Load bearing capacity of existing concrete half-joints

J.B. Ruijgrok

Master Thesis

Delft University of Technology

Faculty of Civil Engineering and Geosciences

Load bearing capacity of existing concrete half-joints

Master Thesis

by

J.B. (Joris) Ruijgrok

A thesis report submitted for partial fulfillment of the requirements for the degree of
Master of Science in Civil Engineering

at the Delft University of Technology
Faculty of Civil Engineering and Geosciences

To be defended publicly on Wednesday February 15, 2023 at 09.00 AM.

Thesis committee:

Dr. ir. Y. Yang *(chair)*	TU Delft
Dr. M. Poliotti	TU Delft
Dr. A.A. Mehrotra	TU Delft
ir. M. Aurik	ARUP
ir. C. Quartel	Rijkswaterstaat

Rijkswaterstaat
Ministry of Infrastructure and the Environment

An electronic version of this thesis is available at
`http://repository.tudelft.nl/`.

Abstract

Concrete half-joints are a specific support detail in reinforced concrete structures, which reduce the construction height of the total structure. The use of concrete half-joints became popular around 1950s, but decreased its interest as a result of new insights on structural behaviour and collapses of these structures. Typical issues regarding concrete half-joints are either due to inadequate reinforcement detailing or due to deterioration mechanisms. The most critical deterioration is when a crack at the re-entrant corner allows for water ingress and thus corrosion of the rebars. This thesis focuses on the negative influence of this corrosion on the load bearing capacity and proposes an assessment method, which includes the reinforcement detailing. Firstly, problematic half-joints have been categorised and studied for reinforcement detailing. Subsequently, they have been analysed using an analytical tool, in which corrosion was implemented on the rebars. The outcomes were validated numerically.

For this thesis research, a series of Dutch concrete bridges has been studied to identify general reinforcement issues and categorise concrete half-joints. It has been observed that the majority showed short transfer- and/or anchorage lengths of the rebars and that all of them showed no shear stirrups as hanger-reinforcement. In stead, only a horizontal- and hanger rebar are present, which can be accompanied with a diagonal rebar, prestressing at the top or nib (or combinations in between).

An analytical tool is designed to calculate the load bearing capacity of (un)corroded concrete half-joints. The analysis is based on a lower-bound approximation using a strut-and-tie approach and an upper-bound approximation using a kinematic approach. The analytical tool is used to determine the load bearing capacity of the series of investigated Dutch concrete half-joints. Both approximations are comparable when rebar failure is the governing failure mechanism. The strut-and-tie approach also incorporates detailing checks, which are not considered in the kinematic approach. Therefore large differences occur when detailing governs the capacity.

The nodes in the strut-and-tie model, in which two ties are connected to one concrete strut, appear to be critical in the lower-bound solutions. The capacity depends on the concrete strength and dimensions of the node. The dimensions are influenced by the mandrel diameter of the hanger-rebar and anchorage length of the horizontal rebar. In order to study the influence of corrosion on the load bearing capacity, the effect of a reduced rebar capacity due to an increasing corrosion rate was implemented in the analytical tool. The kinematic approach appears to be more sensitive to load bearing capacity loss, as this calculation depends mainly on the strength of the rebars. The strut-and-tie approach is able to redistribute forces over the struts and ties and is less sensitive.

In order to verify the analytical results, a numerical study is performed. The specimens are modelled in such a way that rupture of one of the rebars at the re-entrant corner is governing. Both analytical solutions appear to be conservative compared to the numerical results, in which the lower-bound solutions are very conservative. Different crack's angles have been found between the upper-bound calculation and numerical results. If the same angle is applied in the analytical tool, the difference reduces from 7% to 2% for an uncorroded concrete half-joint without diagonal. The differences can be explained by the simplification in the kinematic approach, in which the concrete compression zone is not able to transfer shear stresses

Based on the conclusions of the analytical tool and numerical verification, an assessment method is proposed in which the upper-bound solution is combined with the lower-bound solution. If the load on the concrete half-joint is lower than the calculated lower-bound solution, the concrete half-joint is safe. However, questions arise if the load is between the lower- and upper-bound solution, in which structural safety cannot be guaranteed. The analytical tool is still a useful tool to understand the behaviour and vulnerabilities of the concrete half-joint. The analytical tool is even more useful if the strut-and-tie approach is governed by rupture of the horizontal-, diagonal- or hanger-rebar. The kinematic approach can be extended by implementing the same crack's angle, which occurs in the existing concrete half-joint.

Contents

Chapter 1

Introduction

1.1 Motivation

Concrete half-joints are a specific support detail in reinforced concrete structures, which reduces the construction height of the total structure. Concrete half-joints are also known as Gerber joint, or dapped-end joint.

The total structure consists of a precast beam with dapped-ends supported by a concrete half-joint. An expansion joint is provided at the top of the concrete half-joint to prevent leakage through the joint. Figure 1.1 illustrates a general concrete half-joint structure.

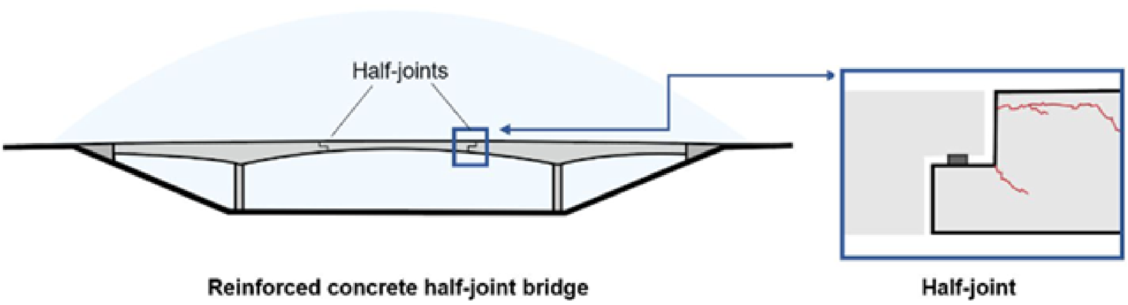

Figure 1.1: General concrete half-joint structure, based on [1]

The use of concrete half-joints in structures was popular around 1950s [2], but decreased its interest in the last years as a result of new insights on structural behaviour and failures of structures, like the collapse of 'De La Concorde overpass' in Quebec (2006) which cost the lives of 5 people and another 6 were wounded [3].

Recent discoveries on a bridge with concrete half-joints in the Netherlands (Nelson Mandela bridge), led to a closure of the structure. A leaking expansion joint, large diagonal cracks at the re-entrant corner and inadequate reinforcement detailing led to a large uncertainty on the structural safety of the structure [4]. Especially, because the failure of a concrete half-joint is a brittle failure mechanism, which shows no ´warning signs´ as large deformations.

The structural behaviour and load bearing capacity of concrete half-joints is questionable, especially if inadequate reinforcement detailing or deterioration like corrosion is present. Therefore, Rijkswaterstaat already decided that new concrete structures can not be provided with half-joints anymore. Nevertheless, there are still at least 200 existing structures with concrete half-joints in their possession and possibly even more in the Netherlands.

1.2 Problem statement

The first crack in a concrete half-joint typically initiates at the re-entrant corner. In the experimental study of Desnerck et al. [5], the diagonal crack initiated at 27-42% of the ultimate load for different reinforcement layouts. Similar results have been found by experiments from Wang et al. [6] (13-45%). Therefore, it can be stated that a (small) diagonal crack is already present at the re-entrant corner of a concrete half-joint at a relatively small load-level, despite the reinforcement layout. Though, the reinforcement layout does have an effect on further propagation and crack-width of the diagonal crack.

A space is left open between the precast beam and concrete slab, so that the concrete components can deform freely due to e.g. temperature. An expansion joint is placed to provide a smooth transition at bridge deck level and to provide a water-sealing function. Unfortunately, the joints are prone to damage due to traffic loads and the water-sealing function is often damaged. (Chloride rich) Surface water is then able to seep through the expansion joint towards the re-entrant corner, in which the diagonal crack is present [1].

The reinforcement of a concrete half-joint are placed near the re-entrant corner and intersect the diagonal crack, see Figure 1.2. As the (chloride rich) surface water seeps through the diagonal crack, corrosion can occur at the reinforcement. Corrosion influences the mechanical properties of the reinforcement and therefore has a major influence on the load bearing capacity of the concrete half-joint.

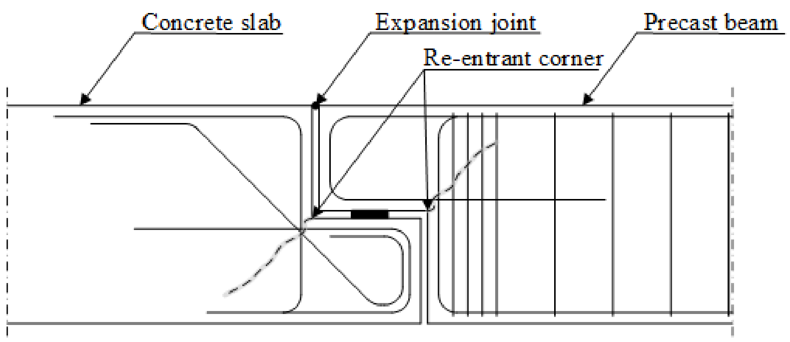

Figure 1.2: Concrete half-joint indication

Additionally, concrete half-joints are difficult to inspect due to the limited space available between the precast beam and concrete slab. Therefore, the condition of the concrete half-joint at the re-entrant corner can only be observed from the side.

1.3 Objectives & research questions

This thesis research focuses on the deterioration due to corrosion of the rebars at the re-entrant corner and reinforcement detailing of a concrete half-joint. The aim is to identify which reinforcement layouts are prone to load bearing capacity loss due to corroded rebars at the re-entrant corner, in order to identify a risk profile of concrete half-joints. And to provide an assessment method for concrete half-joints dealing with deterioration and/or inadequate reinforcement detailing.

The main research question of this thesis research is as follows:

How can concrete half-joints be assessed on load bearing capacity by implementing deterioration and/or inadequate reinforcement detailing?

Which can be subdivided into sub questions as:

- What are the main reinforcement layouts for existing concrete half-joints?
- How does inadequate reinforcement detailing influence the load bearing capacity of concrete half-joints?
- How does deterioration influence the load bearing capacity of concrete half-joints?
- How can the assessment on load bearing capacity of concrete half-joints be improved?

1.4 Methodology

The preliminary study consists of a literature review on concrete half-joints and the influence of corrosion reinforcement and the bond-behaviour between concrete and reinforcement. Additionally, an archive study is performed using technical drawings of Dutch structures with concrete half-joints, provided by Rijkswaterstaat and ´Provincie Gelderland´. In the main research, an analytical parametric tool is proposed to assess concrete half-joints subjected to inadequate reinforcement detailing and deterioration. Subsequently, a numerical study is performed to understand the structural behaviour of concrete half-joints and verify the analytical results. The methodology is illustrated in Figure 1.3.

It is assumed that the corrosion rate of the reinforcement is known and can be used in further calculations. Methods on how to measure corrosion in a concrete structure are not discussed in this thesis research.

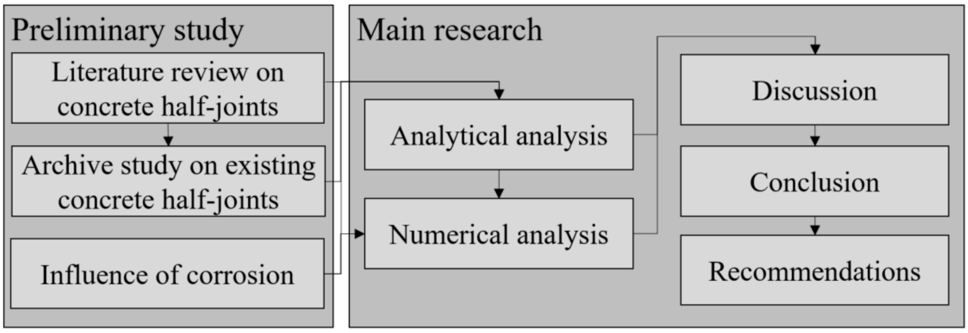

Figure 1.3: Methodology

A brief introduction to each chapter is given below:

Chapter 2: Literature review on concrete half-joints

The structural behaviour of concrete half-joints is analysed, by studying the crack propagation and failure mechanisms. Subsequently, the design- and assessment methods for concrete half-joints are elaborated, to understand the structural idea behind the calculations. At last, three studies are summarised, which are of interest for the main research.

Chapter 3: Categorisation of existing concrete half-joints

The technical drawings of Dutch structures with concrete half-joints are analysed on material- and geometrical properties. A first structural analysis is performed by schematizing a strut-and-tie model, which will be used in further calculations. Subsequently, four general issues have been identified by comparing the observations from the archive study with the literature review on concrete half-joints.

Chapter 4: Literature review on influence of corrosion

The influence of corrosion can be distinguished in influence on the reinforcement itself and bond-behaviour between reinforcement and concrete. A literature study of Imperatore [7] is briefly elaborated, from which a suitable corrosion model is chosen to model the corroded reinforcement at the re-entrant corner of the concrete half-joint.

Chapter 5: Analytical assessments using parametric tool

A analytical parametric tool to assess concrete half-joints is designed and elaborated. The tool uses a strut-and-tie approach (lower-bound) and kinematic approach (upper-bound) to determine the load bearing capacity of a concrete half-joint. The material and geometrical properties of the concrete and reinforcement are used as input and the corrosion is simulated by applying a reduction on the rebars close to the re-entrant corner.

Chapter 6: Numerical verification

A numerical study is performed using DIANA FEA to analyse the structural behaviour of a concrete half-joint with simulated corrosion of the rebars. Subsequently, the analytical results of Chapter 5 are verified.

Chapter 7: Discussion, conclusions and recommendations

At last, the results of this thesis research are discussed and conclusions are drawn. Recommendations are provided for the assessment of concrete half-joint and to improve future research.

Chapter 2

Literature review on concrete half-joints

2.1 Introduction

This chapter elaborates a literature review on concrete half-joints. Attention is paid to the structural behaviour and design/assessment methods. Subsequently, three completed studies are elaborated, which are of interest for this thesis research.

An overview of commonly known advantages and disadvantages of concrete half-joints found in literature is elaborated below:

Advantages

1. The reduction in construction height leads to an equal level between the bridge deck and its support [1]
2. Precast concrete beams can be lifted and installed easily [1]
3. The concrete half-joint makes statically indeterminate structures (e.g. multi-span bridges), statically determinate. They can be considered as hinged connections, which is beneficial for uneven settlements. The freedom to deform does not lead to additional stresses in the structure [2]

Disadvantages

1. Deterioration of concrete and/or corrosion of reinforcement can occur as a result of a leaking expansion joint [1], [3]
2. The area between the concrete half-joint and precast concrete beam is difficult to access for inspection or maintenance [1]
3. There is no general accepted assessment method for concrete half-joints as a result of the complexity of shear failure in reinforced concrete structures [8], [6]

Figure 2.1 illustrates the general geometry of a concrete half-joint including names/labels for specific aspects. A general reinforcement layout with diagonal rebar is also provided, which will be discussed in paragraph 3.5. The sum of hanger-stirrups and hanger-rebars will be referred as hanger-reinforcement.

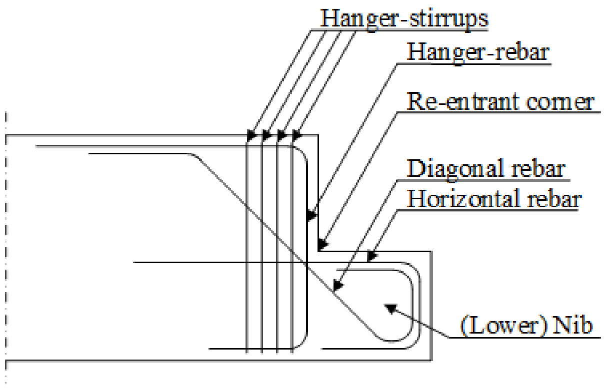

Figure 2.1: Reinforcement layout of concrete half-joint

2.2 Structural behaviour of concrete half-joints

2.2.1 Crack propagation

In general, the load of a concrete structure with concrete half-joint propagates from the precast beam through the concrete half-joint towards the support structure, which can be a shear wall, cantilever structure or column. If the structure would have been continuous, the load would be transferred in accordance with Bernoulli's theorem.

However, this is not the case due to the presence of the concrete half-joint. Therefore it is considered as a discontinuous region, from which Bernoulli's theorem cannot be applied. The discontinuity is illustrated in Figure 2.2 using elastic stress trajectories of an uncracked concrete half-joint.

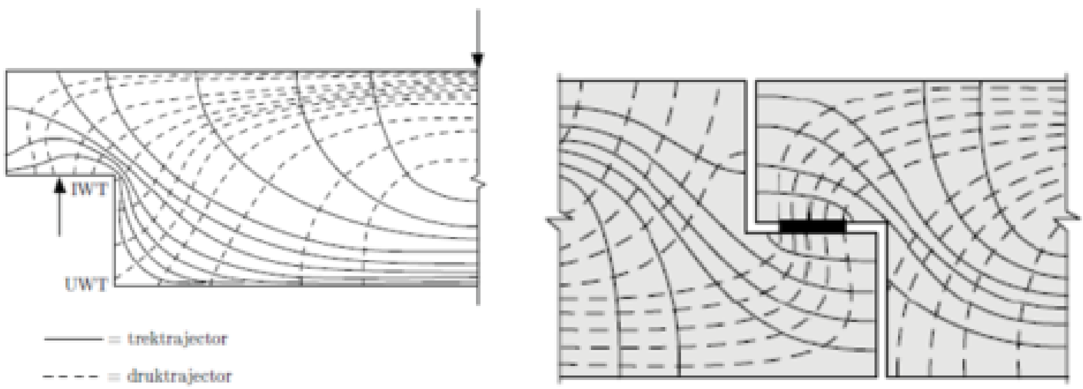

Figure 2.2: Stress trajectories of uncracked concrete half-joint [1],[8]

Figure 2.2 shows that the compressive stresses propagate from the support towards the bottom of the concrete half-joint and the tensile stresses propagate towards the top. The largest tensile stresses occur at the re-entrant corner of the concrete half-joint.

The exact crack propagation relies on the dimensions and material properties of the concrete half-joint. However, the first crack often initiates at the re-entrant corner and propagates diagonally towards the compression zone. At the same time, diagonal cracks occur in the nib. As the load further increases, a large diagonal crack occurs suddenly over the full depth of the concrete beam [6]. Figure 2.3 shows the crack pattern of the example given above:

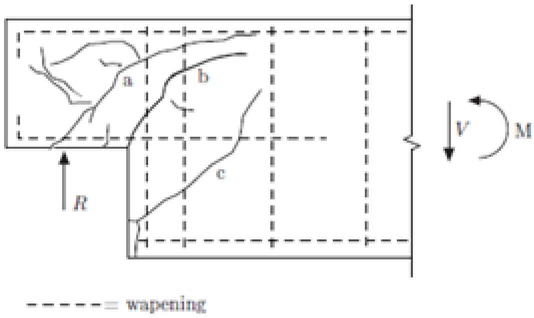

Figure 2.3: Crack pattern just before failure of specimen B2.22 [6], [8]

The crack width of the crack at the re-entrant corner can be limited by providing a diagonal rebar perpendicular to the crack. If applied properly with sufficient anchorage length, this also leads to a higher load bearing capacity [6].

2.2.2 Strut-and-tie model

A strut-and-tie model for a concrete half-joint can be designed using the stress trajectories in Figure 2.2 and crack propagation in Figure 2.3. The reinforcement layout can be distinguished in a layout with or without diagonal rebar, which leads to the following commonly used strut-and-tie models: [9]:

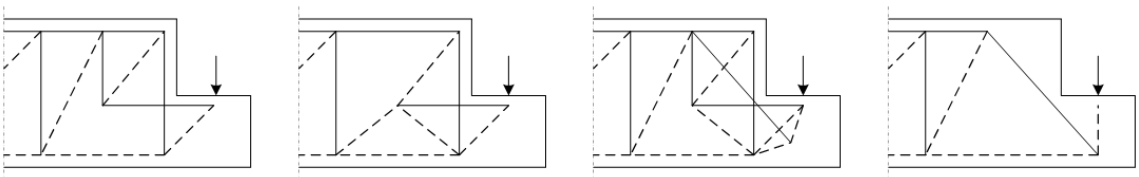

(a) (b) (c) (d)

Figure 2.4: Commonly used strut-and-tie models for concrete half-joints, based on [9]

An introduction to strut-and-tie modelling is provided in paragraph 5.2.

2.2.3 Failure mechanisms

The concrete half-joint shows typical crack patterns at failure, also called failure modes. Literature describes 4 potential failure modes that can occur [8], [6], [9], [10]:

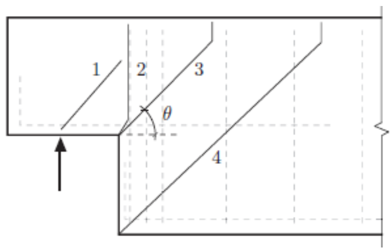

Figure 2.5: Failure modes of concrete half-joints [8]

Table 2.1: Failure modes with failure mechanisms of concrete half-joints

	Failure mode	Failure mechanism
1.	Diagonal crack in nib	Concrete compressive or tensile strength is exceeded
2.	Direct shear crack	Rupture of horizontal rebar in nib
3.	Diagonal crack in re-entrant corner	Rupture of horizontal rebar, hanger-reinforcement and/or diagonal rebar
4.	Diagonal crack over full depth	Rupture of hanger-reinforcement or inadequate detailing of reinforcement

Which failure mode and mechanism occurs, depends on the dimensions (e.g. height/ depth ratio) of the concrete half-joint and material properties of the applied concrete and the reinforcement. Desnerck et al. [5] describe that the most common failure modes of a concrete half-joint are mode 3 and 4. However, the structural interactions of these failure modes are complex and sensitive to reinforcement detailing and/or strength reductions as a result of deterioration of concrete [11].

Houwen [8] studied the concrete half-joint (without diagonal rebar) with experiments and observed that the failure modes were a combination of failure mode 2 and 3. The failure modes can be distinguished as illustrated in Figure 2.6:

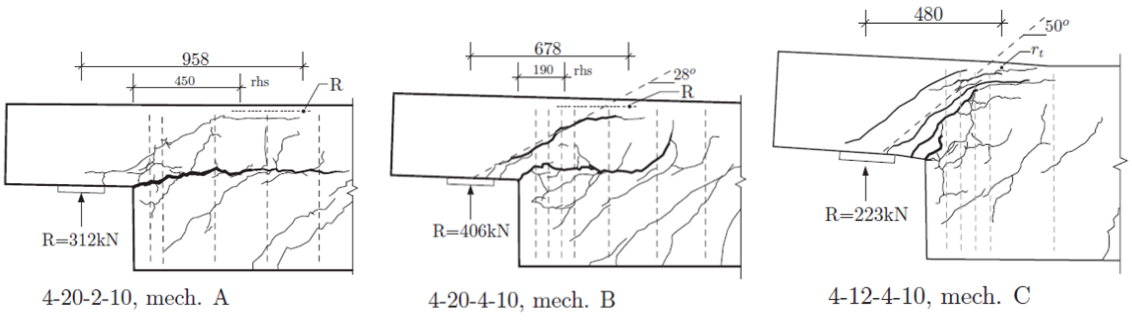

(a) Mechanism A (b) Mechanism B (c) Mechanism C

Figure 2.6: Crack pattern at failure [8]

Failure mechanism A: Rupture of hanger-reinforcement

Failure mechanism A occurs if the hanger-reinforcement ruptures before the horizontal rebar reaches its yield strength. The crack pattern at failure shows that the critical crack follows a horizontal line. Houwen used this crack pattern to model the concrete nib as a cantilever fixed to the main beam.

Failure mechanism B: Yielding of hanger-reinforcement and horizontal rebar

Failure mechanism B occurs if the hanger-reinforcement and horizontal rebar both reach the yield strength. Besides the horizontal crack that also occurs in failure mechanism A, diagonal cracks are present. The cracks initiate at the re-entrant corner and propagate towards the compression zone. This initiates a second failure mechanism.

Failure mechanism C: Rupture of horizontal rebar

Failure mechanism C occurs if the horizontal rebar ruptures before the total hanger-reinforcement reaches its yield strength. The hanger-reinforcement prevents the propagation of the horizontal crack. Therefore, the crack pattern at failure shows a critical diagonal crack, similar to the second failure mechanism of B.

2.3 Design of concrete half-joints

The first Dutch design codes for reinforced concrete structures were published in 1912 and only contained approximately 20 pages. In the following years, more research and requirements led to an expansion of the design codes. An overview of all design codes for reinforced concrete structures used in the Netherlands is given below:

- GBV series (1912, 1918, 1930, 1940, 1962)
- VB series (1974, 1978) also known as NEN 3880
- VBC series (1990, 1995) also known as NEN 6720
- Eurocode (2010)

This paragraph elaborates the design method of concrete half-joints in accordance with recent and previous code provisions to understand the design principles of existing structures.

2.3.1 NEN6720

The design method of a concrete half-joint in accordance with NEN 6720 is based on a strut-and-tie model, in which the hanger-reinforcement, horizontal rebar and shear capacity needs to be considered.

Hanger-reinforcement

The hanger-reinforcement must be able to transfer the complete load from the bottom of the beam to the top of the concrete half-joint (NEN6720 art. 9.11.7.2). The amount of hanger-reinforcement is based on the strut-and-tie model in Figure 2.4(a). If a different strut-and-tie model is used, for example in Figure 2.4(b), the tensile force in the hanger-reinforcement would be larger [12].

The hanger-reinforcement needs to be placed over a length of $h_i \cdot cot\theta_i$, in which θ_i is an arbitrary value between 30° and 60° (NEN6720 art. 9.11.7.2):

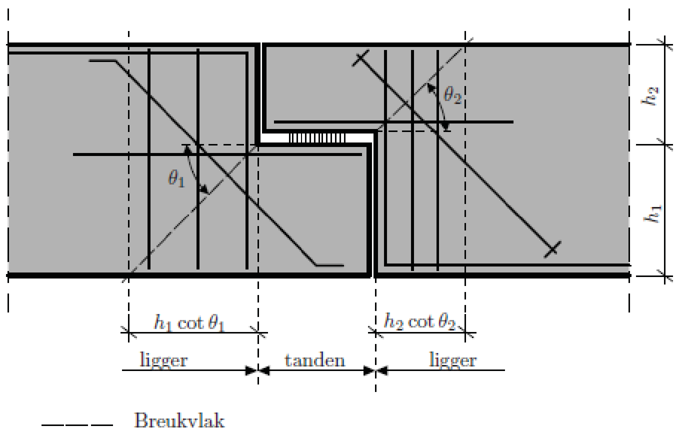

Figure 2.7: Spacing of hanger-reinforcement [8]

The detailing of the hanger-reinforcement needs to be sufficient in order to transfer the load from the compressive strut towards the hanger-reinforcement itself. The detailing is elaborated in further depth in paragraph 2.5.1.

Horizontal rebar

The horizontal rebar must be able to transfer the tension force caused by the bending moment of the support reaction and hanger reinforcement. The horizontal lever arm a which causes the bending moment, is the distance between the support and resultant force in the hanger-reinforcement. In addition, the horizontal rebar must be able to transfer horizontal forces caused by shrinkage or temperature variations. Figure 2.8 elaborates how the forces and lever arms are determined in accordance with NEN6720:

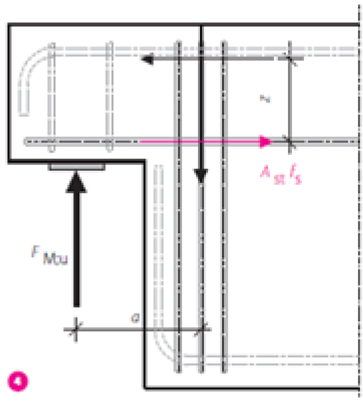

Figure 2.8: Calculation of tension force in horizontal rebar [12]

The horizontal rebar needs sufficient anchorage length in order to transfer the total tension force. The anchorage length must be determined using the strut-and-tie model in Figure 2.4(a).

Shear capacity

The shear capacity needs to be verified by comparing the shear stress with the shear resistance of the concrete. If the shear stress is larger than the shear resistance, additional stirrups need to be provided. The shear strength can be determined as (NEN 6720 art. 8.2.3.1):

$$\tau_1 = 0.4 f_b k_\lambda k_h \sqrt[3]{\omega_0} \tag{2.1}$$

In which:

f_b	is the design value of the tensile strength of concrete
k_λ	is a coefficient depending on the span-to-depth ratio ("dwarskrachtslankheid")
k_h	is a coefficient depending on the height of the structure
ω_0	is the longitudinal reinforcement ratio

The coefficient k_λ can be determined, if a proper compressive strut can be formed, as:

$$k_\lambda = \frac{12}{g_\lambda} \sqrt{\frac{A_0}{b \cdot d}} \leq 1 \tag{2.2}$$

In other situations, k_λ must be equal to 1. Paragraph 2.5.1 provides additional recommendations on whether the coefficient can be reduced or not.

2.3.2 Eurocode

The design method of a concrete half-joint in accordance with Eurocode 2 is fully based on a strut-and-tie model. Figure 2.9 shows the provided models in accordance with NEN-EN 1992-1-1 (incl. NB) art. 10.9.4.6(1) which may be used:

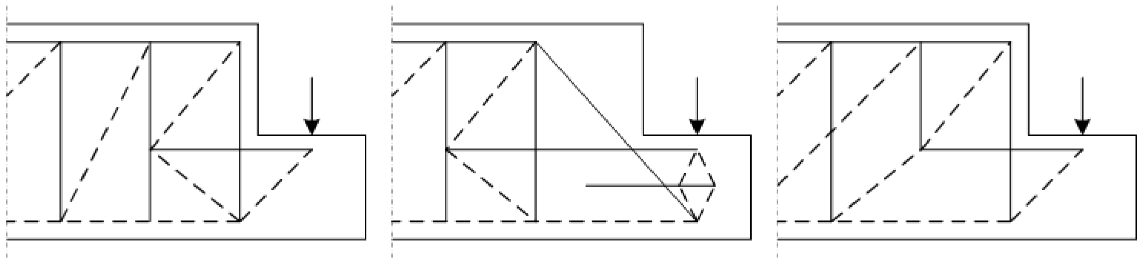

(a) (b) (c)

Figure 2.9: Possible strut-and-tie models for concrete half-joints

Eurocode 2 does not give any further guidance on the design. The general rules of strut-and-tie modelling and detailing must be applied, see paragraph 5.2..

2.4 Assessment of existing concrete half-joints

In the Netherlands, concrete structures are assessed in accordance with the 'bouwbesluit ´, which refers to NEN 8700 for the structural safety of existing structures. Rijkswaterstaat provides additional guidelines for the assessment of existing structures in the RBK1.2. An outline of the RBK1.2 is provided in Appendix A.

Rijkswaterstaat approved the CUR40 method (also known as kinematics-based method) to assess concrete half-joints with prestressing (RBK1.2 art. 3.1.3.1). This method is elaborated below.

2.4.1 CUR40 method

The CUR40 method uses the presence of diagonal crack to determine the load bearing capacity of the concrete. The torn-off concrete part can be modelled as a free-body diagram, in which the load at the bearing plate leads to a rotation. The rebars in the concrete half-joint provide a restoring force and moment. The torn-off part is illustrated in Figure 2.10.

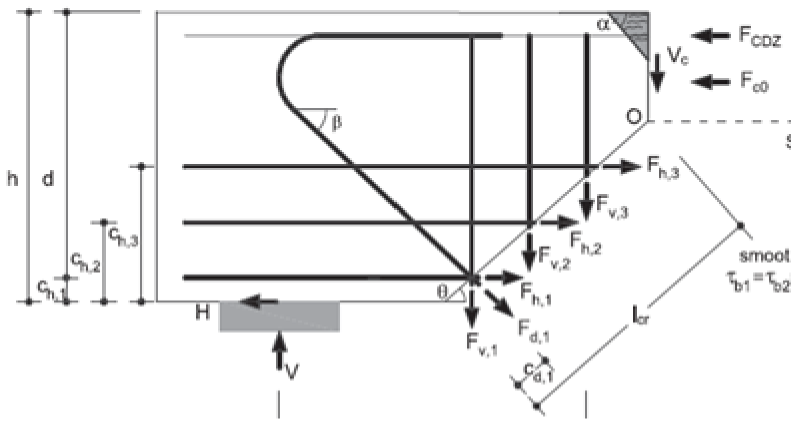

Figure 2.10: Free body diagram of torn-off concrete part [13]

The CUR40 method assumes that the reinforcement is detailed properly, and tensile forces are able to develop up to the yield capacity. The tensile forces in the rebars are therefore not dependent on the crack-width. CUR commission validated this method using a full-scale experiment using a concrete half-joint with and without prestressing with satisfactory results [14]. The method is elaborated in further depth in paragraph 5.5.

The method can also be extended by determining the tensile forces in the rebars in accordance with the crack-width in the concrete and the strain in the concrete and rebars. Rajapakse et al. [13] proposed and validated [15] this method using experiments. The strains in the reinforcement are determined using an iterative procedure depending on the crack-width in the direction of the reinforcement. Subsequently, the horizontal force equilibrium is checked and the compressive zone height is adjusted if necessary.

2.5 Overview of completed studies

This paragraph elaborates completed studies, which are of interest for this thesis research.

2.5.1 Nokken met die tanden

In 2006, prof.ir. C. Kleinman started research on the structural design of concrete half-joints in accordance with NEN 6720 (Dutch design standard, also known as VBC 1995) [16] [17] [18] [19]. The design method of concrete half-joints is assumed to be similar to corbels, in which the load transfer function between support and the beam (concrete half-joint) is assumed to be fulfilled by hanger-reinforcement. In corbels, the load is transferred directly into the column. The hanger-reinforcement can be provided in the form of hanger-stirrups or by bending the lower longitudinal reinforcement towards the top of the beam and back (hanger-rebar).

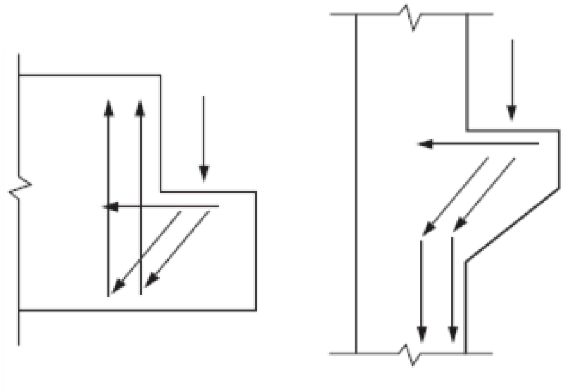

(a) Concrete half-joint (b) Corbel

Figure 2.11: Load transfer in corbel and concrete half-joint, based on [8]

In engineering practice, the concrete half-joint was considered as a deep beam (Dutch: “gedrongen ligger”) with a span-to-depth ratio smaller than 1, which results in a higher shear resistance of concrete than slender beams [16] [17]. An overestimation of the shear resistance of concrete can lead to a shortcoming of hanger-reinforcement.

The incorrectness of the assumption that concrete half-joints behave similar to corbels and can be considered as a deep beam was researched by Kleinman using numerical modelling and experiments. The experimental set-up was as follows:

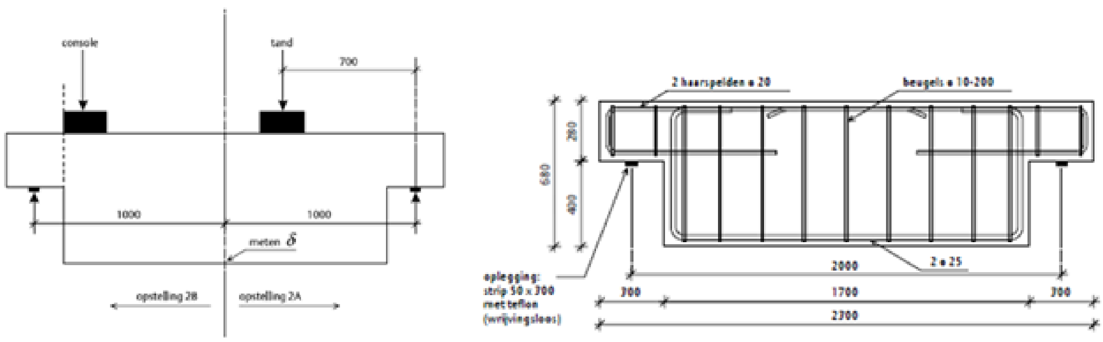

Figure 2.12: Experimental set-up and reinforcement layout [17]

The hanger-reinforcement is provided by bending the longitudinal bottom reinforcement to the top of the beam. The concrete half-joint is considered as a deep beam, with sufficient shear strength and therefore no additional hanger-stirrups need to be provided.

The results of the experiment confirmed the hypothesis of Kleinman. The concrete half-joint failed at a load of 170 kN (design load: 231 kN and ultimate load: 326 kN). The crack pattern indicates that failure occurred at the curved part of the hanger reinforcement. This indicates that the load cannot be transferred properly to the hanger reinforcement. The corbel failed at a load of 360 kN, in which the load is transferred directly from the support to bearing plate, as indicated in Figure 2.11. The crack patterns at failure are shown in Figure 2.13a and Figure 2.13b:

(a) Concrete half-joint (b) Corbel

Figure 2.13: Crack pattern at failure [17]

Kleinman concluded that the load transfer mechanism of a concrete half-joint differs from a corbel, because a proper compressive strut can be formed in the corbel and not at the hanger-rebar in the concrete half-joint. Hanger-stirrups need to be provided in the concrete half-joint to create a proper node which can transfer the load between the compressive strut and the hanger-reinforcement [17].

Kleinman proposed an alternative method to lower the shear resistance of concrete by using linear interpolation [18].

NEN 6720 art 9.11.7.2 states that the hanger-stirrups must be placed over a certain length from the re-entrant corner of the half joint, see Figure 2.7. The standard provision does not state any guidelines about the placement or spacing between the hanger-stirrups.

Kleinman investigated three different shear reinforcement layouts to determine the effectiveness of placement, see Figure 2.14. In Layout I the reinforcement is placed behind the curved part of the bottom reinforcement. Layout II is similar to Layout I, but the reinforcement is placed near the re-entrant corner. Layout III is similar to Layout II, but stirrup 'B' is placed next to 'A'.

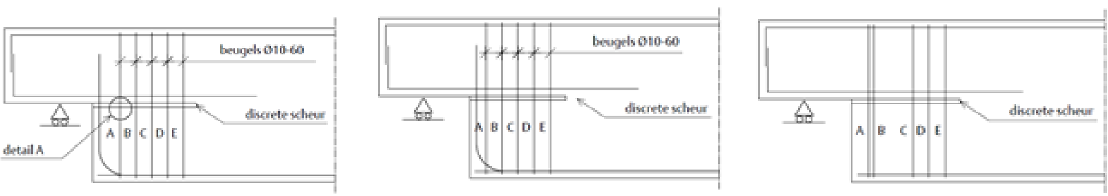

(a) Layout I (b) Layout II (c) Layout III

Figure 2.14: Different hanger reinforcement placements [18]

Yielding of the (first) hanger-stirrup will occur in Layout I and Layout II at a lower load than Layout III. Therefore, it is recommended to place the hanger-stirrups as close as possible towards the re-entrant corner. This conclusion has also been confirmed from experiments by Houwen [8]. Additionally, the crack width at the re-entrant corner is limited by applying this layout.

The results of the research led to additional recommendations for NEN6720 [12]:

- The coefficient depending on the span-to-depth ratio (k_λ) may only be reduced if proper detailing is provided between compressive strut and hanger-reinforcement

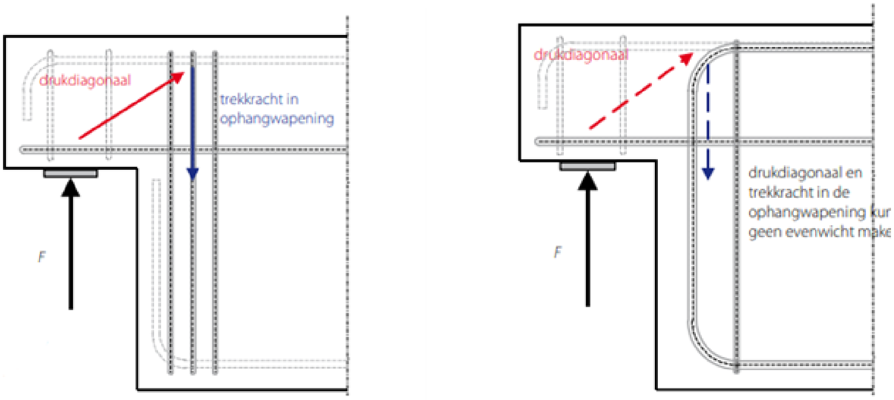

(a) Good detailing (b) Bad detailing

Figure 2.15: Different reinforcement layouts for k_λ [12]

- The hanger-stirrups needs to be placed as close to the re-entrant corner as possible, see Layout III in Figure 2.14c. This is also beneficial for the tension force in the horizontal rebar as the horizontal levers arm decreases.

- A different reinforcement layout is proposed, in which the hanger rebar is bend the other way. In this case, the compressive strut is captured properly by the hanger rebar, see Figure 2.16 [20], [21], [22]:

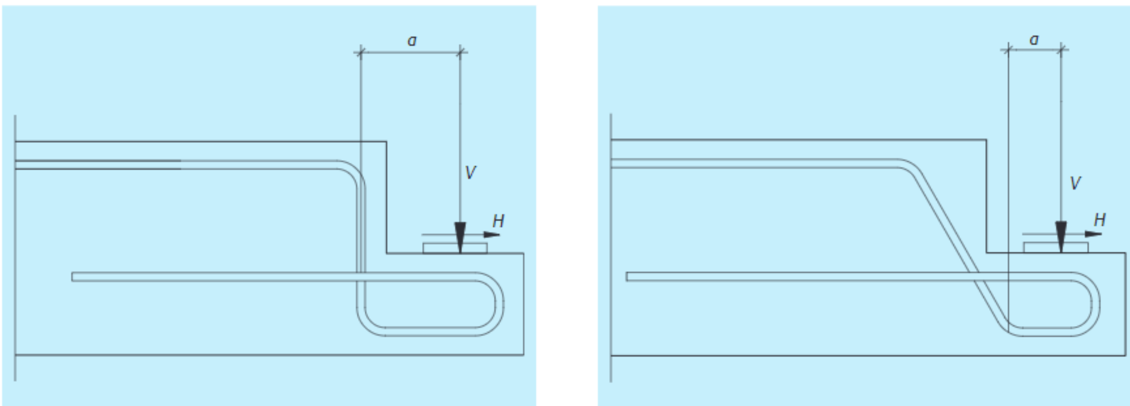

(a) 90° hanger-rebar (b) 60° hanger-rebar

Figure 2.16: Proper detailing of hanger-rebar [20], [21], [22]

2.5.2 Deteriorated concrete half-joints

In 2014, Desnerck et al. started research on: *Structural integrity implications of reinforcement detailing and deterioration*, which led to multiple published articles. This paragraph addresses the articles related to the research with overlap of this thesis research briefly.

The first article provides an introduction to the problem with deteriorated concrete half-joints [1]. The design of new concrete half-joint structures is usually based on strut-and-tie models. Code provisions usually do not give guidelines on assessment of load bearing capacity if deterioration or repair works are present. Additionally, it is unclear to what extent deterioration should be considered by assessors.

To identify the influence of deterioration on the load-bearing capacity, a numerical study is performed. The deterioration is simulated on the rebars by reducing the diameters and/or concrete properties, by reducing the compressive strength by 50% (the tensile strength and Young's modulus are adjusted in accordance with the new obtained compressive strength). The reinforcement layout of the studied concrete half-joint is illustrated in Figure 2.17:

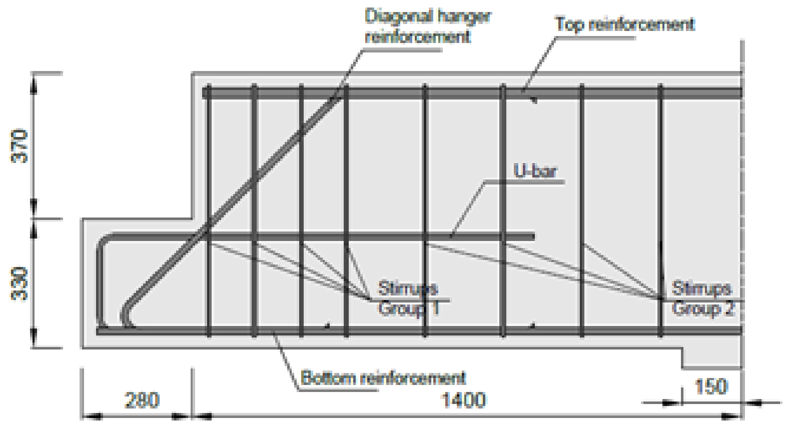

Figure 2.17: Reinforcement layout for numerical analysis [11]

The failure mechanism of the concrete half-joint in the numerical study was rupture of the longitudinal reinforcement, which obviously also appeared to be the most vulnerable for load bearing capacity loss. All other reductions of rebars did not significantly change the load bearing capacity. However, if the reductions are present in all the rebars at the re-entrant corner, the reduction increased even more as redistribution of forces over the rebars is limited [11].

Additionally, an experimental study is performed to identify the influence of reinforcement layouts of the load-bearing capacity [5]. A reference reinforcement layout is used with a horizontal rebar, diagonal rebar and hanger stirrups, and three different layouts are used, in which one of the rebars/stirrups is/are absent. The design load of the reference model is determined using a strut-and-tie model as 300 [kN], which is much larger than the failure load of 402.3 [kN]. This indicates that the strut-and-tie approach for this reinforcement layout and dimensions is conservative. The greatest impact on the load bearing capacity was the absence of diagonal rebar, which had a failure load of 244.9 [kN]. It was noticeable that the first cracks initiated at the re-entrant corner for each specimen and are therefore not dependent on the reinforcement layout.

The results of the previous studies are further analysed using experiments, by incorporating different reinforcement layouts with different deterioration mechanisms [23]. The authors used two different effects caused by corrosion: reduction in rebar diameter and reduction in bond-strength due to the formation of a weak layer of corrosion products and cracking of concrete surrounding the rebar. In total, 9 specimens were used, in addition to the already experimented specimens in [5]. A local reduction of the diameter of the rebars at the re-entrant corner of 50% resulted in a reduction of 35% of the load bearing capacity.

Using the results from the numerical- and experimental study, a strut-and-tie method is proposed for deteriorated reinforced concrete half-joints [9]. Three different strut-and-tie models were used, based on the reinforcement layouts:

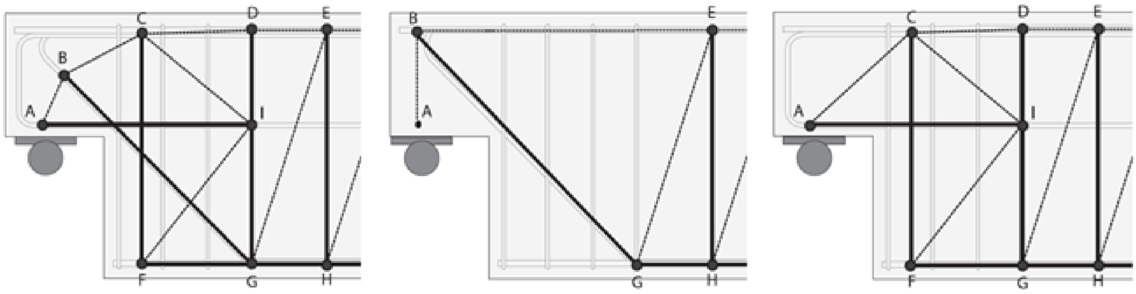

(a) STM for NS/LS-REF (b) STM for NS-NU (c) STM for NS-ND

Figure 2.18: Strut-and-tie models [9]

Corrosion of the rebars can be incorporated by reducing the rebar diameter, which leads to a reduction of the tie. Insufficient or deteriorated anchorage zones can be incorporated by using a proportional reduction of the tie capacity or by penalising the residual bond-strength. The authors suggest reduction factors between 0.3-0.85 [-] depending on the confinement condition and crack state. The strut-and-tie models are verified on the experimental results of [11]-[23] and lead to conservative results within a difference between 16-57%. The developed strut-and-tie models sometimes seem to be unable to pick up alternative load paths that develop as soon as the capacity of a certain tie is reached.

At last, an improved concrete half-joint bridge inspection is proposed, based on existing structures in England with concrete half-joints and the results of the study. In total 428 structures were identified, in which most structures are built between 1960-1970. Approximately 25% of the investigated structures contained reinforced concrete half-joints without pretensioning.

The authors proposed an inspection method using an improved data classification to link a 'Defect type', with a 'Defect Group' and subsequently a 'Defect class'. The inspector can also be provided with a zonal layout of a concrete half-joint, in which deterioration and cracks can be identified. The knowledge of which crack occurs in which zone, leads to an improved decision on whether the defect is affecting the load bearing capacity. Figure 2.19 illustrates such a zonal layout for a concrete half-joint.

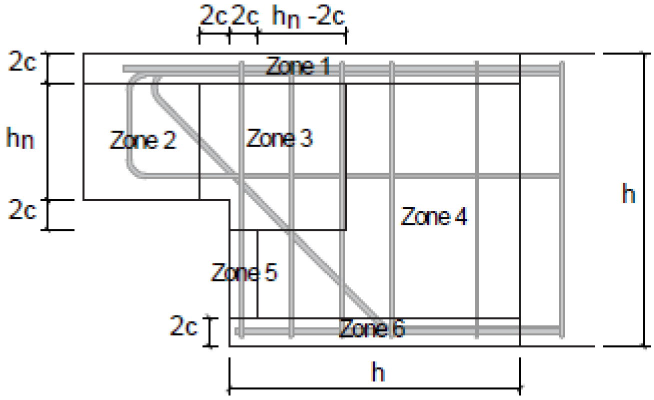

Figure 2.19: Zonal layout of concrete half-joint [24]

The proposed inspection method could possibly be incorporated in the inspection of Dutch structures with concrete half-joints. However, for concrete half-joints reinforced as a slab, different zonal layouts and data classification could arise due to the absence of stirrups and different concrete mixtures.

2.5.3 Collapse of the de la Concorde overpass

On 6 September 2006, five people died and another 6 people were injured as a result of the collapse of the de la Concorde overpass. The overpass was located near Montreal, Canada and consists of prestressed concrete beams, which were supported by concrete half-joints, see Figure 2.20:

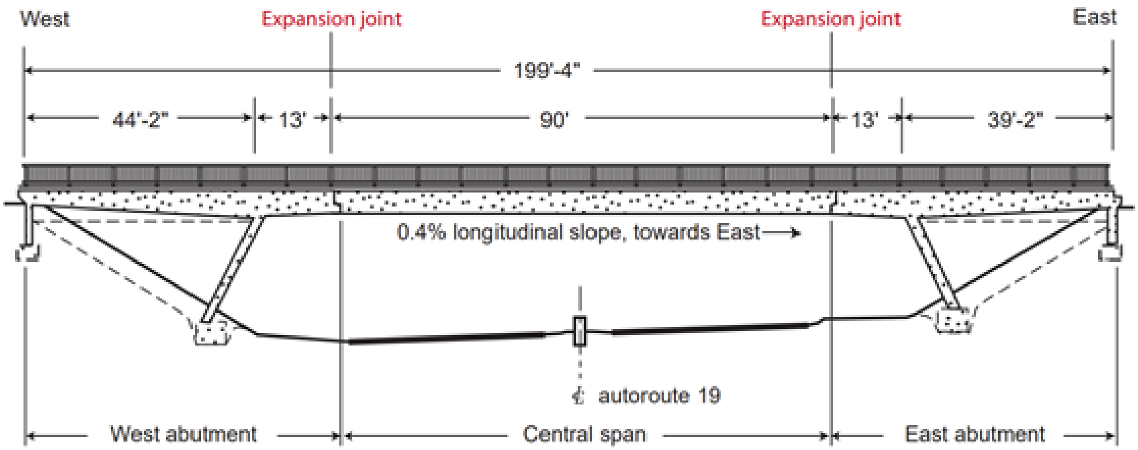

Figure 2.20: Side view of the de la Concorde overpass [3]

The structure was built in 1968 and had an expected lifespan of 70 years. The original design fulfilled the requirements of the standards at that time (CSA-S6-1966 code). Therefore, no shear reinforcement was required, and the disturbed region was designed using strut-and-tie modelling [25]. Figure 2.21 illustrates the reinforcement layout in the disturbed region (concrete half-joint) as designed and as built.

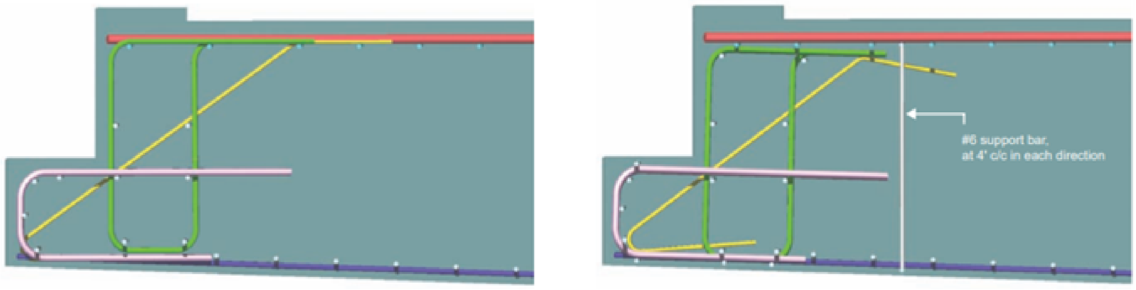

(a) As Designed (b) As Built

Figure 2.21: Reinforcement layout of concrete half-joint [3]

It can be observed that the hanger-rebar (green) is properly designed, but not properly installed. This creates a weak zone at the top of the concrete half-joint. The hanger-rebar must be placed in line with the top rebar. Additionally, diagonal rebar is not properly installed as well.

In 1985, it was observed that the expansion joints were leaking. These were replaced in 1992 during a large repair program, which also involved installation of a waterproof membrane, concrete repair, and the placement of new asphalt. The concrete half-joint already showed some degradation and a large shear crack [3], see Figure 2.22(a):

(a) Span before failure (b) Span after failure

Figure 2.22: Collapse of the de la Concorde overpass [3]

Eventually, the expected lifespan was not reached, and the overpass collapsed suddenly. The Government of Québec established a Commission of inquiry to investigate the collapse and determine the causes. The commission concluded that the overpass collapsed as a result of shear failure, which was caused by deterioration of the concrete and not from the rebar. A crack initiated above the upper rebars, starting from the beam seat, and propagated towards the abutments. Freeze-thaw cycles weakened the concrete and created a zone of weakness at the crack [3].

The commission supposes that the following principal physical causes can have led to the collapse [3]:

- Inadequate rebar detailing during design (weak plane, by placing all reinforcement in one plane)
- Inadequate rebar installation at the time of construction
- Low quality concrete used in the abutments (concrete half-joints)

The commission also supposes some additional physical causes, which can have contributed to the collapse [3]:

- Lack of shear reinforcement in the thick slab
- Surface of the thick slab was not watertight
- Damage caused during the 1992 repair works

The commission provided recommendations to prevent such collapses in the future. Some are outlined below [3]:

- A revision of code provisions in order to require at least minimum shear reinforcement in thick slabs
- Update the inspection and evaluation manuals
- Improve policies and control between different parties, which contribute to the design, execution and maintenance of structures

Furthermore, the commission provided many recommendations on the assessment and maintenance on existing structures, as most of Québec's infrastructure was built in the same years as the de la Concorde overpass [3].

2.6 General categorisation

Figure 2.23 illustrates the reinforcement layouts for concrete half-joints, which have been found in literature. It is possible that concrete half-joints consist of a combination of reinforcement layouts.

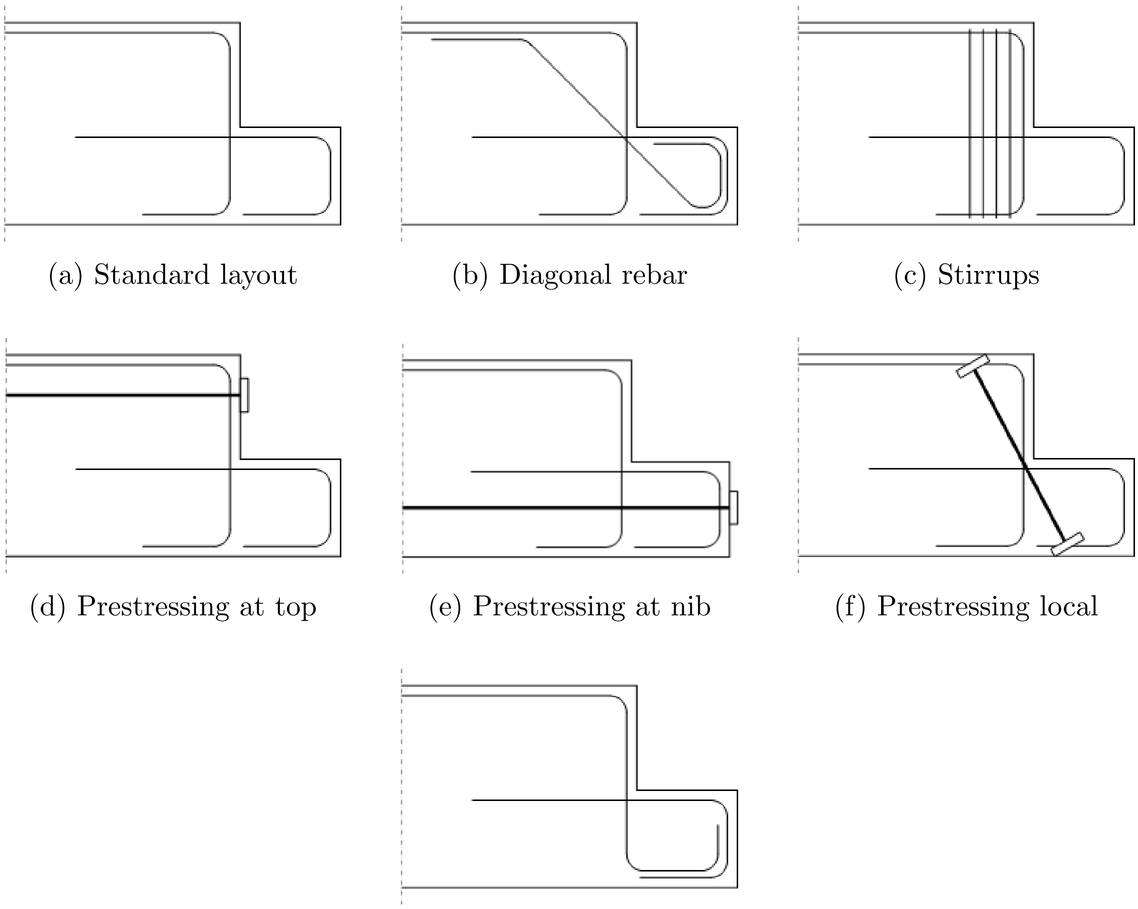

(a) Standard layout

(b) Diagonal rebar

(c) Stirrups

(d) Prestressing at top

(e) Prestressing at nib

(f) Prestressing local

(g) Different bending

Figure 2.23: Reinforcement layouts of concrete half-joints based on literature

Chapter 3

Categorisation of existing concrete half-joints

3.1 Introduction

An archive study on existing bridges with concrete half-joints is performed to categorize the concrete half-joints and to get an overview of the general issues. Rijkswaterstaat and ´Provincie Gelderland´ provided technical drawings of seven existing concrete bridges with concrete half-joints in the Netherlands.

3.2 Overview of existing bridges with concrete half-joints

This paragraph gives an overview of the provided technical drawings, including the year of origin and material properties. A summary of the technical aspects and material properties of the observed concrete half-joints are given in Table 3.1 and 3.2. Subsequently, the concrete half-joints are illustrated and schematically analysed using strut-and-tie modelling. The struts are illustrated as blue, ties as red and anchorage length as orange.

3.2.1 Summary of existing concrete half-joints

Table 3.1: Summary of reinforcement layouts of investigated series of concrete half-joints

Name	Year of origin	Diagonal rebar	Prestressing		
			Global		Local
			Top	Nib	
KW111 Geldermalsen - Nijmegen	1972	Yes	No	No	No
KW38 Bullewijk	1973	No	Yes	Yes	No
KW04 Postwijk	2004	Yes	Yes	No	No
KW16 Purmerend	1973	No	No	No	No
Tegelen	1994	Yes	Yes	No	No
Knooppunt Terbregseplein	1972	No	Yes	Yes	No
KW10 Deventer - Bathmen	1970	Yes	No	No	No

Table 3.2: Summary of material properties of investigated series of concrete half-joints

Name	Concrete		Reinforcement		Prestressing	
	Quality	f_{ck}	Quality	f_{yk}	Quality	f_{pk}
KW111 Geldermalsen - Nijmegen	K300	19	FeB 40	400	-	-
KW38 Bullewijk	unk.	-	QR 40	400	unk.	-
KW04 Postwijk	B45	35	FeB 500	500	FeP 1860	1860
KW16 Purmerend	unk.	-	QR 40	400	-	-
Tegelen	B45	35	FeB 500	500	FeP 1860	1860
Knooppunt Terbregseplein	LC25/28	25	QR 40	400	QP 170	1670
KW10 Deventer - Bathmen	unk.	-	QR 40	400	-	-

The material qualities are provided on the technical drawings for (almost) each concrete half-joint. Due to the different years of origin, the qualities are rewritten to their characteristic strength value using RBK1.2. Some material properties were not provided in the technical drawings or calculations. The characteristic strength values can be determined using the method elaborated in Appendix A.

3.2.2 KW 111 Geldermalsen-Nijmegen

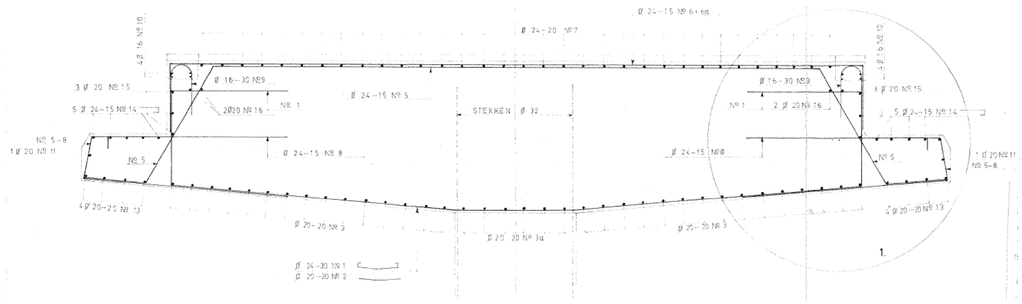

Figure 3.1: KW111 Geldermalsen-Nijmegen - Sideview

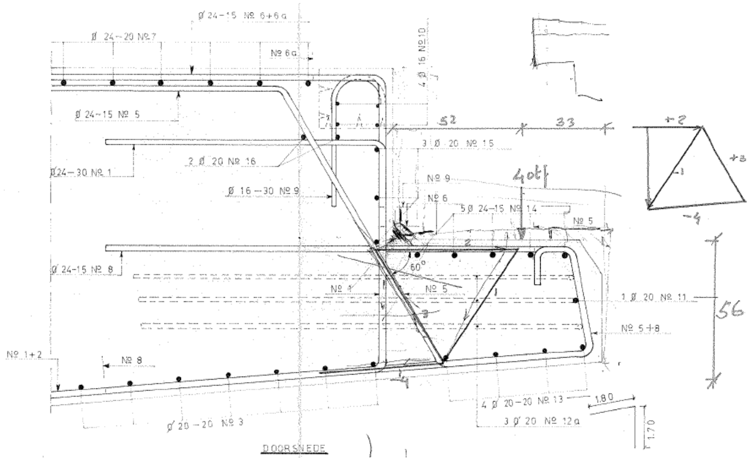

Figure 3.2: KW111 Geldermalsen-Nijmegen - Half joint detail

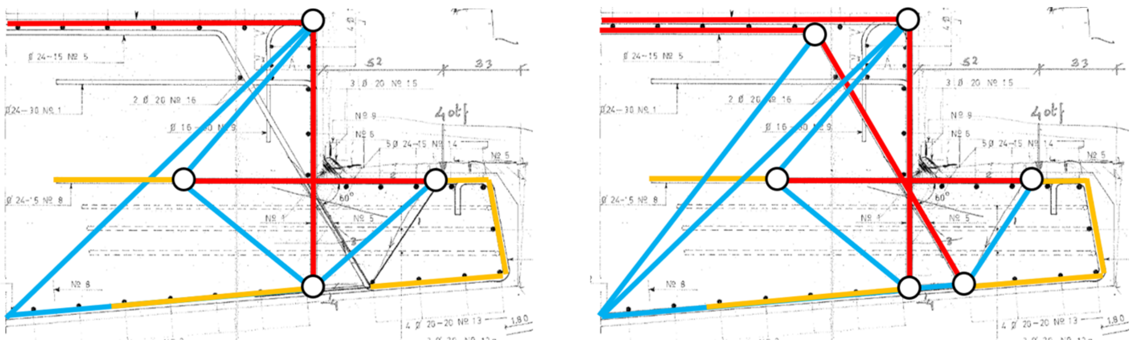

(a) STM1 (b) STM2

Figure 3.3: KW111 Geldermalsen-Nijmegen - Strut-and-tie models

Year of origin	1972
Concrete	K 300
Concrete cover	30 mm
Reinforcement steel	FeB 40
Prestressing steel	-

Table 3.3: KW111 Geldermalsen-Nijmegen - Material properties

3.2.3 KW38 Bullewijk

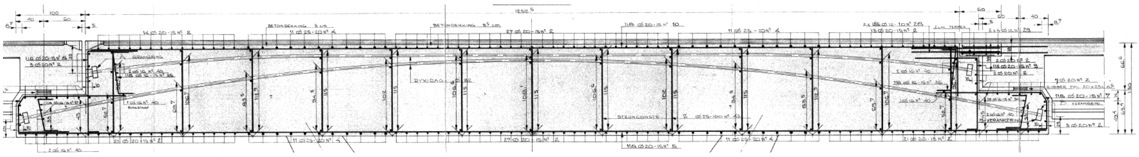

Figure 3.4: KW38 Bullewijk - Sideview

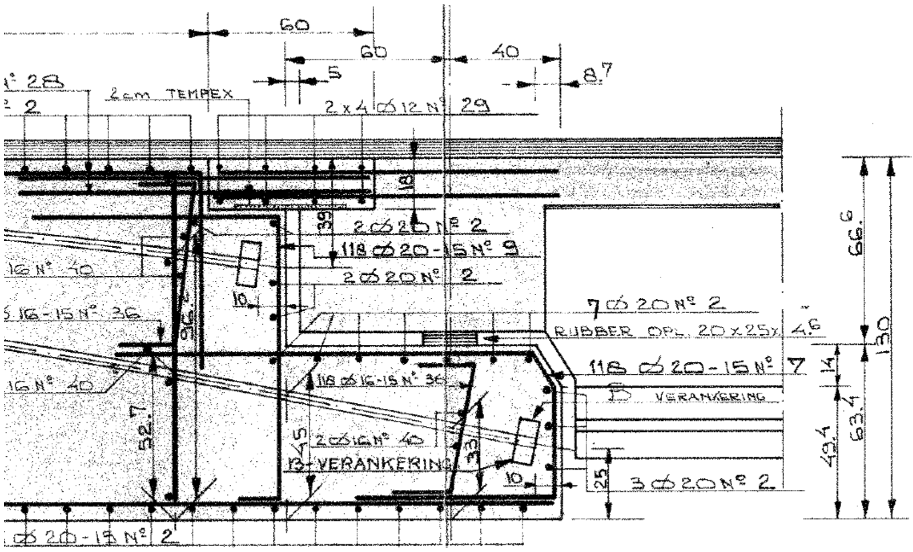

Figure 3.5: KW38 Bullewijk - Half joint detail

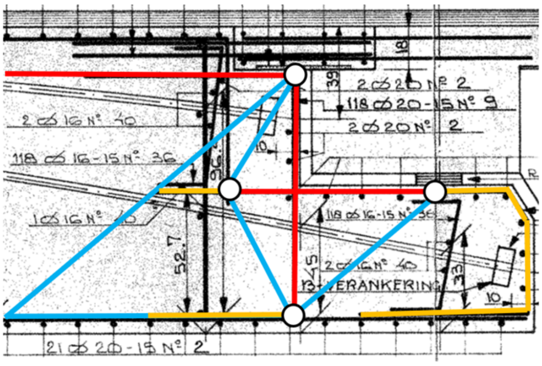

Figure 3.6: KW38 Bullewijk - Strut-and-tie model

Year of origin	1973
Concrete	unknown
Concrete cover	30 mm
Reinforcement steel	QR 40
Prestressing steel	unknown

Table 3.4: KW38 Bullewijk - Material properties

3.2.4 KW04 Postweg

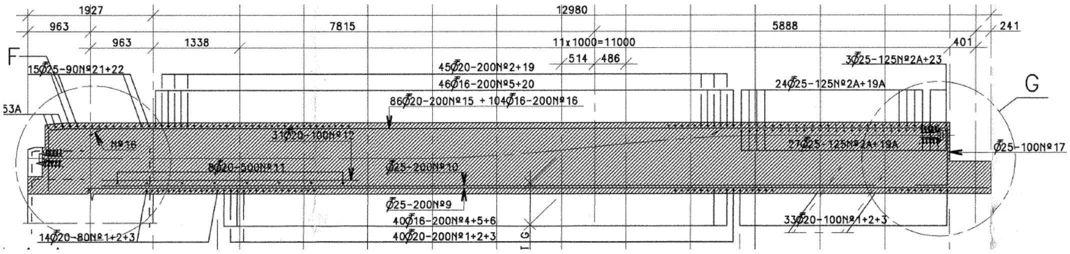

Figure 3.7: KW04 Postweg - Sideview

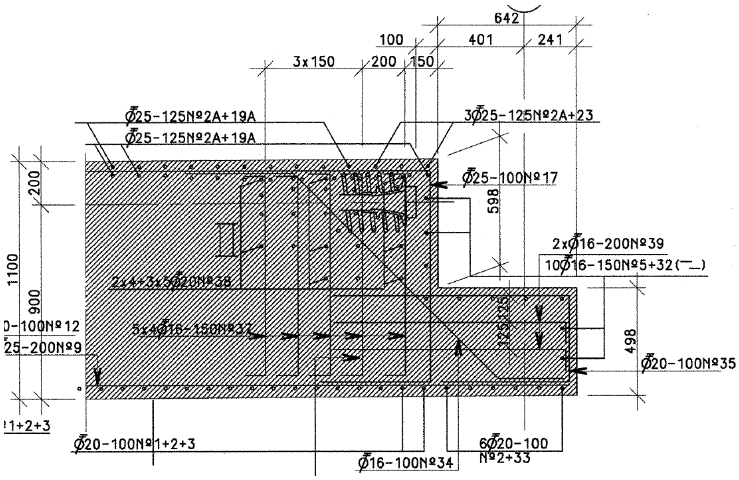

Figure 3.8: KW04 Postweg - Half joint detail

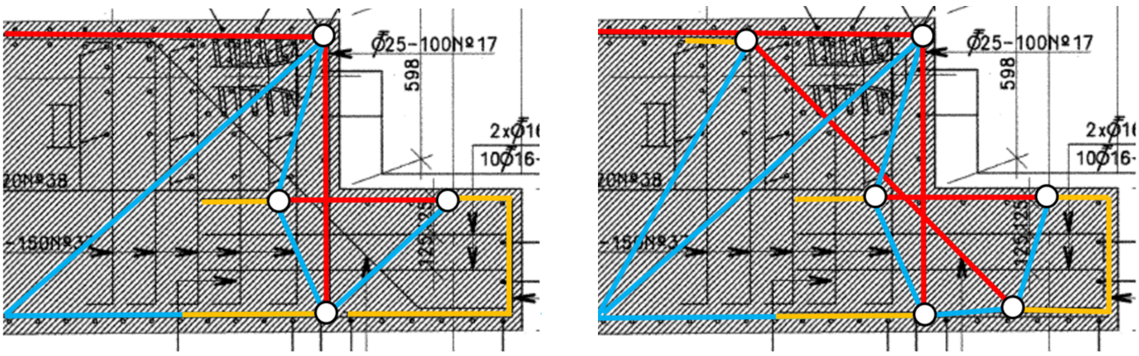

(a) STM1 (b) STM2

Figure 3.9: KW04 Postweg - Strut-and-tie models

Year of origin	2004
Concrete	B45
Concrete cover	35 mm
Reinforcement steel	FeB 500
Prestressing steel	FeP 1860

Table 3.5: KW04 Postweg - Material properties

3.2.5 KW16 Purmerend

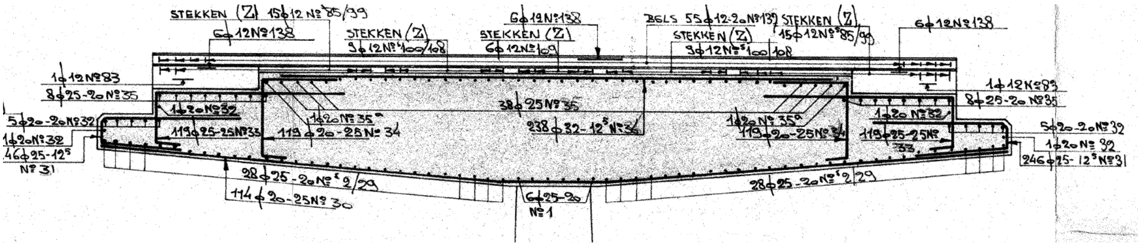

Figure 3.10: KW16 Purmerend - Sideview

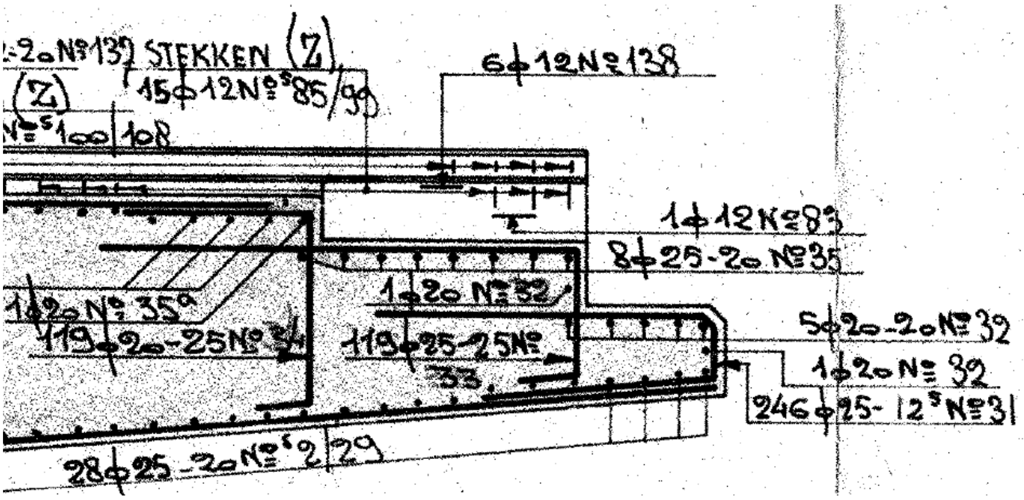

Figure 3.11: KW16 Purmerend - Half joint detail

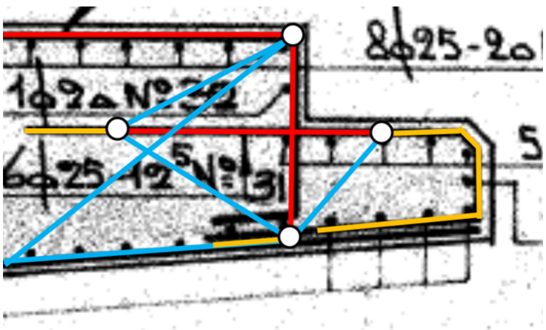

Figure 3.12: KW16 Purmerend - Strut-and-tie model

Year of origin	1973
Concrete	unknown
Concrete cover	30 mm
Reinforcement steel	QR 40
Prestressing steel	-

Table 3.6: KW16 Purmerend - Material properties

3.2.6 Tegelen

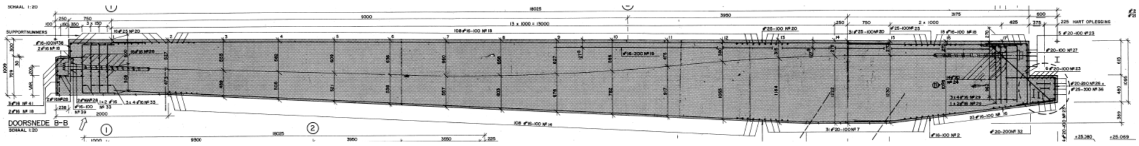

Figure 3.13: Tegelen - Sideview

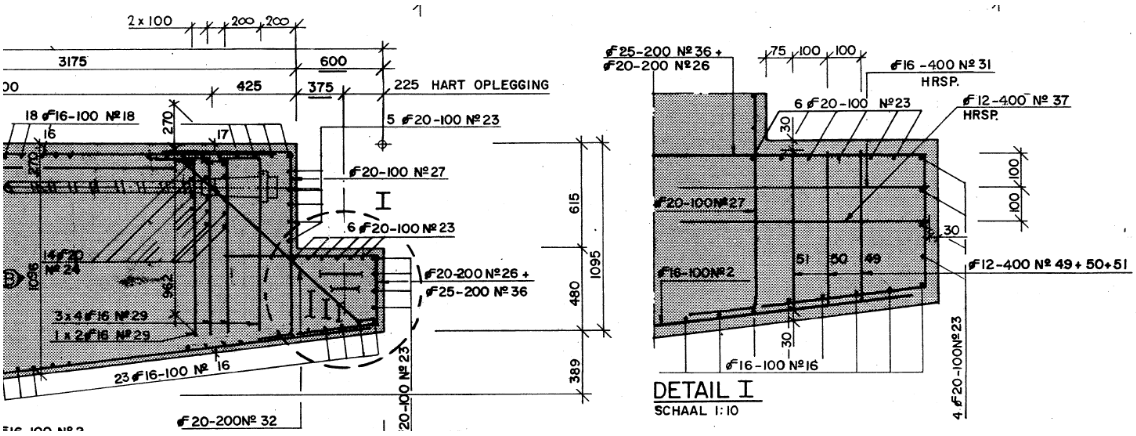

Figure 3.14: Tegelen - Half joint detail

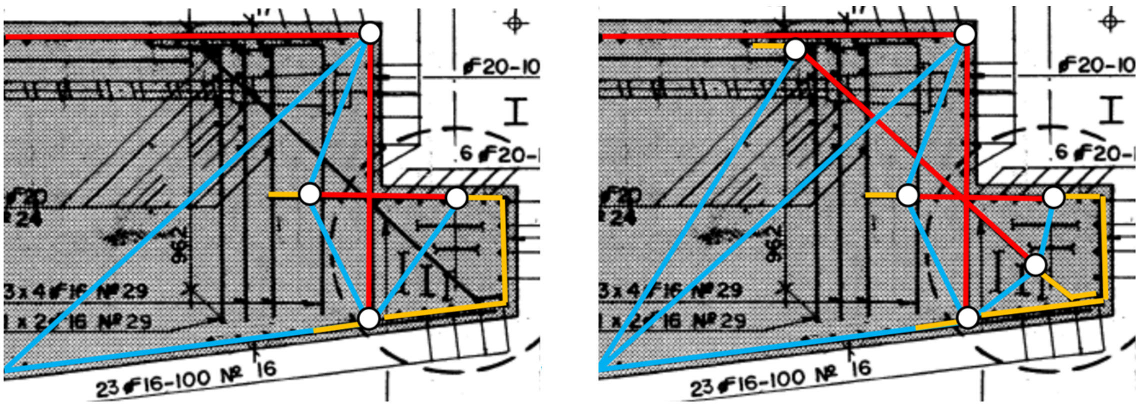

(a) STM1 (b) STM2

Figure 3.15: Tegelen - Strut-and-tie models

Year of origin	1994
Concrete	B45
Concrete cover	30 mm
Reinforcement steel	FeB 500
Prestressing steel	FeP 1860

Table 3.7: Tegelen - Material properties

3.2.7 Knooppunt Terbregseplein

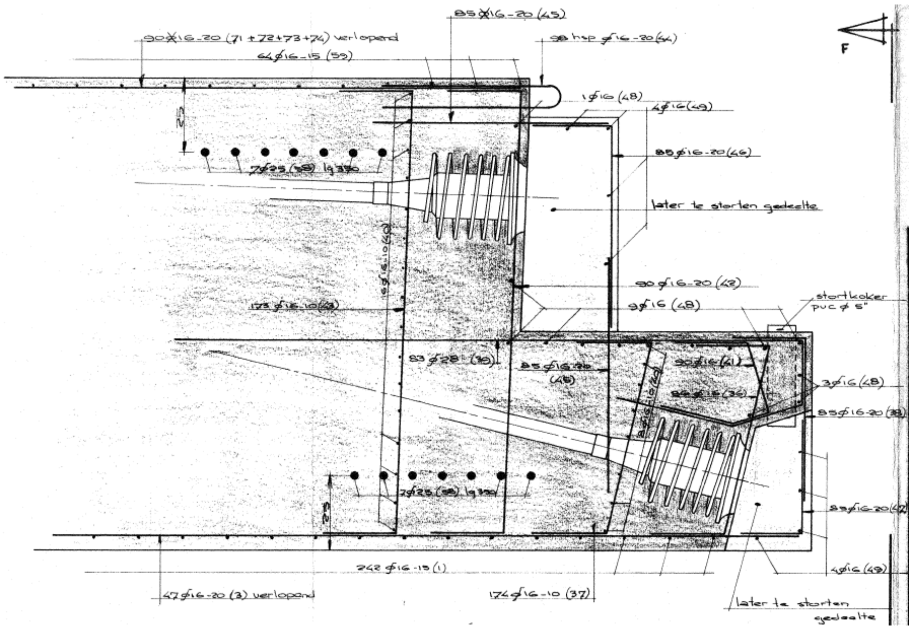

Figure 3.16: Knooppunt Terbregseplein - Half joint detail

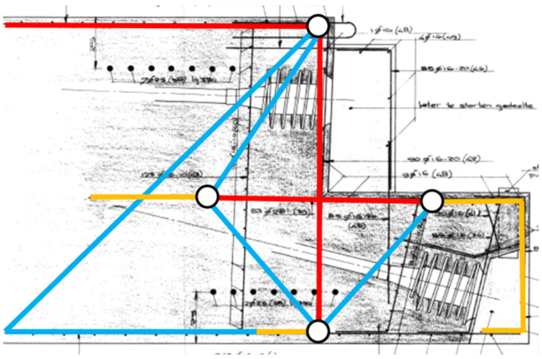

Figure 3.17: Knooppunt Terbregseplein - Strut-and-tie model

Year of origin	1972
Concrete	LC25/28
Concrete cover	unknown
Reinforcement steel	QR 40
Prestressing steel	QP 170

Table 3.8: Knooppunt Terbregseplein - Material properties

3.2.8 KW10 Deventer-Bathmen

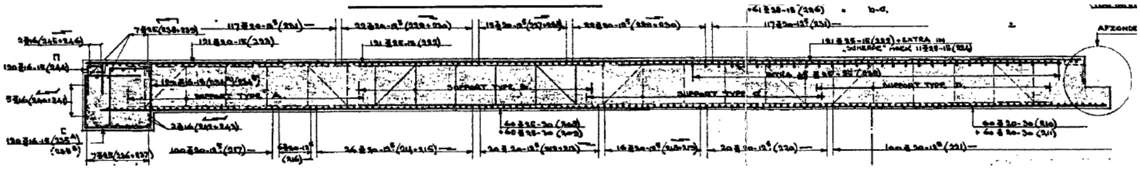

Figure 3.18: KW10 Deventer-Bathmen - Sideview

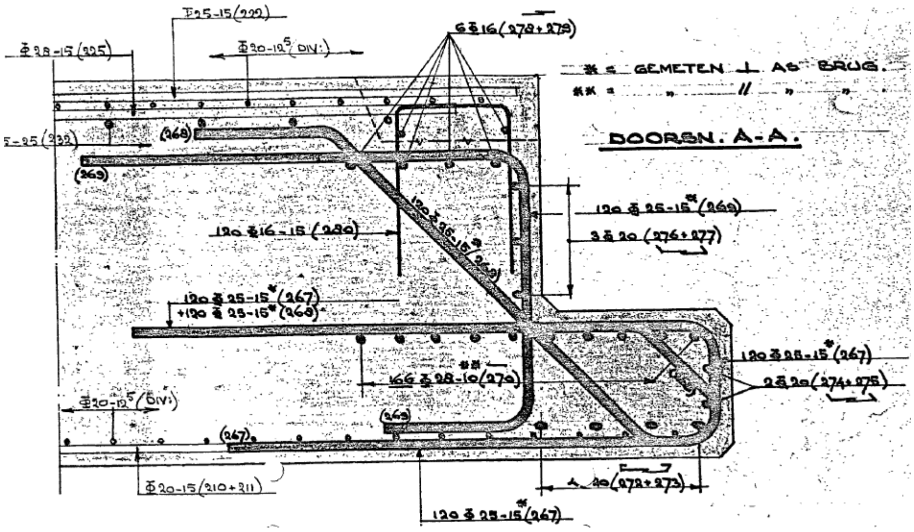

Figure 3.19: KW10 Deventer-Bathmen - Half joint detail

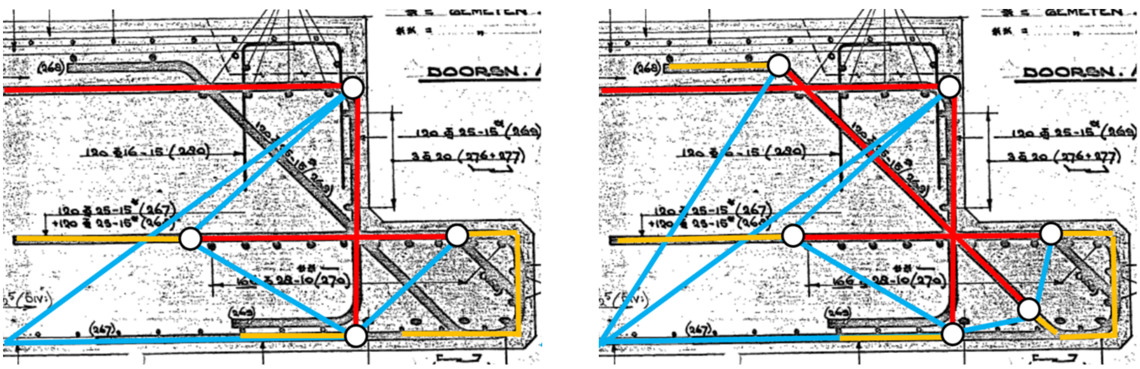

(a) STM1 (b) STM2

Figure 3.20: KW10 Deventer-Bathmen - Strut-and-tie models

Year of origin	1970
Concrete	unknown
Concrete cover	30 mm
Reinforcement steel	QR 40
Prestressing steel	-

Table 3.9: KW10 Deventer-Bathmen - Material properties

3.3 Observations

This paragraph elaborates the observations from the technical drawings, which will be used to identify general issues in paragraph 3.4.

Strut-and-tie models

It has been observed that the investigated series of concrete half-joints can all be analysed using one or two strut-and-tie models. All concrete half-joints contain a general reinforcement layout with a horizontal- and vertical rebar, which can be analysed using STM-1. In the case of the presence of a diagonal rebar, the load bearing capacity can be analysed by the sum of STM-1 and STM-2, which can be respresented by STM-3. This assumption is elaborated in further depth in Chapter 5.4.

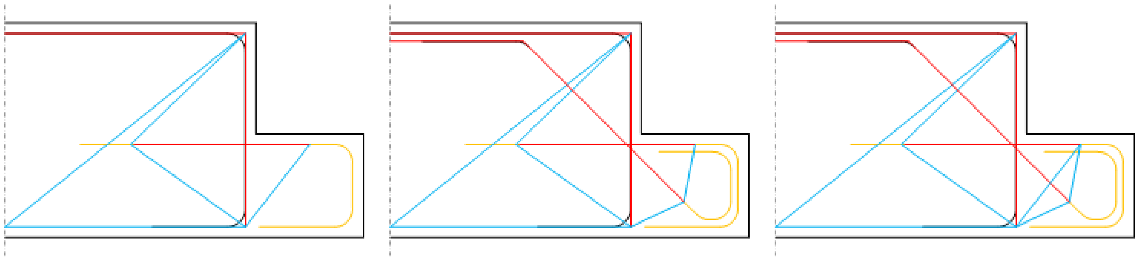

(a) STM-1 (b) STM-2 (c) STM-3

Figure 3.21: Strut-and-tie models based on archive study

If prestressing is present at the top of the concrete half-joint, the horizontal tie in the top can be replaced by this prestressing. If prestressing is present at the nib of the concrete half-joint, the horizontal tie in the nib or diagonal tie can be replaced by this prestressing

No shear reinforcement and hanger-stirrups

It has been observed that the investigated series of concrete half-joints are all designed as a slab, in which no shear reinforcement in the form of stirrups is applied. The shear resistance of the concrete in a concrete slab is typically designed to be sufficient to transfer the shear stresses.

However, these stirrups are also not provided as hanger-stirrups at the concrete half-joints detail, which is the cases elaborated in paragraph 2.5. The hanger-reinforcement of the investigated series of concrete half-joints is only provided with a hanger-rebar and/or diagonal rebar.

Inadequate bending of hanger-rebar

The hanger-rebar is curved into the slab in all investigated concrete half-joints, in which the compressive strut from the bearing plate cannot be transferred properly. As mentioned in paragraph 2.5.1, this can be improved by bending the hanger-rebar the other way [20], [21], [22]. However, this research was published in 2008 and most of the structures with concrete half-joint were build around 1970.

Insufficient anchorage/transfer length of diagonal rebar

A diagonal rebar is placed in some of the concrete half-joints, which limits the crack-width at the re-entrant corner. However, if the diagonal rebar is also placed to transfer loads, the rebar must be provided with sufficient anchorage/transfer length on both sides. At the top of the concrete half-joint, this appears to be a problem in the cases: KW04-Postweg, Tegelen and KW10 Deventer-Bathmen. At the bottom, the anchorage length is often sufficient.

Insufficient anchorage length of horizontal rebar

The anchorage length of the horizontal rebar in some of the concrete half-joints appears to be rather short in the cases: KW 38 Bullewijk, KW04 Postweg and Tegelen. The anchorage length of the horizontal rebar can be determined using a strut-and-tie approach as follows:

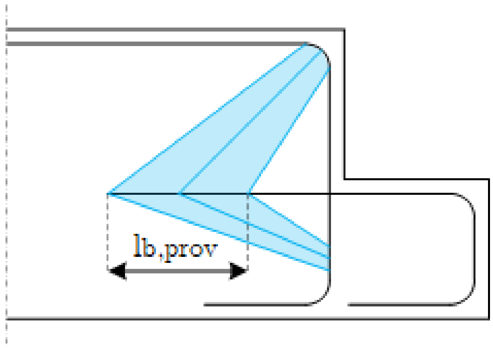

Figure 3.22: Anchorage length of horizontal rebar

Figure 3.22 illustrates how the provided anchorage length can be schematised, with the contributing struts. The angle between the strut and the tie must fulfil the requirements elaborated in paragraph 5.2..

Prestressing

Prestressing is provided in some of the concrete slabs and can be distinguished in local- and global prestressing. Global prestress describes the horizontal prestressing placed in the concrete slab. It can be distinguished into global prestress at the nib and at the top.

Local prestressing describes the vertical- or diagonal prestressing of the concrete half-joint at a local level. An example of local prestressing is given in the experiments of CUR40 [14]. The investigated series of concrete half-joints were not equipped with local prestressing.

Expansion joint

In half of the investigated series of concrete half-joints, a space is left unfilled at the top of the concrete half-joint. This space is needed for expansion joints, which provides the link between the concrete slab and precast concrete beam. The unfilled space leads to a reduction in the height of hanger-reinforcement or an overlap using hairpins.

<u>Rounded- or inclined re-entrant corner</u>

A rounded- or inclined re-entrant corner can be beneficial for the crack initiation. The tensile stresses are able to spread more, which leads to smaller cracks and crack-widths [6] [12]. The inclined re-entrant corner only has been applied in 2 out of 7 investigated concrete half-joints.

<u>Concrete cover</u>

The concrete cover in almost all concrete slabs is equal to 30 [mm], which can indicate on a simplified calculation for concrete cover. As most of the concrete structures were build around 1970, it can be assumed that the GBV 1962 was used as code provision. The concrete cover in accordance with GBV 1962 is determined using Table 3.10:

Table 3.10: Concrete cover in accordance with GBV 1962

Structure	Concrete cover [mm]		
	Inside	Outside	Uncontrollable after pouring
Slabs	10	15	20
Walls	15	20	25
Beams	20	25	30
Columns	25	30	35

- Concrete cover must be increased with 10 [mm], if harmful situations can occur as a result of high temperatures due to fire, seawater or other aggressive fluids
- Concrete cover must be increased with at least 10 [mm], if the cement skin can be damaged due to fabrication after hardening

Nowadays, the concrete cover is determined based on the environment (carbonation, chlorides, freeze-thaw cycles), lifespan, concrete quality, slab-geometry and certain quality control of the concrete structure. Therefore, it can be stated that structures with a simplified calculation for concrete cover can be underestimated and are more prone to corrosion.

3.4 Identified issues from investigated series of concrete half-joints

This chapter elaborates the identified issues, by comparing the completed researches from paragraph 2.5 with the observations from paragraph 3.3.

3.4.1 Deterioration issues

Corrosion of reinforcement at re-entrant corner

The issue with corrosion of the reinforcement at re-entrant corner was already elaborated in the introduction of this thesis research. The investigated series of concrete half-joints confirms the issue even more, as the absence of a rounded- or inclined re-entrant corner has been observed in most of the concrete half-joints.

Corrosion of reinforcement at anchorage zone

Corrosion of reinforcement near the concrete surfaces and edges can lead to a reduction in bond-behaviour as a result of cracking or even spalling from the concrete as a consequence of the increased volume of corrosion product (see paragraph 4.2). The vulnerable regions for bond-failure in a concrete half-joint are indicated in Figure 3.23.

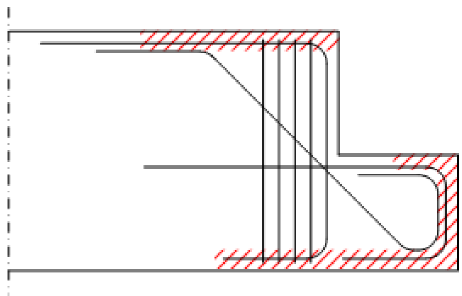

Figure 3.23: Vulnerable regions for bond-failure

The regions partly correspond with the zonal assessment of Desnerck et al. [24] in Figure 2.19. However, it is expected that this issue is less critical than the corrosion of reinforcement at re-entrant corner as a result of cracking. Most concrete structures in the Netherlands are build using blast-furnace-slag cement, which are less prone to deterioration as a result of chloride ingress (see paragraph 4.2). Nevertheless, blast-furnace-slag is more vulnerable to deterioration as a result of carbonation.

3.4.2 Reinforcement layout/detailing issues

Insufficient anchorage length of horizontal and diagonal rebar

The horizontal rebar is critical in the structural behaviour of a concrete half-joint. Sufficient anchorage length must be applied, so the tensile force in the horizontal rebar can develop completely and ductile behaviour can be provided from yielding of the rebar. If the anchorage length is not sufficient, the rebar is not able to develop the tensile strength and the link between rebar and concrete will fail in a brittle way as the bond-strength is reached.

The diagonal rebar limits the crack-width at the re-entrant corner, but it can also transfer load if properly anchored. If anchorage is not properly applied, the contribution to total load transfer is uncertain.

Bending of hanger-rebar

Prof.ir C. Kleinman already indicated that the reinforcement detail, in which the hanger-reinforcement is only equipped with a hanger-rebar can be insufficient, as the concrete compressive strut can not be transferred properly to the hanger-rebar. This reinforcement detail has been found in all of the investigated concrete half-joints. Paragraph 2.5.1 provides a solution to improve the reinforcement layout and how to calculate the load bearing capacity in the absence of hanger-stirrups.

However, there is still some uncertainty about the structural behaviour, if for example the bending radius of the hanger-rebar increases.

3.5 Categorisation of problematic concrete half-joints

Based on the reinforcement layouts of the investigated series of concrete half-joints in paragraph 3.2, the following categorisation is proposed for problematic concrete half-joints in the Netherlands. A standard reinforcement layout can be drawn using a hanger-rebar and horizontal rebar (Category A1). Each concrete half-joint will have at least this reinforcement layout, with or without diagonal rebar or prestressing at the top and/or nib.

The concrete half-joints can be distinguished in the following categories:

Table 3.11: Categorisation of concrete half-joints

	No prestressing	**Global prestressing**		
		At top	At nib	Both
Standard reinforcement layout	Category A1	Category B1-1	Category B1-2	Category B1-3
Standard reinforcement layout with diagonal	Category A2	Category B2-1	Category B2-2	Category B2-3

It needs to be mentioned that this categorisation is based on the investigated series of concrete half-joints and that it is assumed these represent most of the (problematic) concrete half-joints build before 2000 in the Netherlands.

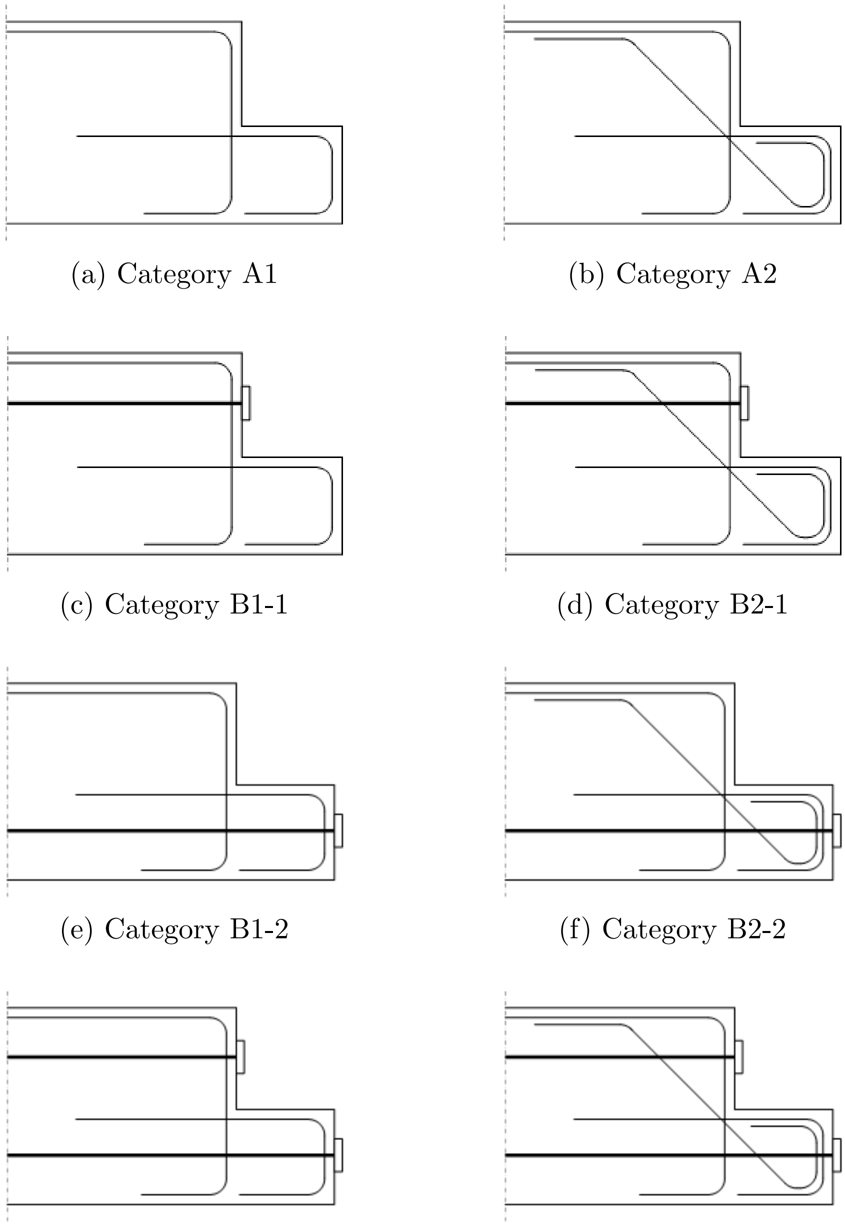

(a) Category A1

(b) Category A2

(c) Category B1-1

(d) Category B2-1

(e) Category B1-2

(f) Category B2-2

(g) Category B1-3

(h) Category B2-3

Figure 3.24: Reinforcement layouts of concrete half-joints based on archive study

Chapter 4

Literature review on corrosion

4.1 Introduction

The reinforcement is embedded in a layer of concrete, which forms a protective layer to prevent corrosion. However, concrete is not an impermeable material and contains small open spaces: voids. If these voids are large, the permeability is large as well and the protective layer can be damaged. The layer can also be damaged as a result of cracking. Both causes, allow water/moisture and oxygen to reach the reinforcement steel, which can lead to corrosion.

4.2 Chemical background on corrosion process

The corrosion process involves an anodic reaction, in which an electron is released from the metal and the metal becomes positively charged:

$$2Fe \rightarrow 2Fe^{2+} + 4e^-$$

The electron is used in the cathodic reaction with water/moisture and oxygen to form hydroxide:

$$4e^- + 2H_2O + O^2 \rightarrow 4OH^-$$

Eventually, the hydroxide reacts with the positively charged iron and forms iron-hydroxide, also known as corrosion:

$$2Fe^{2+} + 4OH^- \rightarrow 2Fe(OH)_2$$

The formation of iron hydroxide leads to an increase in volume, depending on the state of oxidation. The volume increase can be as large as 600% of the original product [26]. Additionally, a thin impermeable protective layer is formed around the reinforcement bar, which prevents iron molecules to participate in the anodic reaction. This layer stops the corrosion process until the layer is damaged, which can happen as a result of carbonation of chloride attack.

Carbonation

The protective layer of reinforcement steel can be damaged if the pH value of the surrounding concrete decreases below 11.5. Usually, the alkaline environment of concrete ensures that the pH value does not decrease to the critical level. However, the pH level in the concrete can be reduced as a result of carbonation.

Carbonation is the process in which carbon dioxide from the atmosphere reacts with alkalis and calcium-hydroxide to carbonates [27]:

$$Ca(OH)_2 + CO_2 \rightarrow CaCo_3 + H_2O$$

$$2NaOH + CO_2 \rightarrow Na_2Co_3 + H_2O$$

$$2KOH + CO_2 \rightarrow K_2Co_3 + H_2O$$

The removal of alkalis and calcium-hydroxide from the pore solution (alkaline solution in hydrated cement) leads to a reduction in pH. If the carbonation depth is bigger than the concrete cover, the protective layer of the reinforcement will be damaged. Subsequently, corrosion of the rebars can occur in the presence of water/moisture and oxygen. However, carbonation also leads to the formation carbonates, which leads to a decrease in overall porosity and the permeability of concrete.

The degree of carbonation depends on: type of cement, cement composition, aggregate size, water/cement ratio, temperature, moisture conditions and concentration levels of carbon dioxide in the atmosphere.

Corrosion resulting from carbonation can be defined as uniform corrosion, which will be elaborated in further depth in paragraph 4.3.1.

Chloride attack

The protective layer of reinforcement can also be damaged if chlorides are present in the surrounding concrete. These chlorides originate from seawater or de-icing agents and can lead to chloride-initiated corrosion. Chlorides penetrate the protective layer and react with iron ions. This results in iron-chloride [27] [28]:

$$Fe^{2+} + 2CL^{-} \rightarrow FeCL_2$$

Subsequently, iron-chloride reacts with water/moisture and forms corrosion [27] [28]:

$$FeCL_2 + 2H_2O \rightarrow 2Fe(OH)_2 + 2HCL$$

The formation of hydrochloric acid drops the pH value as well and therefore accelerates the corrosion process [27]. Additionally, the chloride ions can be regenerated and can be used in new reactions [28]. Cracks in concrete accelerate the chloride ingress. The ingress depends on the crack-width, large cracks will lead to a higher chloride ingress [27].

Corrosion resulting from chloride attack can be defined as local or pitting corrosion, which will be elaborated in further depth in paragraph 4.3.1.

4.3 Influence of corrosion on reinforcement

Corrosion influences the structural properties of reinforcement. The influence can be distinguished into reduction in effective cross-sectional area, ductility and yield-/ultimate strength of the rebar.

4.3.1 Influence on cross-sectional area

The corrosion process leads to an increase of the total cross-sectional area. However, this is the result of the formation of iron-hydroxide (corrosion). The effective cross-sectional area of the rebar is reduced, as iron from the rebar is used for the corrosion process. The remaining cross-sectional area of the rebar is called the residual cross-sectional area.

Corrosion of the rebar can be distinguished in uniform- and local-/pitting corrosion. The differences are illustrated in Figure 4.1:

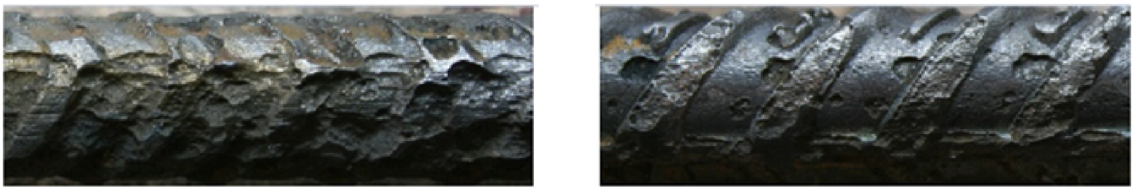

(a) Uniform　　(b) Local-/pitting

Figure 4.1: Corrosion of rebar [29]

Uniform corrosion occurs in the presence of carbonation and leads to a uniform reduction in cross-sectional area of the rebar. This reduction can occur symmetrical or asymmetrical. Asymmetrical reduction occurs if the deterioration process is driven from one side, which is schematically illustrated in Figure 4.2:

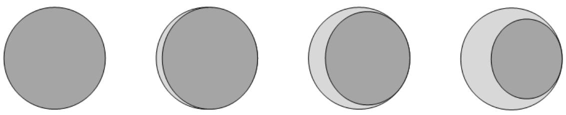

Figure 4.2: Asymmetrical reduction in cross-sectional area of rebar

Local-/pitting corrosion occurs in the presence of chlorides and leads to a notch in the rebar, which can propagate inwards the rebar. The corrosion process is schematically presented in Figure 4.3:

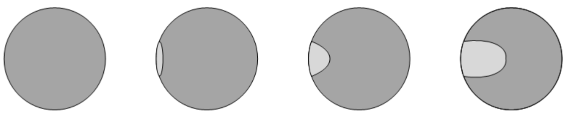

Figure 4.3: Local reduction in cross-sectional area of rebar

The corrosion rate is defined as the average loss of mass of the rebar due to corrosion and can thereby directly be related to the cross-sectional area. As the residual cross-sectional area is not harmed by corrosion [30], the area can be determined as:

$$A_{s,corr} = A_{s,0}(1 - 0.01 \cdot Q_{corr}) \tag{4.1}$$

In which:

$A_{s,corr}$	is the residual cross-sectional area of corroded rebar
$A_{s,0}$	is the original cross-sectional area of rebar
Q_{corr}	is the average corrosion rate [%]

4.3.2 Influence on mechanical properties

Much research has been done on the mechanical properties of corroded reinforcement using mechanically indented bars [31], [7], [32] artificially corroded bars [33], [30], [34], [35], [36] or naturally corroded bars [31], [35], [37]. The properties can be determined by testing the tensile behaviour of a corroded rebar. Unfortunately, the cross-sectional area of a corroded rebar is not uniform over the whole length and has local reductions. Therefore, the reference cross-sectional area plays a key role in determining the stress-strain behaviour [7].

Imperatore [7] researched the influence of the reference cross-sectional area on the stress-strain relationship of the corroded rebar. If the nominal cross-sectional area is considered, the corrosion leads to a large reduction in yield strength, see Figure 4.4(a). However, if the minimum cross-sectional area is considered, the mechanical properties appears to be improved for a corroded rebar, see Figure 4.4(b). If the average cross-sectional area in the gauge length is considered, the results appears to be more reasonable , see Figure 4.4(c).

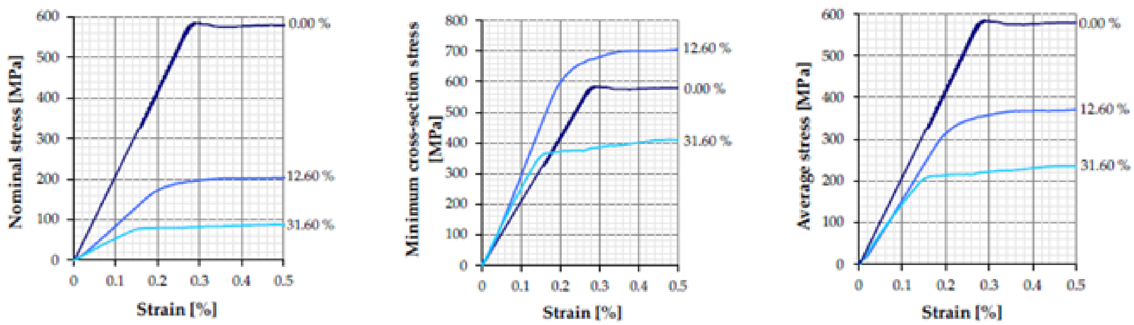

(a) Nominal (b) Minimal (c) Average

Figure 4.4: Stress-strain relationship of corroded rebar [7]

The influence of corrosion on the mechanical properties of the rebar are related to the corrosion rate and differs for uniform- and local-/pitting corrosion. Imperatore [7] performed a literature study, in which many experimental results were collected and compared. The reduction of yield-/ultimate strength and ultimate strain of a corroded rebar can be related to the corrosion rate as follows:

Yield-/ultimate strength:

$$f_{y,corr} = f_{y,0}(1 - \alpha_y \cdot Q_{corr}) \tag{4.2}$$

$$f_{u,corr} = f_{u,0}(1 - \alpha_u \cdot Q_{corr}) \tag{4.3}$$

Ultimate strain*:

$$\varepsilon_{u,corr} = \varepsilon_{u,0}(1 - \alpha_{\varepsilon,lin} \cdot Q_{corr}) \tag{4.4}$$

$$\varepsilon_{u,corr} = \varepsilon_{u,0} \cdot \exp(-\alpha_{\varepsilon,exp} \cdot Q_{corr}) \tag{4.5}$$

In which:

$f_{y,corr}$	is the yield strength of corroded rebar
$f_{y,0}$	is the original yield strength of rebar
$f_{u,corr}$	is the ultimate strength of corroded rebar
$f_{u,0}$	is the original ultimate strength of rebar
$\varepsilon_{u,0}$	is the original ultimate strain of rebar
α	is an empirical coefficient
Q_{corr}	is the corrosion rate [%]

* a linear relation and exponential relation have been found in literature.

The empirical coefficients for local-/pitting corrosion based different research have been determined as [7]:

Table 4.1: Empirical coefficients for local-/pitting corrosion [7]

Specimen	Author	Q_{corr}	α_y	α_u	$\alpha_{\varepsilon,lin}$	$\alpha_{\varepsilon,eps}$
Mechanically indented bars	Cairns et al. [32]	0-3	0.012	0.011	0.03	-
	Finozzi et al. [38]	0-57	0.129	0.0182	-	0.041
Artificially corroded bars	Du et al. [33], [30]	0-16	0.015	0.015	0.044	-
	Lee and Cho [34]	0-35	0.0198	0.0157	0.0259	-
	Ou et al. [35]	0-31	0.0127	0.0116	0.0281	-
	Imperatore et al. [36]	0-53	0.0120	0.0186	-	0.0547
Naturally corroded bars	Ou et al. [35]	0-82	0.0123	0.0115	0.0125	-
	Vanama and Ramakrishnan [37]	0-80	0.0122	0.0119	-	0.0292

The scatter in empirical coefficients (especially for ultimate strain) for mechanical properties of corroded rebars can be related to the following aspects:

- The corrosion of the rebar is simulated in different ways (mechanically indented bars, artificially bars and naturally corroded bars)

- Imperatore [7] states that reinforcement steel composition can influence the structural behaviour of corroded rebars
- Zhu and François [31] researched this, by performing experiments using naturally corroded rebars and mechanically indented bars, simulating: uniform corrosion, asymmetrical pitting corrosion and symmetrical pitting corrosion. They concluded that symmetrical distribution of corrosion resulted in better ductile behaviour than asymmetrical corrosion
- The reference cross-sectional area of the rebar, from which the stress-strain relationship are determined, have influence on the mechanical results, see Figure 4.4.

The empirical relations for yield-/ultimate strength and ultimate strain for corroded rebars are plotted over the domain over which the corrosion study is performed in Figure 4.5 and Figure 4.6

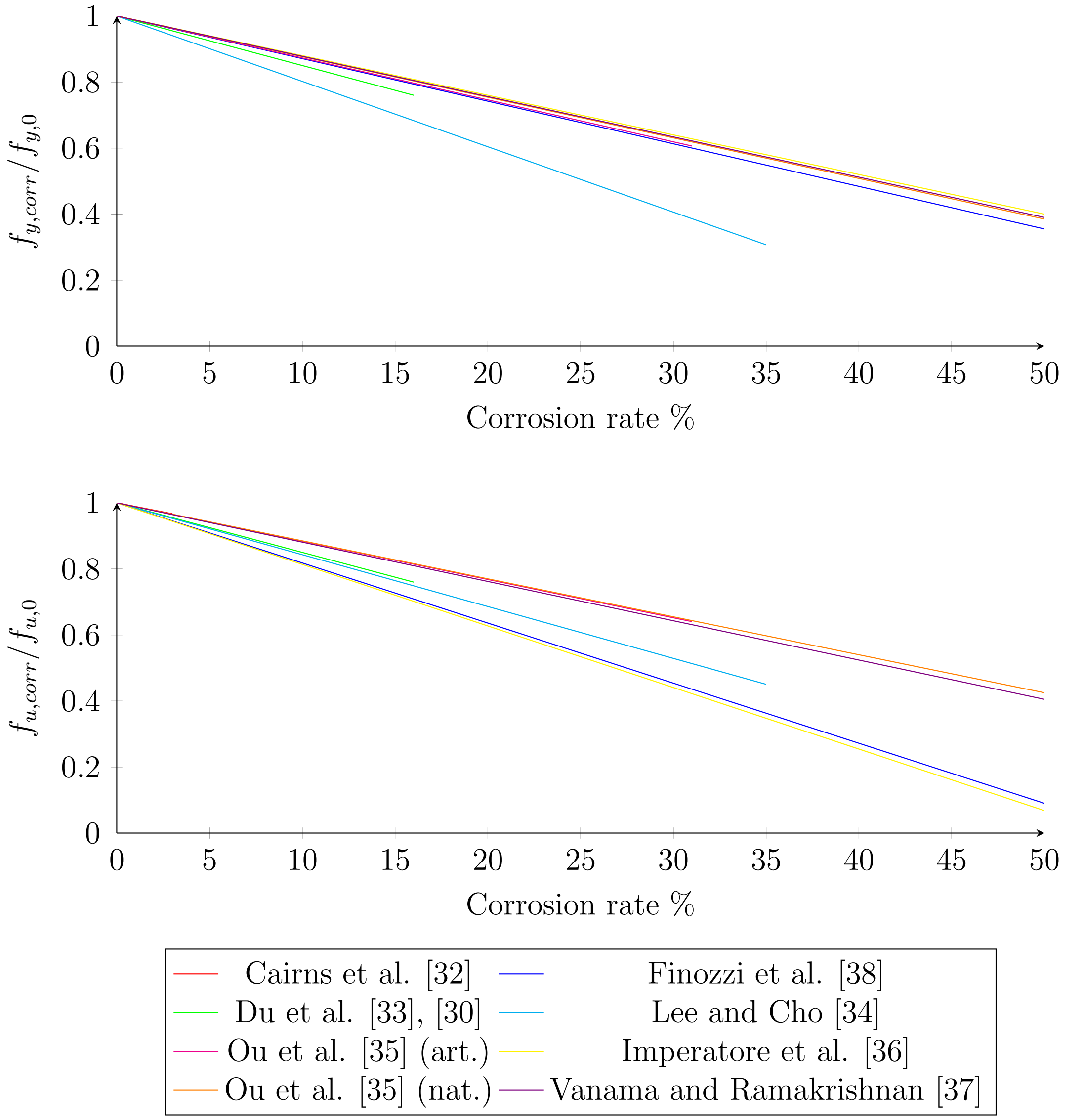

Figure 4.5: Empirical relations for yield- and ultimate strength of corroded rebars [7]

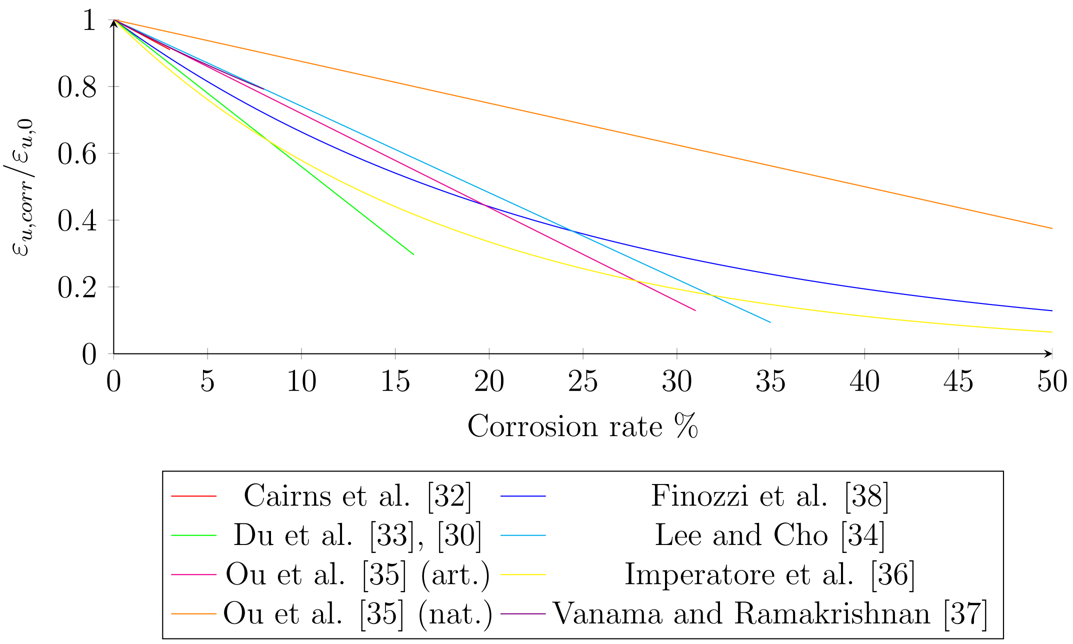

Figure 4.6: Empirical relations for ultimate strain of corroded rebars [7]

The graph of the empirical relations show a larger scatter when it comes to the ultimate strain of corroded rebars than for the yield- and ultimate strength. Possible causes have already been discussed before.

4.4 Influence of corrosion on bond-behaviour

The influence of corrosion on the bond-behaviour can be distinguished in the influence on bond-strength and bond-slip. A semi-empirical formulation for the bond-strength is given for the prediction of anchorage length and a local bond-slip model is given, which can be used in coherence with *fib* Model Code 2010.

The bond-behaviour between concrete and a rebar depends on various parameters as indicated in Appendix 5.2.8. In case of corrosion, the bond-behaviour is influenced even more by the weakening of concrete confinement as a result of concrete cover cracking and stirrup corrosion, the presence of corrosion products at the structural interface and reduction of bond index in ribbed bars as a result of cross-sectional reduction [39] [40].

4.4.1 Influence on bond-strength

The bond-strength between rebars and concrete with corrosion cannot be described with a generalised bond strength equation. Therefore, Prieto et al. [39] proposed a semi-empirical model for assessing bond strength, which is generally applicable for non-corroded and corroded reinforcement.

The model is obtained by applying a linear regression model on 650 bond experiments from various authors. The bond-strength for ribbed bars can be determined as [39]:

$$f_{bd} = f_{cm}^{2/3}\left(m\left(\frac{1}{\text{Ø}^2}+1\right)^{9.052}\left(\left(\frac{\text{Ø}}{l_b}\right)^2+1\right)^{8.13} e^{-0.129\frac{f_{cm}}{40}}\left(\left(\frac{a}{\text{Ø}}\right)^4+1\right)^{0.058}\right.$$
$$\left.\left(K_{tr}^2+K_{tr}+1\right)^{0.498}\left(Q_{corr}+1\right)^{-0.016}-1\right) \quad (4.6)$$

In which:

f_{cm}	is the mean compressive strength
m	is a variable that takes into account the bond conditions, confinement and corrosion of reinforcement
Ø	is the rebar diameter
l_b	is the anchorage length of rebar
a	is the tensile ring radius
K_{tr}	describes the confinement as a result of transverse reinforcement
Q_{corr}	is the corrosion rate

It can be observed that the proposed bond-strength model depends on many variables and coefficients. Therefore, Prieto et al. [39] also describes a simplified equation based on the *fib* Model Code 2010:

$$f_{bd} = f_{cm}^{2/3}\left(\eta_1\eta_2\eta_3\eta_4\eta_5\eta_6 - 1\right) \quad (4.7)$$

In which:

f_{cm}	is the mean compressive strength
η	is a coefficient which can be determined using Table 4.2

The coefficients are obtained from the mean values of the database of 650 bond experiments researched by Prieto et al. [39].

It needs to be mentioned that the η values and approach on bond-strength by Prieto et al. differs from Eurocode 2. Eurocode 2 provides the bond-strength depending on the bond condition, bar diameter and design value of tensile strength of concrete. The influence of transverse reinforcement, concrete cover is taken into account in the calculation of anchorage length. The calculation is elaborated in paragraph 5.4.4.

Table 4.2: Values for η's for Eq. 4.7

η	Parameter	Values	
η_1	Rate of corrosion	Non-corroded bars: Corroded bars $< 5\%$ Corroded bars $> 5\%$	$\eta_1 = 1.24$ $\eta_1 = 1.16$ $\eta_1 = 1.12$
η_2	Bond condition	Good bond condition Otherwise	$\eta_2 = 1.03$ $\eta_2 = 1.00$
η_3	Bar diameter	$Ø \leq 10[mm]$ $10 \leq Ø \leq 20[mm]$ $Ø \geq 20[mm]$	$\eta_3 = 1.10$ $\eta_3 = 1.04$ $\eta_3 = 1.02$
η_4	Transverse reinforcement confinement	No confinement Confinement with $K_{tr} \leq 0.05$ Confinement with $K_{tr} > 0.05$	$\eta_4 = 1.00$ $\eta_4 = 1.04$ $\eta_4 = 1.06$
η_5	Concrete cover	$a/Ø \leq 1.5$ $1.5 < a/Ø \leq 3.5$ $a/Ø > 3.5$	$\eta_5 = 0.97$ $\eta_5 = 1.06$ $\eta_5 = 1.26$
η_6	Anchorage length	$l_b/Ø \leq 10$ $l_b/Ø > 10$	$\eta_6 = 1.50$ $\eta_6 = 1.04$

4.4.2 Influence on bond-slip

Lundgren et al. [40] used a large number of studies to organise the influencing parameters and proposed an engineering model to take into account the influence of corrosion. The model is based on the local bond-slip model from the fib Model Code 2010.

The engineering model is referred to as "ARC model" and can be used in nonlinear numerical analyses. The model has been calibrated on approximately 500 pull-out and beam tests, in which most of the rebars were artificially corroded and thus mainly included uniform corrosion [40]. The corrosion is incorporated into the bond-slip model by using the observation that the bond-slip curve of fib Model Code 2010 can be shifted towards the slip direction. This observation is illustrated in Figure 4.7:

The effective slip can now be written as:

$$s_{eff} = s + s_{eq} \tag{4.8}$$

In which:

s is the mechanical slip

s_{eq} is the equivalent slip to account for the effect of corrosion

The equivalent slip can be approximated by [41]:

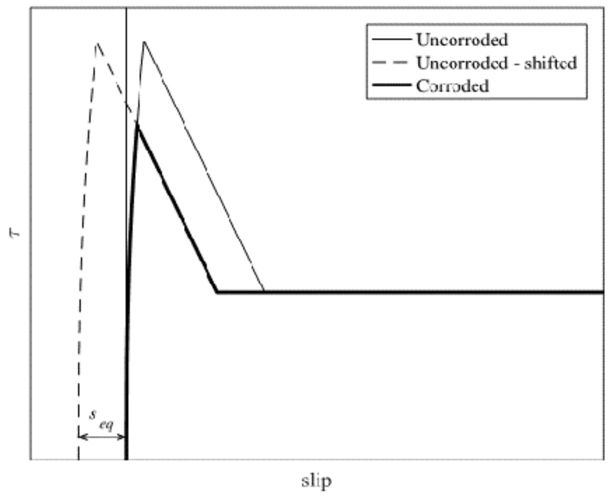

Figure 4.7: "ARC model" [40]

$$s_{eq,nostir} = 2.9Q_{corr} \tag{4.9}$$

$$s_{eq,stir} = 13.6Q_{corr} \tag{4.10}$$

The model is calibrated on cases in which the corrosion ratio was between 0% - 15% for the case without stirrups and between 0% - 20% for the case with stirrups [41].

The model can be used for corrosion cases with uniform corrosion and splitting bond-failure. For the corrosion cases with pull-out bond-failure, the bond capacity can increase as a result of the increase of total cross-sectional area until the concrete cover cracks [40]. However, the research does not state any information on the bond-behaviour in the case of local-/pitting corrosion.

4.5 Corrosion input for analysis

The analytical- and numerical analyses use the corrosion rate of the rebar at the re-entrant corner to model corrosion. It is assumed that the corrosion rate is known and can be used as input in the analysis. This is a hypothetical assumption and follow-up research needs to be done, on how this can be implemented.

The corrosion of reinforcement at the re-entrant corner can be distinguished as local-/pitting corrosion [23], as it is very localised and induced by (chloride rich) surface water. The influences on the mechanical properties of the reinforcement and bond-behaviour between the reinforcement and concrete for local-/pitting corrosion are elaborated below.

4.5.1 Cross-sectional area

The reduction of cross-sectional area of corroded rebars is directly related to the corrosion rate as discussed in paragraph 4.3.1 as:

$$A_{s,corr} = A_{s,0}(1 - 0.01 \cdot Q_{corr}) \tag{4.11}$$

4.5.2 Mechanical properties

The mechanical properties for corroded rebars are introduced in paragraph 4.3.2. Different methods were used to simulate the corrosion (mechanically indented, artificially corroded and naturally corroded rebar), which also led to different results. Ou et al. [35] studied the influence by using naturally corroded rebars and comes closest to the case with the corrosion at the re-entrant corner of concrete half-joints. The results of study are elaborated below.

Corroded rebars from a residential building exposed to natural chloride attack were experimentally tested on their tensile behaviour. The building was located near the coastline of northern Taiwan and constructed in the 1970s. The investigated series of corroded rebars had an initial diameter between 13 [mm] and 19 [mm], and showed a corrosion rate between 6% and 82% [35].

The corrosion rate of the rebars was quantified by the ratio between average mass loss of the corroded rebar and initial mass of the uncorroded rebar, which is commonly used in literature [35].

The stress-strain relationships of the corroded rebars were obtained by a tensile test, in which the strain of the tested rebar was determined by dividing the increase in gauge length by the initial gauge length. The gauge length of the tested rebars was set to be approximately eight times the nominal diameter of the uncorroded rebar. The tensile stress in the tested rebar was determined using the nominal cross-sectional area of the uncorroded rebar. This method was used in most of the previous studies and the authors wanted to compare the results with these studies [35]. Therefore, the reduction in yield- and ultimate strength is overestimated as elaborated in Figure 4.4. The mechanical properties of the corroded rebars have been normalised to their corresponding uncorroded properties. This makes it able to compare the results between rebars with different corrosion rates.

Ou et al. [35] found the following empirical relations for mechanical properties of corroded rebars:

$$f_{y,corr} = f_{y,0}(1 - 0.0123 \cdot Q_{corr}) \tag{4.12}$$

$$f_{u,corr} = f_{u,0}(1 - 0.0130 \cdot Q_{corr}) \tag{4.13}$$

$$\varepsilon_{u,corr} = \varepsilon_{u,0}(1 - 0.0125 \cdot Q_{corr}) \tag{4.14}$$

4.5.3 Bond-behaviour

The influence of corrosion on the bond-behaviour at the re-entrant corner is very localised and will have a small impact on the total load bearing capacity. Additionally, the rebars are not anchored in this region. Therefore, the influence of corrosion on bond-behaviour will be neglected in this thesis research. However, the reduction of bond-behaviour can be of importance if the influence of corrosion of reinforcement at anchorage zones is studied (which is not in the scope of this thesis research), as discussed in paragraph 3.4.1 and Figure 3.23.

Chapter 5

Analytical assessments using parametric tool

5.1 Introduction

The load bearing capacity of concrete half-joints is analysed analytically using a strut-and-tie approach and kinematic approach, which provide a lower-bound approximation and upper-bound approximation. An analytical parametric tool is designed, in which the geometry and material properties of concrete and reinforcement are used as input parameter. The results are optimised by determining the lowest upper-bound approximation and highest lower-bound approximation.

The analytical tool can be used for the following half-joint categories:

A1: standard reinforcement layout

A2: standard reinforcement layout with diagonal rebar

B1-1: standard reinforcement layout with prestressing at top

B2-1: standard reinforcement layout with diagonal rebar and prestressing at top

The analytical tool was initially designed for Category A1 and A2 only. However, the application of prestressing at the top was easy to implement and therefore Category B1-1 and B2-1 can also be calculated in the analytical tool. Prestressing in the nib is more difficult as a new strut-and-tie model arises. However, the strut-and-tie model is similar to the models used for a Category A2 half-joint.

This chapter elaborates the design principles and background of the analytical tool in accordance with Eurocode 2 and RBK1.2. Firstly, the strut-and-tie modelling approach is introduced. Followed by the elaboration of the input of geometry and material properties for the analytical tool. Next, the strut-and-tie approach and kinematic approach are elaborated as used in the analytical analysis. At last, the implementation of corrosion and results of the load bearing capacity of the concrete half-joints from the archive study are discussed. An extended manual for the analytical tool can be found in Appendix B

5.2 Introduction to strut-and-tie modelling

Schlaich, Schäfer and Jennewein [42] proposed a general design model to determine the load bearing capacity of reinforced concrete structures in a consistent way. The method is based on the truss analogy of Ritter and Mörsch [43], [44] and various other authors and can be applied on geometrical discontinuous situations as: supports (point loads), corbels and recesses. These regions used to be designed with rules of thumb and experience, but can also be designed using a strut-and-tie model [42]. This leads to a more consistent design of reinforced concrete structures. This chapter provides an introduction of the strut-and-tie model and a brief overview of how this method is applied in code provisions.

5.2.1 Plasticity theory

Strut-and-tie models are based on lower-bound plasticity theory [42], which implies that any model is safe provided [42] [45]:

- Force equilibrium is satisfied
- The structure has sufficient deformation capacity, so forces in struts and ties can develop
- Struts and ties are proportioned to resist the design forces

A general formulation of the lower-bound plasticity theory is given by Vrouwenvelder as [45]:

"Each arbitrary moment distribution, that is in equilibrium with the external load and for which nowhere the yield condition is violated, delivers a lower bound for the limit load"

The advantage of a lower-bound model is that it always provides a solution on the safe side. However, the solution can be uneconomical as a result of applying to much reinforcement. Nevertheless, this method is commonly used in practice due to its application without using expensive and time consuming finite element programs.

5.2.2 B-& D regions

The stress flow in the middle of a beam is almost continuous and compressive struts occur parallel to each other. This region is called 'B´ region, because it fulfils the classical beam theory, in which plane sections remain plane (Bernoulli).

If the stress flow is not continuous and the strain distribution is nonlinear, the classical beam theory cannot be applied. This region is called a 'D´ region (discontinuity or disturbed), see Figure 5.1:

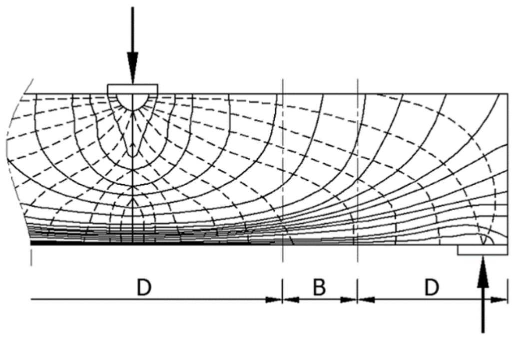

Figure 5.1: B-& D region of a beam [46]

This principle can also be applied on more complicated structures, see Figure 5.2:

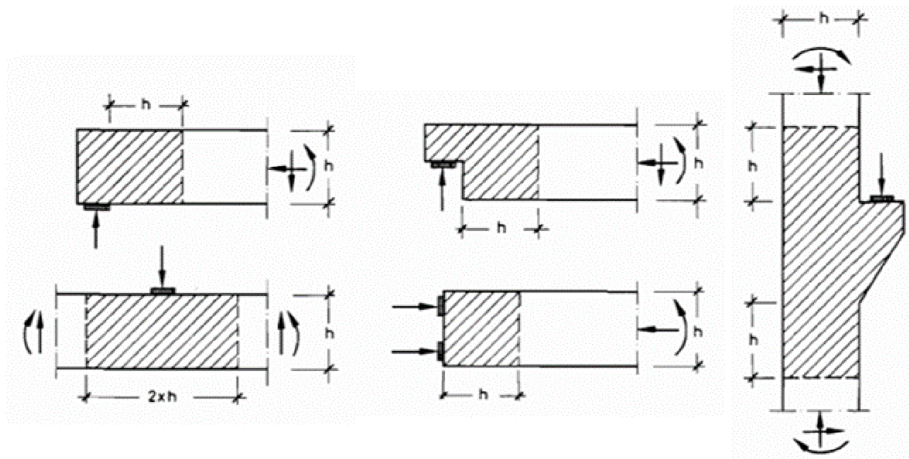

Figure 5.2: B-& D region of structures [46]

The disturbed region must provide compatibility with the continuous region along their boundary to transfer the compressive and tensile stresses. The length of the disturbed region can be determined using Saint-Vénants principle, which states that the disturbed region can be approximated as the width or height of the beam over which the forces are distributed [47].

5.2.3 Model

The orientation of the struts and ties can be based on the principal stress trajectories and elastic stresses of the uncracked concrete structure. The direction of the compressive struts corresponds with the mean direction of principal compressive stresses. The struts and ties can also be located and designed using the centre of gravity of the stress diagram [42], see Figure 5.3:

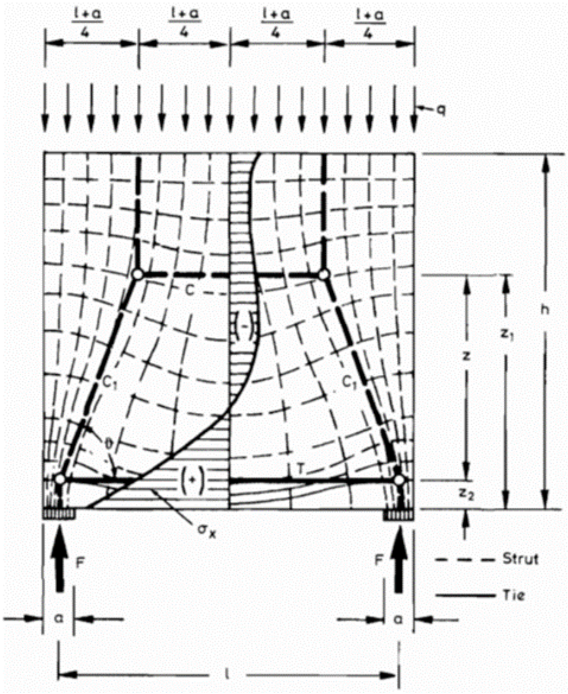

Figure 5.3: Stress trajectories in D-region [46]

If the elastic stresses have not been evaluated (yet), load paths can also be used to determine the orientation of struts and ties. Load paths can be drawn using the compatibility between the continuous region and the disturbed region. The elastic stress along the boundary can be determined using the classical beam theory, which will be used to determine resulting forces in the centre of gravity of the stress diagram. This is illustrated in Figure 5.4:

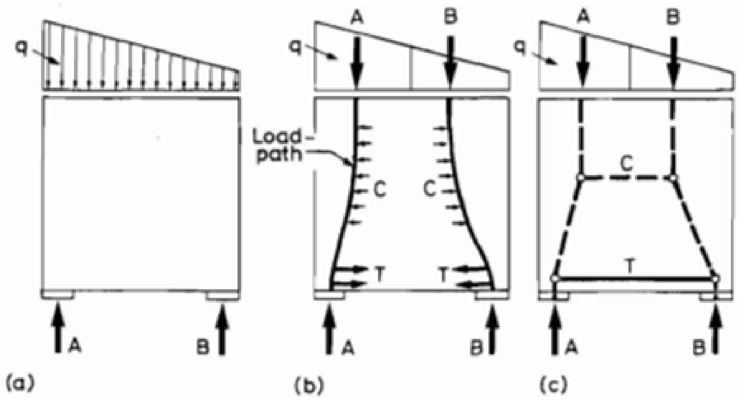

Figure 5.4: Load paths and strut-and-tie model [46]

However, it is possible that multiple load paths can be drawn for the same situation and thereby also multiple strut-and-tie models. This is illustrated in Figure 5.5, in which both models fulfil the requirements, but have different strut-and-tie models.

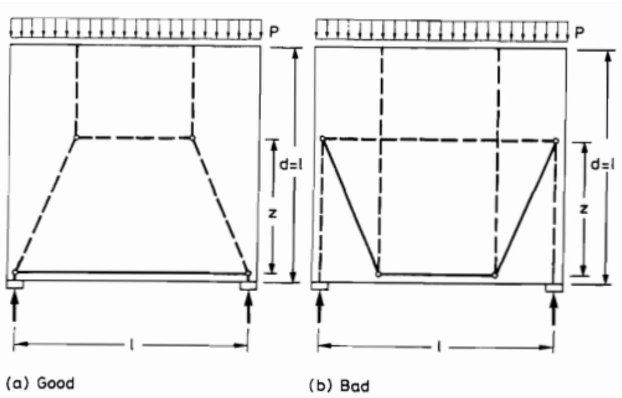

Figure 5.5: Load paths of two different strut-and-tie models for the same case [46]

Model (a) has one large tie (rebar) at the bottom and Model (b) consists of one tie at the bottom and two inclined ties. From a practical point of view, Model (a) is preferred over Model (b). However, the question arises which model is correct from an engineering point of view. Loads try to use the load path with the least forces and deformations. Therefore, we can optimise the model using strain energy as follows [42]:

$$E = F \cdot u \tag{5.1}$$

In which:

F is the force in the strut or tie

u is the deformation of the strut or tie

The most favourable option for the strut-and-tie model from an engineering point of view can therefore be found by finding the model with the least strain energy. Since ties (reinforcement) will deform significantly more than struts (concrete), the model with the least and shortest ties is the best option [42].

5.2.4 Deformation capacity

The strut-and-tie model must have sufficient deformation capacity in order to develop all forces up to maximum capacity of the struts and ties. Sufficient deformation capacity can be provided by the ductile behaviour of the reinforcement, in combination with proper anchoring. The structure must be designed in such a way that the reinforcement yields before the concrete starts to crush. The same holds for assessment.

However, the reinforcement must be able to transfer a force equal to the yield capacity of the rebar to the surrounding concrete. This can be an issue, if the angle between the struts and ties is rather small, in combination with the different stress-strain behaviour of the concrete and reinforcement. Concrete is a much more brittle material than reinforcement steel.

Eurocode 2 does not state any requirements for the angle between a strut and a tie in a strut-and-tie model and only states a requirement for members requiring design shear reinforcement ($1.0 \leq \cot\theta \leq 2.5$). Literature usually limits the value in a strut-and-tie model between approximately $25° \leq \theta \leq 65°$.

5.2.5 Struts

In a strut-and-tie model, concrete struts are designed as two- or three-dimensional compressive stress fields between two nodes. Struts can occur in different forms, which are illustrated in Figure 5.6:

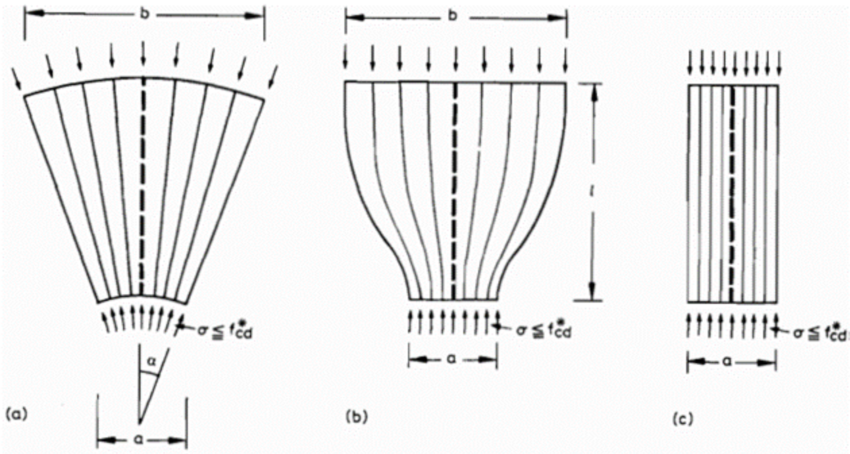

Figure 5.6: Different compressive stress fields [46]

a) Fan: The compressive stress field spreads radially and the compressive stress trajectories are approximately straight. Therefore, the transverse tensile stresses are negligible small
b) Bottle: The compressive stress field spread and narrow between the nodes. The stress trajectories follow the same bottle shape and therefore transverse tensile stresses occur
c) Prism: The prism is a simplified stress field in which the compressive stress field is parallel and therefore constant. This simplification is often used in a one-dimensional stress field

Eurocode 2 only considers the compressive strength based on whether or not tensile stresses in the transverse direction are present. The corresponding equations for the compressive strength of the nodes are as follows:

- If tensile stresses do not occur in transverse direction (NEN-EN 1992-1-1 art. 6.5.2(1)):
$$\sigma_{Rd,max} = f_{cd} \tag{5.2}$$
- If tensile stresses do occur in transverse direction (NEN-EN 1992-1-1 art. 6.5.2(2)):
$$\sigma_{Rd,max} = 0.6\nu' f_{cd} \tag{5.3}$$

In which:

f_{cd} is the design value of concrete compressive strength

$\nu^{'}$ is a value which takes into account transverse tension and can be determined as: $\nu^{'} = 1 - f_{ck}/250$

5.2.6 Ties

In a strut-and-tie model, the concrete is assumed to have no tensile strength and therefore all tensile forces need to be transferred through the reinforcement (or prestressing), which are designed as ties. The capacity of a tie is equal to the yield strength of the reinforcement steel (or tensile strength of prestressing steel) multiplied by the cross-sectional area of the rebar(s) (or prestressing). The tensile force in the tie needs to be transferred to the concrete by applying proper anchorage.

5.2.7 Nodes

The area of concrete in which the struts and ties are connected are called nodes. These nodes provide force equilibrium as compressive stresses and tensile forces come together. Schlaich, Schäfer and Jennewein describe four different nodes [42], CCC, CCT, CTT and TTT, in which C is 'compression´ and T is 'tension´. The latter node is not applied in practice and is therefore not considered in the Eurocode and this thesis.

It is possible to have more than three struts and/or ties connected in one node. However, these nodes can be split in two or more (sub)nodes in order to be designed using the nodes described in this paragraph.

The compressive strength capacity of each node depends on its stress state. Eurocode 2 provides the following equations (NEN-EN 1992-1-1 art. 6.5.4 incl. NB):

$$\sigma_{Rd,max} = k_i v' f_{cd} \tag{5.4}$$

In which:

$k_1 = 1.0$ for CCC node

$k_2 = 0.85$ for CCT node

$k_3 = 0.75$ for CTT node

The modelling and structural behaviour of each node type is considered below:

CCC node

A CCC node connects three compressive struts. The node often occurs at the inside of a concrete structure or at a bearing plate. The stress state is advantageous for the compressive strength as a two-dimensional compressive stress state occurs. A CCC node can occur in a hydrostatic- and non-hydrostatic stress state, see Figure 5.7.

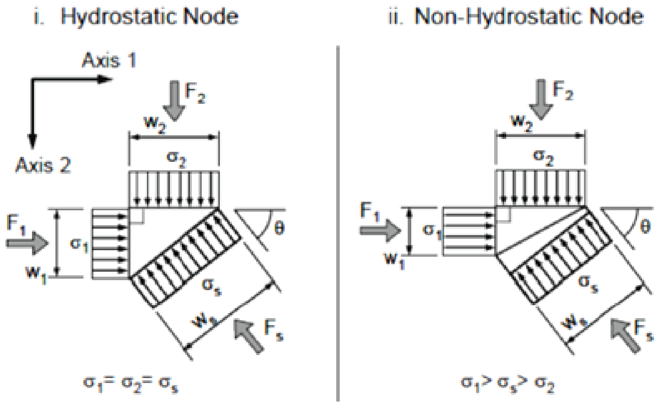

Figure 5.7: Hydrostatic- and non hydrostatic nodes [48]

Hydrostatic nodes occur if the compressive stress acting on each face of the node is equivalent ($\sigma_1 = \sigma_2 = \sigma_3$) and perpendicular to the surface of the node. Therefore no shear stresses occur at the face of the node. However, hydrostatic nodes are impractical as a result of geometric configurations in an STM and therefore difficult to model. Therefore, non-hydrostatic nodes can be used in which shear stresses occur. Eurocode 2 does not distinguishes hydrostatic- and non hydrostatic nodes. Nevertheless, node should be enclosed properly by applying rebars.

In order to guarantee the node its structural safety, it must be checked if the compressive strength is not exceeded in any of the faces. See Figure 5.8:

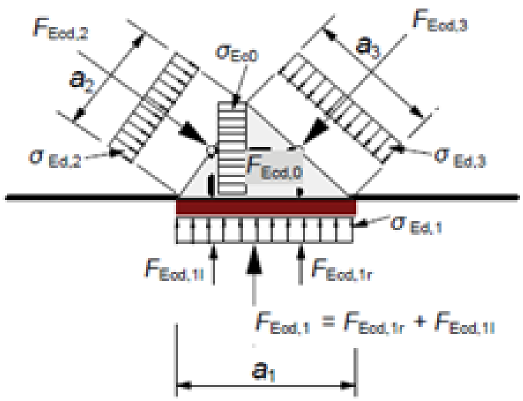

Figure 5.8: Model of CCC node in accordance with Eurocode 2

CCT node

A CCT node connects two compressive struts to one tie. This type of node often occurs near a bearing plate and in a concrete half-joint. The stress state is less advantageous than the CCC node, due to the presence of the tie. An important aspect of the node is the anchorage of the tie. Anchoring can be done using an anchor plate or by providing sufficient anchorage length.

Anchoring is usually provided using sufficient anchorage length in the Netherlands. Anchor plates can be used, if sufficient anchorage length cannot be applied. However, this is not preferred, as a result of expensive costs and practical difficulties. Therefore, anchorage plates are not considered in this thesis. The anchorage length of the rebar l_{bd} is illustrated in Figure 5.9 and propagates until the end of the rebar.

The size of the node depends on the bearing width and the distance between the bearing and the rebar, which is illustrated in 5.9. The compressive stresses need to be verified similar to a CCC node, but with a different k_i value. The tensile force can not exceed the yield- or prestressing strength of the rebar.

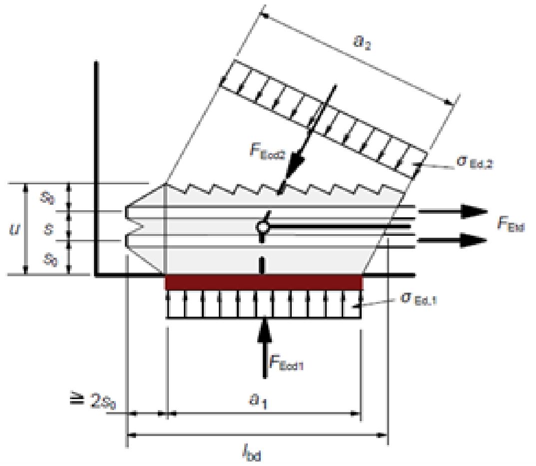

Figure 5.9: Model of CCT node in accordance with Eurocode 2

CTT node

A CTT node connects one compressive strut to two ties. The node has the least advantageous stress state in comparison with a CCC- and CCT node. The ties represent one bent rebar or two anchored rebars with or without anchor plates

The compressive stresses need to be verified on the face perpendicular to the strut in the curved part of the rebar. The width of the face depends on the mandrel diameter of the rebar and the angle with the strut, see Figure 5.10:

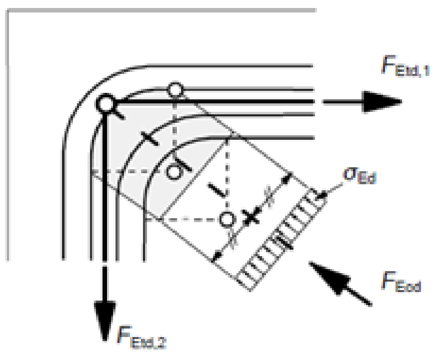

Figure 5.10: Model of CTT node in accordance with Eurocode 2

5.2.8 Anchorage

Sufficient anchorage length must be provided in order to transfer tensile forces to compression forces into the concrete. The principle of anchoring a rebar using sufficient anchorage length is illustrated in Figure 5.11:

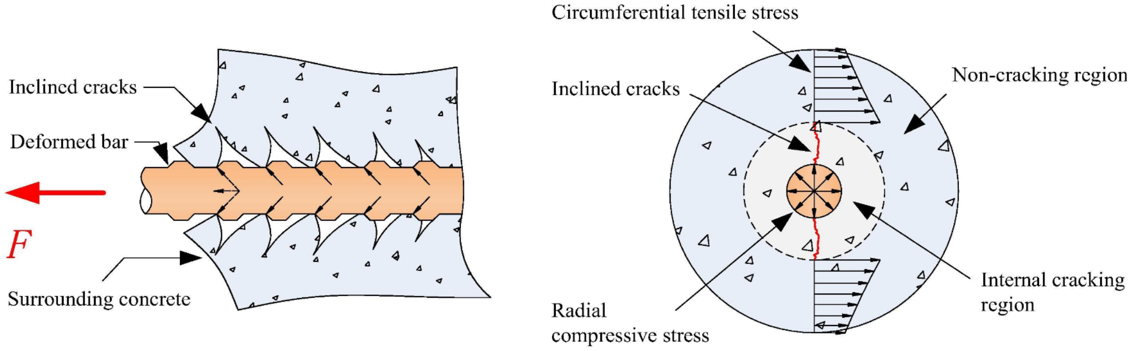

Figure 5.11: Principle of anchoring with sufficient anchorage length [49]

The bond-strength provides the load transfer between rebar and concrete. It depends on the presence of micro-cracks and the application of ribbed or smooth rebars. Eurocode 2 provides a simplified calculation that determines a constant bond-strength (NEN-EN 1992-1-1 art. 8.4.2(2)):

$$f_{bd} = 2.25\eta_1\eta_2 f_{ctd} \tag{5.5}$$

In which:

η_1	is a coefficient that accounts for the bonding conditions
η_2	is a coefficient that accounts for the rebar diameter
f_{ctd}	is the design tensile strength of concrete

A basic required anchorage length needs to be applied in order to transfer the tensile force to the concrete. It can be determined as (NEN-EN 1992-1-1 art. 8.4.3(2)):

$$l_{b,rqd} = \frac{\text{Ø}}{4}\frac{\sigma_{Rd}}{f_{bd}} \tag{5.6}$$

In which:

Ø	is the rebar diameter
σ_{Rd}	is the design tensile stress in rebar

Other design aspects can influence the anchorage capacity of a rebar as well. For example, by bending the rebar or applying (welded) rebars transverse to the tie. These effects are taken into account in (NEN-EN 1992-1-1 art. 8.4.4(1)):

$$l_{bd} = \alpha_1 \alpha_2 \alpha_3 \alpha_4 \alpha_5 l_{b,rqd} \geq l_{min} \tag{5.7}$$

In which:

α_1 is a coefficient for the form of rebar, assuming sufficient concrete cover

α_2 is a coefficient for the concrete cover

α_3 is a coefficient for the effect of confinement by transverse reinforcement

α_4 is a coefficient for the influence of welded transverse bars

α_5 is a coefficient for the effect of transverse pressure

5.3 Geometry and material properties

This chapter elaborates the geometry and material properties for the analytical tool. A distinction is made between concrete, reinforcement steel and prestressing.

5.3.1 Concrete

Geometry

The geometry of the concrete half-joint, as used in the analytical tool, is illustrated in Figure 5.12.

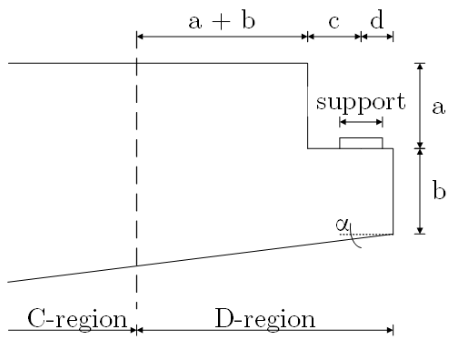

Figure 5.12: Geometry of concrete in parametric tool

The analytical tool uses a depth of 1000 [mm] (into the plane of the page) and the load bearing capacity is therefore calculated in: [kN/m^1]. The discontinuous region is determined using St. Venants principle as the sum of the height of the concrete half-joint and the length of the nib [42].

Material

The material properties for concrete can be determined using the characteristic compressive cylinder strength and different coefficients: partial safety factors and coefficients for long-term effects. The design values for compressive- and tensile strength can be determined using NEN-EN 1992-1-1 art. 3.1.6 as:

$$f_{cd} = \frac{\alpha_{cc} f_{ck}}{\gamma_C} \tag{5.8}$$

$$f_{ctd} = \frac{\alpha_{ct} f_{ctk,0.05}}{\gamma_C} \tag{5.9}$$

In which:

$\alpha_{cc/ct}$	is the coefficient taking account for long term effect on the compressive- or tensile strength and unfavourable effects resulting from the way the load is applied. NEN-EN 1992-1-1-NB suggests a value of 1.0
f_{ck}	is the characteristic compressive cylinder strength of concrete at 28 days
$f_{ctk,0.05}$	is the characteristic axial tensile strength of concrete (5% fractional)
γ_C	is the partial factor for concrete

The RBK1.2 suggests that the compressive cylinder strength of the concrete can be determined using material research or without material research. If the strength is determined at an age $t > 28$ days, the values $\alpha_{cc/ct}$ must be reduced by a factor k_t. NEN-EN 1992-1-1(-NB) art. 3.1.2 suggests a value of 0.85. Using the RBK1.2, multiple possibilities arise to determine this coefficient:

1. Compressive strength of concrete without material research:
   - (a) Using original design value of technical drawing: ($\alpha_{cc} = \alpha_{ct} = 1.0$)
   - (b) Using lowest design value of original design standard: ($\alpha_{cc} = \alpha_{ct} = 1.0$)
   - (c) Using results from samples of similar structures: ($\alpha_{cc} = \alpha_{ct} = 0.85$)
2. Compressive strength of concrete with material research:
   - (a) Using results from samples of structure: ($\alpha_{cc} = \alpha_{ct} = 0.85$)

5.3.2 Reinforcement

Geometry

The reinforcement of the concrete half-joint, as used in the analytical tool, is illustrated in Figure 5.13. The rebars are reformulated in the analytical tool as follows:

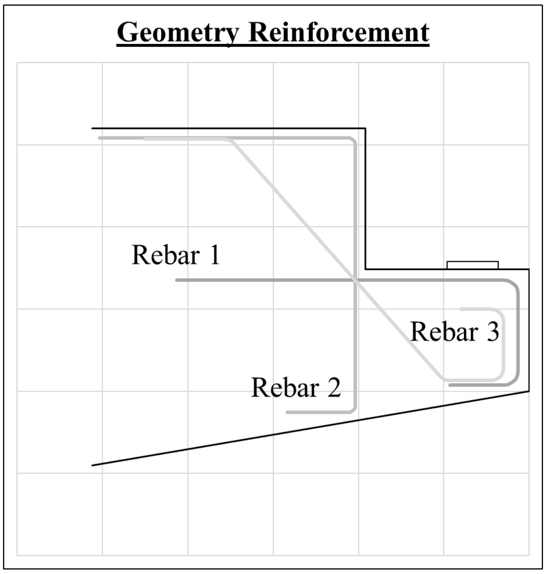

Figure 5.13: Geometry of reinforcement in parametric tool

Material

The design yield strength of reinforcement steel can be determined using NEN-EN 1992-1-1 art. 3.2.7 as:

$$f_{yd} = \frac{f_{yk}}{\gamma_S} \tag{5.10}$$

In which:

f_{yk}	is the characteristic yield strength of reinforcement steel
γ_S	is the partial factor for reinforcement steel

The RBK1.2 suggests to determine the design yield strength based on the original design standard, which could be different than eq. 5.10. RBK1.2 Table 2.6 elaborates the design yield strengths based on the original design standards.

5.3.3 Prestressing

Geometry

The prestressing of the concrete half-joint, as used in the analytical tool, is illustrated in Figure 5.14.

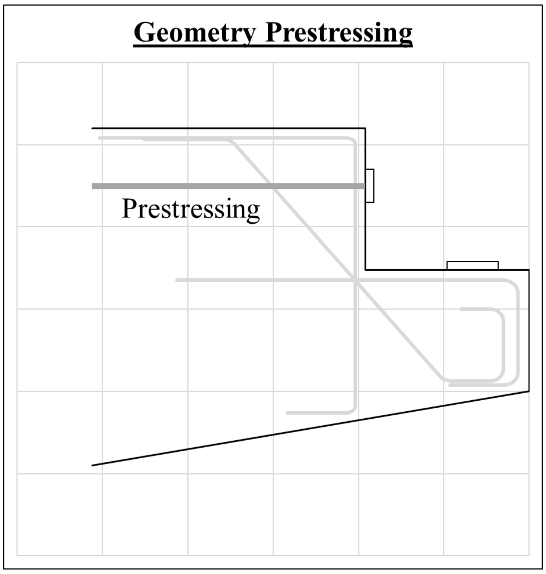

Figure 5.14: Geometry of the prestressing in parametric tool

Material

The mean prestress force $P_{m,t}(x)$ is equal to the maximum force P_{max} imposed at the end, minus the immediate losses and the time dependent losses. RBK1.2 Table 2.7 suggests to use the mean prestressing of the original calculations or maximum permissible mean prestressing according to original design codes.

5.4 Strut-and-tie approach

The introduction of the strut-and-tie approach in paragraph 5.2 is about design, in which the support load is known and the concrete and reinforcement needs to be calculated. In the case of assessment, the concrete and reinforcement are known and the support load or load bearing capacity needs to be calculated.

Therefore, the analytical tool uses a unit load to determine the load distribution between the struts and ties. Subsequently, the load capacity of each strut, node and tie is calculated, in which the lowest maximum load bearing capacity is governing. The structural analysis and assumptions are elaborated in paragraph 5.4.3 - 5.4.4 and the optimisation method is elaborated in paragraph 5.4.5.

5.4.1 Nodes

The node modelling for the strut-and-tie analysis, as used in the analytical tool, is illustrated in Figure 5.15:

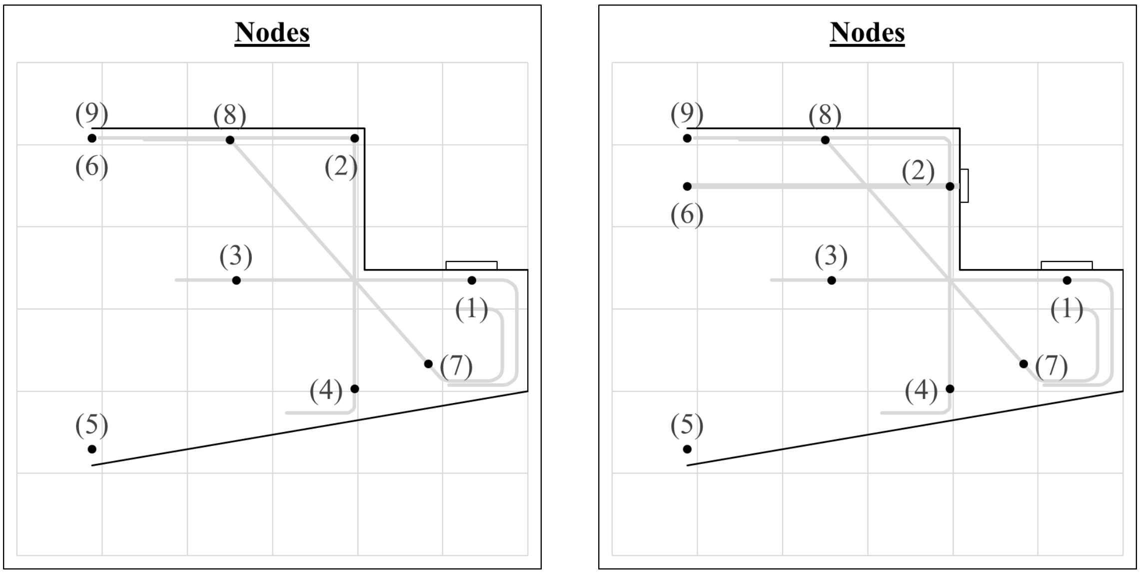

(a) Without prestressing (b) With prestressing

Figure 5.15: Node numbering

If prestressing is present in the concrete half-joint, Nodes (2) and (6) are replaced from the upper rebar towards the prestressing.

The nodes for the strut-and-tie analysis are not all fixed to its position and can shift in x- or y-direction, or along the corresponding rebar. A shift in position can lead to an increase of anchorage length, but also to an increase in forces in struts or ties. The optimisation of finding the most favourable positions is elaborated in paragraph 5.4.5. An overview of the fixed- and movable nodes are given in Table 5.1:

Table 5.1: Fixed- an movable nodes in strut-and-tie analysis

Fixed nodes	**Movable nodes**
Node (1)	Node (3) (x-direction)
Node (2)	Node (4) (y-direction)
Node (6)	Node (5) (y-direction)
Node (8)	Node (7) (along Rebar 3)
Node (9)	

5.4.2 Strut-and-tie model

The strut-and-tie analysis is elaborated on the basis of a Category A2 half-joint (with diagonal rebar, but without prestressing). Other categories can be analysed similarly, with only a few adjustments:

Category A1:	Only strut-and-tie model 1 is used, without predefined load factor
Category B1-1:	Strut-and-tie model 1 is used, without predefined load factor and the prestressing is added to tie T3 in the strut-and-tie model (including change of Node (2) from CTT to CCT)
Category B2-1:	Only the prestressing is added to tie T3 in the strut-and-tie model (including change of Node (2) from CTT to CCT)

The strut-and-tie tool is based on two different strut-and-tie models for a Category A2 half-joint, which are summed using a predefined load factor. The strut-and-tie models are illustrated in Figure 5.16:

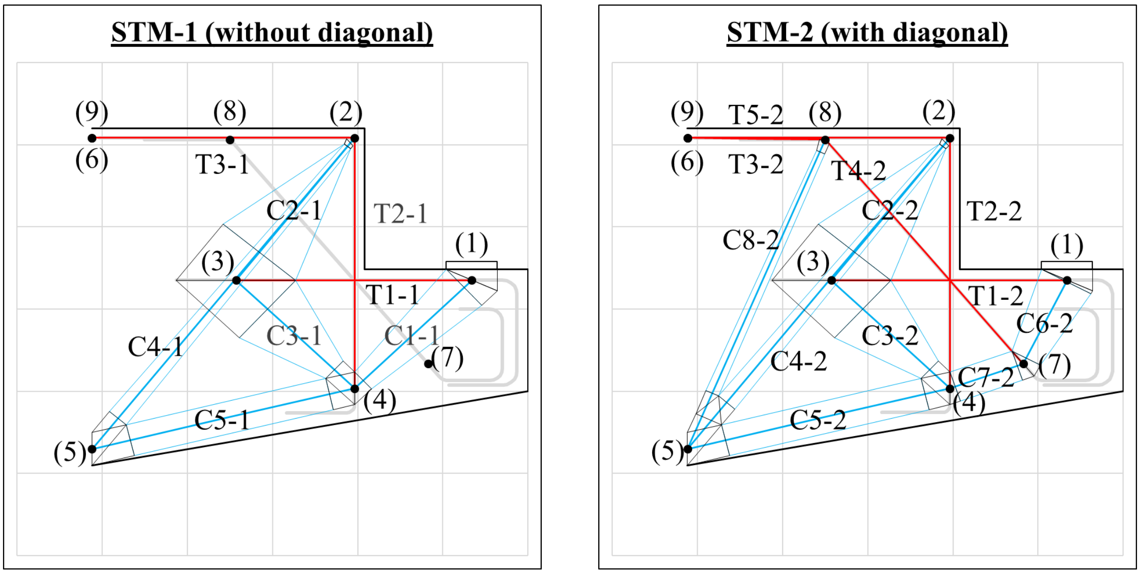

(a) Strut-and-tie model 1

(b) Strut-and-tie model 2

Figure 5.16: Strut-and-tie models 1 and 2

For each strut-and-tie model, the forces in the struts and ties are calculated using a unit load. Subsequently, the two strut-and-tie models can be summed to a new strut-and-tie model (STM3), which is illustrated in Figure 5.17. A predefined load factor is introduced, which distributes the load over the two strut-and-tie models.

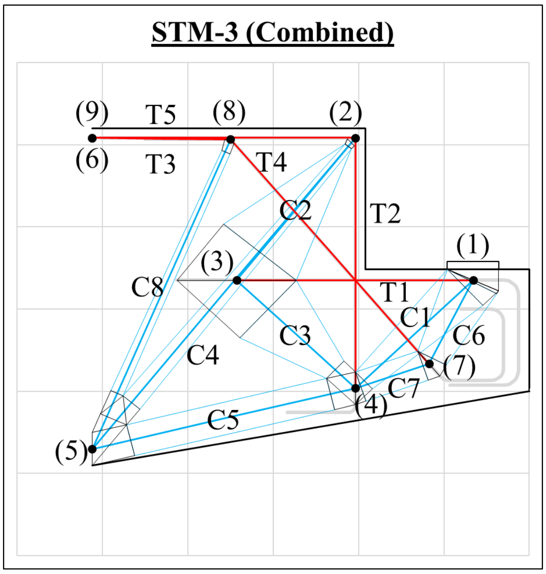

Figure 5.17: Strut-and-tie model 3

The unit force per strut and tie in STM3 is determined as follows:

$$F_{unit,i} = F_{unit,i,STM1} \cdot Q_{STM} + F_{unit,i,STM2} \cdot (1 - Q_{STM}) \tag{5.11}$$

In which:

$F_{unit,i,STM1}$ is the unit force in strut or tie i of STM-1

$F_{unit,i,STM2}$ is the unit force in strut or tie i of STM-2

Q_{STM} is the load factor, which is a value between 0 and 1.

The optimisation of the most favourable load factor is elaborated in paragraph 5.4.5.

Alternative strut-and-tie models

Strut C4 transfers the load from Node (2) to Node (5) directly. However, it can be argued that the load should be transferred through Node (3). Nevertheless, if the length of the horizontal rebar increases or decreases, this could lead to unusual strut-and-tie models. The differences are illustrated in Figure 5.18 and Figure 5.19:

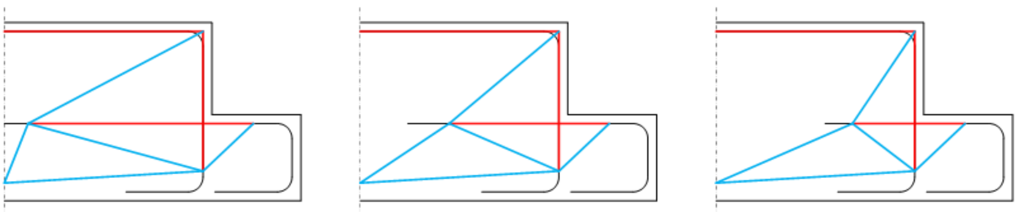

Figure 5.18: Strut C4 from Node (3) to Node (5) (indirect)

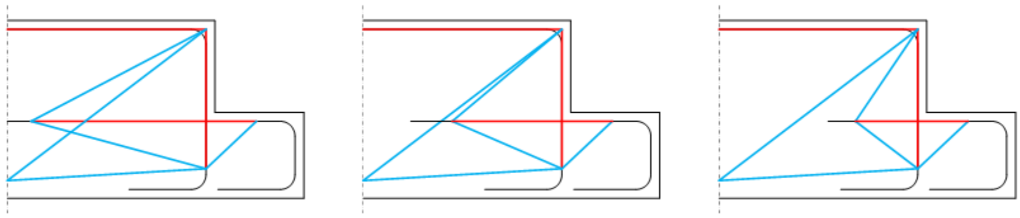

Figure 5.19: Strut C4 from Node (2) to Node (5) (direct)

Special care is taken in modelling and calculating Node (2) in the analytical tool, which will be elaborated in paragraph 5.4.3.

It can also be argued that the strut-and-tie model is not compatible as a slab, as the compressive and shear stresses localize in Node (5) at the bottom, see Figure 5.20(a). Shear stresses are distributed over the uncracked section of the slab. Therefore, it can be argued that strut C4 should transfer the compressive stress to the middle of the slab, see Figure 5.20(b).

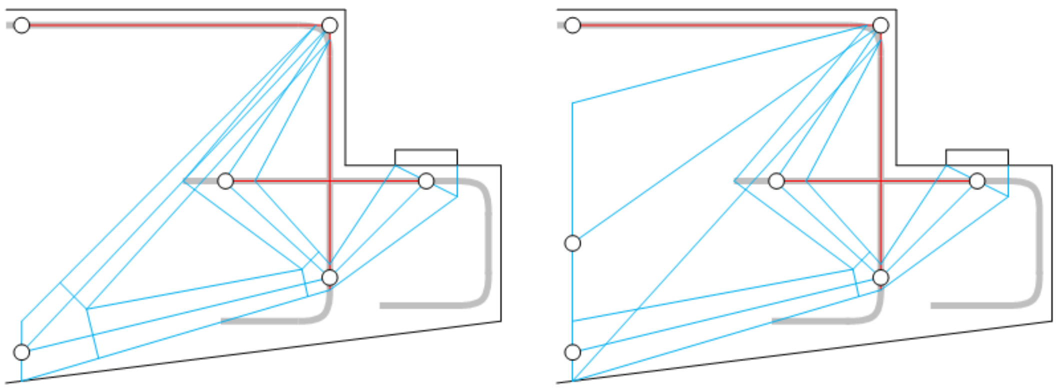

(a) Strut C4 to bottom

(b) Strut C4 to middle

Figure 5.20: Strut-and-tie model in as a slab

The same holds for strut C8, which occurs in the presence of a diagonal rebar. However, is it unknown over which height the concrete section is uncracked. Therefore, the strut-and-tie model of Figure 5.20a will be used in further calculations.

5.4.3 Node modelling

This paragraph briefly elaborates the modelling of the nodes in the strut-and-tie model. The dimensions of the nodes are extensively elaborated in Appendix B.

The nodes are verified at the face in which the strut is connected to the nodes, by checking the compressive strength. An additional check is performed for Node (1), (2), (4) and (5), in which multiple struts are coupled. The individual forces are projected perpendicular to the face and summed. The face of each node over which the additional check is performed, is elaborated below.

Node (1)

Node (1) is a CCT node and connects strut C1 (and C6) with tie T1 and the bearing plate. The anchorage of tie T1 in Node (1) is indicated in orange in Figure 5.21, it starts at the left of Node (1) and ends at the end of rebar 1.

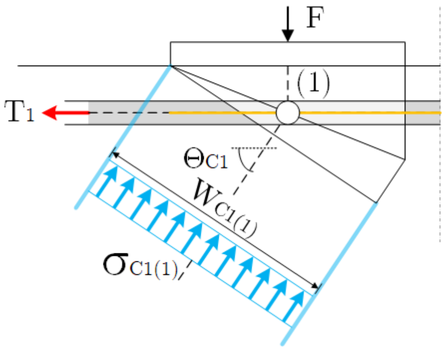

(a) Individual

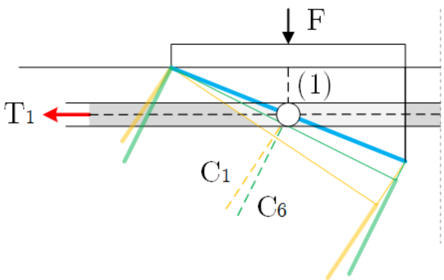

(b) Extra check

Figure 5.21: Node (1)

For a Category A2 half-joint, strut C1 and C6 are coupled to Node (1). An additional check is performed on the diagonal face, which is indicated in blue in Figure 5.21(b).

Node (2)

Node (2) is a CTT node and connects strut C2 and C4 with tie T2 and T3. The width of the face of strut C2 and C4 depends on the mandrel diameter of rebar 2 and the strut's angle. If the mandrel diameter decreases, or the strut's angle deviates from 45°, the width of the faces decrease rapidly.

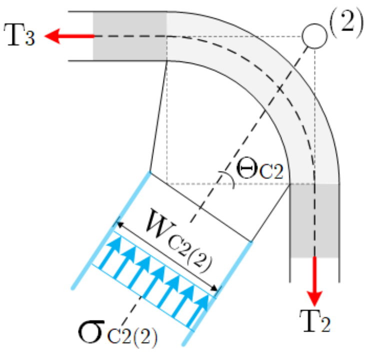

(a) Individual

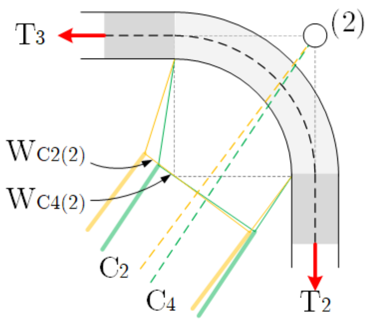

(b) Extra check

Figure 5.22: Node (2)

Strut C2 and C4 are coupled to Node (2). An additional check is performed on the minimum width of the face of strut C2 and C4: $w_{C2/C4(2)} = \min(w_{C2(2)}, w_{C4(2)})$.

Node (2) changes from a CTT node to a CCT node (similar to Node (1)) in the presence of prestressing.

Node (3)

Node (3) is a CCT node and connects strut C2 and C3 with tie T1. The node can be shifted along rebar 1 (in x-direction), which can increase or decrease the anchorage length and strut's angle. The offset of the node is indicated by $\Delta_{(3)}$. The anchorage length of tie T1 in Node (3) is equal to twice the offset of Node (3).

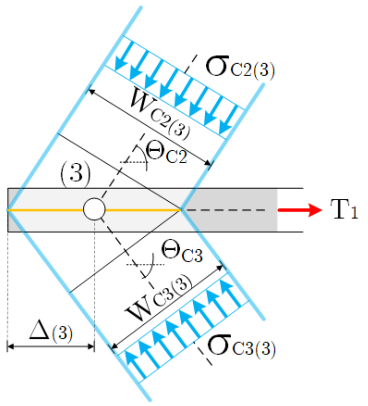

(a) Individual

Figure 5.23: Node (3)

Node (4)

Node (4) is a CCT node and connects strut C1, C3, C5 (and C7) with tie T2. The node can be shifted along rebar 2 (in y-direction), in which the minimum offset start at the bending of the rebar. The offset of the node is indicated by $\Delta_{(4)}$

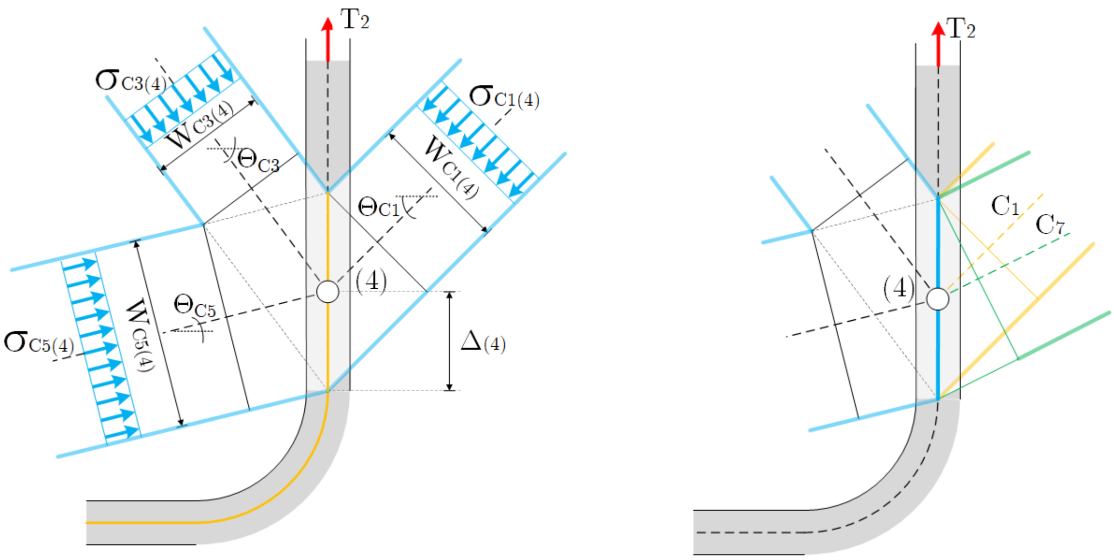

(a) Individual

(b) Extra check

Figure 5.24: Node (4)

For a Category A2 half-joint, strut C1 and C7 are coupled to Node (4). An additional check is performed on the vertical face, which is indicated in blue in Figure 5.24(b).

Node (5)

Node (5) is a CCC node and connects strut C4, C5 (and C8) to the continuous region. The modelling of Node (5) leads to a concentration of compressive stresses, which are not present in reality. It is expected that strut C4 and C8 spread their stress fields over the height of the concrete half-joint and transfer the shear stresses through the concrete. Therefore, the modelling of Node (5) is a conservative assumption.

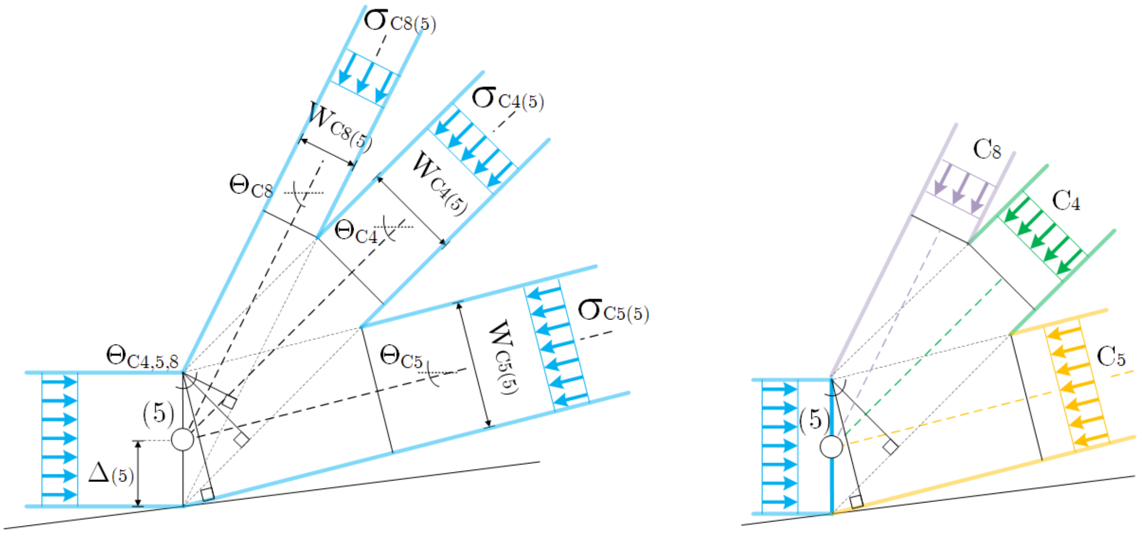

(a) Individual

(b) Extra check

Figure 5.25: Node (5)

Struts C4, C5 (and C8) are coupled in Node (5). An additional check is performed on the vertical face of Node (5), which is illustrated in blue in Figure 5.25.

Node (7)

Node (7) is a CCT node and connects strut C6 and C7 to tie T4. The node can be shifted along rebar 3 (in local-direction), in which the minimum offset start at the bending of the rebar. The offset of the node is indicated by $\Delta_{(7)}$

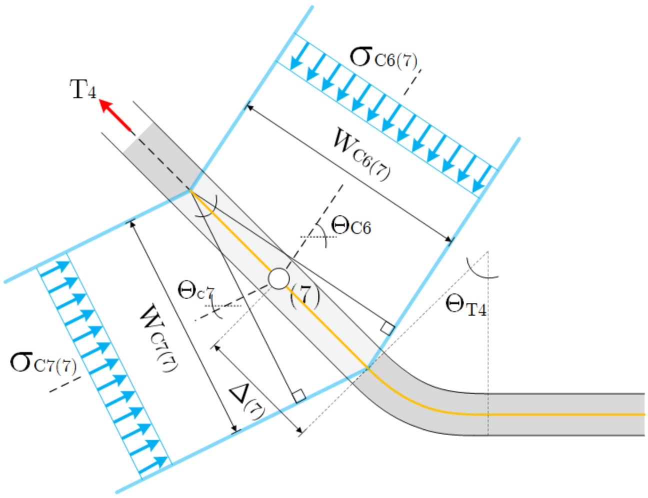

(a) Individual

Figure 5.26: Node (7)

No additional checks need to be performed.

Node (8)

Node (8) is a CTT node and connects strut C8 to tie T4 and T5. The width of the face of strut C8 depends on the mandrel diameter of rebar 3 and the strut's angle. If the mandrel diameter decreases, or the strut's angle deviates from $\Theta_{T4}/2$, the width of the faces decrease rapidly.

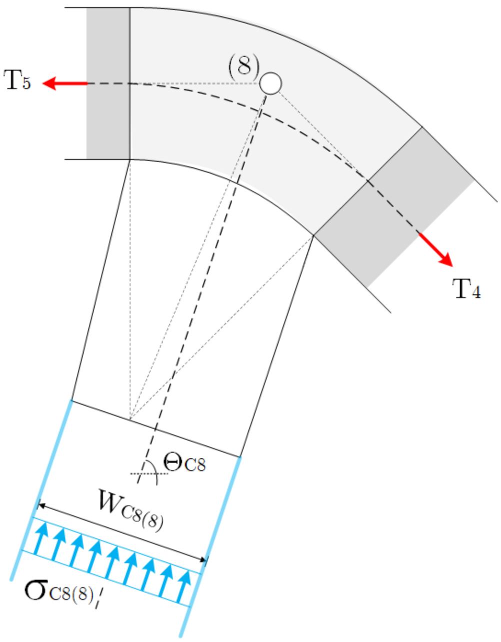

(a) Individual

Figure 5.27: Node (8)

5.4.4 Checks

The load bearing capacity of each strut, node and tie is calculated using the unit force. The analytical tool refers a strut or tie by: i, which is connected by two nodes: j and k.

Struts

The design compressive strength of a concrete strut is elaborated in paragraph 5.2.5 The analytical tool assumes conservatively that transverse tension is present in the struts. The capacity of the concrete strut i is determined in the analytical tool as follows:

$$C_{max,C,i} = \sigma_{Rd,max} \cdot \min(w_{i(j)}, w_{i(k)}) \cdot b \tag{5.12}$$

In which:

$w_{i(j/k)}$ is the width of concrete strut i at node j or node k

b is the depth of the nib as illustrated in Figure 5.12

Based on the capacity of concrete strut i, the maximum bearing capacity can now be determined as:

$$F_{max,C,i} = \frac{C_{max,C,i}}{F_{unit,i}} \tag{5.13}$$

Nodes

The capacity of the face of concrete strut i at node j or k is determined in the analytical tool as follows:

$$C_{max,i(j/k)} = \sigma_{Rd,max} w_{i(j/k)} \cdot b \tag{5.14}$$

In which:

$w_{i(j/k)}$ is the width of the concrete strut i at node j or k

Based on the capacity of the face of concrete strut i at node j or k, the maximum bearing capacity can now be determined as:

$$F_{max,i(j/k)} = \frac{C_{max,i(j/k)}}{F_{unit,i}} \tag{5.15}$$

Ties

The design tensile strength of the tie is determined using the total cross-sectional area of the corresponding rebar over the considered width and design yield strength as:

$$T_{max,T,i} = A_{s,i,tot} \cdot f_{yd} \tag{5.16}$$

Based on the capacity of the tie, the maximum bearing capacity can now be determined as:

$$F_{max,T,i} = \frac{T_{max,T,i}}{F_{unit,i}} \tag{5.17}$$

Anchorage length

The calculation of design anchorage length in accordance with Eurocode 2 is elaborated in paragraph 5.2.8. In the presence of insufficient anchorage length, the rebar is only partially anchored. As the structural behaviour of a partial anchored rebar is unknown, the solution is not valid and not taken into account in the optimisation.

5.4.5 Optimisation

The load bearing capacity using the strut-and-tie analysis is optimised by shifting Node (3), (4), (5) and (7) over a predefined range with a certain step-size. Subsequently, the load factor (Q_{STM}) is also be optimised. In each step, all forces are checked in each element of the strut-and-tie model (struts, ties and (combined) nodes) again. The best solution can be found as the highest solution of all lower bound solutions. The analytical tool calculates all possible solutions and presents the highest lower-bound solution, including failure mechanism. The sequence of finding this value is elaborated below:

1. The analysis starts by setting the offsets of the nodes and load factor to zero.
2. The anchorage and angle limitations are verified and if both are correct, the solution will be stored in a database
3. Node (7) will be shifted by a predefined step-size and loop returns to 2. until the predefined range is met.
4. Node (5) will be shifted by a predefined step-size and loop returns to 2. until the predefined range is met.
5. Node (4) will be shifted by a predefined step-size and loop returns to 2. until the predefined range is met.

6. Node (3) will be shifted by a predefined step-size and loop returns to 2. until the predefined range is met.
7. The load factor (Q_{STM}) will be increased by the predefined step-size and loop returns to 2. until the load factor is equal to 1.
8. The highest solution from the database is the highest lower-bound solution for the load bearing capacity of the concrete half-joint.

An example of the optimisation of the load factor is illustrated in Figure 5.28.

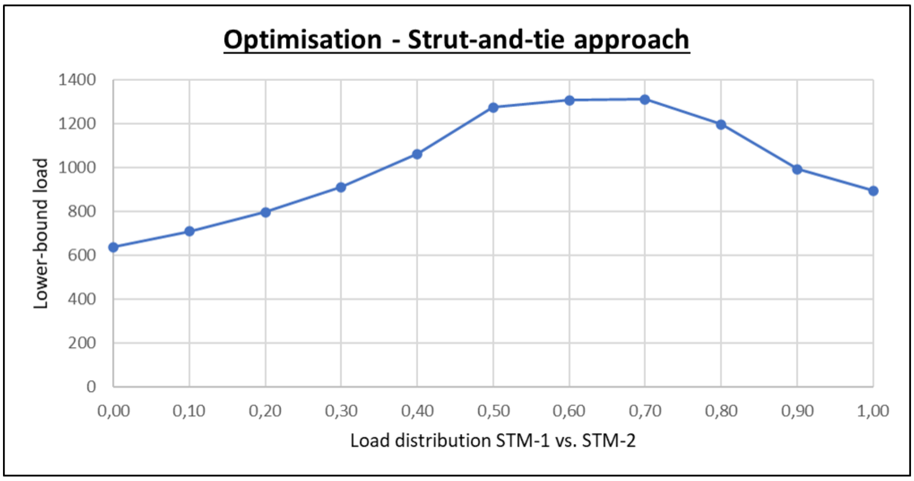

Figure 5.28: Optimisation of load factor

The x-axis shows the distribution of the load over STM-1 and STM-2. If the load factor is equal to 0, the load is distributed over STM-2 only (with diagonal) and if the load factor is equal to 1, the load is distributed over STM-1 only (without diagonal). The most optimised solution can usually be found somewhere in between.

It is recommended to start with a large step-size and predefined range, and adjust the values based on the results to save computational time.

5.5 Kinematic approach

The kinematic approach (also known as CUR40-method) uses the (expected) presence of the diagonal crack at the re-entrant corner to determine the load bearing capacity. The crack corresponds with failure mechanism 2 and 3 (see paragraph 2.2.3, in which the hanger-rebar or horizontal rebar ruptures.

The approach is based on an upper-bound approximation, which can be formulated as [45]:

"Starting from an arbitrary mechanism, the corresponding equilibrium equation will provide an upper-bound solution for the limit load"

The results of the kinematic approach are usually more accurate than the strut-and-tie approach for concrete half-joints, despite that this is an upper-bound approximation. The structural analysis and assumptions are elaborated in paragraph 5.5.1 and an optimisation method is elaborated in paragraph 5.5.2.

5.5.1 Calculation

The diagonal crack initiates at the re-entrant corner and propagates with a certain angle until horizontal- or vertical force equilibrium can no longer be fulfilled. The torn-off concrete part can be considered as a free-body diagram, as illustrated in Figure 5.29:

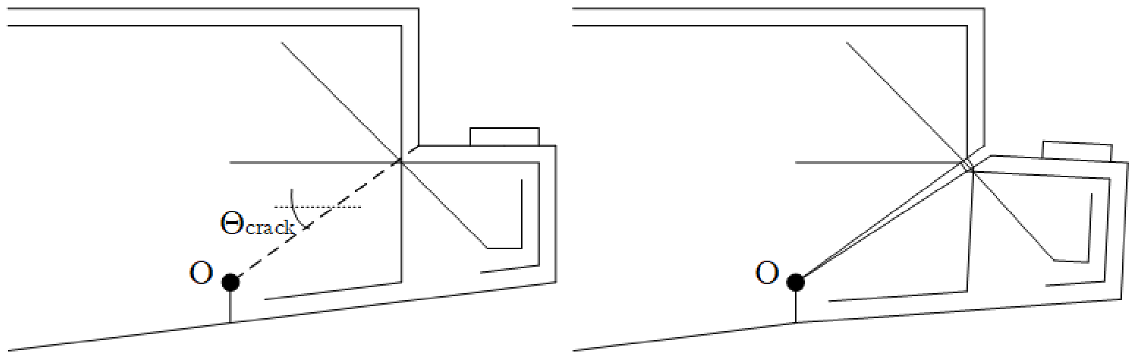

Figure 5.29: Diagonal crack in concrete half-joint

The free-body diagram rotates around point O, due to the load on the support and self-weight of the torn-off concrete part. The latter one can be neglected due to its minor contribution compared to the total load on the support. The rotation leads to an increase of strain and tensile stress in the rebars, which acts as a resistance mechanism. Additionally, the compressive stresses in the concrete compression zone increase. Both contribute to the load bearing capacity of the concrete half-joint, which can be determined using horizontal- and vertical force equilibrium and moment equilibrium.

The free-body diagram with forces is illustrated in Figure 5.30.

The load bearing capacity can calculated as follows:

1. Approximate the (minimum) concrete compression zone using horizontal force equilibrium
2. Determine contributions/resistance of rebars and concrete
3. Determine the load on the support, using moment equilibrium
4. Check vertical force equilibrium and increase concrete compression zone if needed.

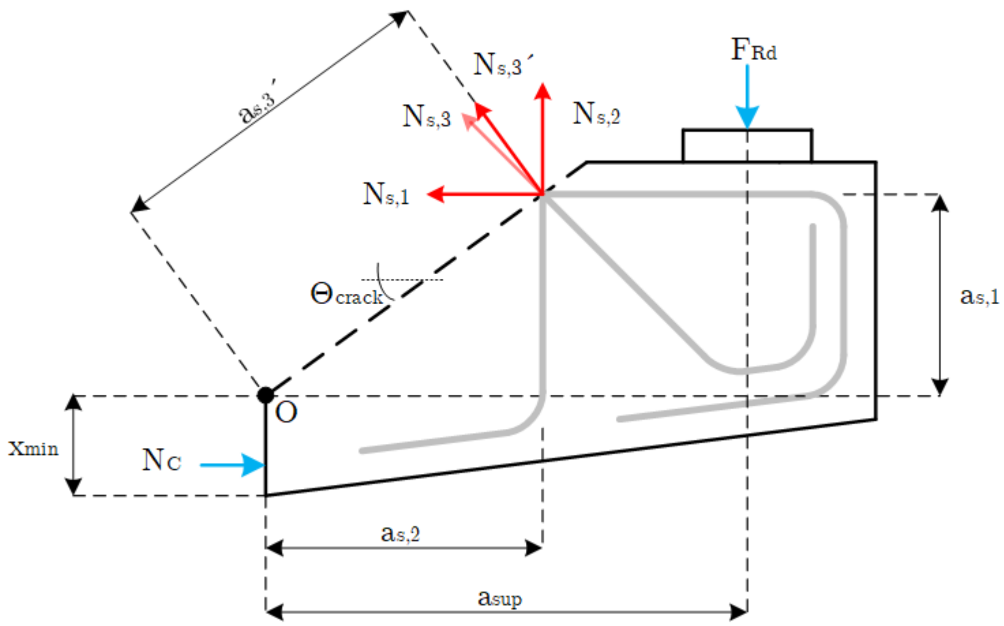

Figure 5.30: Free-body diagram for kinematic approach

(Minimum) Concrete compression zone

The minimum concrete compression zone is determined using the tensile forces in the rebars, which have a horizontal component (horizontal rebar and diagonal rebar). It is assumed that both rebars are able to develop its yield strength and must be in horizontal force equilibrium with the concrete:

$$\sum H = \sum N_{s,x} + N_c = 0 \tag{5.18}$$

In which:

$\sum N_{s,x}$ is the sum of the horizontal components of the tensile forces in the rebars (horizontal rebar and diagonal rebar)

N_c is the compressive force in the concrete

It is initially assumed that the concrete crushes in the concrete compression zone. The compressive force in the concrete can therefore be determined as:

$$N_c = 0.75 \cdot x_{min} \cdot b \cdot f_{cd} \tag{5.19}$$

From which, a minimum concrete compression zone can be determined as:

$$x_{min} = \cdot (A_{s,1,tot} + A_{s,3,tot} \cdot \cos\phi) \cdot \frac{f_{yd}}{0.75 \cdot b \cdot f_{cd}} \tag{5.20}$$

The concrete compression zone can be increased if vertical force equilibrium cannot be fulfilled.

Resistance of rebars and concrete

It is assumed that the rebars are detailed properly and able to develop its yield strength. Therefore, the restoring moments around point O due to the rebars can be determined as:

$$M_s = \sum_{n=1}^{3} N_{s,i} \cdot a_{s,i} = \sum_{n=1}^{3} A_{s,i,tot} f_{yd} \cdot a_{s,i} \tag{5.21}$$

In which:

$A_{s,i,tot}$	is the total cross-sectional area of rebar i over the width
$a_{s,i}$	is the lever arm of rebar i
f_{yd}	is the design yield strength of the rebar

The tensile force in the diagonal rebar is projected perpendicular to the crack ($N_{s,3}$').

The concrete is initially assumed to be crushing in the concrete compression zone. The compression zone is than modelled using a bi-linear diagram, from which the axial compression force centers at $0.39 \cdot x_{min}$. The restoring moment due to the concrete can be determined as:

$$M_c = N_c \cdot (1 - 0.39) \cdot x_{min} \tag{5.22}$$

If vertical force equilibrium cannot be fulfilled, the concrete compression zone can be increased. Subsequently, it is assumed that the concrete is not crushing. The compressive stresses in the concrete compressive zone are linearly distributed. The restoring moment due to the concrete can in that case be determined as:

$$M_c = N_c \cdot (1 - 0.33) \cdot (x_{min} + \Delta x) \tag{5.23}$$

Load on the support

The load on the support can be determined using moment equilibrium around point O, using the restoring moments due to rebars and concrete. It can be determined as:

$$\sum M^O = M_s + M_c + F_{Rd} \cdot a_{sup} = 0 \tag{5.24}$$

From which, the load on the support can be determined as:

$$F_{Rd} = \frac{\sum M_s + M_c}{a_{sup}} \tag{5.25}$$

The load on the support is equal to the load bearing capacity of the concrete half-joint

Vertical force equilibrium

The difference between the vertical forces of the rebars and load on the support is transferred in shear stresses through the concrete compression zone to fulfil vertical force equilibrium. The shear resistance of the concrete compression zone can be determined in accordance with NEN-EN 1992-1-1 art. 6.2.2 as:

$$V_{Rd,c} = \nu_{min} \cdot b \cdot x_{min} \tag{5.26}$$

In which:

ν_{min} is the shear strength of the concrete

The shear strength of the concrete can be determined as:

$$\nu_{min} = 0.035k^{3/2} \cdot f_{ck}^{1/2} \tag{5.27}$$

In which:

k $= 1 + \sqrt{\frac{200}{x_{min}}} \leq 2.0$

If vertical force equilibrium cannot be fulfilled, the concrete compression zone is increased and the analysis needs to be executed again. It is still assumed that the concrete is crushing in the compression zone, despite the increase in height.

5.5.2 Optimisation

The load bearing capacity is calculated using an arbitrary value for the crack's angle θ_{crack}. No guidance is given on which angle must be taken. Rajapakse et al. [13], [15] compared experimental results of half-joints with analytical results and found that angles ranging between 30° and 70° provide adequate approximations.

Therefore, multiple calculations need to be made within this range, in which the lowest solution is the best upper-bound approximation of the load bearing capacity of the concrete half-joint, see Figure 5.31.

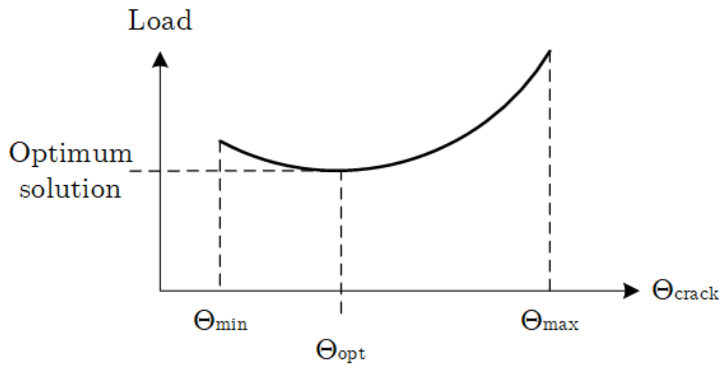

Figure 5.31: Optimisation of kinematic approach

The lowest upper-bound approximation is determined using range of the crack's angles provided by Rajapakse et al. [13], [15].

5.6 Corrosion

The analytical tool is able to perform a corrosion study on the load bearing capacity of a concrete half-joint. The corrosion is simulated in the strut-and-tie approach on tie T1, T2 and T4, and in the kinematic approach on the rebars that intersect the diagonal crack.

The corrosion is simulated by reducing the cross-sectional area and/or yield strength, as elaborated in paragraph 4.5

5.7 Results

The existing concrete half-joints from the archive study are analysed using the analytical tool. The concrete half-joints of Bullewijk and Terbregseplein are not analysed, because prestressing is present in the nib. The analytical tool is not able to determine the load bearing capacity of these half-joints (yet). The results are distinguished in the cases with- and without corrosion. The results from the analytical tool are added in Appendix C.

5.7.1 Uncorroded concrete half-joints.

The upper-bound and lower-bound solutions of the analytical analysis are illustrated in Figure 5.32 and Table 5.2.

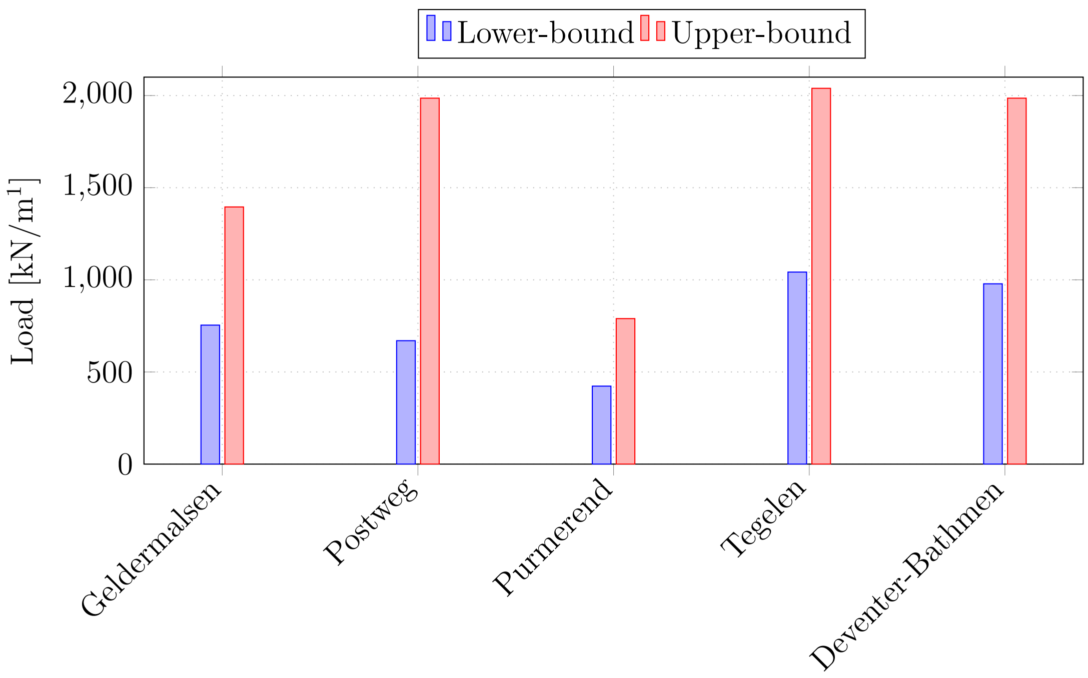

Figure 5.32: Analytical results of uncorroded concrete half-joints

Table 5.2: Overview of analytical results and failure mechanisms

Name	**Category**	**Lower-bound**		**Upper-bound**
		[kN/m^1]	Mech.	[kN/m^1]
Geldermalsen	A2	754.2	T1	1395.4
Postweg	B2-1	669.7	Node (8)	1985.8
Purmerend	A1	423.2	T2	789.6
Tegelen	B2-1	1042.1	Node (8)	2039.2
Deventer-Bathmen	A2	978.4	Node (8)	1985.8

The following aspects can be observed from the analytical analyses:

- The upper-bound results are always higher than the lower-bound results. However, the differences are very large in the case where concrete strength governs the load bearing capacity in the strut-and-tie model. The differences are smaller for the case in which rupture of tie T1 or T2 occurs. However, a difference of 46% can still be observed.

- The CTT nodes in the strut-and-tie approach appear to be vulnerable for the load bearing capacity. As indicated in paragraph 5.4.3, the stress state of CTT nodes is already unfavourable and the dimensions of Node (2) and (8) strongly depends on the mandrel diameter of the rebar and inclination of the strut. Failure in Node (2) has not been observed in the calculations, because the dimensions of this node are adjusted to a CCT node due to the presence of prestressing.

- The failure mechanism of the nodes is not captured in the kinematic approach, which assumes that all rebars are yielding and checks the concrete compression zone only. Reinforcement detailing (e.g. mandrel diameters or anchorage length) is considered to be adequate and therefore not considered in the calculation. This might be another reason for the large differences.

- The investigated series of concrete half-joint are mainly built with a relatively low concrete strength ($f_{ck} = 30 - 35$ [N/mm^2]) and a normal yield strength of the reinforcement ($f_{yk} = 400 - 500$ [N/mm^2]). In combination with the high sensitivity for concrete strength and the presence of CTT nodes, the differences in results can be explained.

5.7.2 Corroded concrete half-joints.

The upper-bound and lower-bound solutions of the analytical analysis for corroded concrete half-joints are elaborated in this paragraph. The influence of corrosion is distinguished in reduction of cross-sectional only and in combination with the yield-strength.

Geldermalsen

The concrete half-joint can be categorised as Category A2. The design load bearing capacity is calculated using: $f_{cd} = 20$ [N/mm^2] and $f_{yd} = 330$ [N/mm^2]. Figure 5.33 illustrates the design load bearing capacity for different corrosion rates:

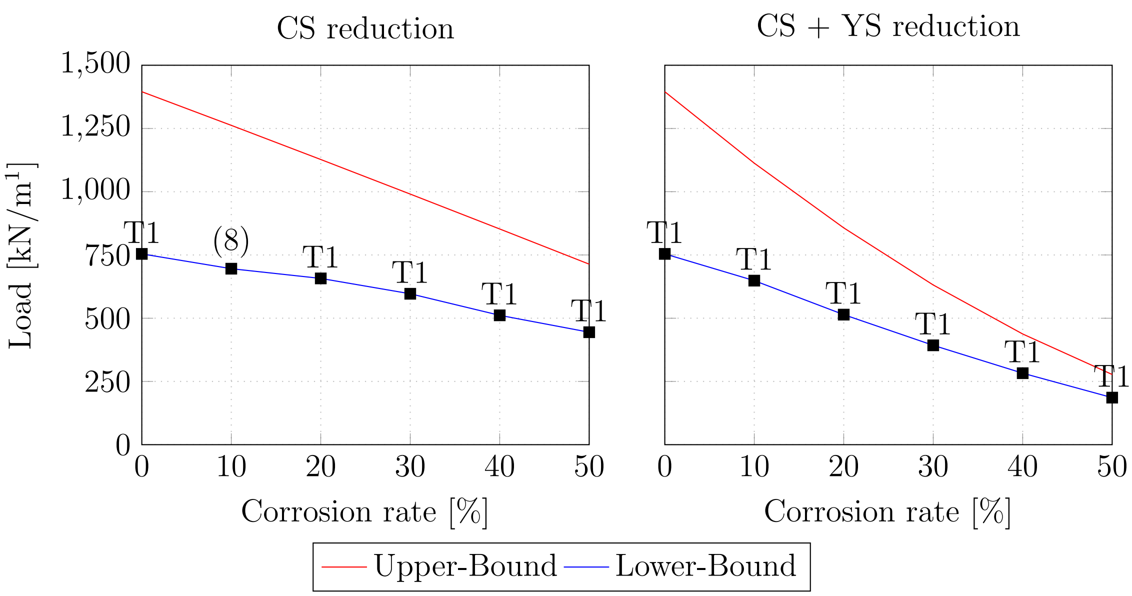

Figure 5.33: Analytical results for ´Geldermalsen´

Postweg

The concrete half-joint can be categorised as Category B2-1. The design load bearing capacity is calculated using: $f_{cd} = 23.3$ [N/mm^2] and $f_{yd} = 435$ [N/mm^2]. Figure 5.34 illustrates the design load bearing capacity for different corrosion rates:

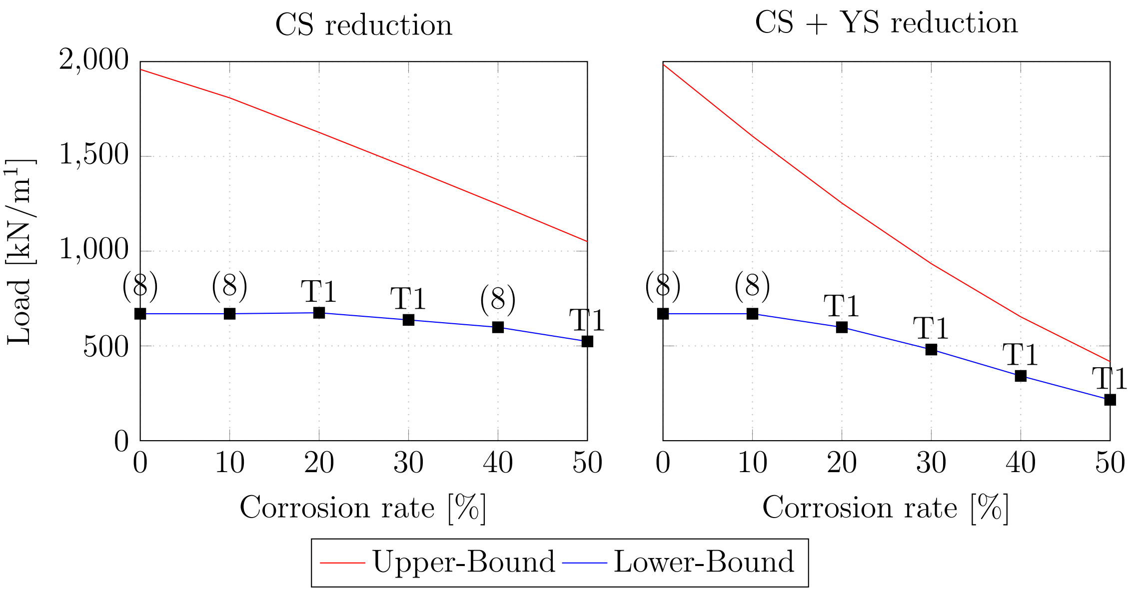

Figure 5.34: Analytical results for ´Postweg´

Purmerend

The concrete half-joint can be categorised as Category A1. The design load bearing capacity is calculated using: $f_{cd} = 20$ [N/mm^2] and $f_{yd} = 330$ [N/mm^2]. Figure 5.35 illustrates the design load bearing capacity for different corrosion rates:

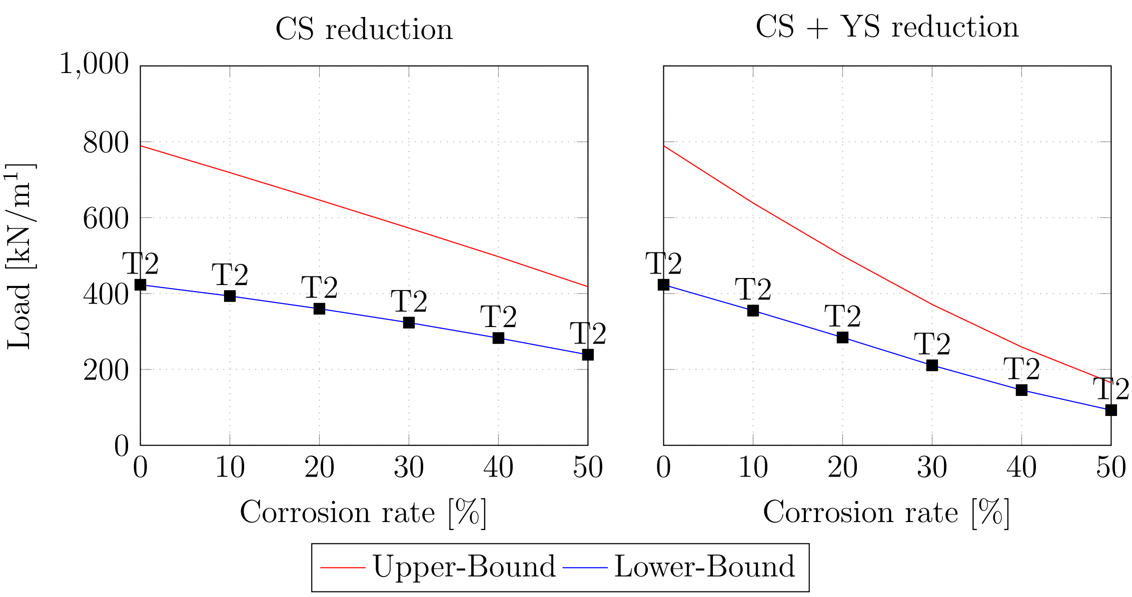

Figure 5.35: Analytical results for ´Purmerend´

Tegelen

The concrete half-joint can be categorised as Category B2-1. The design load bearing capacity is calculated using: $f_{cd} = 23.3$ [N/mm^2] and $f_{yd} = 435$ [N/mm^2]. Figure 5.36 illustrates the design load bearing capacity for different corrosion rates:

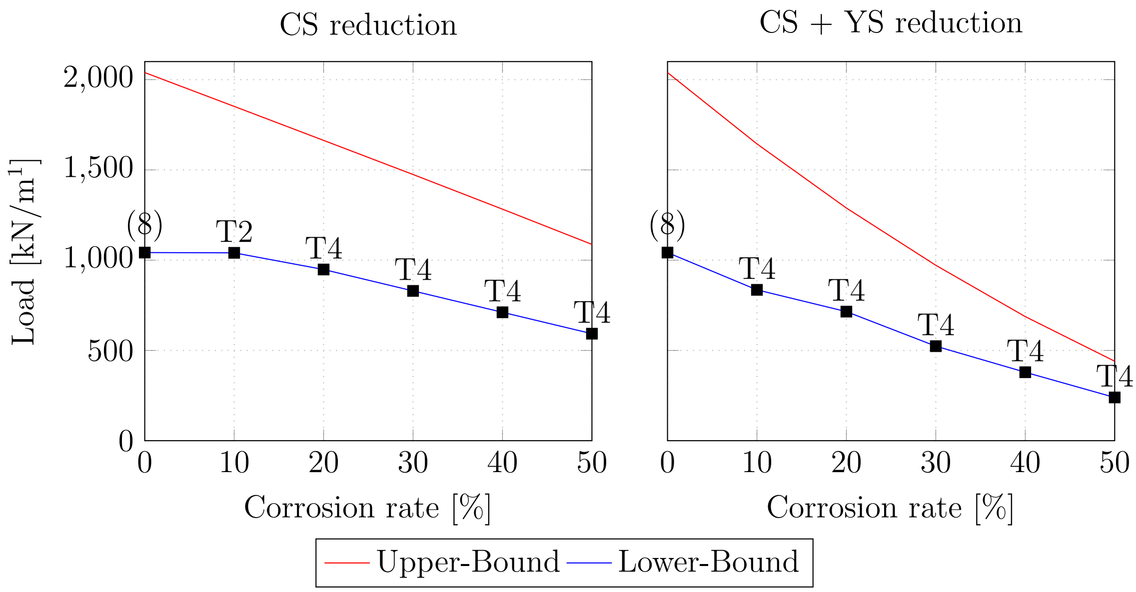

Figure 5.36: Analytical results for ´Tegelen´

Deventer-Bathmen

The concrete half-joint can be categorised as Category A2. The design load bearing capacity is calculated using: $f_{cd} = 23.3$ [N/mm^2] and $f_{yd} = 330$ [N/mm^2]. Figure 5.37 illustrates the design load bearing capacity for different corrosion rates:

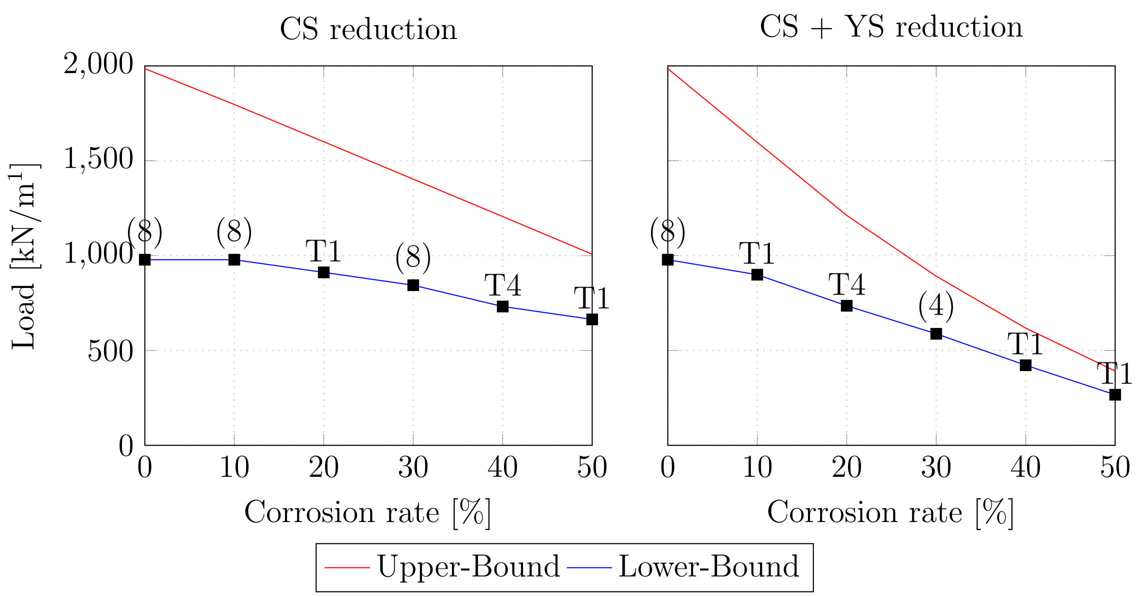

Figure 5.37: Analytical results for ´Deventer-Bathmen´

The following observations and conclusions can be drawn from the analytical analyses of the corroded concrete half-joints:

- The kinematic approach appears to be more vulnerable for load bearing capacity loss due to corrosion than the strut-and-tie approach.
- The load bearing capacity loss in the kinematic approach is linear in the case of only cross-sectional area reduction and quadratic in the combination with yield-strength reduction.
- The load bearing capacity loss in the strut-and-tie approach is less trivial. Due to redistribution of the forces over the struts and ties, it is possible that the load bearing capacity loss is not linear or quadratic. If the concrete strength governs in the strut-and-tie approach, the load bearing capacity loss due to corrosion is minimal. Especially in the cases of ´Postweg´, ´Tegelen´ and ´Deventer-Bathmen´. The loss in those cases appears to be slightly bi-linear in case of cross-sectional reduction only.

Additional sensitivity study

The lower-bound solutions of ´Postweg´, ´Tegelen´ and ´Deventer-Bathmen´ appear to be heavily punished by the low concrete strength and therefore Node (2) and (8) are vulnerable. The solutions were calculated using their original design values. However, it is expected that the concrete strength increased over the years. This would lead to a higher concrete strength and possibly a higher lower-bound solution. Additionally, the dimensions of Nodes (2) and (8) are sensitive to the mandrel diameters and inclination of the strut. Some can say, that the modelling of these nodes is too conservative and the dimensions should be increased.

Therefore, two additional analytical analyses have been performed to study the sensitivity on concrete strength and Nodes (2) and (8). The case of ´Deventer-Bathmen´ will be used, as there is no pretensioning present and concrete governs the load bearing capacity and only a cross-sectional area reduction will be applied. In the first analysis, it is assumed that the characteristic compressive strength of the concrete increased from 35 towards 50 [N/mm^2], from which a design value can be obtained as 33.3 [N/mm^2] (k_t = 1 for educational reasoning). In the second analysis, the checks of Node (2) and (8) are ignored in the strut-and-tie calculation. The results are shown in Figure 5.38:

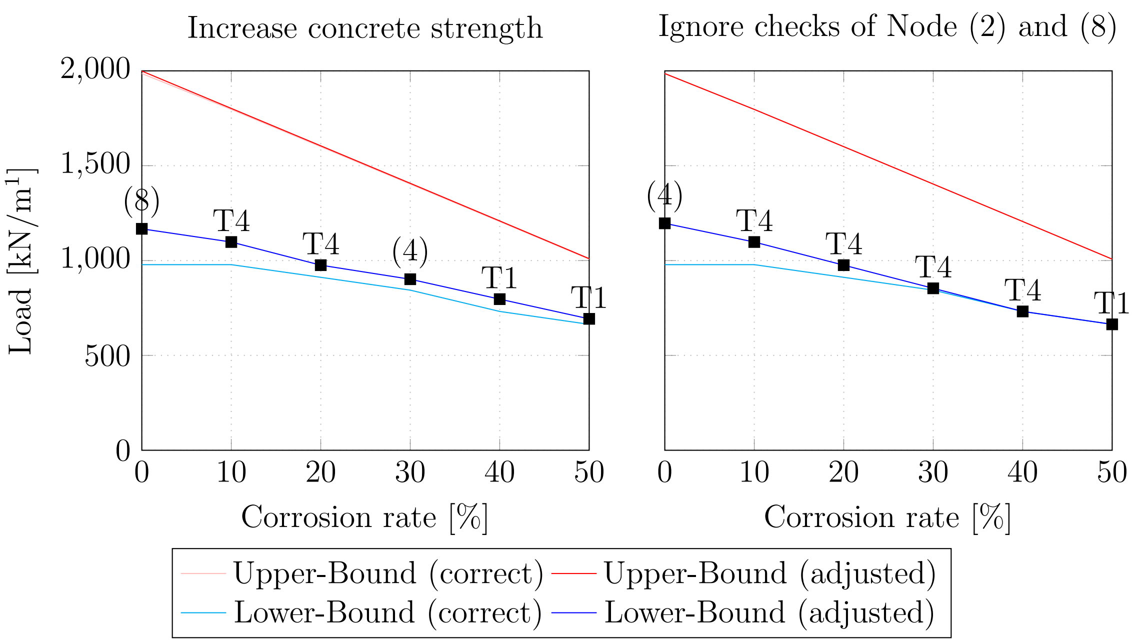

Figure 5.38: Additional analytical results for ´Deventer-Bathmen´

It can be observed that the upper-bound solutions are hardly affected by the increase in concrete strength or ignoring of Node (2) and (8). However, the load bearing capacity increased for the lower-bound solution with approximately 20% for both uncorroded cases. Nevertheless, the differences decreased as the corrosion rate increased.

Chapter 6

Numerical verification

6.1 Introduction

A numerical study is performed using DIANA FEA 10.5 to analyse the structural behaviour and to verify the analytical results of a Category A1 and A2 half-joint. Concrete half-joints with prestressing are not covered in this chapter.

6.2 Description of cases

The dimensions of the Category A1 and A2 half-joint are based on the specimen of the numerical- and experimental study of Desnerck et al. [9], [5], [11], [23], which is already elaborated in paragraph 2.5.2 and Figure 2.17. Figure 6.1 illustrates the dimensions and reinforcement layout of the analysed Category A2 half-joint of this chapter.

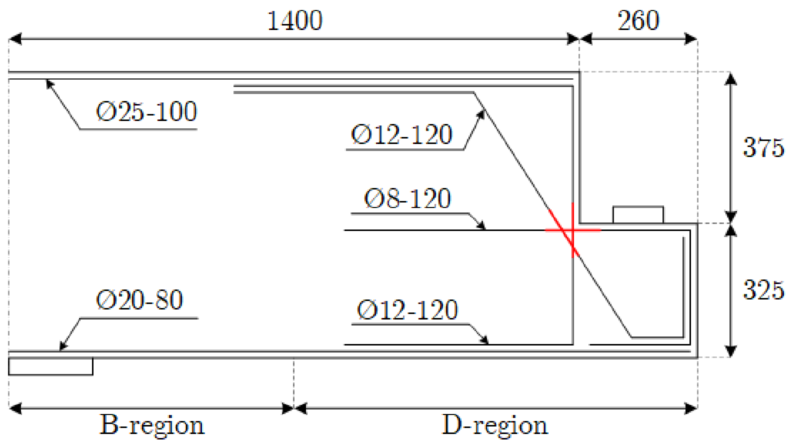

Figure 6.1: Dimensions and reinforcement layout of Category A2 half-joint

The dimensions and reinforcement layout of the Category A1 half-joint are similar, but reinforced without diagonal rebar.

The reinforcement layout of [23] is adjusted to agree the Category A1 and A2 half-joint. The first three hanger-stirrups of are replaced by hanger-rebars in the numerical study and the other stirrups are removed. Additionally, the diameter of the diagonal rebar is reduced to capture the cooperation between the two strut-and-tie models elaborated in paragraph 5.4.

The material properties are adjusted to meet the results of the archive study. Desnerck et al. [23] used a cubic concrete compressive strength of 50.8 [N/mm^2] and a yield strength between 539-578 [N/mm^2]. For the analytical- and numerical study, a concrete quality of C45/55 and reinforcement yield strength of 400 [N/mm^2] are used, which are comparable to the concrete half-joints found in the archive study. Table 6.1 provides the material properties used in the numerical study.

Table 6.1: Material properties

Concrete		
f_c	53	[N/mm^2]
f_{ct}	3.80	[N/mm^2]
E_c	36283	[N/mm^2]
ν	0.2	[-]
G_F	0.104	[Nmm/mm^2]
G_C	31.66	[Nmm/mm^2]

Reinforcement		
f_y	400	[N/mm^2]
f_u	400	[N/mm^2]
E_s	200000	[N/mm^2]
ν	0.3	[-]
ε_y	0.002	[-]
ε_u	0.05	[-]

6.3 Finite element modelling

The numerical study is performed in accordance with ´RTD - Guidelines for Nonlinear Finite Element Analysis of Concrete Structures´ [50] (referred to as RTD).

6.3.1 Finite elements

The concrete is modelled as two-dimensional quadratic plane stress elements. The reinforcement is modelled as bond-slip reinforcement or embedded reinforcement. Bond-slip reinforcement allows relative slip to the continuum element (or ´mother-element´) and is connected to the continuum elements with interface elements. The bond-slip reinforcement is discretised as truss-elements and therefore only captures axial behaviour. Embedded reinforcement allows no relative slip and also captures axial behaviour only.

6.3.2 Material models

Concrete

The concrete is modelled using a total strain-based rotating crack model. The linear-elastic material properties of the concrete are based on the Young's modulus and Poisson ratio. The Poisson ratio is reduced based on damage (cracking).

The tensile softening behaviour of the concrete is based on a smeared cracking approach. RTD suggests Hordijk's tension softening curve [50], [51]. After reaching the ultimate tensile strain ε_u, the tensile resistance is equal to zero. Figure 6.2 illustrates the stress-strain relationship of Hordijk's tension softening curve:

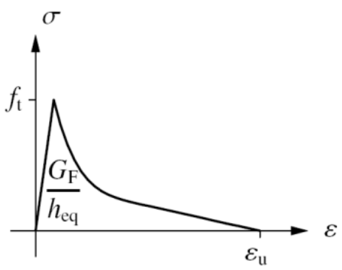

Figure 6.2: Hordijk's tension softening curve [51], [52]

The area under the stress-strain curve is equal to the tensile fracture energy divided by the equivalent length (crack-band width). RTD suggests the Govindjee's Projection method [53], which calculates the crack-band width dependent on the orientation of the crack [52]. This method is also used in the numerical analyses.

The compressive softening behaviour is based on a parabolic compressive curve with softening branch.

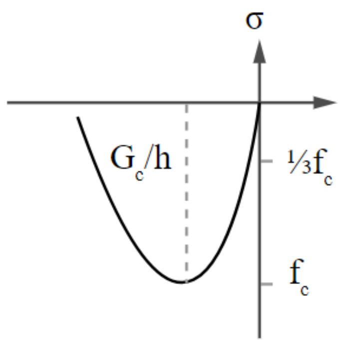

Figure 6.3: Parabolic compressive softening curve [52]

A reduction in compressive strength resulting from lateral cracking needs to be taken into account in accordance with RTD art. 2.4.1.5. The tension-compression interaction can be modelled using a reduction model, which is based on a reduction coefficient for compressive strength: β_{cr}. The model from Vecchio and Collins 1993 [54] is suggested by RTD and will be used with a lower-bound reduction coefficient of: $\beta_{cr}^{min} = 0.4[-]$

Reinforcement

The material model for the reinforcement is based on an elasto-plastic model without hardening. The linear-elastic branch is based on the Young's modulus and yield-strength of the reinforcement. The post-yielding behaviour is modelled as perfectly plastic (no hardening).

Concrete/reinforcement interaction

The interaction between concrete and reinforcement can be modelled as perfect bond (no relative slip) or using a bond-slip failure model. For the later one, RTD suggests the bond-slip relation from *fib* Model Code 2010, which distinguishes bond-slip relations for confined (pull-out failure) and unconfined (splitting failure) concrete. Figure 6.4 illustrates the bond-slip relations used in the numerical study:

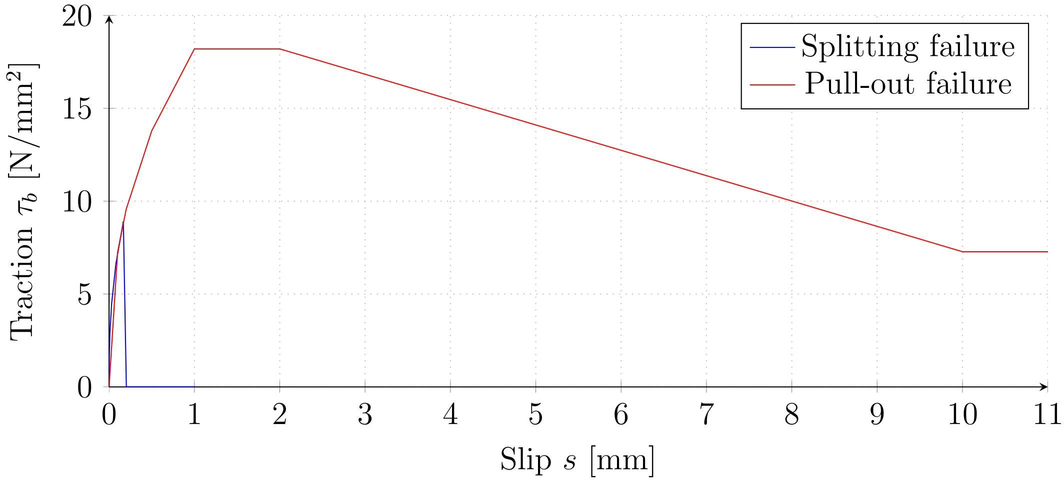

Figure 6.4: Bond-slip relations

Additionally, normal- and shear stiffness modulus must be provided to the interface elements, which are set relatively high such that there is little relative displacement between the concrete and reinforcement. The bond-slip failure model will be used in the sensitivity study on mesh-size and bond-behaviour.

Other interactions, such as tension-stiffening and dowel-action are not considered, which makes the numerical study a conservative approximation.

6.3.3 Corrosion

The corrosion is simulated in a range from 0-50% in steps of 10%. The corrosion is applied locally on the hanger-rebar and horizontal rebar (and diagonal rebar). The length over which the corrosion is applied is elaborated in further depth in paragraph 6.6.1. Table 6.2 elaborates the material properties and Table 6.3 the geometries of the corroded rebars.

Table 6.2: Material properties for corroded rebars

	Corrosion rate						Units
	0%	10%	20%	30%	40%	50%	
f_y	400	351	302	252	203	154	[N/mm^2]
ε_u	0.05	0.044	0.038	0.031	0.025	0.019	[-]

Table 6.3: Geometries for corroded rebars

		Corrosion rate						Units
		0%	10%	20%	30%	40%	50%	
Ø8	A_s	419	377	335	293	251	209	[mm^2]
	u_s	209	188	168	147	126	105	[mm]
Ø12	A_s	942	848	754	660	566	471	[mm^2]
	u_s	314	283	251	220	189	157	[mm]

In which:

u_s is the circumference of the residual cross-sectional area of (un)corroded rebar

6.3.4 Model, constraints and load

The concrete half-joint is constraint in horizontal direction at the edge of the boundary and vertically at the bottom of the boundary. The half-joint is loaded with a prescribed vertical displacement of 1 [mm] at the loading plate. Figure 6.5 illustrates the boundary conditions and load of the numerical study:

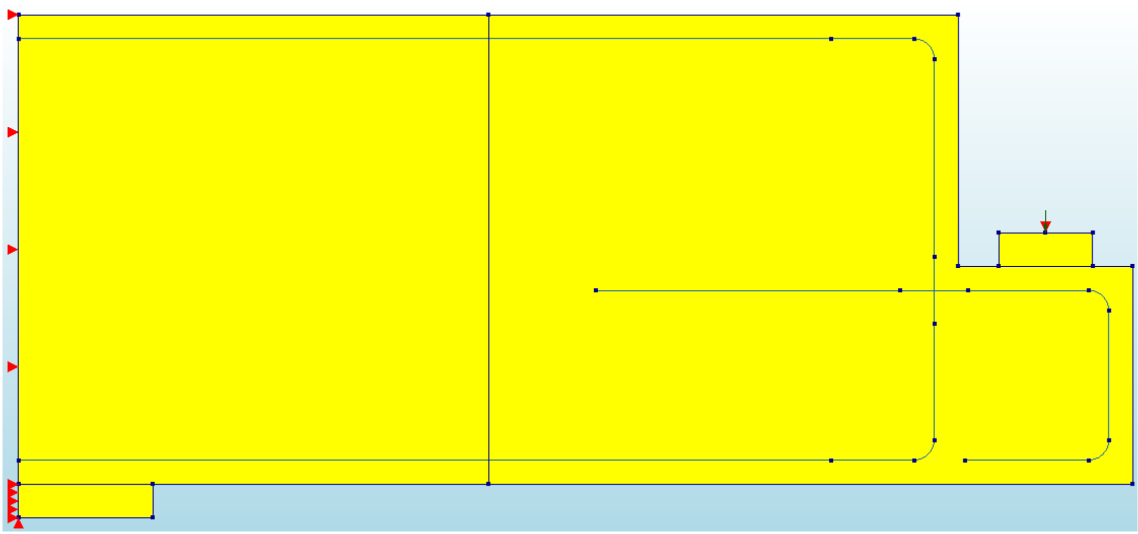

Figure 6.5: Model, constraints and load

The concrete is split in two parts (see Figure 6.1), as we are only interested in the behaviour in the discontinuous region. The continuous region (left) is modelled with elastic material properties and the discontinuous region with nonlinear material properties.

6.3.5 Analysis

The numerical study is executed with the following solution parameters:

Load incremention:	Different for each analysis	
Equilibrium iteration:	150 iterations (maximum)	
	Regular Newton-Raphson method	
Convergence criteria (or):	Force norm:	0.01
	Energy norm:	0.001

6.4 Base-model

A base-model is modelled for a Category A1 half-joint, in which all further analyses are calculated with small adjustments. This paragraph elaborates the input for the base-model and results of the analysis.

6.4.1 Input

The base-model for the numerical study contains the following properties:

Mesh (elastic part):	25 [mm]
Mesh (nonlinear part):	10 [mm]
Bond-slip:	Perfect bond
Corrosion:	No corrosion

6.4.2 Results

The results of the analysis of the base-model are elaborated in this paragraph. The analytical analysis provided an upper-bound solution of 442.2 [kN/m^1] and a lower-bound solution of 307.1 [kN/m^1].

Load-displacement diagram

Figure 6.6 elaborates the load-displacement diagram of the numerical analysis for the base-model. Four characteristic points are indicated in the diagram. The loads and displacements of these points are shown in Table 6.4.

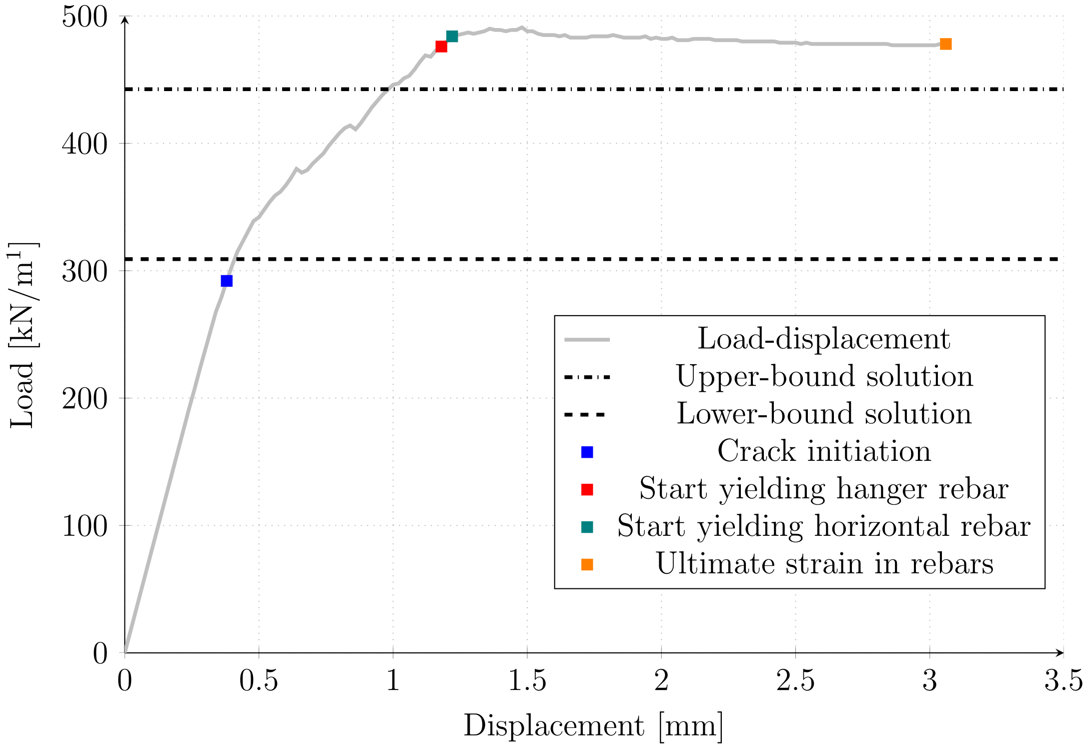

Figure 6.6: Load-displacement diagram of base-model

Table 6.4: Characteristic points in base-model

Characteristic points	**Load** [kN/m^1]	**Displacement** [mm]
Crack initiation	291.9	0.38
Start yielding hanger rebar	475.9	1.18
Start yielding horizontal rebar	483.9	1.22
Ultimate strain in rebar	477.6	3.06

Stress fields/diagrams & crack patterns

The stress fields/diagrams and crack patterns of the results for three characteristic point are illustrated below. The start yielding of hanger- and horizontal rebar are combined, as the point are close to each other.

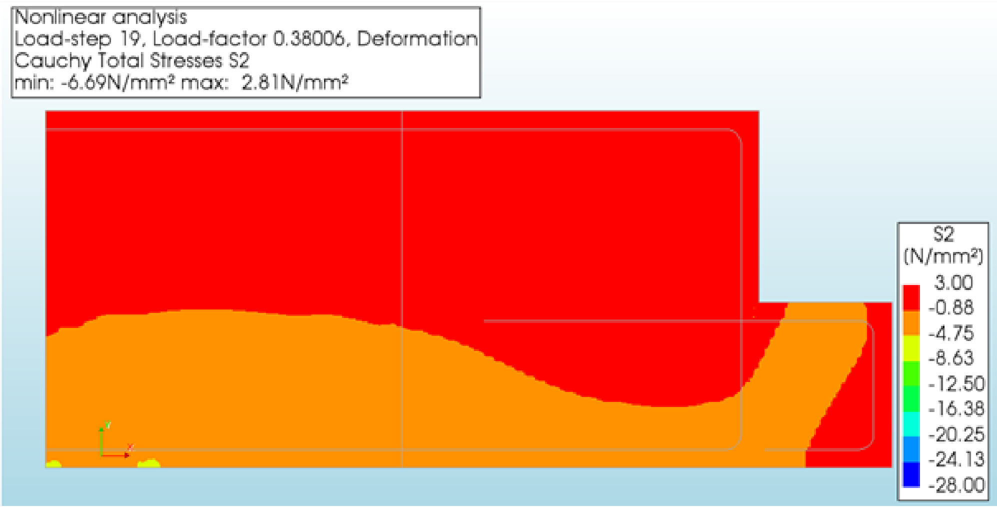

(a) Loadfactor 0.38 (Loadstep 19)

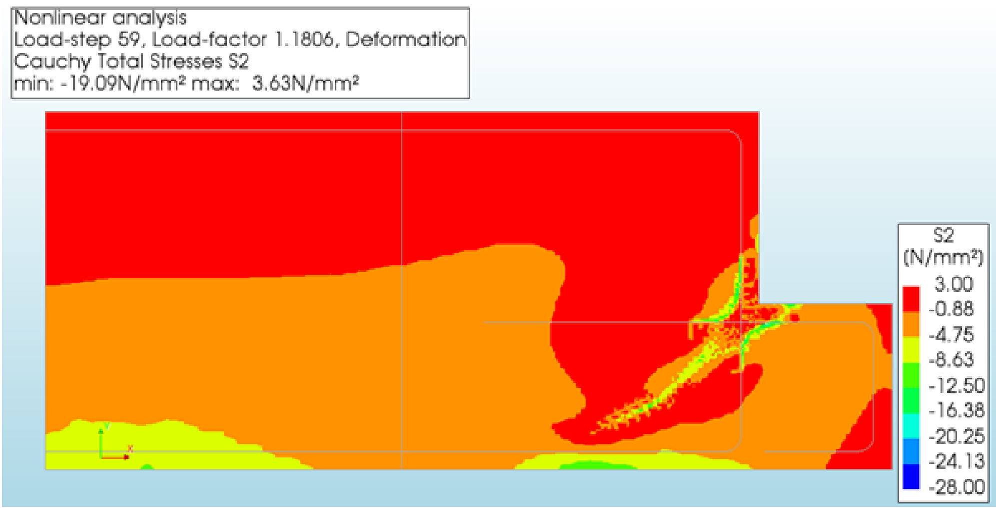

(b) Loadfactor 1.18 (Loadstep 59)

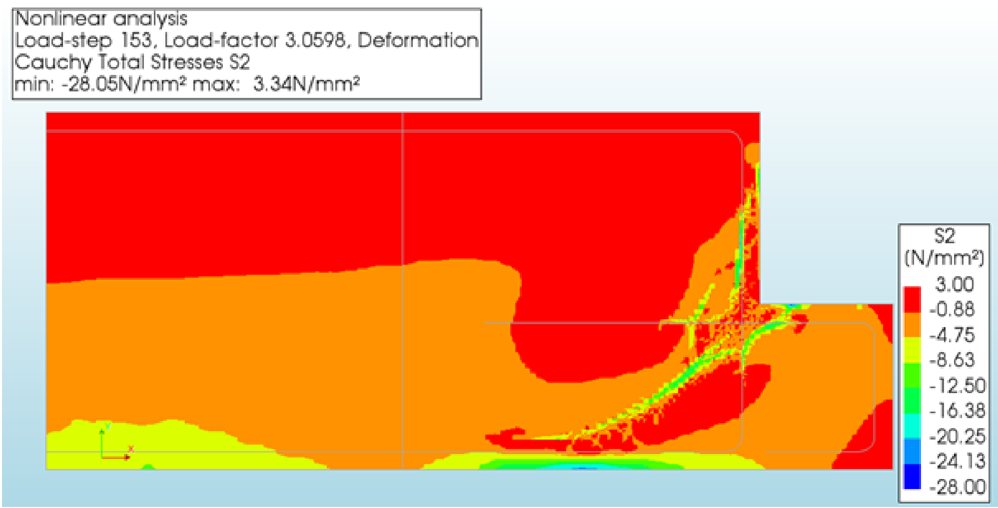

(c) Loadfactor 3.06 (Loadstep 153)

Figure 6.7: Minimum stress of concrete

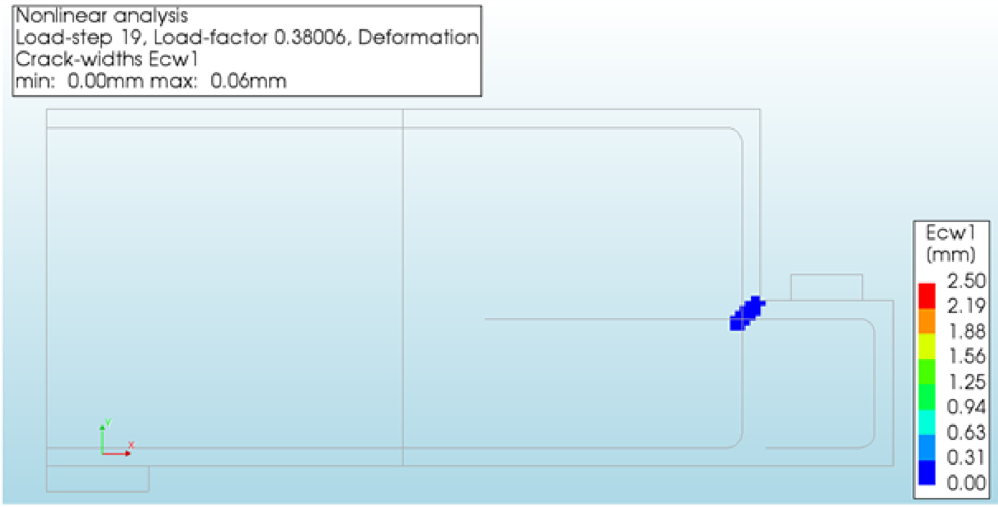

(a) Loadfactor 0.38 (Loadstep 19)

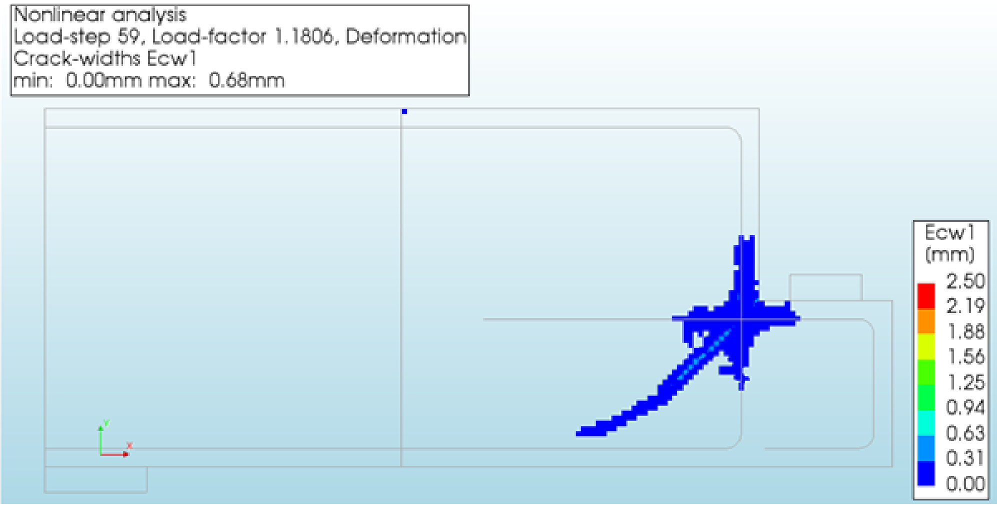

(b) Loadfactor 1.18 (Loadstep 59)

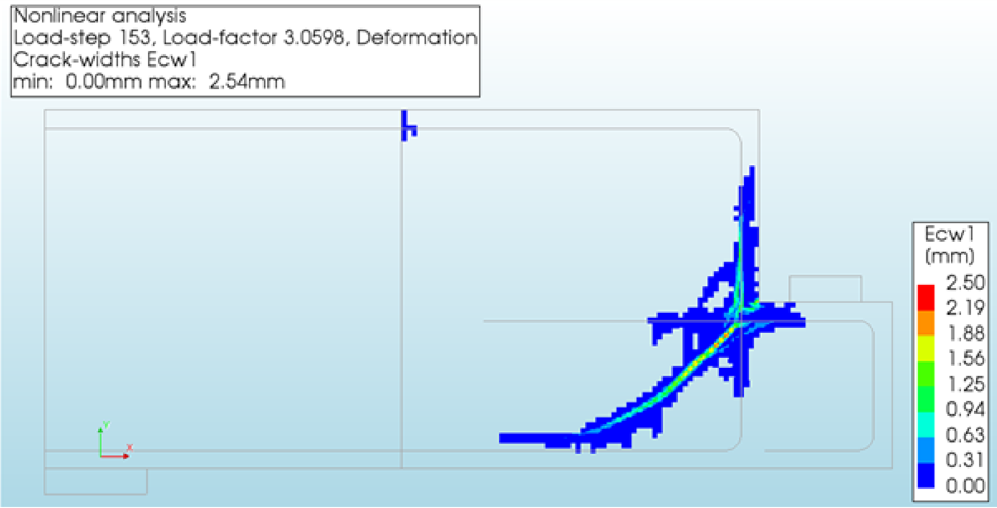

(c) Loadfactor 3.06 (Loadstep 153)

Figure 6.8: Crackwidth of concrete

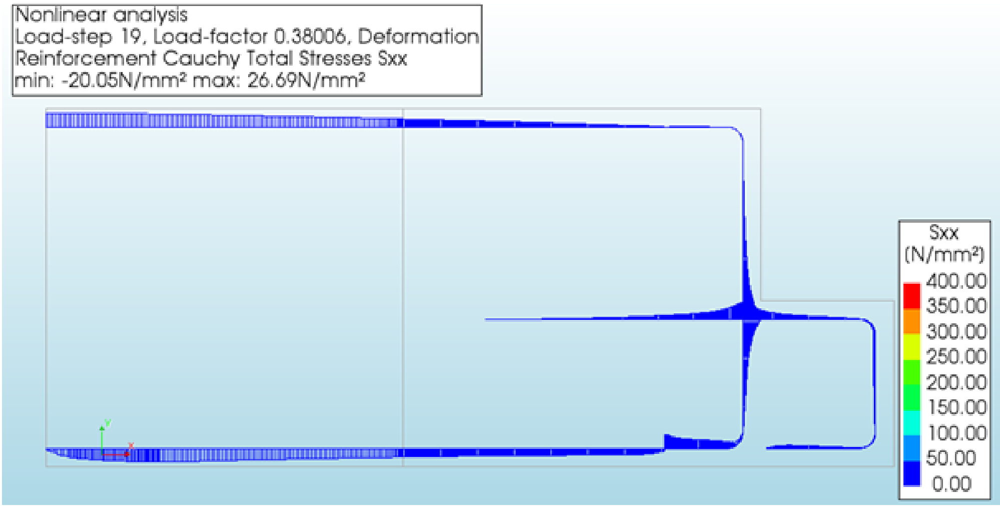

(a) Loadfactor 0.38 (Loadstep 19)

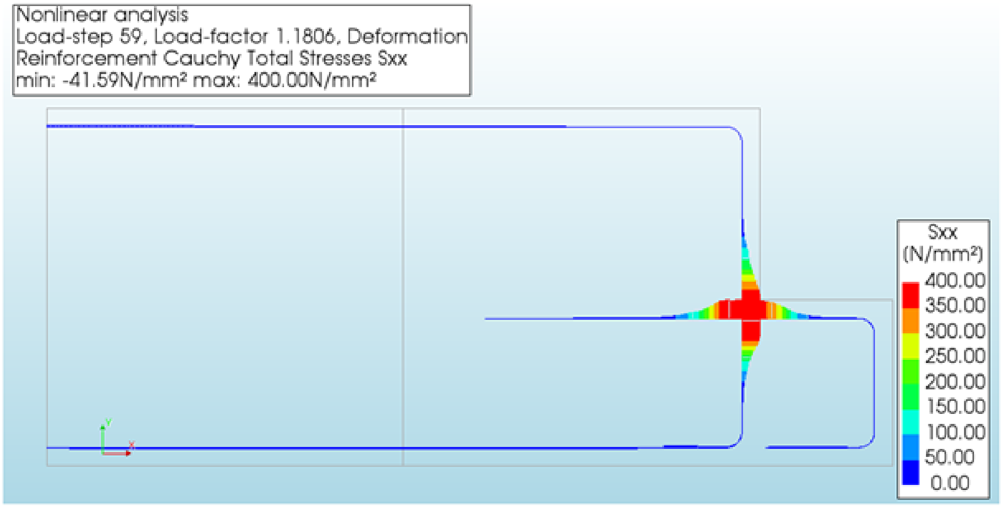

(b) Loadfactor 1.18 (Loadstep 59)

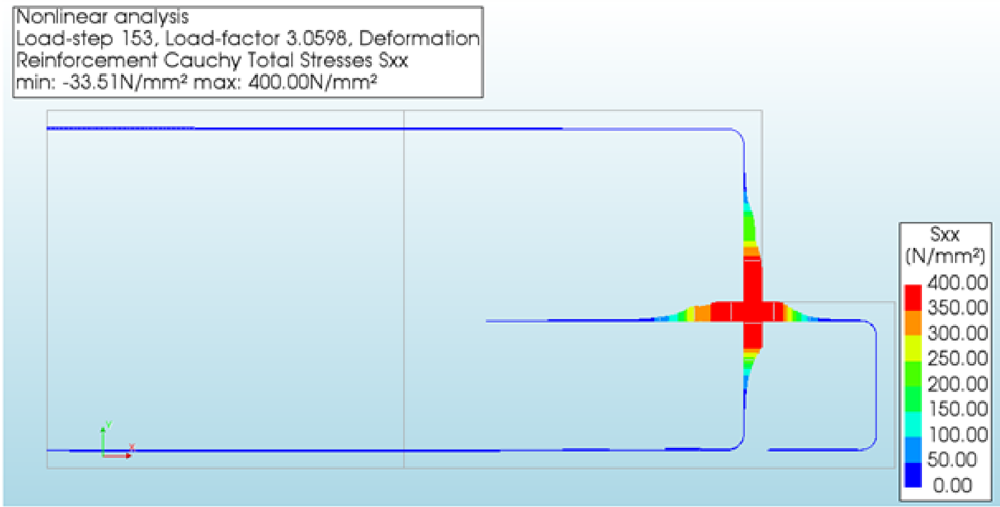

(c) Loadfactor 3.06 (Loadstep 153)

Figure 6.9: Stress in reinforcement

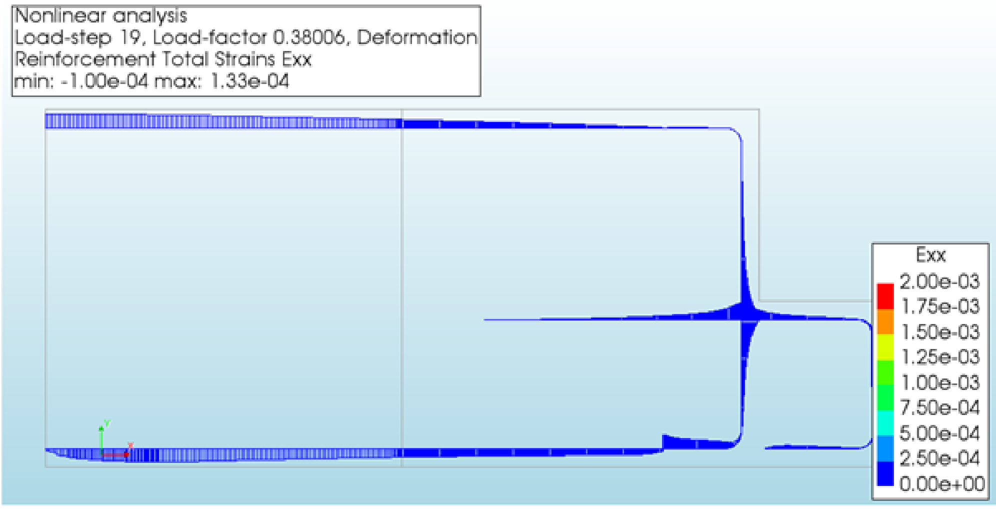

(a) Loadfactor 0.38 (Loadstep 19)

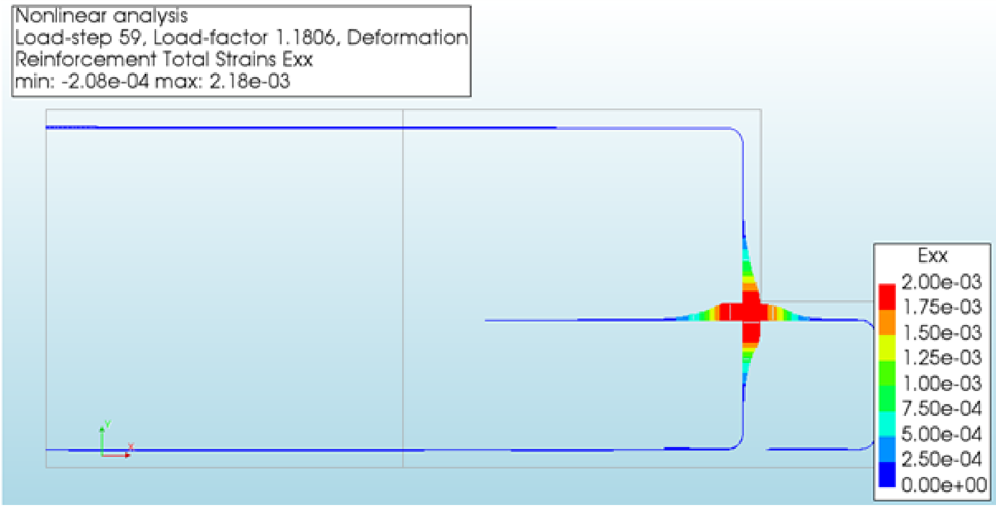

(b) Loadfactor 1.18 (Loadstep 59)

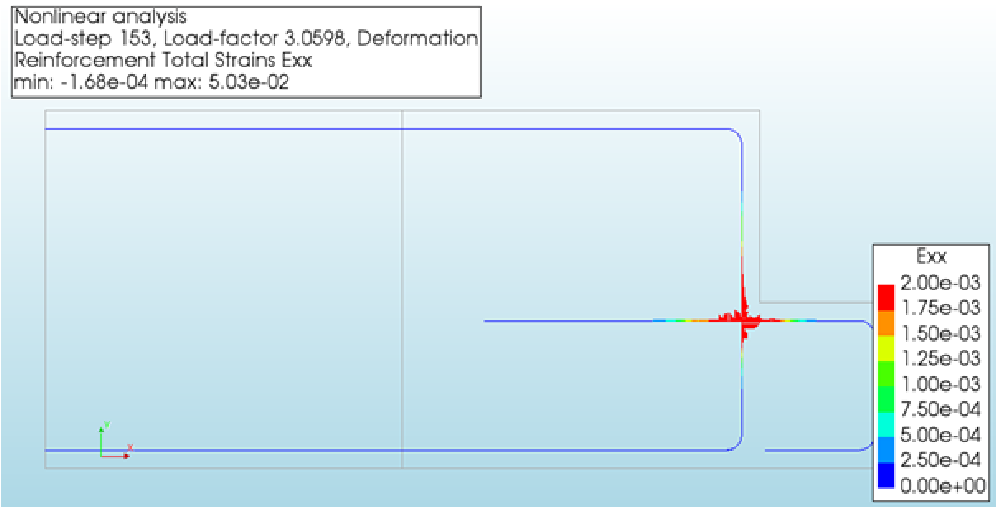

(c) Loadfactor 3.06 (Loadstep 153)

Figure 6.10: Strain in reinforcement

6.4.3 Discussion

Load at crack initiation

It can be observed from Figure 6.6 that the diagonal crack initiates at 60% of the ultimate load, which is much higher than expected. In the experimental study of Desnerck et al. [5], the diagonal crack initiated at 27-42% of the ultimate load for different reinforcement layouts. Similar results have been found by experiments from Wang et al. [6] (13-45%). However, the material properties in this case are adjusted to meet the materials from the archive study. The material properties for the concrete were comparable to the experimental study of Desnerck [5], but the yield strength of the rebars is significantly less. Therefore, the load at crack initiation is not affected, but the ultimate load is.

Load at start yielding

It can be observed from Figure 6.6 that the hanger- and horizontal rebars yield at almost the same load, which is the consequence of the geometries and material properties of the concrete half-joint and reinforcement. The behaviour can be different for different geometries and/or material properties.

It can be observed from Figure 6.7(b) & Figure 6.9(b) that when the rebars starts to yield, the concrete did not reached its compressive strength yet. This indicates that the rebars yield before the concrete crushes.

Load at ultimate strain

After the hanger- and horizontal rebars yield, the load-displacement reaches a plateau. The material model for the reinforcement is modelled as perfectly plastic after yielding, which can also be observed in the load-displacement diagram. The load between yielding and reaching ultimate strain does not significantly change. The diagonal crack-length did also not increase further after the reinforcement started to yield. Only the crack-width increased.

The failure mechanism in the base-model is rupture (reaching ultimate strain) of the hanger-rebar. The strain in the horizontal rebar is 60 [%] of the ultimate strain (0.03 [-]) and the compressive stress in the concrete is 53 [%] of the compressive strength (53 [N/mm^2].

Comparison with lower-bound solution

The lower-bound solution (strut-and-tie approach) is lower than the numerical solution, which is expected. The tensile strength of hanger-rebar is governing for the lower-bound solution, which is also the failure mechanism in the numerical analysis.

Comparison with upper-bound solution

The upper-bound solution (kinematic approach) is also lower than the numerical solution, which is not expected. The difference between the numerical solution and upper-bound solution is 7%. The kinematic approach uses a crack's angle over a range of 30°-70°. The governing crack's angle is 30° in the analytical tool. However, Figure 6.8 shows that the crack appears at an angle of approximately 45°.

The kinematic approach is a simplified method, which assumes that all rebars are yielding and no shear stresses are transferred through the concrete compression zone. However, the concrete is able to transfer shear stresses in the numerical model. This could have caused the differences in crack's angle.

If the upper-bound solution is recalculated with an angle of 45° degrees, the solution increased to 469.5 [kN/m^1]. The difference between the numerical solution is now reduced to 2%, which is a much better approximation. In further calculations, the upper-bound solution will be analysed using the kinematic approach with a range of crack's angles and the crack's angle of the numerical analysis.

6.5 Sensitivity study

This chapter elaborates the influence of mesh-size and bond-behaviour on the load bearing capacity and deformation capacity.

6.5.1 Input

The bond-behaviour is distinguished in a ´perfect bond´-model and ´bond-slip´-model. In the ´perfect bond´-model, there is no bond-slip failure and the bond-behaviour only depends on the stiffness of the interface. In the ´bond-slip´-model, the bond-slip failure is modelled as discussed in paragraph 6.3.2. Figure 6.11 illustrates, which bond-slip relation is applied on each rebar in the model:

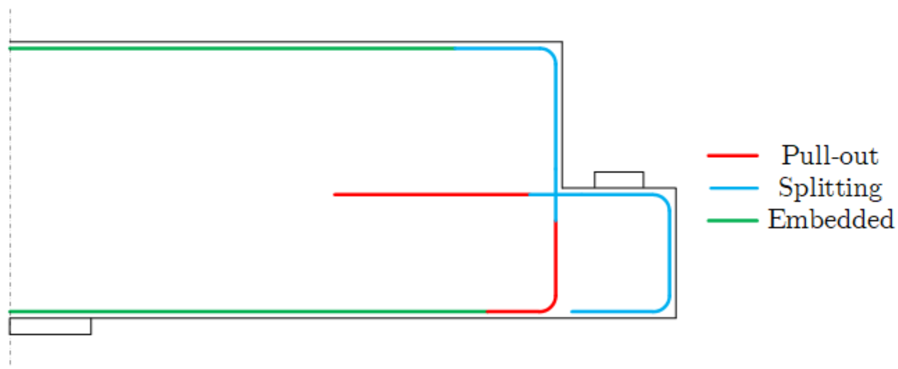

Figure 6.11: Bond-slip relations on rebars

Additionally, it is studied whether the model is mesh dependent by comparing a mesh-size of 10 [mm] with 25 [mm].

6.5.2 Results

The results of the sensitivity study on the base-model are elaborated in this paragraph. For sake of clearness, the analytical results are not presented in the graphs. Renderings are provided for the model with a mesh-size of 10 [mm] and bond-slip failure, to compare with the results from the base-model.

Load-displacement

Figure 6.12 shows the load-displacement diagrams for the studied models and Table 6.5 gives the displacement and load at crack initiation of concrete, start yielding and reaching the ultimate strain in the reinforcement.

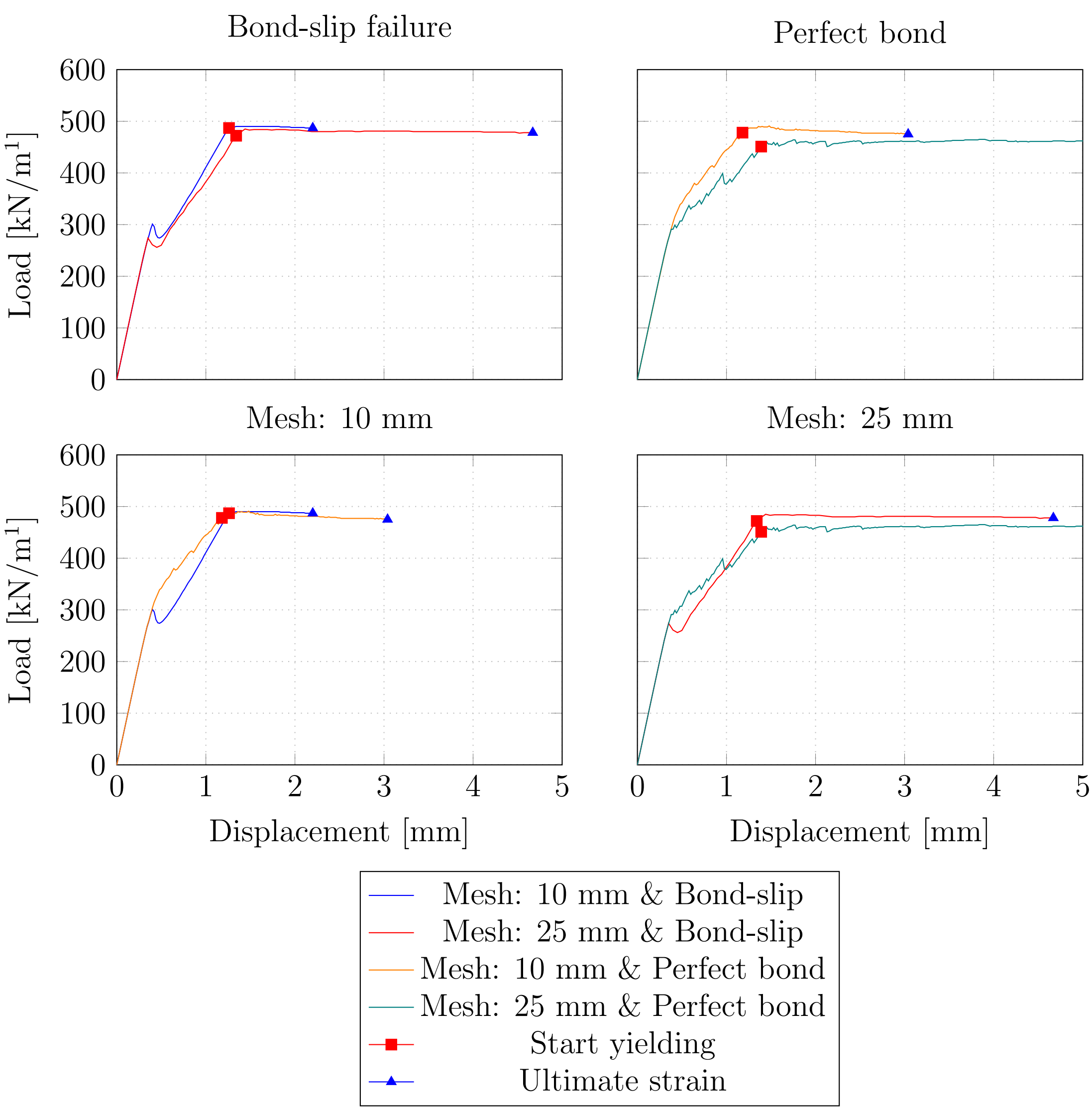

Figure 6.12: Load-displacement diagram of mesh-size and bond-behaviour study

Table 6.5: Results of mesh-size and bond-behaviour study

Analysis	**Crack initiation**		**Start yielding**		**Ultimate strain**	
	Displ. [mm]	Load [kN/m^1]	Displ. [mm]	Load [kN/m^1]	Displ. [mm]	Load [kN/m^1]
Mesh: 10 mm & Bond-slip	0.38	290.7	1.26	487.2	2.20	486.9
Mesh: 25 mm & Bond-slip	0.35	273.9	1.34	471.9	4.67	478.3
Mesh: 10 mm & Perfect bond	0.38	291.9	1.18	475.9	3.06	477.6
Mesh: 25 mm & Perfect bond	0.38	290.9	1.39	450.6	6.46	460.4

Stress diagrams & crack patterns: (Mesh: 10 mm & Bond-slip)

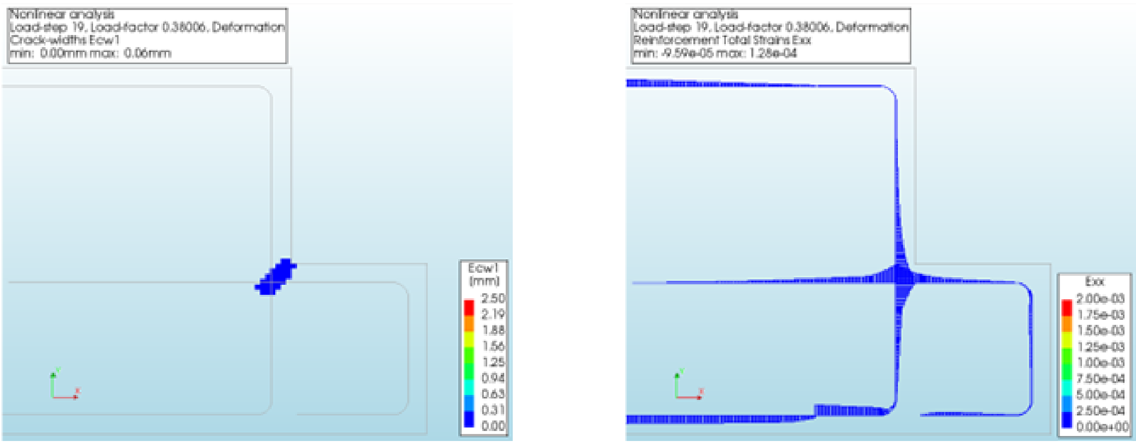

(a) Crackwidth (b) Strain reinforcement

Figure 6.13: Crack initiation of concrete

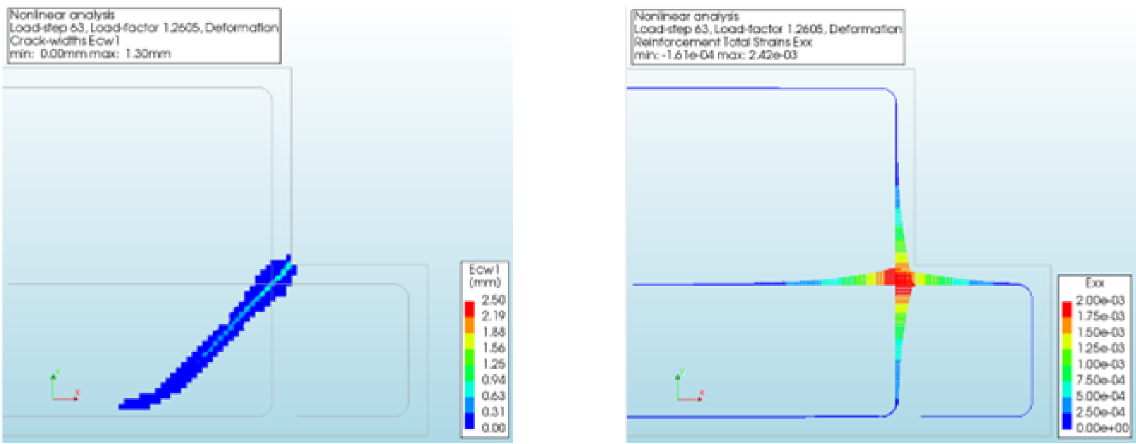

(a) Crackwidth (b) Strain reinforcement

Figure 6.14: Start yielding of reinforcement

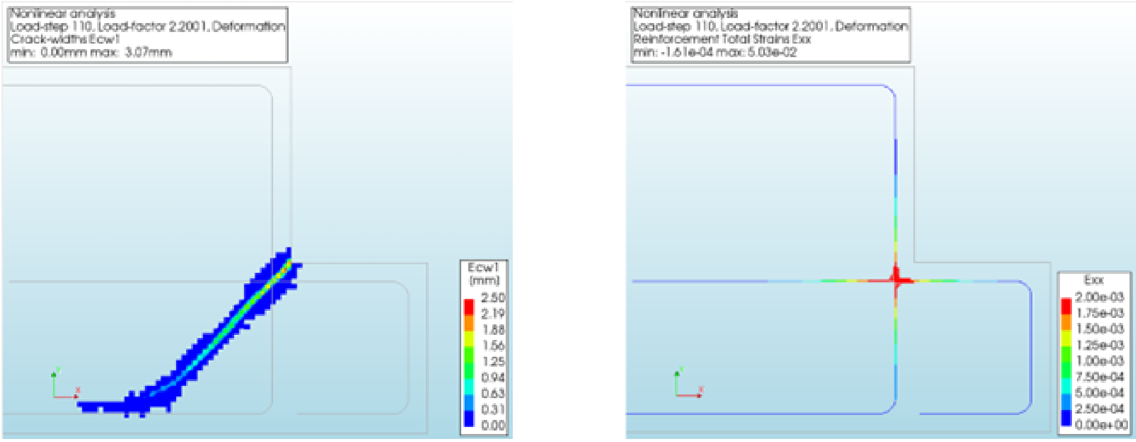

(a) Crackwidth (b) Strain reinforcement

Figure 6.15: Ultimate strain of reinforcement reached

6.5.3 Discussion

Load at crack initiation

The load-displacement diagram in Figure 6.12 for the models with bond-slip failure shows a drop as soon as the diagonal crack initiates in the half-joint. The crack initiation is also captured in the models with perfect bond, but does not show a drop in the load-displacement diagram.

Load at start yielding

As the diagonal crack is formed, the reinforcement starts to yield at approximately the same loads. The crack-width of the bond-slip model is larger than the model with a perfect bond relation. In the model with a perfect bond relation, splitting cracks occur around the hanger- and horizontal rebar. In the model with a bond-slip relation, the reinforcement already slipped.

In the models with mesh-size 25 [mm], the diagonal crack propagates differently than the models with mesh-size 10 [mm]. The crack is more spread around the re-entrant corner for the model with larger mesh-size. The crack in the model with smaller mesh-size is much more localised.

Load at ultimate strain

At reaching the ultimate strain in the reinforcement, the load did not significantly increase compared to the load when the reinforcement started to yield. However, a large difference can be observed at the displacement, in which the reinforcement reaches ultimate strain (deformation capacity). It appears that the deformation capacity reduces if the mesh-size decreases and/or a bond-slip relation is introduced. Figure 6.16 illustrates the strain in the reinforcement of the case with a mesh-size of 10 [mm] and a perfect bond relation vs. bond-slip relation:

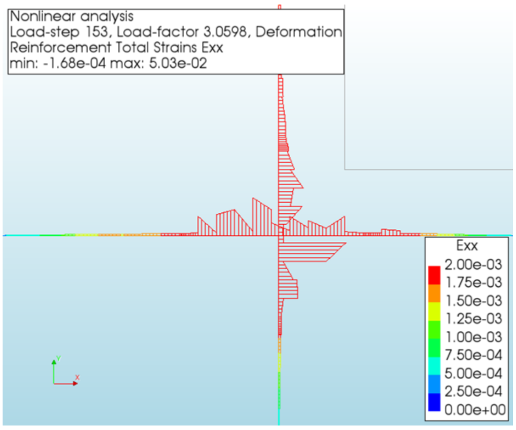

(a) Perfect bond

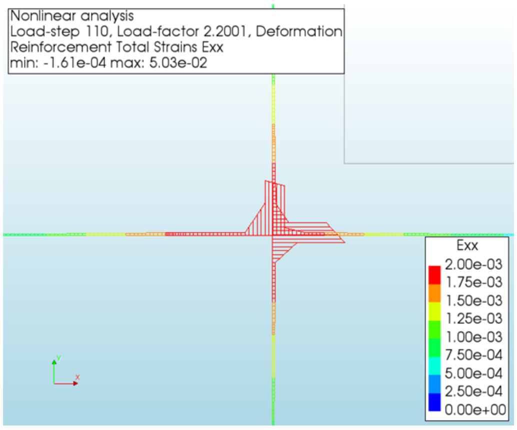

(b) Bond-slip relation

Figure 6.16: Ultimate strain of reinforcement

It can be observed that the strain in the reinforcement is localised at the place where the diagonal crack crosses the reinforcement. For the model with a bond-slip relation, the crack is more localised than for the perfect bond model. For the model with a mesh-size of 25 [mm], the crack is much more spread, which appears to provide larger deformation capacity of the half-joint.

Conclusion

It can be concluded that the models are mesh- and bond-slip dependent, when it comes to deformation capacity (displacement to reach ultimate strain in the reinforcement). The model is only able to predict the load at crack initiation, start yielding of the reinforcement and reaching the ultimate strain in the reinforcement.

The most suitable model appears to be the model with mesh-size 10 [mm] and a perfect bond relation. The diagonal crack is more localised, compared to a model with mesh-size 25 [mm]. The model with a mesh-size 25 [mm] showed a more spread crack pattern, which can lead to problems when corrosion is simulated over a certain length. Additionally, the bond-slip relations are simplified by assuming a perfect bond relation, which have no influence on the characteristic loads (crack initiation, start yielding and ultimate strain) in the load-displacement diagram.

6.6 Corrosion studies

This chapter elaborates the results of the numerical study, in which corrosion is simulated on a part of the reinforcement in the concrete half-joint. First, the influence of corrosion ´length´ is analysed.

Subsequently, an adequate corrosion ´length´ is chosen and applied on a Category A1- and A2 half-joint. The influence of corrosion is split in a simulation with only a reduction of cross-sectional area and one with a reduction of cross-sectional area and yield strength. The reduction in ultimate strain is not taken into account, as the model is not able to predict the deformation capacity.

6.6.1 Corrosion ´length´

This chapter elaborates the influence of the corrosion ´length´ on the load bearing capacity and deformation capacity. The corrosion ´length´ is defined as the part over which the corrosion is present on the rebar and is illustrated in Figure 6.17.

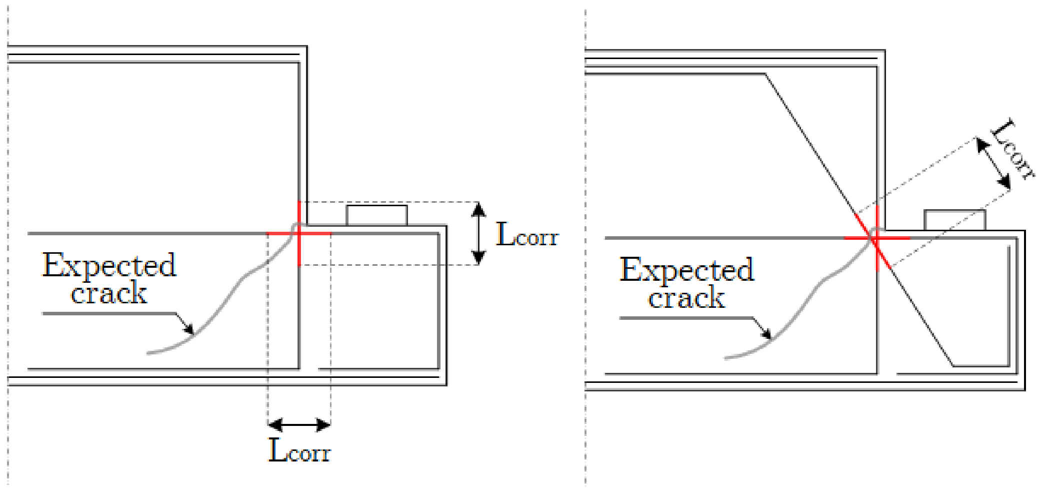

(a) Category A1 (b) Category A2

Figure 6.17: Corrosion lengths

Four different lengths are considered on the base-model (Category A1) to simulate corrosion: 10 [mm], 25 [mm], 50 [mm] and 100 [mm]. The corrosion is simulated by applying a reduction of cross-sectional area for a corrosion rate of 20%.

Results

Figure 6.18 shows the load-displacement diagrams for the studied corrosion ´lengths´ and Table 6.6 gives the displacement and load at crack initiation of concrete, start yielding and reaching the ultimate strain in the reinforcement.

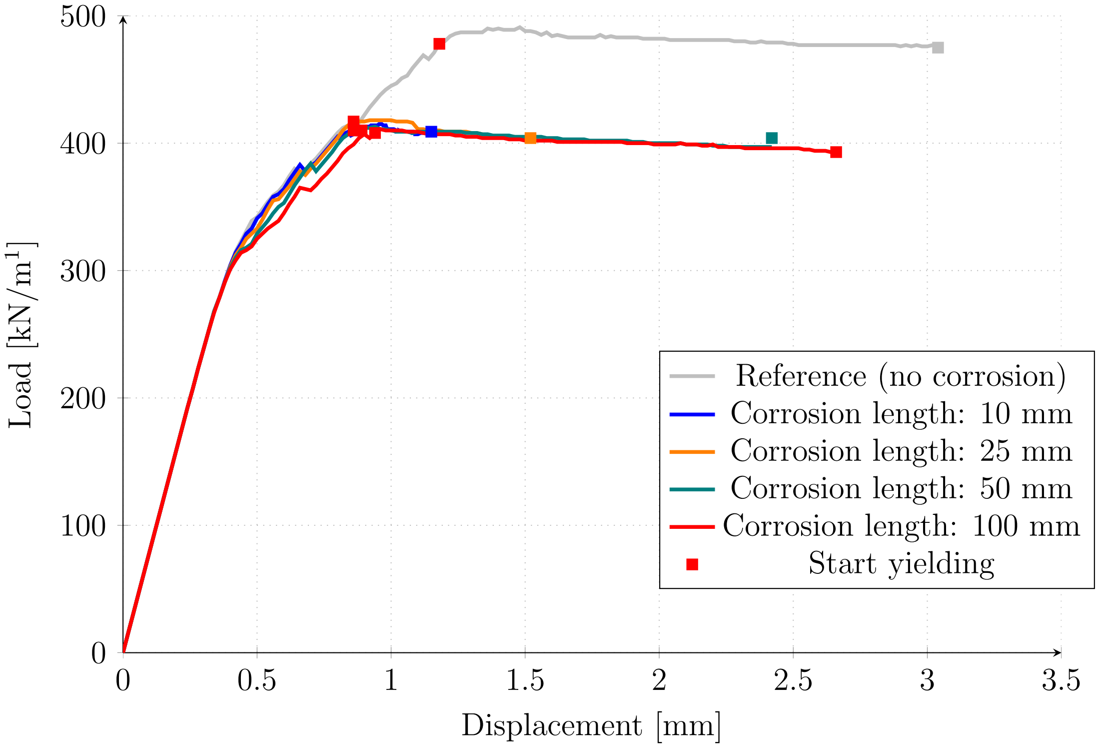

Figure 6.18: Load-displacement diagram of corrosion ´length´ study

Table 6.6: Results of corrosion ´length´ study

Analysis	**Crack initiation**		**Start yielding**		**Ultimate strain**	
	Displ. [mm]	Load [kN/m^1]	Displ. [mm]	Load [kN/m^1]	Displ. [mm]	Load [kN/m^1]
Reference (no corrosion)	0.38	291.9	1.18	475.9	3.06	477.6
20% Corrosion, 10 [mm]	0.38	291.6	0.89	410.1	1.15	409.5
20% Corrosion, 25 [mm]	0.38	291.0	0.86	417.0	1.52	403.8
20% Corrosion, 50 [mm]	0.38	290.8	0.86	410.4	2.42	396.8
20% Corrosion, 100 [mm]	0.38	290.6	0.94	408.3	2.66	393.4

Discussion

It can be observed from Figure 6.18 that the load in which the reinforcement starts to yield is comparable to each other and did not significantly increase until the ultimate load was reached. Again, the deformation capacity is influenced by the corrosion length. The shorter the corrosion length, the shorter the deformation capacity. This is as expected as the corroded part of the rebar is more localised, which makes redistribution of stresses in the rebar more difficult.

The corrosion ´length´ of 10 [mm] showed a peak strain at the transition from corroded to uncorroded rebar, which also led to many computational issues. The peak strain occurred, because the mesh-size is also 10 [mm]. Therefore, it can be stated that the corrosion ´length´ needs to be at least larger than the mesh-size in the numerical model.

The study of Ou et al. [35], which have been used to determined mechanical properties of corroded rebars, used a gauge length of 8 times the diameter of the rebar. The diameter of the hanger-rebar and horizontal rebar is 12 [mm], which corresponds with a gauge length of 96 [mm]. It makes sense to use approximately the same length for simulating the corrosion in the numerical study. Therefore, the corrosion ´length´ of 100 [mm] will be used in further analyses.

6.6.2 Category A1

Cross-sectional reduction

The load-displacement diagrams of the Category A1 half joint with a cross-sectional reduction due to corrosion is illustrated in Figure 6.19. Additional stress diagrams and crack patterns are provided in Appendix D.

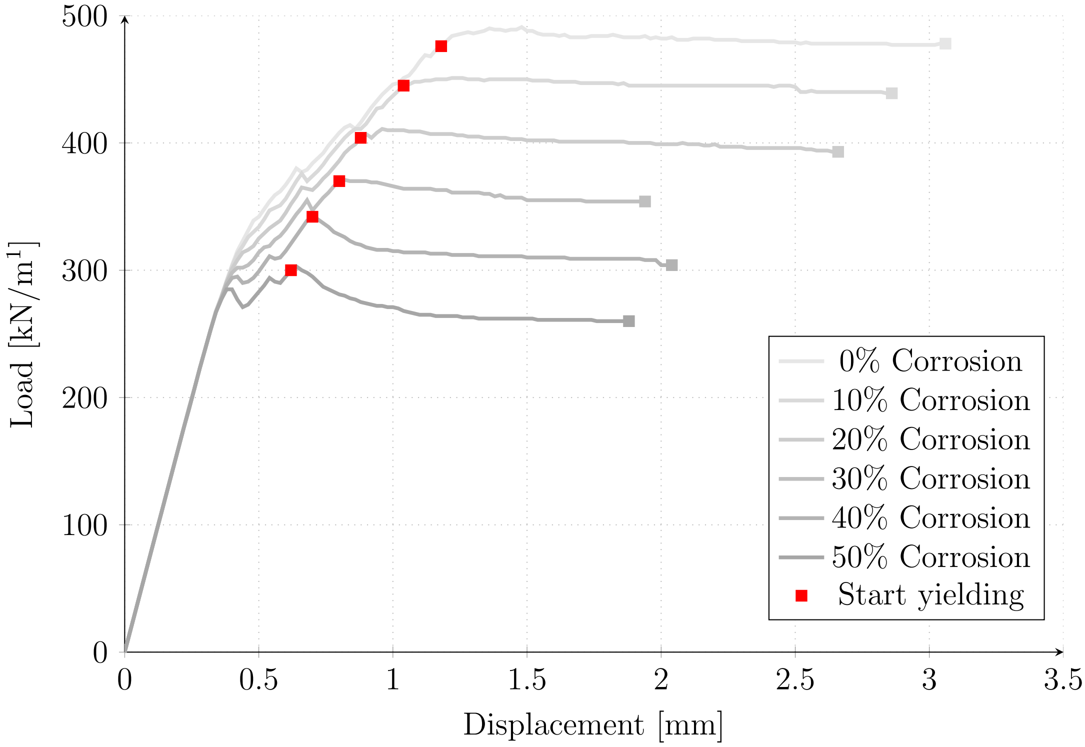

Figure 6.19: Cross-section reduction Category A1

The following observations and conclusions can be drawn from the load-displacement diagram:

- In the corroded models, the stresses in the rebars localize at the corroded part of the rebar and the uncorroded part of the rebar does not yield anymore. As the corrosion rate increases, the difference in stress between the uncorroded- and corroded part of the rebar increases as even more.
- The difference in load bearing capacity loss is similar for each corrosion rate. For each step, the load bearing capacity decreases with 45 [kN/m^1]
- The load-displacement in each analysis reaches a plateau after yielding of the reinforcement until the ultimate strain is reached. The load at the plateau is the load bearing capacity of (un)corroded concrete half-joint. It can be argued that the peak load (at start yielding) should be used as load bearing capacity. However, this peak is accompanied with a sudden drop. If the load would increase slightly at this peak, the concrete half-joint will fail in a brittle manner.

The comparison between the analytical- and numerical analyses is illustrated in Figure 6.20:

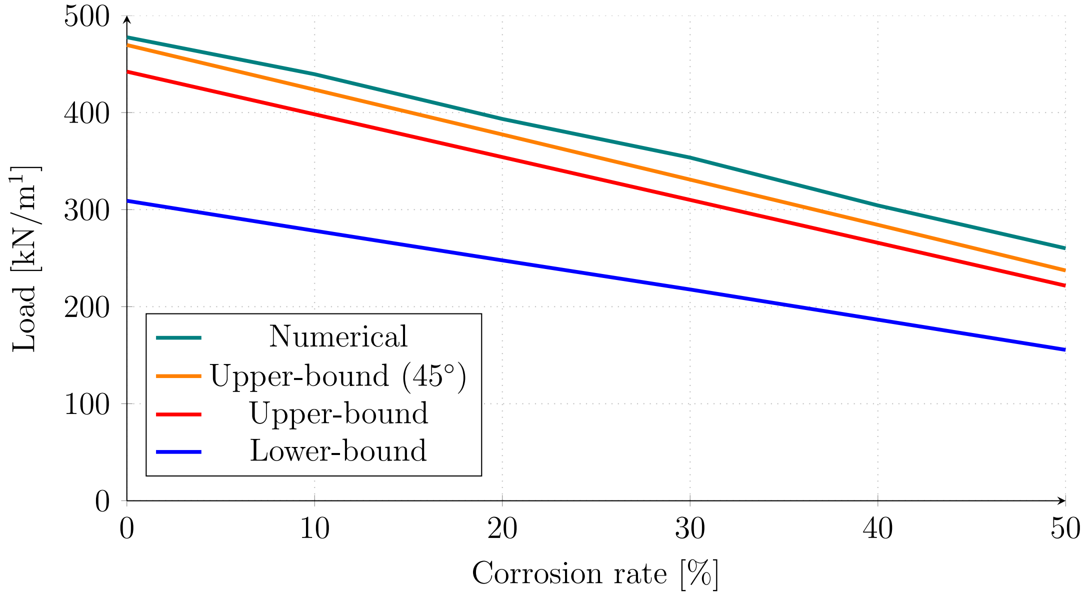

Figure 6.20: Comparison with cross-sectional reduction Category A1

The following observations and conclusions can be drawn from the comparison between analytical- and numerical analyses:

- The load bearing capacity of the numerical analysis is higher than both analytical solutions. Therefore, both the strut-and-tie approach (lower-bound) and kinematic approach (upper-bound) are conservative analyses.
- A linear reduction is observed for the load bearing capacity, for both the analytical and numerical analysis. The linear reduction is similar for the upper-bound- and numerical analysis, but the reduction is less for the lower-bound analysis. The linear reduction is the consequence of the reduced cross-sectional area of the rebars.
- The upper-bound solution can again be optimised by using the initial inclination of the crack.

Cross-sectional & yield strength reduction

The load-displacement diagrams of the Category A1 half joint with a cross-sectional and yield-strength reduction due to corrosion is illustrated in Figure 6.21.

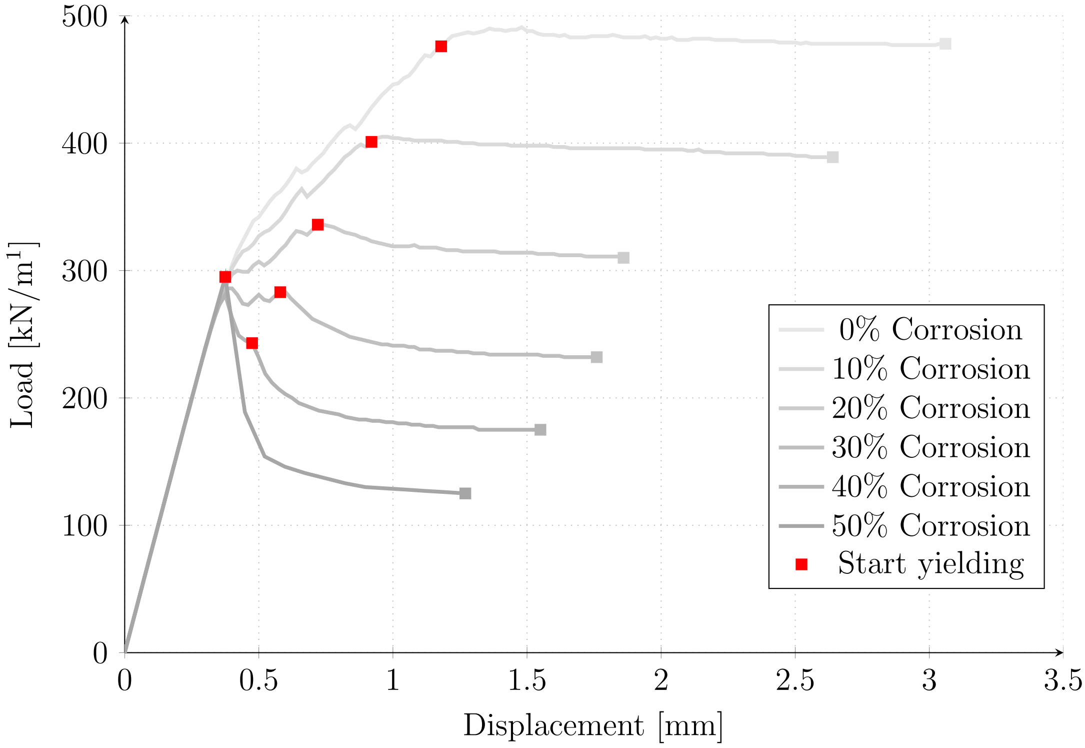

Figure 6.21: Cross-section and yield strength reduction Category A1

The following observations and conclusions can be drawn from the load-displacement diagram:

- A similar drop in load bearing capacity is observed in Figure 6.21. However, the drop is more significant than the case with only a reduction in cross-sectional area. At a corrosion rate of more than 30%, the load at start yielding of reinforcement is even lower than the load at crack initiation.
- In the model with 50% corrosion, the crack initiated at the same load-level as start yielding. The steep drop after crack initiation led to many computational difficulties and it can be argued that the results are not reliable. Therefore, this simulation is not displayed in Figure 6.22 and not taken into account in further comparisons.
- The difference in load bearing capacity loss is larger for low corrosion rates than for high corrosion rates. The load bearing capacity decreased with 90 [kN/m^1] between 0%-10% corrosion and with 57 [kN/m^1] between 30%-40%.

The comparison between the analytical analyses and numerical analysis is illustrated in Figure 6.22:

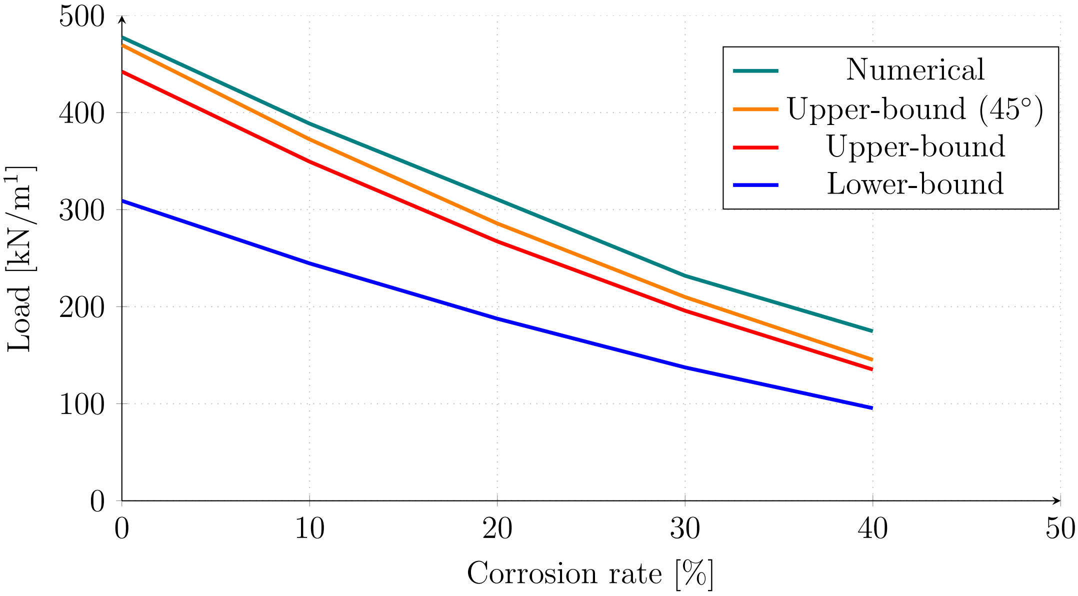

Figure 6.22: Comparison with cross-sectional and yield-strength reduction Category A1

The following observations and conclusions can be drawn from the comparison between analytical- and numerical analysis:

- The same conclusions can be drawn from Figure 6.22 as Figure 6.20. The analytical analyses are conservative, compared to the numerical analysis and the upper-bound solution can be improved by taking the same crack's inclination as the numerical analysis.
- The differences between kinematic analysis with a crack's inclination of 45° and numerical analysis appear to increase as the corrosion rate increases. Nevertheless, the solution approximates the numerical solution better than the original upper-bound solution.
- A quadratic decay is observed for the load bearing capacity, for both the analytical- and numerical analysis. The reduction is again similar for the upper-bound- and numerical analysis, but the reduction is less for the lower-bound analysis. The quadratic reduction is the consequence of the combination of reduced cross-sectional area and yield-strength of the rebars.

6.6.3 Category A2

Cross-sectional reduction

The load-displacement diagrams of the Category A2 half joint with a cross-sectional reduction due to corrosion is illustrated in Figure 6.23.

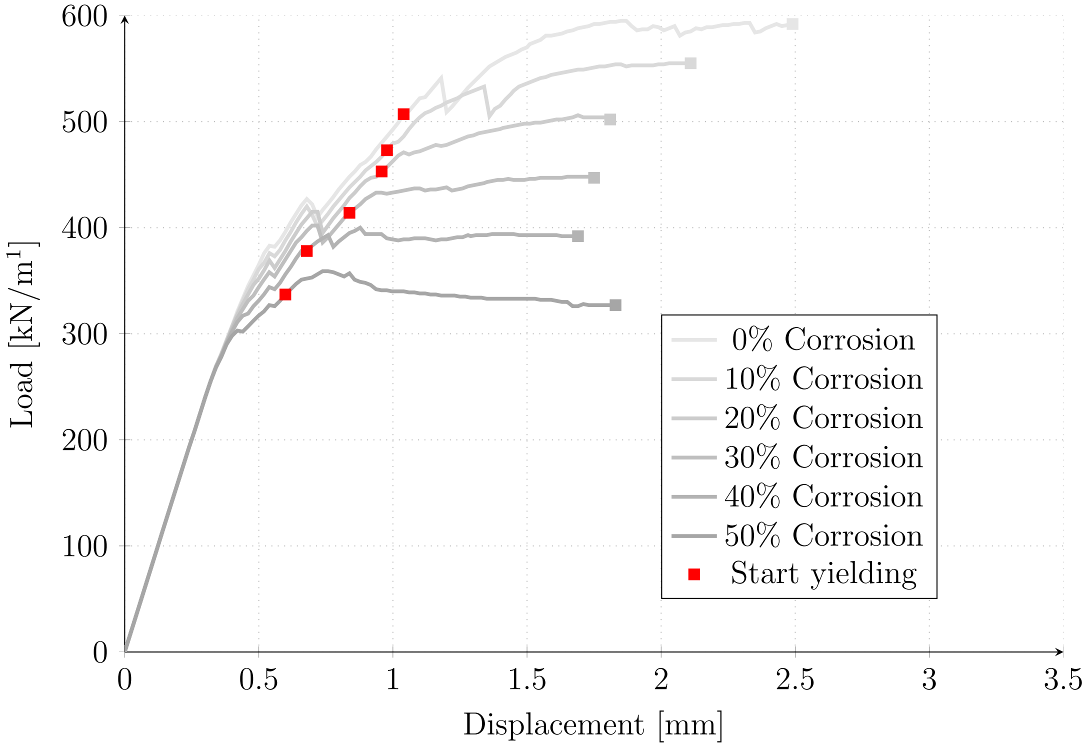

Figure 6.23: Cross-section reduction Category A2

The following observations and conclusions can be drawn from the load-displacement diagram:

- The load-displacement does not reaches a plateau or decrease immediately after the reinforcement starts to yield. The reinforcement in the concrete half-joint is able to redistribute the forces over the rebars. This distribution is also covered in the analytical analysis, in which two strut-and-tie models are considered.
- Despite the increase in load bearing capacity, the deformation capacity reduced slightly compared to the Category A2 half-joint.
- The drop in load-displacement for the cases with 0% and 10% corrosion at approximately 540 [kN/m^1] is caused by a vertical crack between elastic part and nonlinear part. It can be observed that the load-displacement recovers after a few load-steps.
- The difference in load bearing capacity loss is similar for each corrosion rate. For each step, the load bearing capacity decreases with approximately 50-65 [kN/m^1]

The comparison between the analytical analyses and numerical analysis is illustrated in Figure 6.24:

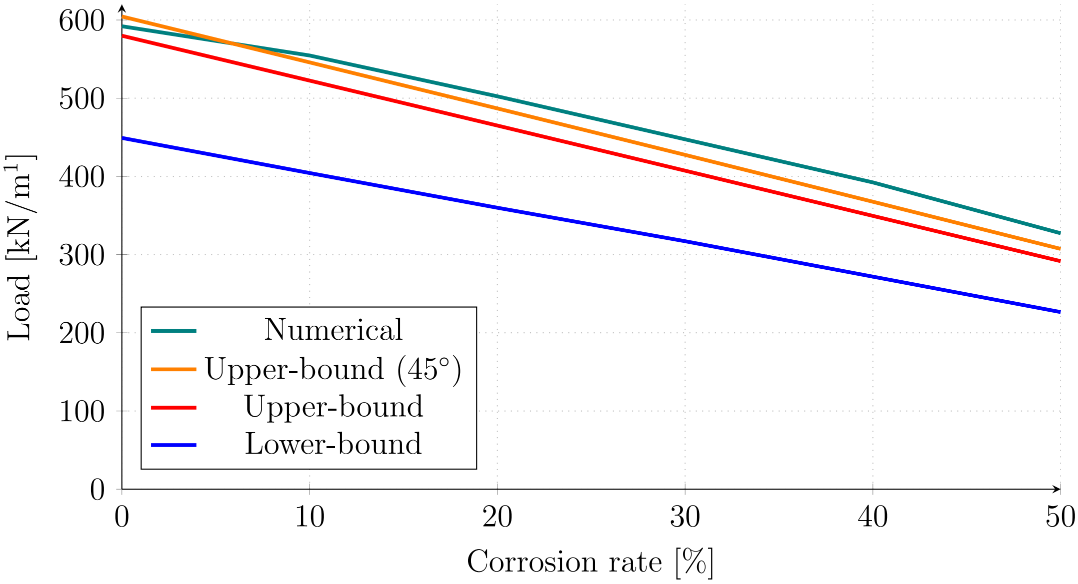

Figure 6.24: Comparison with cross-sectional reduction Category A2

The following observations and conclusions can be drawn from the comparison between analytical- and numerical analysis:

- The same conclusions can be drawn from Figure 6.24 as Figure 6.20. The analytical analyses are conservative, compared to the numerical analysis and the upper-bound solution can be improved by taking the same crack's inclination as the numerical analysis.
- However, it appears that the upper-bound solution with crack's angle of 45° is larger than the numerical solution. It can be observed that the trend of the numerical solution bends at a corrosion rate of 10%. The plot of the numerical solution of 0% shows a slight ´bumpy´ plateau, which is caused by the appearance of (splitting) cracks in the concrete. This might be the cause of the differences.

Cross-sectional & yield strength reduction

The load-displacement diagrams of the Category A2 half joint with a cross-sectional and yield-strength reduction due to corrosion is illustrated in Figure 6.25.

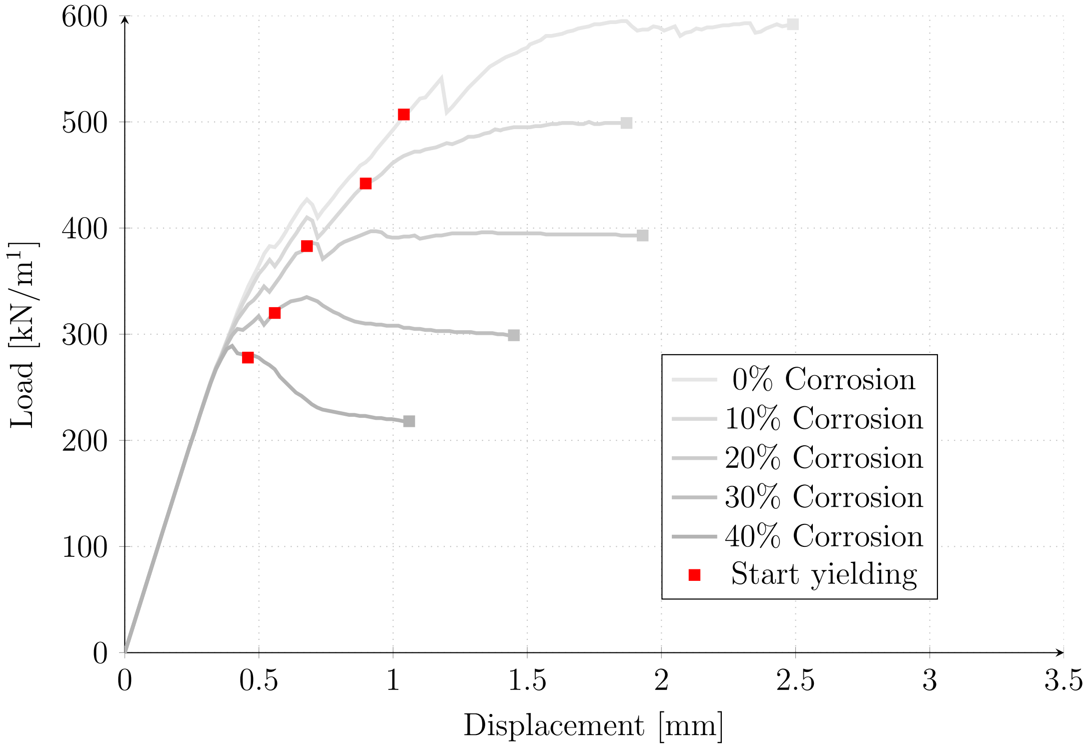

Figure 6.25: Cross-section and yield strength reduction Category A2

The following observations and conclusions can be drawn from the load-displacement diagram:

- The load-displacement for the case with 50% is not shown, for the same reasoning as the Category A1 half-joint.
- The difference in load bearing capacity loss is similar for each corrosion rate. For each step, the load bearing capacity decreases with approximately 80-100 [kN/m^1]

The comparison between the analytical analyses and numerical analysis is illustrated in Figure 6.26:

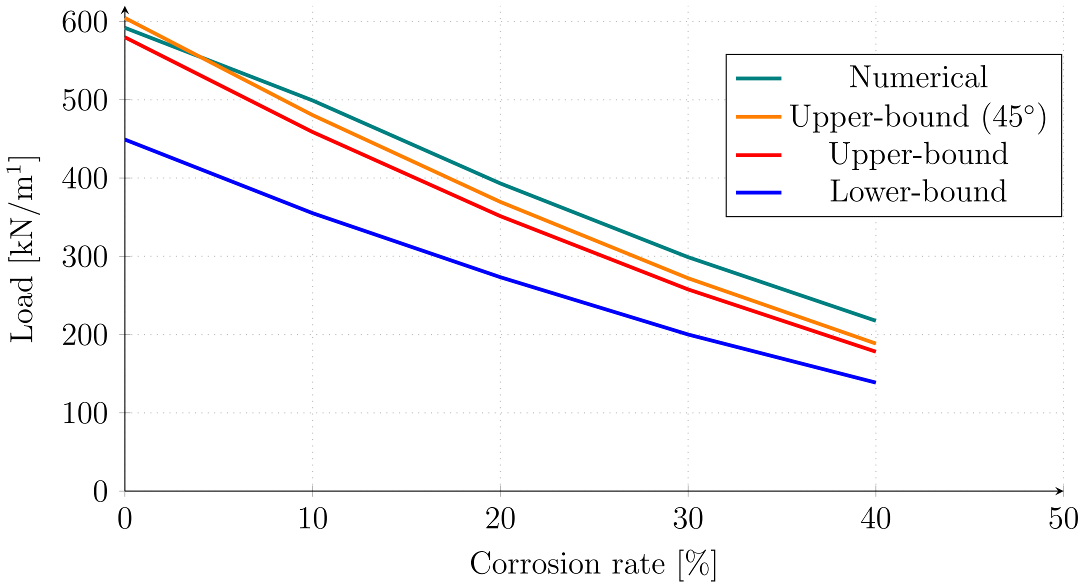

Figure 6.26: Comparison with cross-sectional and yield-strength reduction Category A2

The following observations and conclusions can be drawn from the comparison between analytical- and numerical analysis:

- The same conclusions can be drawn from Figure 6.24 as Figure 6.20. The analytical analyses are conservative, compared to the numerical analysis and the upper-bound solution can be improved by taking the same crack's inclination as the numerical analysis.

6.6.4 Comparison between Category A1 and Category A2

The numerical results of the previous paragraphs are used to compare the reduction in load bearing capacity for different corrosion rates. Figure 6.27 shows the relative load bearing capacity compared to the uncorroded concrete half-joint for Category A1 and Category A2.

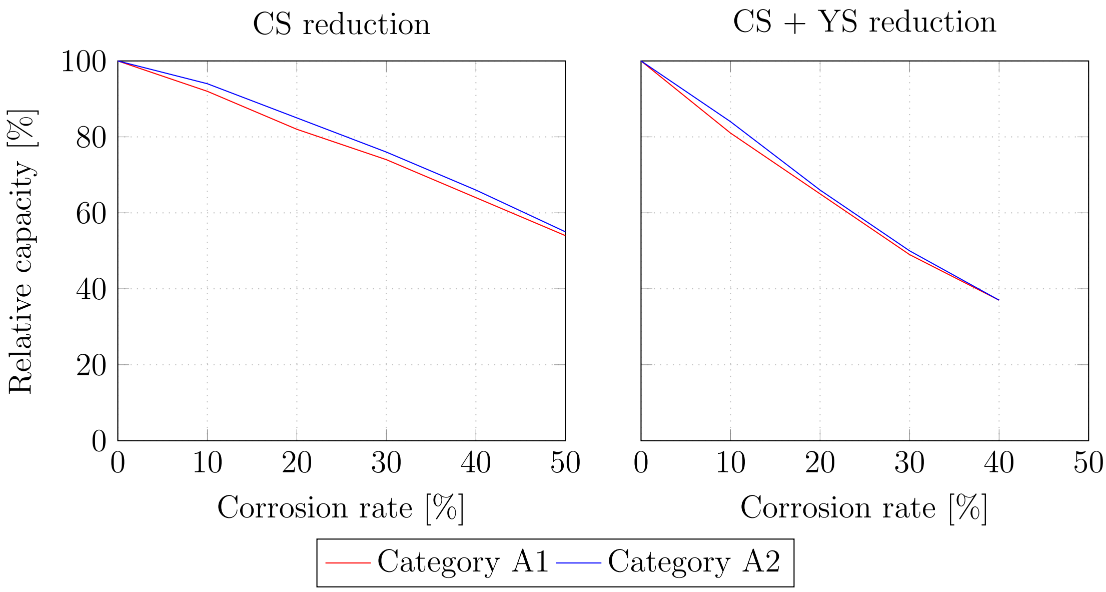

Figure 6.27: Relative load bearing capacity compared to uncorroded half-joint

The reduction in load bearing capacity of corroded concrete half-joints is similar for a Category A1 and A2. This could imply that the relative reduction of load bearing capacity is similar for both categories.

However, the diagonal rebar in the Category A2 half-joint limits the crack-width of the crack at the re-entrant corner and therefore limits the possibility of moisture and oxygen reaching the reinforcement and form corrosion. Contour plots of the global crack width for the uncorroded Category A1 and A2 half-joint at failure are illustrated in Figure 6.28.

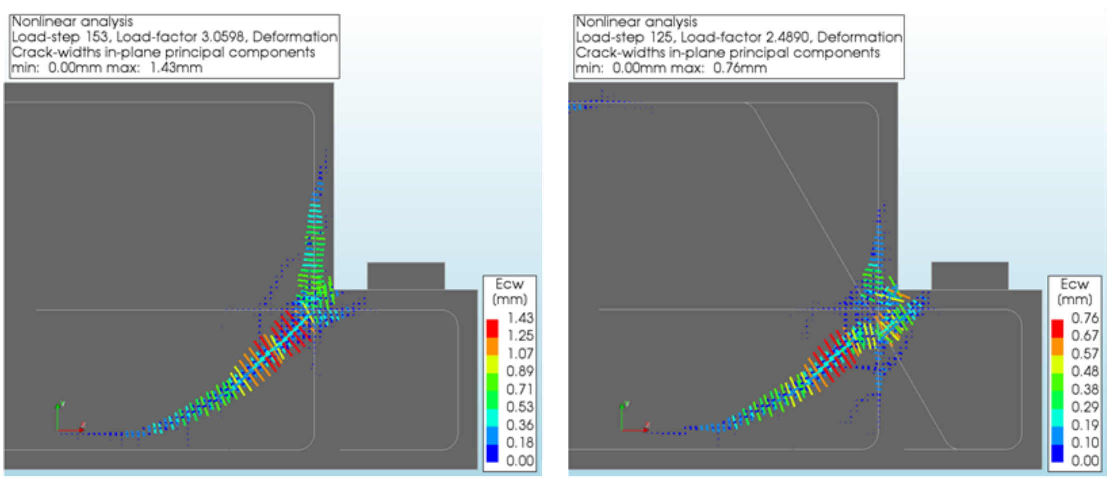

(a) Category A1 (P_{max} = 477.6 [kN/m^1]) (b) Category A2 (P_{max} = 592.0 [kN/m^1])

Figure 6.28: Crackwidth at failure

It can be observed that the crack width of the Category A2 half-joint is half the crack width of the Category A1 half-joint. Therefore, results of the numerical study should be interpreted in accordance with the set-up and assumptions of the model.

Chapter 7

Discussion, conclusions and recommendations

7.1 Discussion

This paragraph provides a discussion on the assumptions and results of this thesis research.

Categorisation of concrete half-joints

The investigated series of concrete half-joints consisted of seven structures from the Netherlands. It is assumed that these structures represent most of the (problematic) concrete half-joints build before 2000 in the Netherlands. The investigated series is used to design the analytical tool, which calculates the load bearing capacity. From similar research in Chapter 2, it is known that reinforcement layouts after 2000 and/or in other countries can be different. Nevertheless, it is expected that these are not present in the Dutch infrastructure and/or not problematic for load bearing capacity.

Material properties of corroded rebars

This paragraph contains an overview of discussion points of the material properties of corroded rebars:

- The material properties of corroded rebars are determined using the experimental study of Ou et al. [35]. The corroded rebars were obtained from a residential building exposed to natural chloride attack. The yield- and ultimate strength of the corroded rebars were obtained using the nominal diameter of the uncorroded rebar. Imperatore [7] elaborated that the use of nominal diameters leads to a major reduction in observed strength. The use of average diameter (minimum- and nominal diameter) appears to be more reasonable. Therefore, the load bearing capacity of corroded concrete half-joint is underestimated if both a cross-sectional area and yield-strength reduction is applied.

- The studies on corroded rebars contained local-/pitting corrosion over the whole length and the corrosion rate was determined as the ratio between average mass loss and initial mass of the (un)corroded rebar of the studied specimen. It can be argued that the corrosion of a rebar in a concrete half-joint is different in shape, as the diagonal crack localizes the area exposed to moisture and oxygen. The corrosion could appear more in the shape of an hour-glass, which has a localised reduction instead of a reduction over a certain length. The localisation of corrosion can lead to a reduction in deformation capacity.
- In this thesis research, it is assumed that the corrosion rate and influence on mechanical properties are known. However, the re-entrant corner of concrete half-joints is difficult to inspect and the measurement of corrosion of rebars in the concrete even more. Therefore, a suitable inspection method should be implemented or invented to measure these quantities.

Results of strut-and-tie approach

This paragraph contains an overview of discussion points of the results of the strut-and-tie approach:

- The lower-bound solutions are always lower than the upper-bound solutions. However, large differences can be observed in the analyses. The results of the strut-and-tie approach appears to be sensitive for the concrete strength and presence of the CTT Nodes (2) and (8). The stress state of these nodes is already unfavourable and dimensions strongly depends on the mandrel diameter of the hanger-rebar and inclination of the strut. In the presence of a small rebar diameter for the hanger-rebar (or diagonal rebar) and low concrete strength, the failure mechanism at the nodes could be governing. In which, corrosion of the rebars does not lead to a reduction in load bearing capacity immediately.
- It can be argued that the modelling approach of the CTT nodes is conservative in the strut-and-tie model. The compressive strut is only captured at the inside of the mandrel diameter and not distributed over e.g. the centre-line of the rebar or a certain length from the bending. In Figure 5.38, the influence of the CTT nodes is studied on the load bearing capacity. It can be seen that the capacity of uncorroded concrete half-joint increased from 978.4 [kN] to 1196.3 [kN], if the checks on CTT nodes are neglected. The increase of approximately 20% shows that there is some space for improvements left. A literature review on different standard provisions and/or numerical studies could provide more background on the structural behaviour of these nodes and whether the capacity can be increased.
- The inclination of strut C2 influences the dimensions of Node (2) and depends on the anchorage length of the horizontal rebar. Short anchorage lengths could have punished the capacity of Node (2) in the calculations. However, it can also be argued that the calculation of anchorage length is too conservative, which leads to an overestimation of the required anchorage length. This leads to a

steeper inclination of strut C2. This issue is difficult to observe in the results of the calculations, because partially anchored rebars are not taken into account. A literature review on different standard provisions and/or numerical studies could provide more background on the structural behaviour and whether the capacity can be increased.

- If an alternative strut-and-tie model, as discussed in Figure 5.20, is used, the vulnerability of the critical CTT Nodes (2) and (8) could be improved. The shear stresses are distributed over the uncracked section of the slab and do not locate at Node (5). This leads to a less steep inclination of strut C2 and C8.

Results of kinematic approach

This paragraph contains an overview of discussion points of the results of the kinematic approach:

- The kinematic approach appears to be less sensitive to the concrete strength, but more sensitive to corrosion of the rebars. The calculation verifies the compressive stress in the concrete compressive zone and assumes that the rebars are able to reach its yield strength. Reinforcement details, such as anchorage length and mandrel diameters are not considered.

- Prof.ir. C. Kleinman [16], [17], [18], [19] already proved that the load bearing capacity of concrete half-joints depend on the load transfer between the compressive strut in the nib and hanger-rebar. An increase of mandrel diameter leads to unfavourable situations, which are not covered by the kinematic approach.

- Short anchorage lengths of the horizontal rebar are not covered by the kinematic approach, which could lead to an overestimation of the actual capacity

- The kinematic approach is a simplification of the reality and it assumed that the concrete does not transfer shear stresses. Therefore, the solution can be an underestimation of the actual capacity.

- The formation of strains in the rebars depend on the crack's angle. The calculation assumes that the rebars are all yielding. However, for small crack's angles (e.g. 30°), the increase in strain is much larger for the hanger-rebar than for the horizontal rebar. For large crack's angles (e.g. 70°), the strain distribution is the other way around.

Results of numerical study

This paragraph contains an overview of discussion points of the results of the numerical study:

- The numerical model consists of plane stress elements, in which out-of-plane stresses are zero. It can be argued that plane strain elements should be used, as the concrete half-joint is modelled as a slab. In that case, the out-of-plane strains are zero. Plane strain elements appear to approximate the behaviour of thick elements loaded in one plane very well [55]. However, it makes sense to use plane stress elements to compare the numerical results with the analytical results, as they also do not capture out-of-plane stresses.
- The modelling of corrosion in the numerical study is different than it will happen in existing structures. In the numerical study it is assumed that corrosion is already present at the beginning of the analysis. In existing structures, the diagonal crack must be initiated at the re-entrant corner of the concrete half-joint in order to corrode the rebar. The expected diagonal crack can be used to formulate a discrete cracking model. Additionally, the accessibility of moisture and oxygen (and so corrosion) depends on the size of the crack width.
- The numerical model to study the load bearing capacity of corroded concrete half-joints appears to be sensitive for mesh-size changes and bond behaviour, when it comes to deformation capacity (reaching the ultimate strain in the rebars). If the mesh-size decreases and bond-slip is included, the diagonal crack propagates very localised and strains in the reinforcement localize as well. However, it appears that the mesh-size and/or bond behaviour does not influence the load at crack initiation, yielding (first) rebars or ultimate load.

7.2 Conclusions

The main research question of this thesis research is as follows:

How can concrete half-joints be assessed on load bearing capacity by implementing deterioration and/or inadequate reinforcement detailing?

For this, an analytical tool is designed based on a strut-and-tie approach and kinematic approach, in which corrosion can be implemented on the rebars at the reentrant corner.

Based on a series of investigated Dutch bridges with concrete half-joints a general reinforcement layout have been found with a hanger-rebar and horizontal-rebar. The layout can be extended by adding a diagonal rebar or prestressing in the nib and/or top or a combination of these. No shear stirrups have been found in the investigated concrete half-joints, as they were all reinforced as a slab. Adding to that, the majority showed short transfer- and/or anchorage lengths of the rebars.

The analytical tool is used to study the influence of inadequate reinforcement detailing and deterioration on the load bearing capacity of concrete half-joints. Large differences have been found between the strut-and-tie- and kinematic approach. Especially, when reinforcement detailing governs the capacity. This behaviour is well captured by the strut-and-tie approach, as anchorage length and mandrel diameters of the rebars are used in the calculation. The CTT nodes appear to be critical in the calculations. The capacity depends strongly on the concrete strength and its dimensions. The dimensions are influenced by the mandrel diameter of the hanger-rebar and inclination of the strut, which depend on the anchorage length of the horizontal rebar. This behaviour is not captured by the kinematic approach, which is the cause of the large differences

The influence of deterioration is captured by both approaches. However, the kinematic approach appears to be more sensitive to load bearing capacity loss due to corrosion, as this method mainly depends on the capacity of the ties. The strut-and-tie approach is able to redistribute its forces over the struts and ties and therefore less sensitive. If the reinforcement detailing governs the load bearing capacity, it is even possible to have no reduction at all as the corrosion rate increases.

The analytical results are verified by a numerical study for a Category A1 and A2 half-joint. The numerical model is able to predict the characteristic loads, but not the deformation capacity as it is sensitive to the mesh-size and bond-behaviour. The analytical results were conservative, compared with the numerical results and therefore provide safe solutions. The trend of reducing load bearing capacity due to corrosion was also similar. However, different crack's angle have been found between the upper-bound approximation and numerical study, due to simplifications in the analytical analysis. If the same angle is used in the upper-bound approximation, the differences reduce from 7% to 2%.

The assessment of concrete half-joints on load bearing capacity can be improved by using a combination of the strut-and-tie- and kinematic approach, as both analyses cover different failure mechanisms. If the acting load on the concrete half-joint is lower than both the calculated solutions, the structure is safe. If the acting load is between the upper-bound- and lower-bound solution, than the analytical tool is useful to understand the structural behaviour and vulnerabilities. The analytical solutions are even more useful, if the load bearing capacity is governed by the same failure mechanism for both analyses.

7.3 Recommendations

This paragraph provides recommendations based on this thesis research for assessment- and inspection method of existing concrete half-joints. Additionally, improvements for this thesis research are elaborated and suggestions for follow-up studies are given.

Assessment- and inspection method of existing concrete half-joints

This paragraph provides suggestions on how the assessment- and inspection methods of existing concrete half-joint can be improved:

Assessment method of existing concrete half-joints

The assessment method of existing concrete half-joints can be improved by using a combination of the strut-and-tie- and kinematic approach, as elaborated in the previous paragraph. An overview of further improvements are listed below:

- The kinematic approach can be extended by applying the actual presence of the diagonal crack at the re-entrant corner in the calculation.
- The kinematic approach can also be extended by incorporating the strains of the rebars in the calculation. Rajapakse et al. [13], [15] suggested an improved method, which had promising results. Anchorage lengths of the rebars could possibly also be included in this method.

Inspection method of existing concrete half-joints

The analytical parametric tool is useful if the corrosion rate of the rebars at the re-entrant corner of the concrete half-joint is known. However, existing methods are not capable of measuring the corrosion at this place and visual inspections cannot be done. It would help if methods will be developed, which are able to measure the corrosion at the re-entrant corner. These methods exist for general concrete, but are not applicable in concrete half-joints.

Improvements for this thesis research

This paragraph provides suggestions on how this thesis research can be improved:

Extension of analytical tool

The analytical tool is able to calculate the load bearing capacity of half-joints with/without diagonal and/or prestressing at the top. However, prestressing in the nib is not included. For the strut-and-tie approach, a new strut-and-tie model needs to be incorporated and for the kinematic approach, an additional restoring moment needs to be added. Additional studies can be performed to improve the calculations:

- Implementation of improved CTT nodes
- Implementation of improved anchorage length calculation
- Implementation of new strut-and-tie model, as indicated in Figure 5.20

Improved (numerical) study on simulation of corrosion

The corrosion in the numerical (and analytical) study is implemented in a different way than it will happen in existing structures. In the numerical study, the corrosion was already present at the beginning, even before the diagonal crack initiated. However, in reality the diagonal crack must appear, before moisture and oxygen can approach the reinforcement and form corrosion. In addition, the formation of corrosion can be reduced by closing of the diagonal crack, if for example the traffic load reduces.

The numerical study can be improved using a discrete cracking approach. The angle and length of the discrete crack can be predicted by an initial study using the smeared cracking approach and a corrosion rate of 0%. Subsequently, the discrete crack can be modelled and corrosion can be simulated. The corrosion rate can be dependent on time and perhaps be extended on the crack-width.

Follow-up studies

This paragraph provides suggestions for future research:

Study on anchorage/transfer length of horizontal- and diagonal rebar

The archive study showed that the anchorage/transfer length of the horizontal- and/or diagonal rebar can be insufficient. The anchorage of horizontal rebar is crucial for the load bearing capacity of a concrete half-joint. The behaviour of partially anchored rebars is not taken into account in this thesis research. However, it is expected that the influence is major on the structural behaviour. Further research is needed to study this behaviour and whether it is possible to implement this influence into account in analytical analyses. This can be done using a numerical study with a closer look on the anchorage. This can also give insight on whether the Eurocode 2 calculation of the anchorage length is conservative.

Study on prestressing in the nib

Prestressing in the nib of the concrete half-joint has not been studied in this thesis research. It is possible to include the prestressing in the nib in the strut-and-tie models and kinematic model with some adjustments. The prestressing could possibly increase the crack initiation, but limit further propagation. However, the structural behaviour can be studied using a numerical study, in which the behaviour between a concrete half-joint with- and without prestressing is studied.

Study on load distribution from bearings

The bearing plates are assumed to be equally long as the depth of the concrete half-joint in the calculations and are therefore not subdivided in individual bearing plates. In reality, each precast beam is supported with an individual bearing plate on each side. This leads to a localisation of the forces, which eventually spreads over the whole depth of the concrete slab. The structural behaviour can be studied using a 3D numerical study. This can give insight on the 3D distribution of the forces in the concrete slab.

Experimental study

Extensive experimental studies have been performed on concrete half-joints with hanger-stirrups. However, this reinforcement layout has not been observed in the archive study. No experimental studies have been found using this reinforcement layout. The experimental research of Prof.ir. C. Kleinman [16], [17], [18], [19] comes as closest to this layout.

An experimental study on different mandrel diameters, different anchorage lengths or different ratio's between horizontal-, hanger- or diagonal rebars could be very beneficial for understanding the structural behaviour of concrete half-joints.

Bibliography

[1] P. Desnerck, J.M. Lees, and C. Morley, editors. *"Assessment of Reinforced Concrete Half-Joint Structures: Dealing with Deterioration"*, PCI Convention and National Bridge Conference, Washington DC, USA, 2014.

[2] R. Asso. Half-joint assessment of concrete bridges: strut and tie model development and fem validation. Master's thesis, Politecnico di Torino, 2020.

[3] *"Report of Commission of inquiry into the collapse of a portion of the De La Concorde overpass"*. Montreal, 2007.

[4] M.Th.M. Somers and J.W. Vos. Nelson Mandelabrug - Constructieve analyse tandopleggingen bestaande brug. Technical report, Wagemaker, $W22074_RAP02 - V1.1, 2022.$

[5] P. Desnerck, J.M. Lees, and C. Morley. Impact of the reinforcement layout on the load capacity of reinforced concrete half-joints. *Engineering Structures*, 127:227–239, 2016.

[6] Q. Wang, Z. Guo, and P.C. Hoogenboom. Experimental investigation on the shear capacity of RC dapped end beams and design recommendations. *Structural Engineering and Mechanics*, 21(2):221–235, 2005.

[7] S. Imperatore. Mechanical Properties Decay of Corroded Reinforcement in Concrete - An overview. *Corrosion and Materials Degradation*, 3:210–220, 2022.

[8] P. Houwen. Onderzoek naar het gedrag van tandopleggingen. Master's thesis, Delft University of Technology, 2008.

[9] P. Desnerck, J.M. Lees, and C. Morley. Strut-and-tie models for deteriorated reinforced concrete half-joints. *Engineering Structures*, 161:41–54, 2018.

[10] *"PCI Design Handbook"*. Precast/Prestressed Concrete Institute, 2010.

[11] P. Desnerck, J.M. Lees, and C. Morley, editors. *Impact of material deterioration on the strength of reinforced concrete half-joint structures*, IABSE Workshop on Safety, Robustness and Condition Assessments of Structures, Helsinki, Finland, 2015.

[12] J. Gijsbers, C. van der Veen, and S. Wijte. Tandopleggingen volgens NEN 6720. *Cement*, 1:32–39, 2009.

[13] C. Rajapakse, H. Degée, and B. Mihaylov. Assessment of failure along Re-Entrant Corner Cracks in Existing RC Dapped-End Connections. *Structural Engineering International*, 31(2):216–226, 2021.

[14] C.U.R. Committee C 13. *CUR40 Report - Loading test on a full-size suspended beam and a model of this beam for a metro viaduct at Rotterdam.* The Hague, 1969.

[15] C. Rajapakse, H. Degée, and B. Mihaylov. Investigation of shear and flexural failure of dapped-end connections with orthogonal reinforcement. *Engineering Structures*, 260:1–14, 2022.

[16] C. Kleinman. Nokken met die Tanden! *Cement*, 7:56–59, 2006.

[17] C. Kleinman. Nokken met die Tanden!(2). *Cement*, 2:78–80, 2007.

[18] C. Kleinman. Nokken met die Tanden!(3). *Cement*, 3:70–73, 2007.

[19] C. Kleinman. Nokken met die Tanden!(4). *Cement*, 1:6–9, 2009.

[20] W.A. de Bruijn and B.M.A. Slenders. Gezonde tanden. *Cement*, 3:43–48, 2008.

[21] J. den Uijl, W.A. de Bruijn, and B.M.A. Slenders. Gezonde tanden(2). *Cement*, 1:11–15, 2009.

[22] W.A. de Bruijn, B.M.A. Slenders, C. Kleinman, and J. den Uijl. Gezonde tanden(3). *Cement*, 1:17–21, 2009.

[23] P. Desnerck, J.M. Lees, and C. Morley. The effect of local reinforcing bar reductions and anchorage zone cracking on the load capacity of rc half joints. *Engineering Structures*, 152:865–877, 2017.

[24] P. Desnerck, P. Valerio, J.M. Lees, and N. Loudon, editors. *Suggestions for improved reinforced concrete half-joint bridge inspection in England*, MATEC Web of Conferences 199, 2018.

[25] D. Mitchell, J. Marchand, P. Croteau, and W.D. Cook. Concorde Overpass Collapse: Structural Aspects. *Journal of Performance of Constructed Facilities*, 25:545–553, 2011.

[26] P.K. Mehta and P.J. Monteiro. *Concrete - Microstructure, properties and materials.* McGraw-Hill, third edition, 2006.

[27] G. Gaal. *Prediction of Deterioration of Concrete Bridges.* PhD thesis, Delft University of Technology, 2004.

[28] A. Neville. *Properties of Concrete.* Pearson, 5th edition.

[29] Kaveh Andisheh, Allan Scott, and Alessandro Palermo. Preliminary estimation of reduction factors in mechanical properties of steel reinforcement due to pitting simulated corrosion. 2014.

[30] Y. Du, L. Clark, and A. Chan. Residual capacity of corroded reinforcing bars. *Magazine of Concrete Research*, 57(3):135–147, 2005.

[31] W. Zhu and R. François. Experimental investigation of the relationships between residual cross-section shapes and the ductility of corroded bars. *Construction and Building Materials*, 69:335–345, 2014.

[32] J. Cairns, G.A. Plizzari, Y. Du, D.W. Law, and C. Franzoni. Mechanical Properties of Corrosion-Damaged Reinforcement. *ACI Materials Journal*, 102(4):256–264, 2005.

[33] Y. Du, L. Clark, and A. Chan. Effect of corrosion on ductility of reinforcing bars. *Magazine of Concrete Research*, 57(7):407–419, 2005.

[34] Han-Seung Lee and Young-Sang Cho. Evaluation of mechanical properties of steel reinforcement embedded in concrete specimen as a function of the degree of reinforced corrosion. *International Journal of Fracture*, (157):81–88, 2009.

[35] Yu-Chen Ou, Yudas Tadeus Teddy Susanto, and Hwasung Roh. Tensile behaviour of naturally and artificially corroded steel bars. *Construction and Building Materials*, (103):93–104, 2016.

[36] Stefania Imperatore, Zila Rinaldi, and Carlo Drago. Degradation relationships for the mechanical properties of corroded steel rebars. *Construction and Building Materials*, (148):219–230, 2017.

[37] Raghava Kumar Vanama and Balaji Ramakrishnan. Improved degradation relations for the tensile properties of naturally and artificially corroded steel rebars. *Construction and Building Materials*, (249), 2020.

[38] I. Finozzi, A. Saetta, and H. Budelmann. Structural response of reinforcing bars affected by pitting corrosion: experimental evaluation. *Construction and Building Materials*, (192):478–488, 2018.

[39] M. Prieto, P. Tanner, and C. Andrade. Multiple linear regression model for the assessment of bond strength in corroded and non-corroded steel bars in structural concrete. *Materials and Structures*, 49:4749–4763, 2016.

[40] K. Lundgren, M. Blomfors, and T. Chen. What do we know about concrete, steel, and bond-slip relation for corroded bars?. Capacity Assessment of Corroded Reinforced Concrete Structures. In *Proceedings of the fib CACRCS DAYS 2020*, 2020.

[41] Mattias Blomfors, Kamyab Zandi, Karin Lundgren, and Dario Coronelli. Engineering bond model for corroded reinforcement. *Engineering Structures*, 156:394–410, 2018.

[42] J. Schliach, K. Schäfer, and M. Jennewein. "Toward a Consistent Design of Structural Concrete". *PCI Journal*, May-June:74–150, 1987.

[43] W. Ritter. "Die Bauweise Hennebique". *Schweizerische Bauzeitung*, 33(7), 1899.

[44] E. Mörsch. *"Der Eisenbetonbau, seine Theorie und Anwendung"*. Stuttgart, 1908.

[45] A. Vrouwenvelder. *"The Plastic Behaviour and the Calculation of Beams and Frames subjected to bending"*. Delft University of Technology, 2003.

[46] J. Schliach and K. Schäfer. Design and detailing of structural concrete using strut-and-tie models. *The Structural Engineer*, 69(6):113–125, 1991.

[47] J.C. Walraven and S.A.A.M. Fennis. *"Gewapend Beton - Collegedictaat CTB2220/3335"*. Delft University of Technology, 2013.

[48] "M.D. Brown, C.L. Sankovich, O. Barak, J.O. Jirsa, J.E. Breen, and S.L. Wood". *"Design for shear in reinforced concrete using strut-and-tie mdoels"*. 2006.

[49] Le Huang, Lihua Xu, Yin Chi, Fangqian Deng, and Aoli Zhang. Bond strength of deformed bar embedded in steel-polypropylene hybrid fiber reinforced concrete. *Construction and Materials*, (218):176–192, 2019.

[50] Max A.N. Hendriks and Marco A. Roosen. Guidelines for Nonlinear Finite Element Analysis of Concrete Structures. Technical report, Rijkswaterstaat Centre for Infrastructure, Report RTD:1016-1:2019, 2019.

[51] D.A. Hordijk. *Local approach to fatigue of concrete*. PhD thesis, Delft University of Technology, 1991.

[52] DIANA FEA. *Diana User's Manual 10.5*, 2022.

[53] Sanjay Govindjee, Gregory J. Kay, and Juan C. Simo. Anisotropic modelling and numerical simulation of brittle damage in concrete. *Int. Journey for Numerical Methods in Engineering*, 38(21):3611–3633, 1995.

[54] F.J. Vecchio and M.P. Collins. Compression response of cracked reinforced concrete. *Journal of Structural Engineering*, 119(12):3590–3610, 1993.

[55] R. Hurlston. Plane Stress vs Plane Strain - What Are They And Which Should You Choose? https://www.fidelisfea.com/post/plane-stress-vs-plane-strain-what-are-they-and-which-should-you-choose. Accessed: 31-01-2023.

Appendix A

Overview of RBK1.2

A.1 Introduction

This appendix provides a brief overview of the standards applicable to existing structures and describes the assessment procedure as outlined by RBK1.2.

A.2 Code provisions and guidelines

The following NEN-standards and Rijkswaterstaat guidelines are used for assessment of concrete structures:

NEN 8700 - Assessment of existing structures in case of renovation and disapproval - Basic rules

NEN 8700 is coherent to Eurocode 0 and describes the basic principles of structural assessment in accordance with safety, serviceability, and durability in case of renovations and existing structures.

NEN 8701 – Assessment of existing structures in case of renovation and disapproval – Actions

NEN 8701 is coherent to Eurocode 1 and describes the actions imposed in case of renovations and existing structures.

RBK1.2 - Guidelines for assessment of existing structures

RBK1.2 is a document provided by Rijkswaterstaat, which gives additional guidelines on the NEN-standards (and Eurocode) for the assessment of existing structures

A.3 Basis of assessment

Residual service life and reference period

The residual service life is used to assess existing structures, instead of the design working life for the design of new structures. The residual service life is the period in which the minimum safety level cannot be exceeded, which is shorter than the design working life. The reference period is used to determine the magnitude of variable actions and does not need to be the same as residual service life.

Table A.1 describes the values of these period for consequence class CC3 in accordance with RBK1.1 Table 1.2.

Table A.1: Reference period and residual service life for CC3

	Reference period (year)	Residual service life (year)
New structure	100	100
Renovation	30	30
current use	30	30
Disapproval	15	1

Limit states

Assessment of existing structures also uses the principles of limit state design (as for design of new structures):

- EQU: Loss of static equilibrium of the structure or any aspect of it that is considered as a rigid body
- STR: Internal failure or excessive deformation of the structure or structural members, where strength of construction material of the structure governs
- FAT: Fatigue failure of the structure or structural members

Different partial factors need to be used for assessment of existing structures, compared to the design of new structures. Table A.2 describes the differences for consequence class CC3 in accordance with RBK1.1 Table 1.1.

<u>Serviceability limit state</u>

Serviceability limit states need to be considered in the assessment for renovation. However, they do not play a role in the assessment for current use or disapproval (NEN 8700 art. 3.4)

Table A.2: Safety factors CC3

Assessment	β	**Perm. actions**		**Var. actions**		
		$\gamma_{G,j,sup}$		$\gamma_{Q,1}$		
		6.10a	6.10b	Traffic	Wind	Others
New structure [1]	4.3	1.40	1.25	1.50	1.65	1.65
Renovation [2]	3.6	1.30	1.15	1.30	1.60	1.50
current use [3]	3.3	1.25	1.15	1.25	1.50	1.30
Disapproval [4]	3.1	1.25	1.10	1.25	1.50	1.30

in accordance with NEN-EN 1990 Table NB.16-A2.4(B)
in accordance with NEN 8700 Table A2.2(B)
in accordance with NEN 8700 Table A2.2(C)
in accordance with NEN 8700 Table A2.2(C)

A.4 Actions

NEN 8701 describes the actions on existing structures in coherence with Eurocode 1. This paragraph describes the general actions and vertical traffic loads on road bridges

General actions

Permanent- and variable actions cannot be reduced, except for the actions based on shortening of the reference period due to the residual service life, e.g. snow-load (NEN 8701 art. 4.3)

Vertical traffic loads on road bridges

Traffic loads can be reduced by shortening of reference period, the long-term increase, influence length or by changing its actual use. For calculations based on actual use, RBK1.2 distinguishes the traffic loads as follows:

V1: Normal situations, in accordance with current use or planned future use

V2: Emergency, in accordance with NEN-EN 1991-2 and NEN 8701

V3: Temporary deviating situation, in accordance with owner of the structure

A.5 Assessment in accordance with RBK1.2

RBK1.2 distinguishes three different situations/levels to assess existing structures, AI, AII and AIII. First, AI must be considered, followed by AII and AIII.

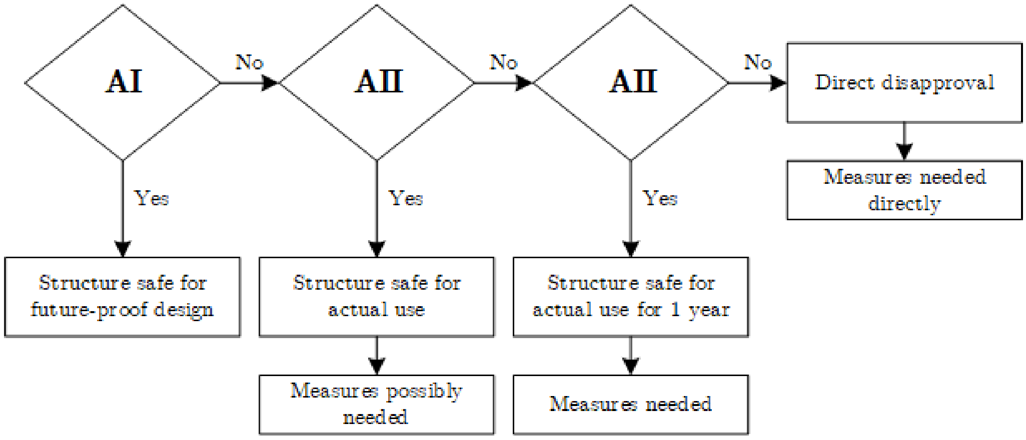

Figure A.1: Assessment of existing structures, translated from RBK1.2

AI: Assessment for future-proof design

- Partial factors, residual service life and reference period in accordance with current use-level
- Traffic load in accordance with NEN 8701, except for actual usage. Instead, use LM1 & LM2 in accordance with NEN-EN 1991-2
- Actual- or desired permanent loads need to be considered

AII: Assessment for actual use

- Partial factors, residual service life and reference period in accordance with current use-level
- Traffic load in accordance with actual usage, see RBK1.2 art. 1.3.2
- Actual permanent load needs to be considered. If there is any intention to change the permanent load in the future, this needs to be considered separately

AIII: Assessment for disapproval

- Partial factors, residual service life and reference period in accordance with disapproval-level
- Traffic load in accordance with actual usage, see RBK1.2 art. 1.3.2
- Actual permanent load needs to be considered.

If the existing structure does not fulfil the requirements, measures need to be taken. This can be done in the form of reducing permanent- or traffic loads, repair the deterioration/damage or strengthening/replacement of structure.

A.6 Material properties in accordance with RBK1.2

RBK1.2 provides different methods to define the material properties of concrete, reinforcement steel and prestressing steel:

1. Determining design values without material research
   (a) Based on original design value in accordance with technical information or on the lowest design value in accordance with original standard provisions (if no technical information is known)
   (b) Based on measurements on similar structure(s)
2. Determining design values with material research

Appendix B

Manual of analytical tool

The analytical tool is a parameterised tool to determine the load bearing capacity of a concrete half-joint. The analysis is based on a lower-bound analysis (strut-and-tie approach) and upper-bound analysis (kinematic approach), in which both analyses are optimised to find the best solutions. The input consists of the geometry and material properties of the concrete, three different rebars and possibly prestressing. Corrosion can be applied on the rebars at the re-entrant corner, which reduce the capacity of the rebars.

This manual provides a guideline for the analytical parametric tool. Firstly, the geometry and material properties are elaborated, followed by the the strut-and-tie- and kinematic approach. At last, the optimisation and corrosion are elaborated.

B.1 Geometry and material properties

B.1.1 Concrete

The geometry of the concrete half-joint, as used in the analytical tool, is illustrated in Figure B.1.

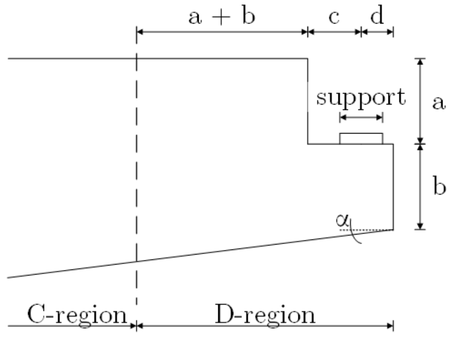

Figure B.1: Geometry of concrete in parametric tool

In which:

Width	is the depth (into the plane of the page) of the concrete half-joint, which is taken as 1000 [mm]
Cover	is the concrete cover, which automatically offsets the rebars
Support	is the width of the support plate
α	is the angle of the bottom surface with respect to the horizontal

Comments:

- The discontinuous region is equal to the sum of the height of the concrete half-joint and width of the nib.
- The width of the support is needed to determine the size of Node (1) in the strut-and-tie models
- The tool provides an input for ´Width´, which will be taken as 1000 [mm]. Therefore the resultant force is calculated as [kN/m^1]
- If $\alpha \leq 10°$, the concrete cover at the bottom needs to be increased with a yet to determine Δ_{bottom}, which can be determined using a graphic tool like AutoCad

The material properties for concrete can be determined using the characteristic compressive cylinder strength and different coefficients: partial safety factors and coefficients for long-term effects. The design values for compressive- and tensile strength can be determined using NEN-EN 1992-1-1 art. 3.1.6 as:

$$f_{cd} = \frac{\alpha_{cc} f_{ck}}{\gamma_C} \tag{B.1}$$

$$f_{ctd} = \frac{\alpha_{ct} f_{ctk,0.05}}{\gamma_C} \tag{B.2}$$

In which:

$\alpha_{cc/ct}$	is the coefficient taking account for long term effect on the compressive- or tensile strength and unfavourable effects resulting from the way the load is applied. NEN-EN 1992-1-1-NB suggests a value of 1.0
f_{ck}	is the characteristic compressive cylinder strength of concrete at 28 days
$f_{ctk,0.05}$	is the characteristic axial tensile strength of concrete (5% fractional)
γ_C	is the partial factor for concrete

The RBK1.2 suggests that the compressive cylinder strength of the concrete can be determined using material research or without material research. If the strength is determined at an age $t > 28$ days, the values $\alpha_{cc/ct}$ must be reduced by a factor k_t. NEN-EN 1992-1-1(-NB) art. 3.1.2 suggests a value of 0.85.

Using the RBK1.2, multiple possibilities arise to determine this coefficient:

1. Compressive strength of concrete without material research:
   (a) Using original design value of technical drawing: ($\alpha_{cc} = \alpha_{ct} = 1.0$)
   (b) Using lowest design value of original design standard: ($\alpha_{cc} = \alpha_{ct} = 1.0$)
   (c) Using results from samples of similar structures: ($\alpha_{cc} = \alpha_{ct} = 0.85$)
2. Compressive strength of concrete with material research:
   (a) Using results from samples of structure: ($\alpha_{cc} = \alpha_{ct} = 0.85$)

B.1.2 Reinforcement

The reinforcement of the concrete half-joint, as used in the analytical tool, is illustrated in Figure 5.13.

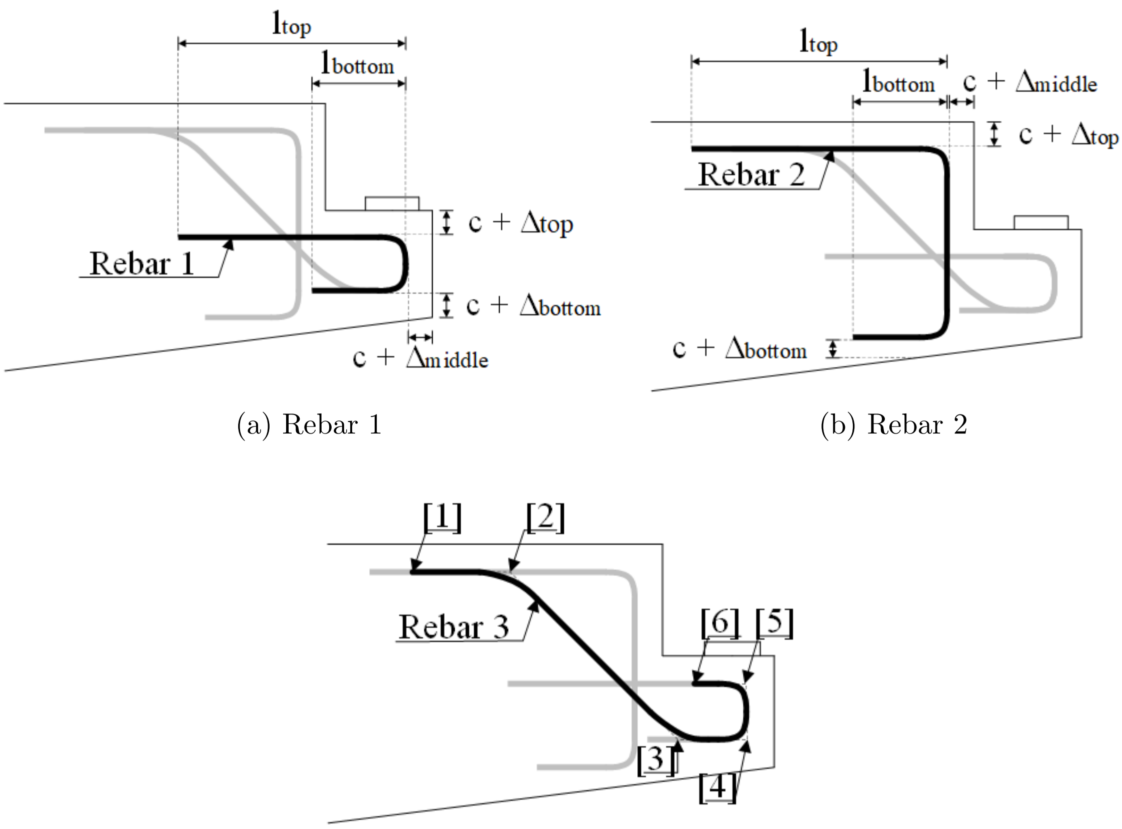

(a) Rebar 1

(b) Rebar 2

(c) Rebar 3

Figure B.2: Reinforcement in analytical tool

Comments:

- The centre-line of the rebars is displayed in the figures of the analytical tool, with a fictitious diameter. However, the stress fields of the strut-and-tie models are defined using the exact diameter

- The bending of the rebars is displayed in the figures of the analytical tool as 5 straight lines. However, the exact length is considered in the calculation of the anchorage length
- The dimensions of rebar 1 and 2 are determined automatically, based on the dimensions of the concrete and concrete cover. An additional offset can be given by Δ
- It is assumed that T3 and T5 have sufficient lap length to transfer the load to the longitudinal reinforcement

The design yield strength of reinforcement steel can be determined using NEN-EN 1992-1-1 art. 3.2.7 as:

$$f_{yd} = \frac{f_{yk}}{\gamma_S} \tag{B.3}$$

In which:

f_{yk}	is the characteristic yield strength of reinforcement steel
γ_S	is the partial factor for reinforcement steel

The RBK1.2 suggests to determine the design yield strength based on the original design standard, which could be different than eq. B.3. RBK1.2 Table 2.6 elaborates the design yield strengths based on the original design standards.

B.2 Strut-and-tie modelling

B.2.1 Nodes

The node modelling for the strut-and-tie analysis, as used in the analytical tool, is illustrated in Figure B.3. If prestressing is present in the concrete half-joint, Nodes (2) and (6) are replaced from the upper rebar towards the prestressing.

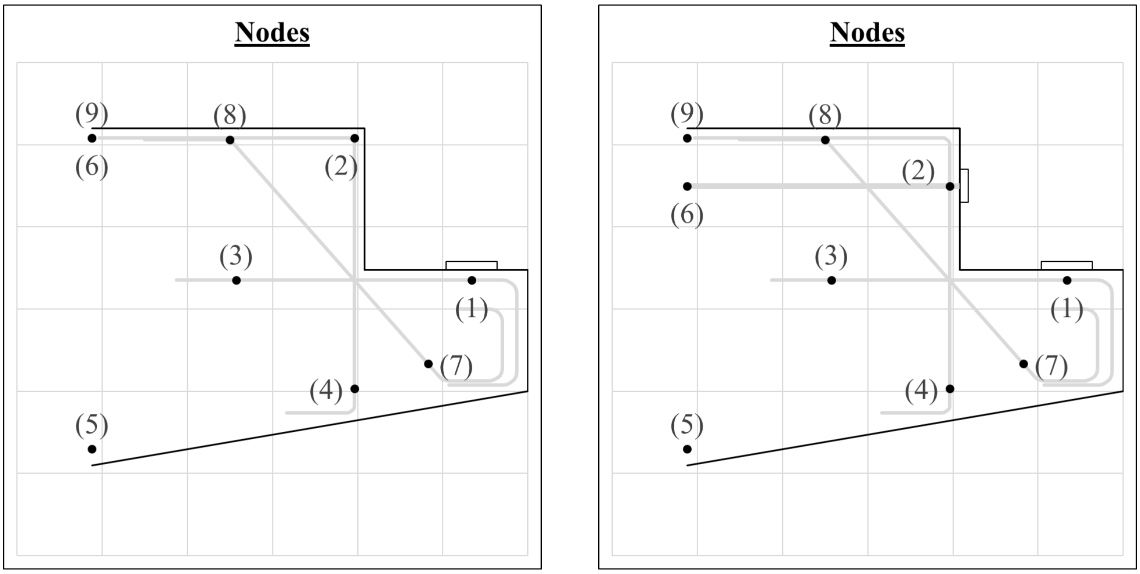

(a) Without prestressing (b) With prestressing

Figure B.3: Node numbering

The nodes for the strut-and-tie analysis are not all fixed to its position and can shift in x- or y-direction, or along the corresponding rebar. A shift in position can lead to an increase of anchorage length, but also to an increase in forces in struts or ties. The optimisation of finding the most favourable positions is elaborated in paragraph 5.4.5. An overview of the fixed- and movable nodes are given in Table B.1:

Table B.1: Fixed- an movable nodes in strut-and-tie analysis

Fixed nodes	**Movable nodes**
Node (1)	Node (3) (x-direction)
Node (2)	Node (4) (y-direction)
Node (6)	Node (5) (y-direction)
Node (8)	Node (7) (along Rebar 3)
Node (9)	

B.2.2 Strut-and-tie model

The strut-and-tie analysis is elaborated on the basis of a Category A2 half-joint (with diagonal rebar, but without prestressing). Other categories can be analysed similarly, with only a few adjustments:

Category A1: Only strut-and-tie model 1 is used, without predefined load factor

Category B1-1: Strut-and-tie model 1 is used, without predefined load factor and the prestressing is added to tie T3 in the strut-and-tie model (including change of Node (2) from CTT to CCT)

Category B2-1: Only the prestressing is added to tie T3 in the strut-and-tie model (including change of Node (2) from CTT to CCT)

The strut-and-tie tool is based on two different strut-and-tie models for a Category A2 half-joint, which are summed using a predefined load factor. The strut-and-tie models are illustrated in Figure B.4:

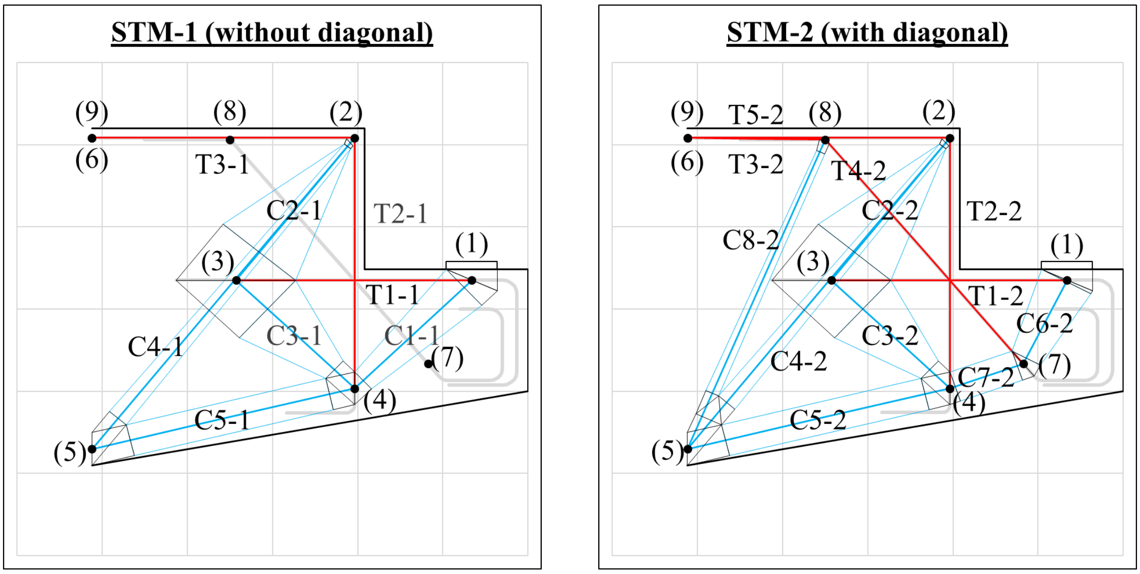

(a) Strut-and-tie model 1

(b) Strut-and-tie model 2

Figure B.4: Strut-and-tie models 1 and 2

For each strut-and-tie model, the forces in the struts and ties are calculated using a unit load. Subsequently, the two strut-and-tie models can be summed to a new strut-and-tie model (STM3), which is illustrated in Figure B.5. A predefined load factor is introduced, which distributes the load over the two strut-and-tie models.

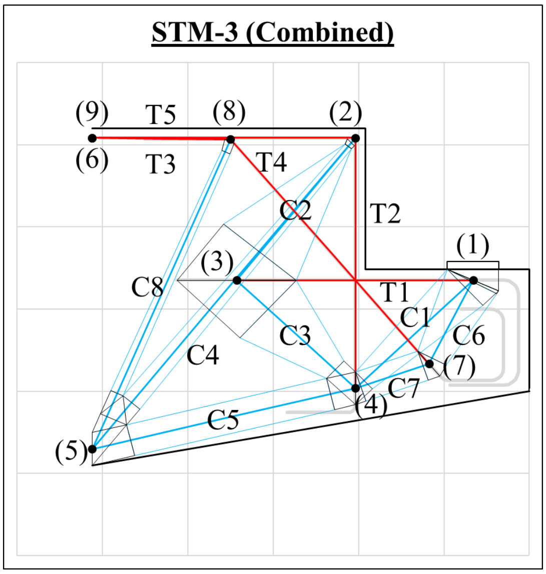

Figure B.5: Strut-and-tie model 3

The unit force per strut and tie in STM3 is determined as follows:

$$F_{unit,i} = F_{unit,i,STM1} \cdot Q_{STM} + F_{unit,i,STM2} \cdot (1 - Q_{STM}) \tag{B.4}$$

In which:

$F_{unit,i,STM1}$ is the unit force in strut or tie i of STM-1

$F_{unit,i,STM2}$ is the unit force in strut or tie i of STM-2

Q_{STM} is the load factor, which is a value between 0 and 1.

B.2.3 Node modelling

This paragraph elaborates the modelling of the nodes in the strut-and-tie model. The nodes are verified at the face in which the strut is connected to the nodes, by checking the compressive strength. An additional check is performed for Node (1), (2), (4) and (5), in which multiple struts are coupled. The individual forces are projected perpendicular to the face and summed. The face of each node over which the additional check is performed, is elaborated below.

Node 1

Node (1) is a CCT node and connects strut C1 (and C6) with tie T1 and the bearing plate. The anchorage of tie T1 in Node (1) is indicated in orange in Figure B.6, it starts at the left of Node (1) and ends at the end of rebar 1.

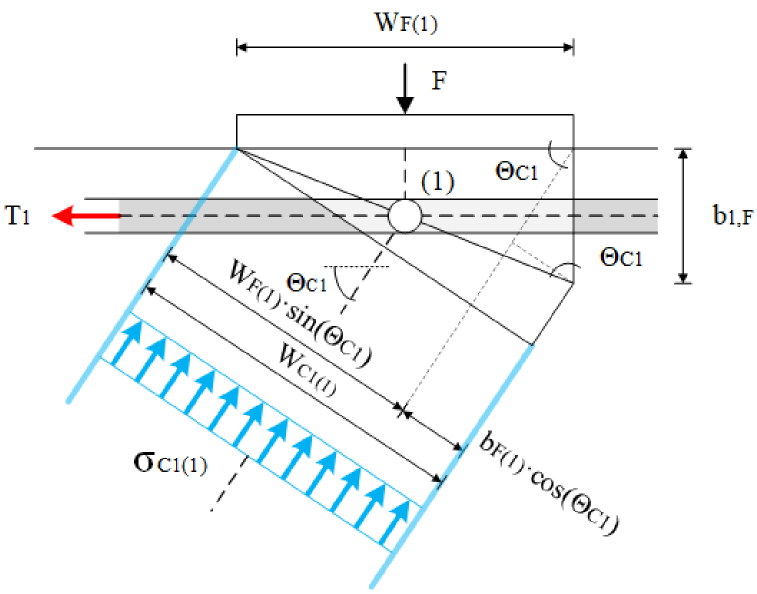

Figure B.6: Modelling of Node (1)

In which:

$W_{F(1)}$ is the width of the support

$b_{1,F}$ is twice the concrete cover + the diameter of the rebar

Θ_{C1} is the inclination of strut C1

- Strut C6 at Node (1) is modelled similarly as strut C1
- The anchorage of T1 at node 1 starts from the left of the support plate towards the end of rebar 1
- For a Category A2 half-joint, strut C1 and C6 are coupled to Node (1). An additional check is performed on the diagonal face, which is indicated in blue in Figure B.7.

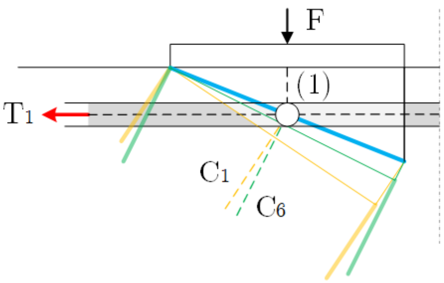

Figure B.7: Combination of Node (1)

Node 2

Node (2) is a CTT node and connects strut C2 and C4 with tie T2 and T3. The width of the face of strut C2 and C4 depends on the mandrel diameter of rebar 2 and the strut's angle. If the mandrel diameter decreases, or the strut's angle deviates from 45°, the width of the faces decrease rapidly.

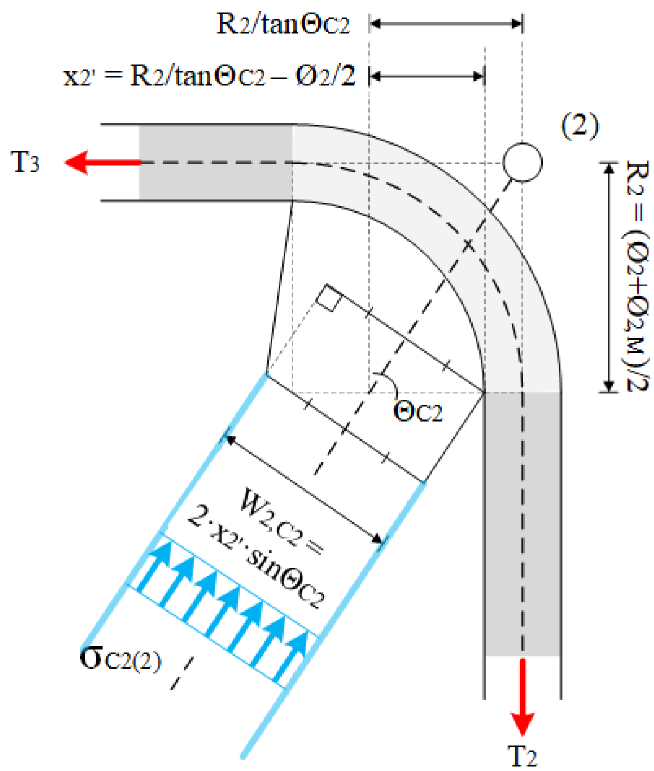

Figure B.8: Modelling of Node (2)

In which:

$\varnothing_2$	is the diameter of rebar 2
$\varnothing_{2,M}$	is the mandrel diameter of rebar 2
Θ_{C2}	is the inclination of strut C2

- Strut C4 at Node (2) is modelled similarly as strut C2
- If $\Theta_{C2} < 45°$, Θ_{C2} becomes $90° - \Theta_{C2}$ is the equation for the width of the node
- If prestressing is included, Node (2) is modelled similarly as Node (1)
- Strut C2 and C4 are coupled to Node (2). An additional check is performed on the minimum width of the face of strut C2 and C4: $w_{C2/C4(2)}$ =min($w_{C2(2)}, w_{C4(2)}$)

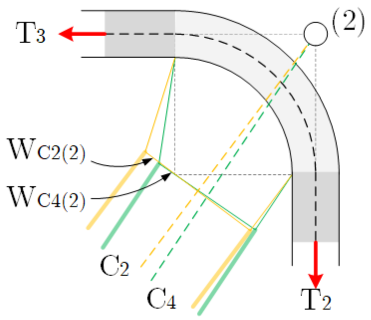

Figure B.9: Combination of Node (2)

Node 3

Node (3) is a CCT node and connects strut C2 and C3 with tie T1. The node can be shifted along rebar 1 (in x-direction), which can increase or decrease the anchorage length and strut's angle. The offset of the node is indicated by $\Delta_{(3)}$. The anchorage length of tie T1 in Node (3) is equal to twice the offset of Node (3).

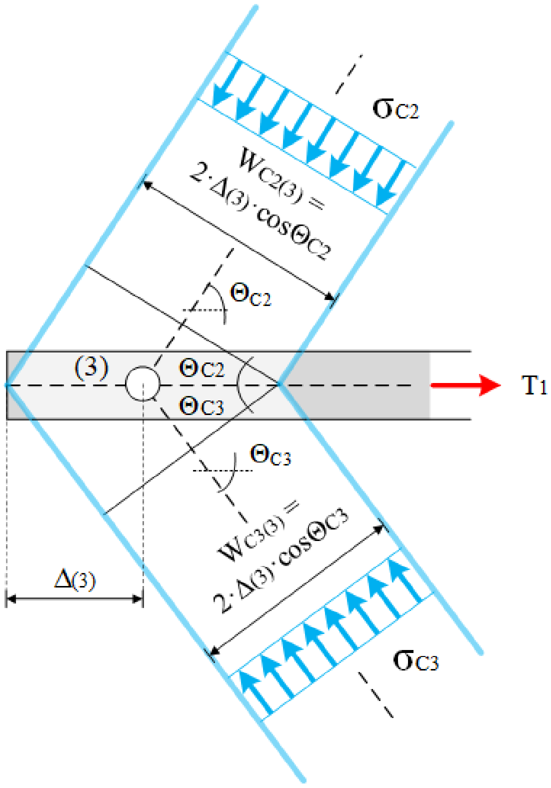

Figure B.10: Modelling of Node (3)

In which:

$\Delta_{(3)}$ is the offset of Node (3)

- The anchorage of T1 at Node (3) start from the end of rebar 1 towards the right side of Node (3)

Node 4

Node (4) is a CCT node and connects strut C1, C3, C5 (and C7) with tie T2. The node can be shifted along rebar 2 (in y-direction), in which the minimum offset start at the bending of the rebar. The offset of the node is indicated by $\Delta_{(4)}$

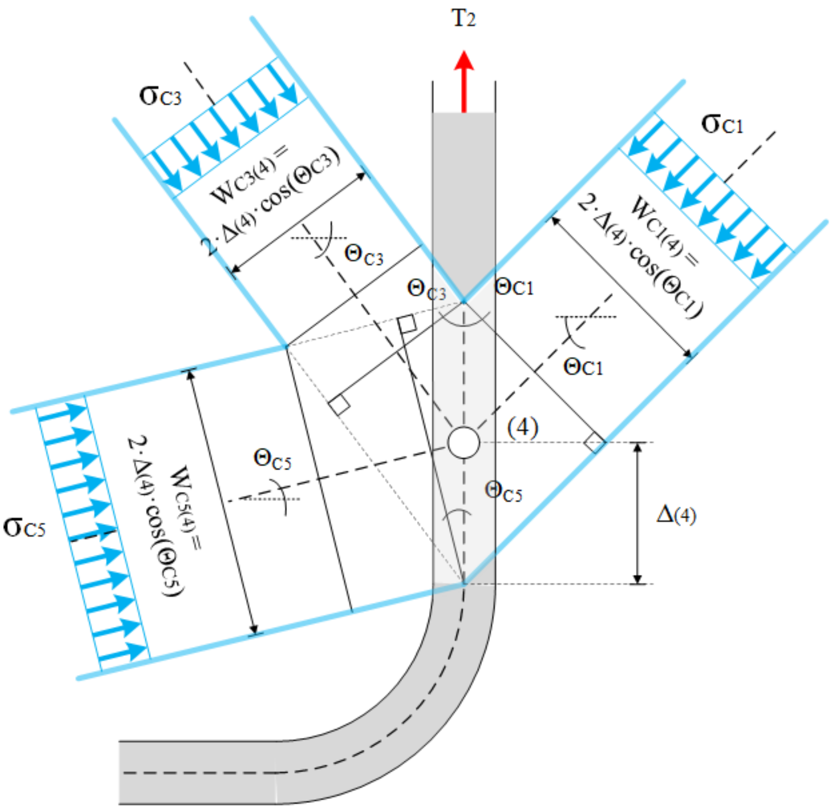

Figure B.11: Modelling of Node (4)

In which:

Θ_{C1}	is the inclination of strut C1
Θ_{C3}	is the inclination of strut C3
Θ_{C5}	is the inclination of strut C5
$\Delta_{(4)}$	is the offset of Node (4)

- Strut C7 is modelled similarly as strut C1
- The anchorage of rebar 2 at Node (4) starts from the end of rebar 2 towards the upper side of Node (4)
- Struts C4, C5 (and C8) are coupled in Node (5). An additional check is performed on the vertical face of Node (5), which is illustrated in blue in Figure B.12.

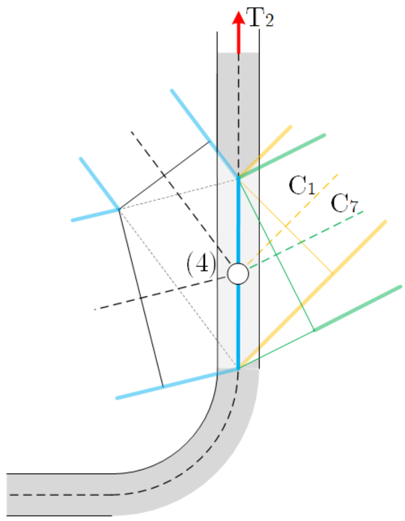

Figure B.12: Combination of Node (4)

Node 5

Node (5) is a CCC node and connects strut C4, C5 (and C8) to the continuous region. The modelling of Node (5) leads to a concentration of compressive stresses, which are not present in reality. It is expected that strut C4 and C8 spread their stress fields over the height of the concrete half-joint and transfer the shear stresses through the concrete. Therefore, the modelling of Node (5) is a conservative assumption.

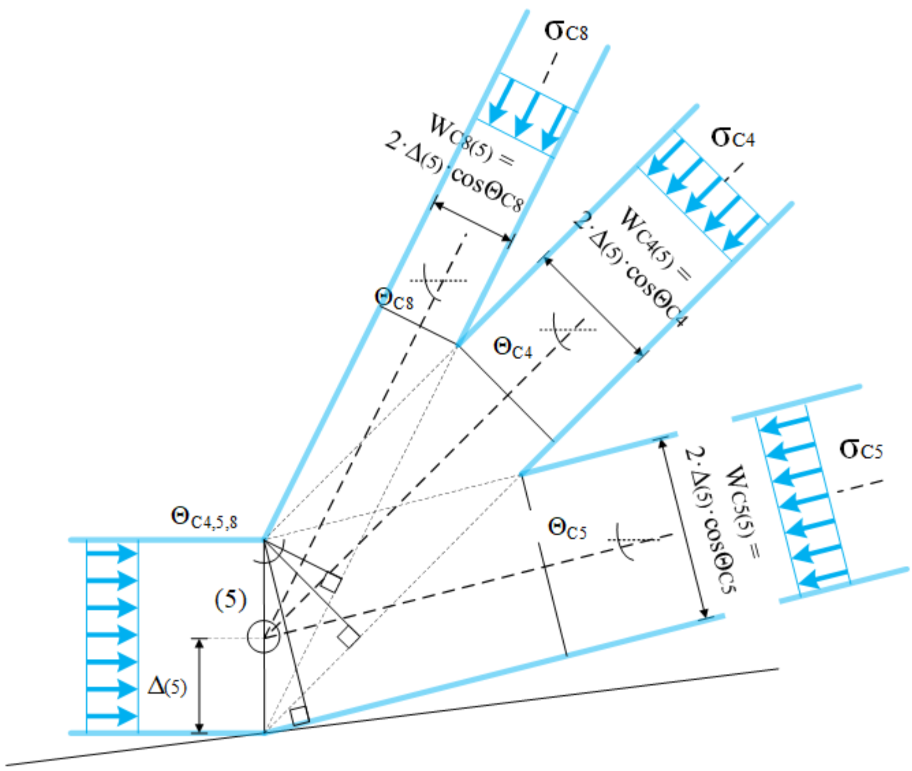

Figure B.13: Modelling of Node (5)

In which:

Θ_{C4}	is the inclination of strut C4
Θ_{C5}	is the inclination of strut C5
Θ_{C8}	is the inclination of strut C8
$\Delta_{(5)}$	is the offset of Node (5)

- Struts C4, C5 (and C8) are coupled in Node (5). An additional check is performed on the vertical face of Node (5), which is illustrated in blue in Figure B.14.

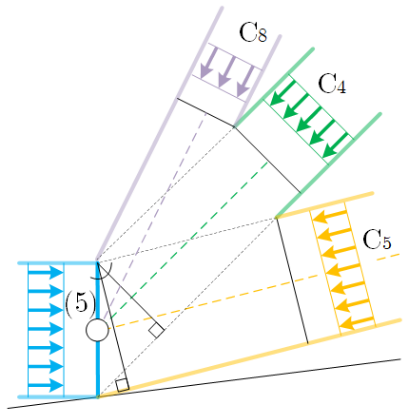

Figure B.14: Combination of Node (5)

Node 7

Node (7) is a CCT node and connects strut C6 and C7 to tie T4. The node can be shifted along rebar 3 (in local-direction), in which the minimum offset start at the bending of the rebar. The offset of the node is indicated by $\Delta_{(7)}$

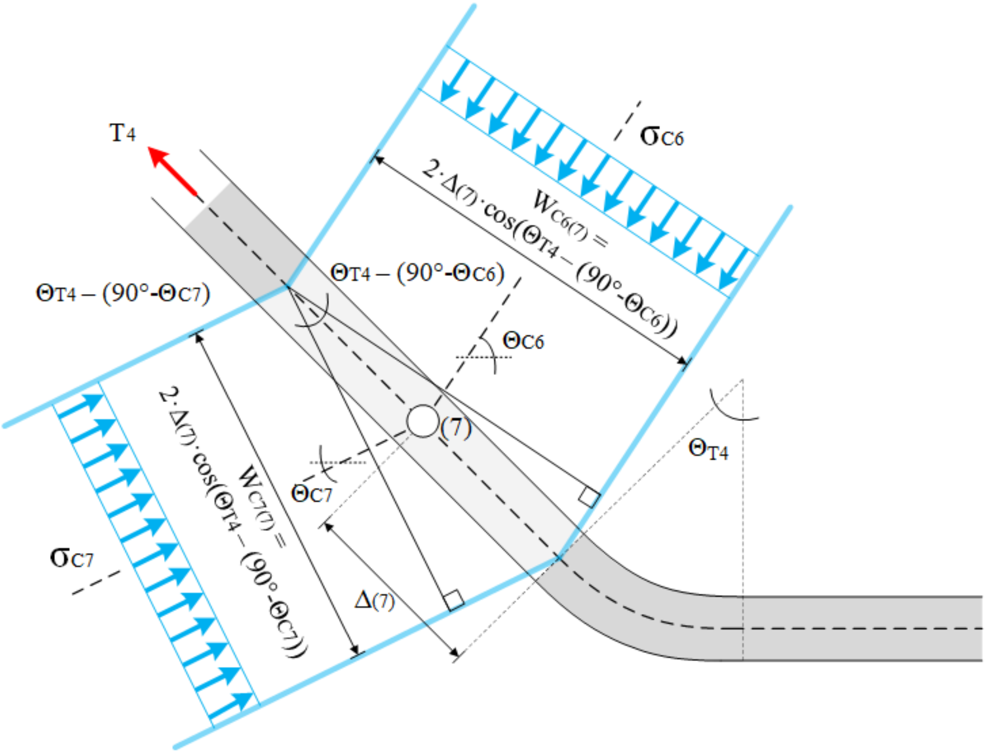

Figure B.15: Modelling of Node (7)

In which:

Θ_{C6}	is the inclination of strut C6
Θ_{C7}	is the inclination of strut C7
$\Delta_{(7)}$	is the offset of Node (7)

- The anchorage of rebar 3 at Node (7) starts from the left side of Node (7) towards the end of rebar 3

Node 8

Node (8) is a CTT node and connects strut C8 to tie T4 and T5. The width of the face of strut C8 depends on the mandrel diameter of rebar 3 and the strut's angle. If the mandrel diameter decreases, or the strut's angle deviates from $\Theta_{T4}/2$, the width of the faces decrease rapidly.

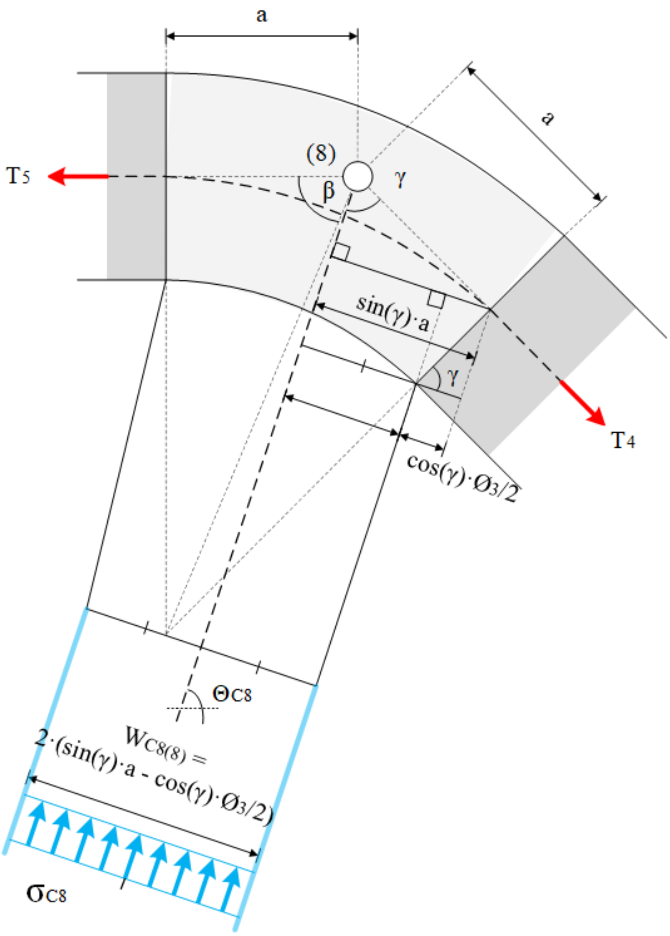

Figure B.16: Modelling of Node (8)

In which:

Θ_{C8}	is the inclination of strut C8
γ	$= \phi - \Theta_{C8}$
ϕ	is the angle of rebar 3
β	$= \tan^{-1}((\varnothing_3 - \varnothing_{M,3})/2/a)$
a	can be found using coordinates

B.2.4 Checks

The load bearing capacity of each strut, node and tie is calculated using the unit force. The analytical tool refers a strut or tie by: i, which is connected by two nodes: j and k.

Struts

Eurocode 2 considers the compressive strength based on whether or not tensile stresses in the transverse direction are present. The corresponding equations for the compressive strength of the nodes are as follows:

- If tensile stresses do not occur in transverse direction (NEN-EN 1992-1-1 art. 6.5.2(1)):
$$\sigma_{Rd,max} = f_{cd} \tag{B.5}$$

- If tensile stresses do occur in transverse direction (NEN-EN 1992-1-1 art. 6.5.2(2)):
$$\sigma_{Rd,max} = 0.6\nu' f_{cd} \tag{B.6}$$

In which:

f_{cd} is the design value of concrete compressive strength

ν' is a value which takes into account transverse tension and can be determined as: $\nu' = 1 - f_{ck}/250$

The analytical tool assumes conservatively that transverse tension is present in the struts. The capacity of the concrete strut i is determined in the analytical tool as follows:

$$C_{max,C,i} = \sigma_{Rd,max} \cdot \min(w_{i(j)}, w_{i(k)}) \cdot b \tag{B.7}$$

In which:

$w_{i(j/k)}$ is the width of concrete strut i at node j or node k

b is the depth of the nib as illustrated in Figure 5.12

Based on the capacity of concrete strut i, the maximum bearing capacity can now be determined as:

$$F_{max,C,i} = \frac{C_{max,C,i}}{F_{unit,i}} \tag{B.8}$$

Nodes

The capacity of the face of concrete strut i at node j or k is determined in the analytical tool as follows:

$$C_{max,i(j/k)} = \sigma_{Rd,max} w_{i(j/k)} \cdot b \tag{B.9}$$

In which:

$w_{i(j/k)}$ is the width of the concrete strut i at node j or k

Based on the capacity of the face of concrete strut i at node j or k, the maximum bearing capacity can now be determined as:

$$F_{max,i(j/k)} = \frac{C_{max,i(j/k)}}{F_{unit,i}} \tag{B.10}$$

Ties

The design tensile strength of the tie is determined using the total cross-sectional area of the corresponding rebar over the considered width and design yield strength as:

$$T_{max,T,i} = A_{s,i,tot} \cdot f_{yd} \tag{B.11}$$

Based on the capacity of the tie, the maximum bearing capacity can now be determined as:

$$F_{max,T,i} = \frac{T_{max,T,i}}{F_{unit,i}} \tag{B.12}$$

Anchorage length

The bond-strength provides the load transfer between rebar and concrete. It depends on the presence of micro-cracks and the application of ribbed or smooth rebars. Eurocode 2 provides a simplified calculation that determines a constant bond-strength (NEN-EN 1992-1-1 art. 8.4.2(2)):

$$f_{bd} = 2.25\eta_1\eta_2 f_{ctd} \tag{B.13}$$

In which:

η_1	is a coefficient that accounts for the bonding conditions
η_2	is a coefficient that accounts for the rebar diameter
f_{ctd}	is the design tensile strength of concrete

A basic required anchorage length needs to be applied in order to transfer the tensile force to the concrete. It can be determined as (NEN-EN 1992-1-1 art. 8.4.3(2)):

$$l_{b,rqd} = \frac{\O}{4}\frac{\sigma_{Rd}}{f_{bd}} \tag{B.14}$$

In which:

$\O$	is the rebar diameter
σ_{Rd}	is the design tensile stress in rebar

Other design aspects can influence the anchorage capacity of a rebar as well. For example, by bending the rebar or applying (welded) rebars transverse to the tie. These effects are taken into account in (NEN-EN 1992-1-1 art. 8.4.4(1)):

$$l_{bd} = \alpha_1\alpha_2\alpha_3\alpha_4\alpha_5 l_{b,rqd} \geq l_{min} \tag{B.15}$$

In which:

α_1	is a coefficient for the form of rebar, assuming sufficient concrete cover
α_2	is a coefficient for the concrete cover
α_3	is a coefficient for the effect of confinement by transverse reinforcement
α_4	is a coefficient for the influence of welded transverse bars
α_5	is a coefficient for the effect of transverse pressure

In the presence of insufficient anchorage length, the rebar is only partially anchored. As the structural behaviour of a partial anchored rebar is unknown, the solution is not valid and not taken into account in the optimisation.

B.3 Kinematic approach

The kinematic approach (also known as CUR40-method) uses the (expected) presence of the diagonal crack at the re-entrant corner to determine the load bearing capacity. The crack corresponds with failure mechanism 2 and 3, in which the hanger-rebar or horizontal rebar ruptures.

The approach is based on an upper-bound approximation, which can be formulated as [45]:

"Starting from an arbitrary mechanism, the corresponding equilibrium equation will provide an upper-bound solution for the limit load"

The results of the kinematic approach are usually more accurate than the strut-and-tie approach for concrete half-joints, despite that this is an upper-bound approximation.

B.3.1 Calculation

The diagonal crack initiates at the re-entrant corner and propagates with a certain angle until horizontal- or vertical force equilibrium can no longer be fulfilled. The torn-off concrete part can be considered as a free-body diagram, as illustrated in Figure B.17:

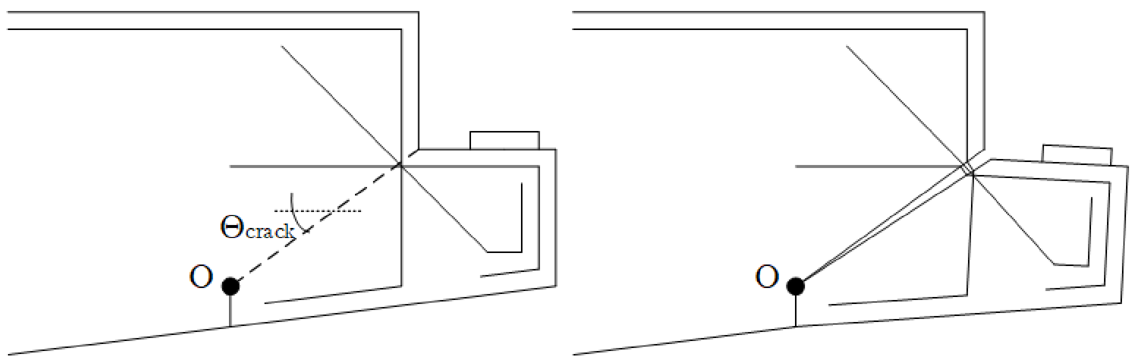

Figure B.17: Diagonal crack in concrete half-joint

The free-body diagram rotates around point O, due to the load on the support and self-weight of the torn-off concrete part. The latter one can be neglected due to its minor contribution compared to the total load on the support. The rotation leads to an increase of strain and tensile stress in the rebars, which acts as a resistance mechanism. Additionally, the compressive stresses in the concrete compression zone increase. Both contribute to the load bearing capacity of the concrete half-joint, which can be determined using horizontal- and vertical force equilibrium and moment equilibrium.

The free-body diagram with forces is illustrated in Figure B.18:

The load bearing capacity can calculated as follows:

1. Approximate the (minimum) concrete compression zone using horizontal force equilibrium
2. Determine contributions/resistance of rebars and concrete
3. Determine the load on the support, using moment equilibrium
4. Check vertical force equilibrium and increase concrete compression zone if needed.

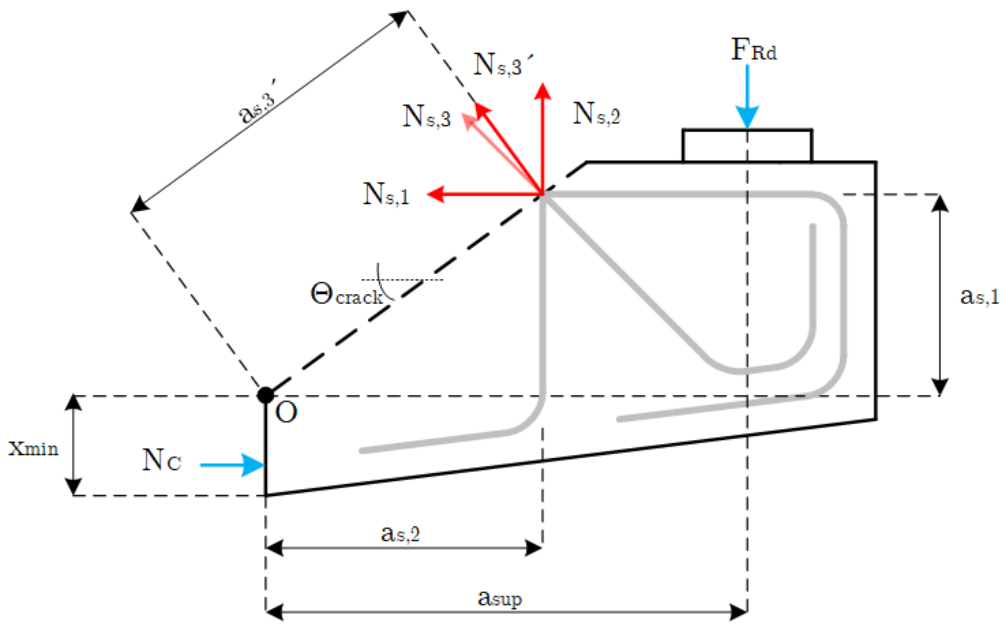

Figure B.18: Free-body diagram for kinematic approach

(Minimum) Concrete compression zone

The minimum concrete compression zone is determined using the tensile forces in the rebars, which have a horizontal component (horizontal rebar and diagonal rebar). It is assumed that both rebars are able to develop its yield strength and must be in horizontal force equilibrium with the concrete:

$$\sum H = \sum N_{s,x} + N_c = 0 \tag{B.16}$$

In which:

$\sum N_{s,x}$ is the sum of the horizontal components of the tensile forces in the rebars (horizontal rebar and diagonal rebar)

N_c is the compressive force in the concrete

It is initially assumed that the concrete crushes in the concrete compression zone. The compressive force in the concrete can therefore be determined as:

$$N_c = 0.75 \cdot x_{min} \cdot b \cdot f_{cd} \tag{B.17}$$

From which, a minimum concrete compression zone can be determined as:

$$x_{min} = \cdot (A_{s,1,tot} + A_{s,3,tot} \cdot \cos\phi) \cdot \frac{f_{yd}}{0.75 \cdot b \cdot f_{cd}} \tag{B.18}$$

The concrete compression zone can be increased if vertical force equilibrium cannot be fulfilled.

Resistance of rebars and concrete

It is assumed that the rebars are detailed properly and able to develop its yield strength. Therefore, the restoring moments around point O due to the rebars can be determined as:

$$M_s = \sum_{n=1}^{3} N_{s,i} \cdot a_{s,i} = \sum_{n=1}^{3} A_{s,i,tot} f_{yd} \cdot a_{s,i} \tag{B.19}$$

In which:

$A_{s,i,tot}$	is the total cross-sectional area of rebar i over the width
$a_{s,i}$	is the lever arm of rebar i
f_{yd}	is the design yield strength of the rebar

The tensile force in the diagonal rebar is projected perpendicular to the crack ($N_{s,3}$').

The concrete is initially assumed to be crushing in the concrete compression zone. The compression zone is than modelled using a bi-linear diagram, from which the axial compression force centers at $0.39 \cdot x_{min}$. The restoring moment due to the concrete can be determined as:

$$M_c = N_c \cdot (1 - 0.39) \cdot x_{min} \tag{B.20}$$

If vertical force equilibrium cannot be fulfilled, the concrete compression zone can be increased. Subsequently, it is assumed that the concrete is not crushing. The compressive stresses in the concrete compressive zone are linearly distributed. The restoring moment due to the concrete can in that case be determined as:

$$M_c = N_c \cdot (1 - 0.33) \cdot (x_{min} + \Delta x) \tag{B.21}$$

Load on the support

The load on the support can be determined using moment equilibrium around point O, using the restoring moments due to rebars and concrete. It can be determined as:

$$\sum M^O = M_s + M_c + F_{Rd} \cdot a_{sup} = 0 \tag{B.22}$$

From which, the load on the support can be determined as:

$$F_{Rd} = \frac{\sum M_s + M_c}{a_{sup}} \tag{B.23}$$

The load on the support is equal to the load bearing capacity of the concrete half-joint

Vertical force equilibrium

The difference between the vertical forces of the rebars and load on the support is transferred in shear stresses through the concrete compression zone to fulfil vertical force equilibrium. The shear resistance of the concrete compression zone can be determined in accordance with NEN-EN 1992-1-1 art. 6.2.2 as:

$$V_{Rd,c} = \nu_{min} \cdot b \cdot x_{min} \tag{B.24}$$

In which:

ν_{min} is the shear strength of the concrete

The shear strength of the concrete can be determined as:

$$\nu_{min} = 0.035k^{3/2} \cdot f_{ck}^{1/2} \tag{B.25}$$

In which:

k $= 1 + \sqrt{\frac{200}{x_{min}}} \leq 2.0$

If vertical force equilibrium cannot be fulfilled, the concrete compression zone is increased and the analysis needs to be executed again. It is still assumed that the concrete is crushing in the compression zone, despite the increase in height.

B.4 Optimisation

B.4.1 Strut-and-tie approach

The load bearing capacity using the strut-and-tie analysis is optimized by shifting Node (3), (4), (5) and (7) over a predefined range with a certain step-size. Subsequently, the load factor (Q_{STM}) is also be optimized. In each step, all forces are checked in each element of the strut-and-tie model (struts, ties and (combined) nodes) again. The best solution can be found as the highest solution of all lower bound solutions. The analytical tool calculates all possible solutions and presents the highest lower-bound solution, including failure mechanism.

The sequence of finding this value is elaborated below:

1. The analysis starts by setting the offsets of the nodes and load factor to zero.
2. The anchorage and angle limitations are verified and if both are correct, the solution will be stored in a database
3. Node (7) will be shifted by a predefined step-size and loop returns to 2. until the predefined range is met.
4. Node (5) will be shifted by a predefined step-size and loop returns to 2. until the predefined range is met.
5. Node (4) will be shifted by a predefined step-size and loop returns to 2. until the predefined range is met.
6. Node (3) will be shifted by a predefined step-size and loop returns to 2. until the predefined range is met.
7. The load factor (Q_{STM}) will be increased by the predefined step-size and loop returns to 2. until the load factor is equal to 1.
8. The highest solution from the database is the highest lower-bound solution for the load bearing capacity of the concrete half-joint.

An example of the optimisation of the load factor is illustrated in Figure B.19.

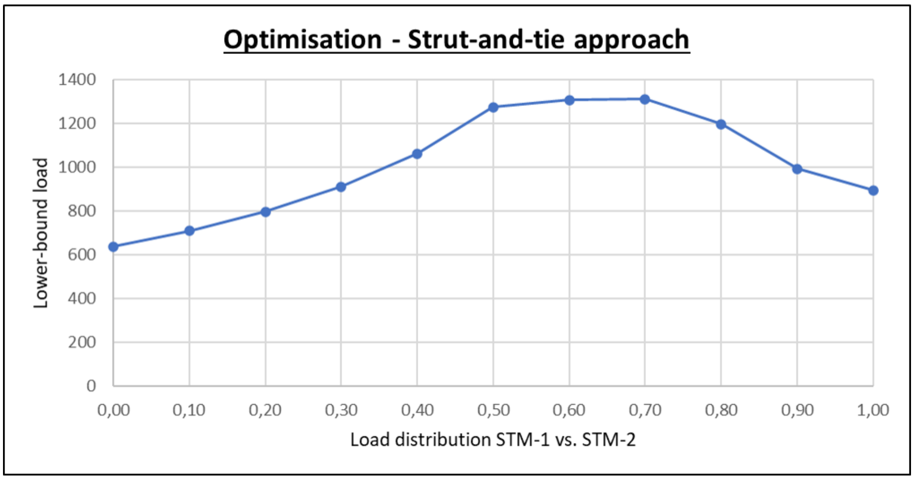

Figure B.19: Optimisation of load factor

The x-axis shows the distribution of the load over STM-1 and STM-2. If the load factor is equal to 0, the load is distributed over STM-2 only (with diagonal) and if the load factor is equal to 1, the load is distributed over STM-1 only (without diagonal). The most optimised solution can usually be found somewhere in between.

It is recommended to start with a large step-size and predefined range, and adjust the values based on the results to save computational time.

B.4.2 Kinematic approach

The load bearing capacity is calculated using an arbitrary value for the crack's angle θ_{crack}. No guidance is given on which angle must be taken. Rajapakse et al. [13], [15] compared experimental results of half-joints with analytical results and found that angles ranging between 30° and 70° provide adequate approximations.

Therefore, multiple calculations need to be made within this range, in which the lowest solution is the best upper-bound approximation of the load bearing capacity of the concrete half-joint, see Figure B.20:

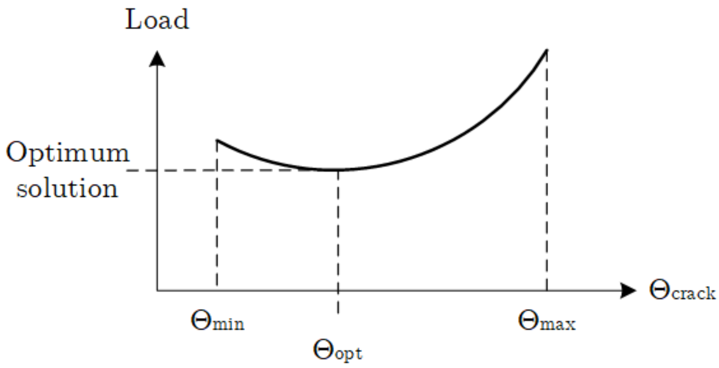

Figure B.20: Optimisation of kinematic approach

The lowest upper-bound approximation is determined using range of the crack's angles provided by Rajapakse et al. [13], [15].

B.5 Corrosion

The analytical tool is able to perform a corrosion study on the load bearing capacity of a concrete half-joint. The corrosion is simulated in the strut-and-tie approach on tie T1, T2 and T4, and in the kinematic approach on the rebars that intersect the diagonal crack.

The corrosion is simulated by reducing the cross-sectional area and/or yield strength, as elaborated in paragraph 4.5

Appendix C

Results of analytical tool

C.1 Geldermalsen

Analytical parametric tool for load bearing capacity of RC half-joints

Project
Geldermalsen

1. Geometry and material properties

1.1 Concrete

1.1.1 Geometry

a	702	[mm]
b	458	[mm]
c	491	[mm]
d	342	[mm]

Width	1000	[mm]
Cover	30	[mm]
Support	250	[mm]
α	4,84	[°]

1.1.2 Material

γ_c	1,5	[-]
k_t	1	[-]

α_{cc}	1	[-]
α_{ct}	1	[-]

f_{ck}	30,0	[N/mm^2]
f_{cm}	38,0	[N/mm^2]
f_{cd}	20,0	[N/mm^2]
v'	0,880	[-]

f_{ctm}	2,90	[N/mm^2]
$f_{ctk,0.05}$	2,03	[N/mm^2]
f_{ctd}	1,35	[N/mm^2]
Mean values?		No

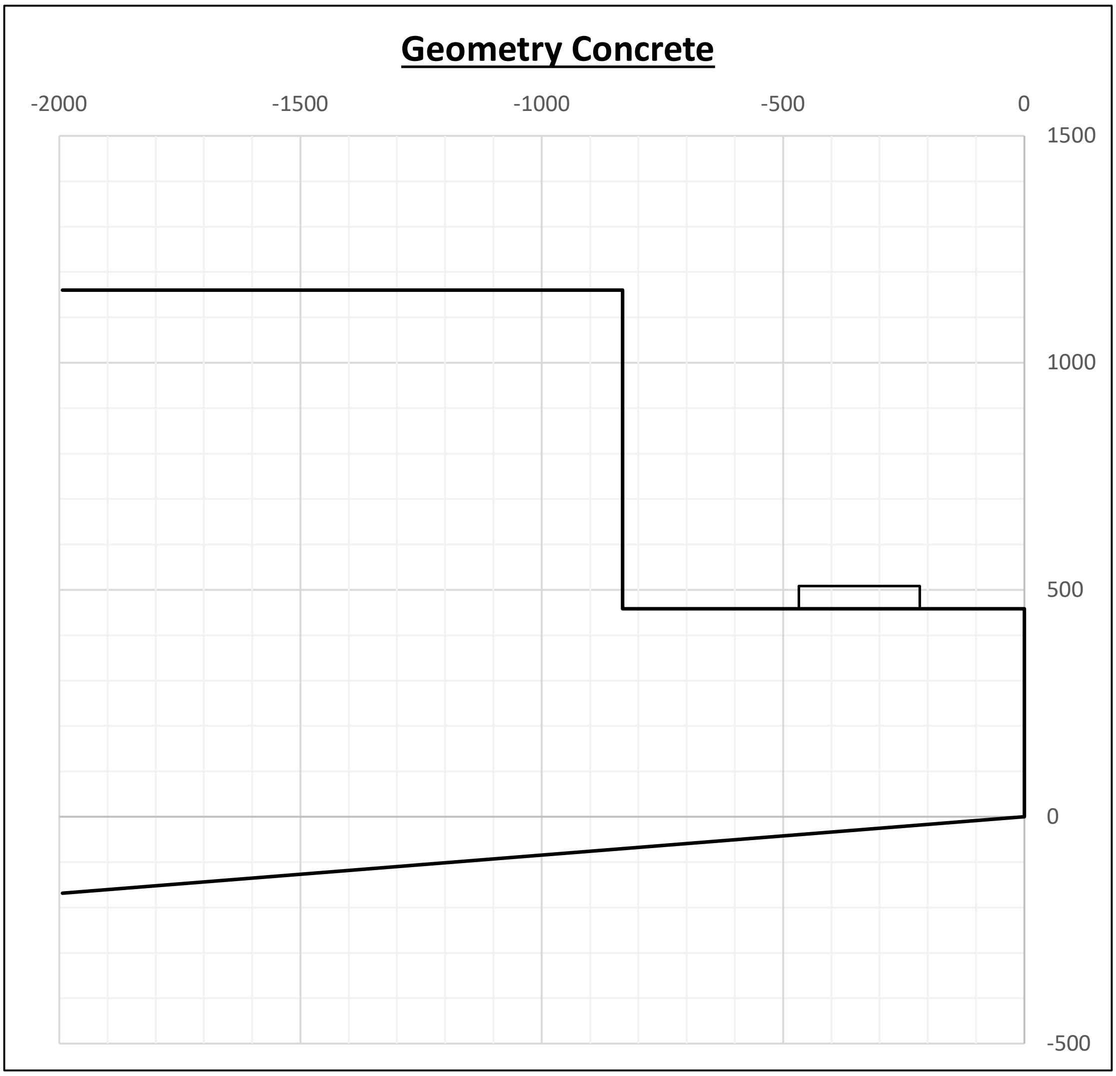

1.2 Reinforcement steel

1.2.1 Geometry

	Rebar 1	Rebar 2	Rebar 3	
Ø	24	24	24	[mm]
$Ø_m$	120	120	120	[mm]
Spacing	150	300	150	[mm]
η_1	1	1	1	[-]
η_2	1	1	1	[-]
η_3	1	1	1	[-]
l_{top}	1700	1000	-	[mm]
l_{bottom}	1700	700	-	[mm]
Δ_{top}	0	0	-	[mm]
Δ_{middle}	0	0	-	[mm]
Δ_{bottom}	0	0	-	[mm]
Corrosion	0%	0%	0%	[-]

Include Rebar 3?	Yes

Coordinates Rebar 3		
x	y	
-2000	1118	[1]
-1250	1118	[2]
-650	33	[3]
-42	33	[4]
-42	416	[5]
		[6]

ϕ	2,1	[rad]
	118,9	[°]

1.2.2 Material

$f_{yd,0}$	330	[N/mm^2]
f_{yd}	330	[N/mm^2]

$\alpha_{corr,y}$	0	[-]
	1,23	

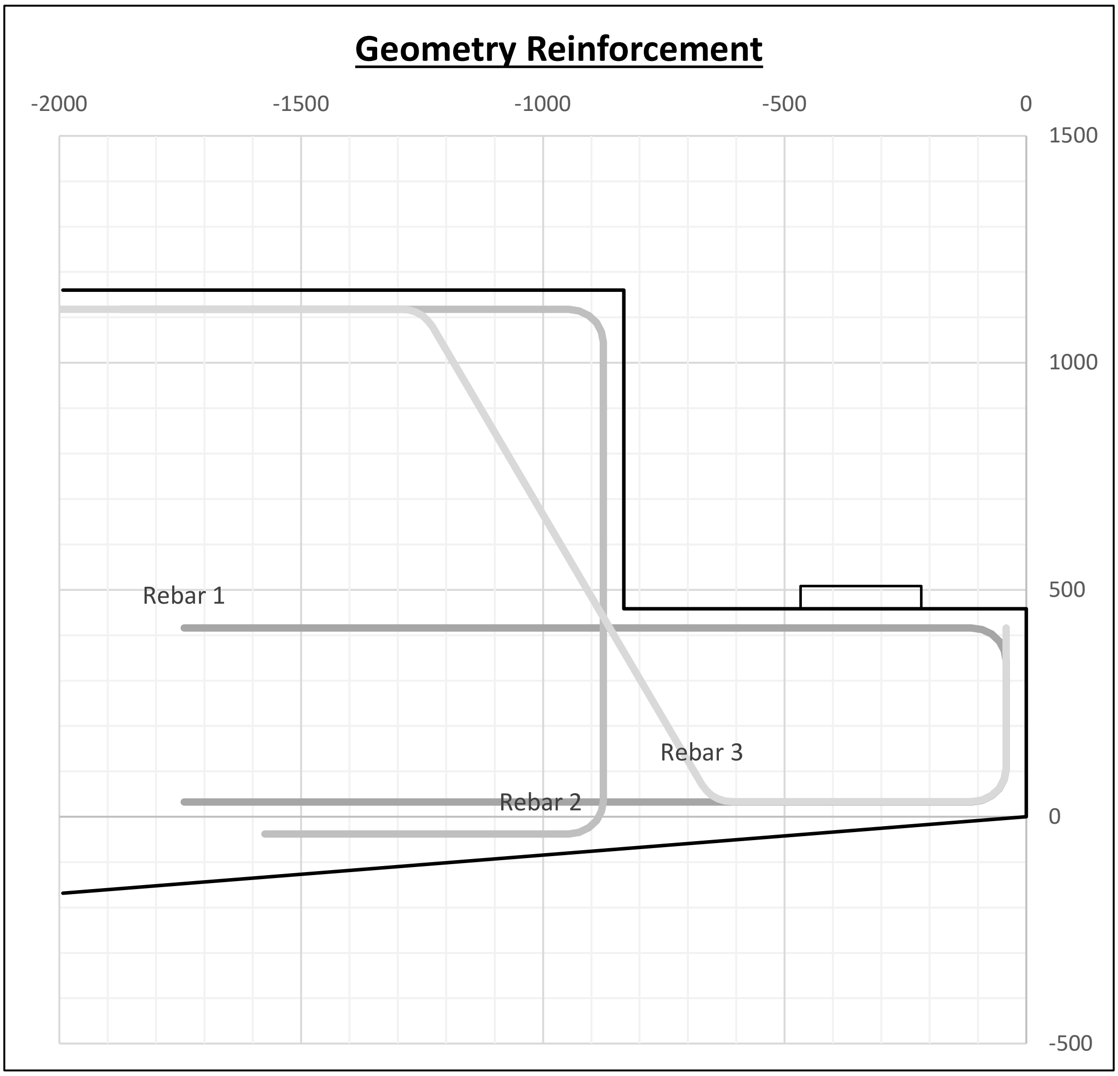

1.3 Pre-stressed steel

1.3.1 Geometry

A_p		[mm^2]
y_p		[mm]
Bearing		[mm]
Spacing		[mm]

Include prestress?	No

1.3.2 Material

σ_{pm}		[N/mm^2]
P_m		[kN]

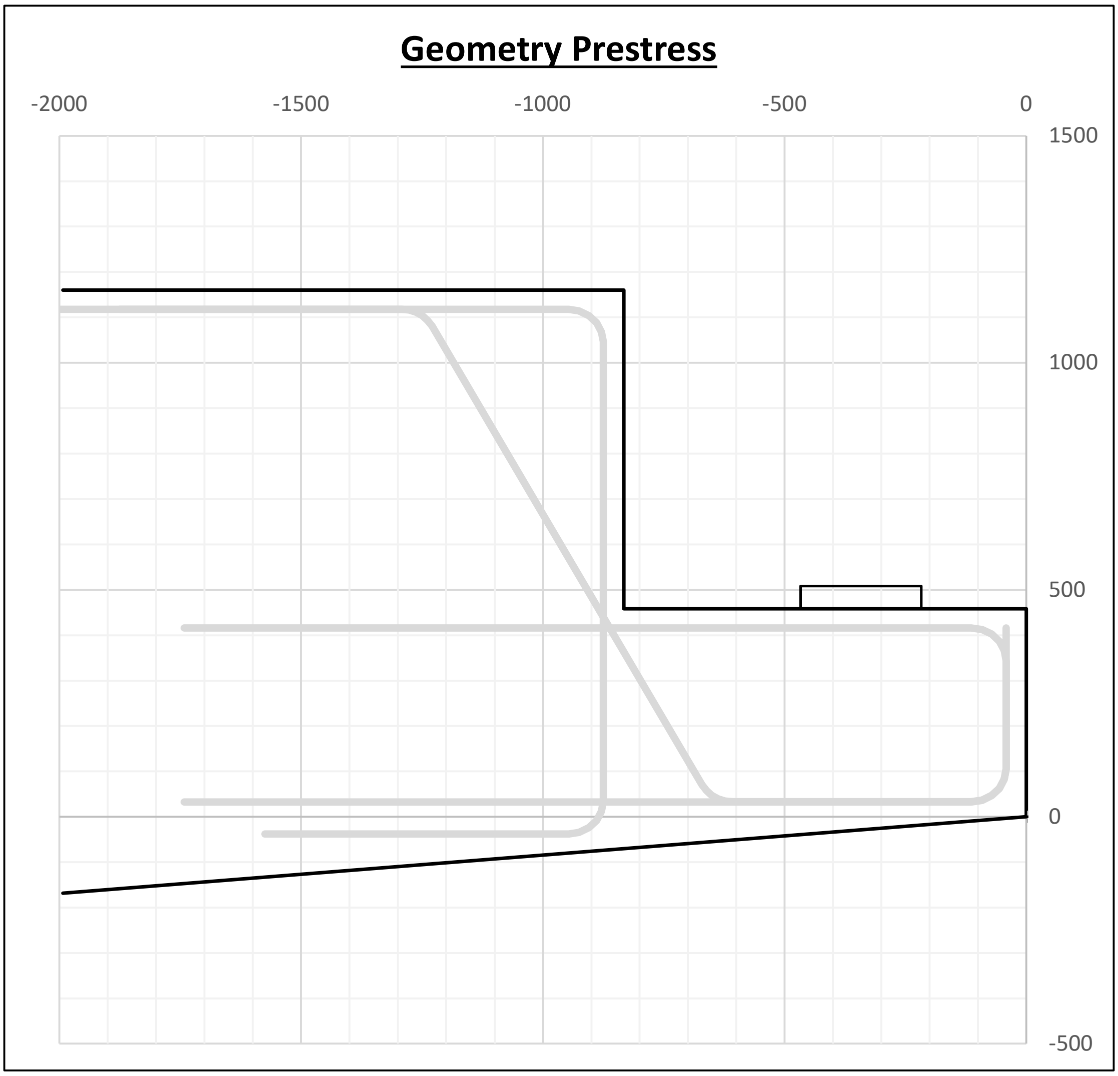

2. Strut-and-tie modelling

2.1 Nodes

	Offset		Coordinates		Type
	x	y	x	y	
(1)	-	-	-342,0	416,0	CCT
(2)	-	0	-875,0	1118,0	CTT
(3)	225	-	-1517,0	416,0	CCT
(4)	-	75	-875,0	108,8	CCT
(5)	-	75	-1993,0	-93,8	CCC
(6)	-		-1993,0	1118,0	-
(7)	70		-704,4	131,4	CCT
(8)	-	-	-1250,0	1118,0	CTT
(9)	-	-	-1993,0	1118,0	-

F_{unit}	1,00	[-]

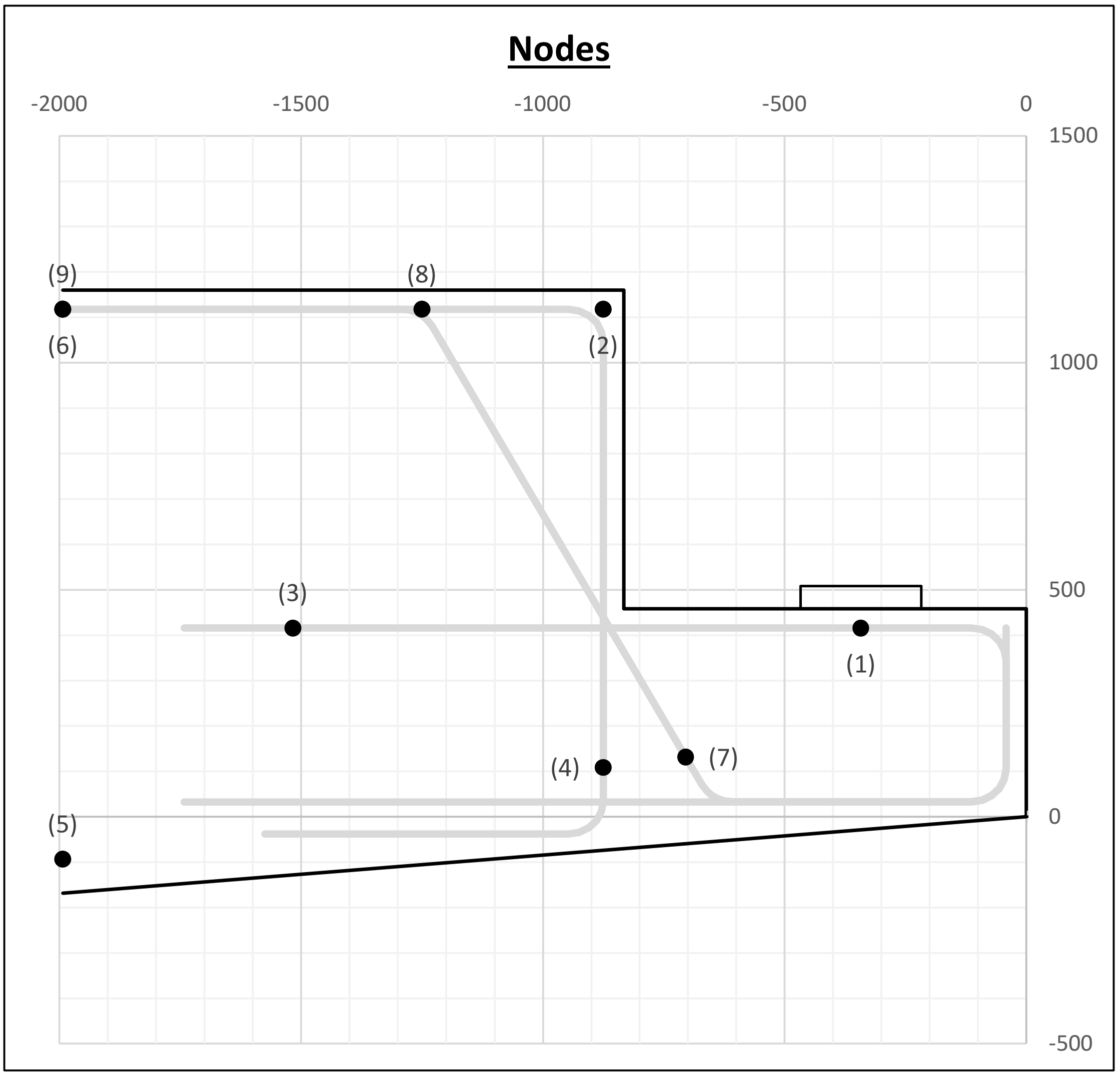

2.2 STM-1 (without diagonal)

	Node (j)	Node (k)	$F_{unit,STM1}$	Length	Angles	
			[-]	[mm]	[rad]	[°]
C1-1	(1)	(4)	-2,00	615,2	0,5228	30,0
C2-1	(2)	(3)	-0,78	951,3	0,8300	47,6
C3-1	(3)	(4)	-1,34	711,7	0,4463	25,6
C4-1	(2)	(5)	-1,23	1648,7	0,8256	47,3
C5-1	(4)	(5)	-0,54	1136,2	0,1792	10,3
T1-1	(1)	(3)	1,74	1175,0	0	0,0
T2-1	(2)	(4)	1,48	1009,2	1,5708	90,0
T3-1	(2)	(6)	1,36	1118,0	0	0,0

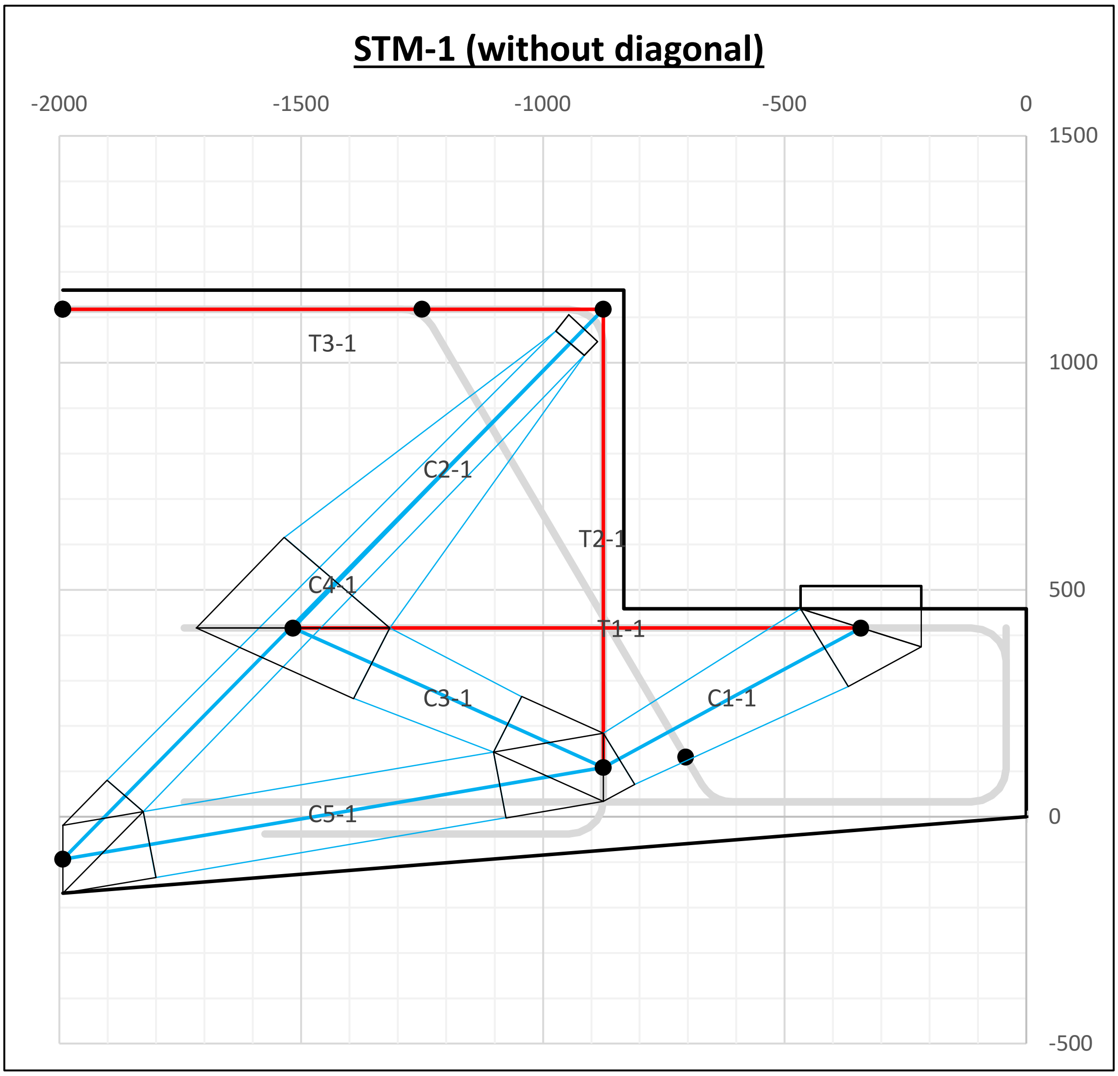

2.3 STM-2 (with diagonal)

	Node (j)	Node (k)	$F_{unit,STM2}$	Length	Angles	
			[-]	[mm]	[rad]	[°]
C2-2	(2)	(3)	-0,57	951,3	0,8300	47,6
C3-2	(3)	(4)	-0,98	711,7	0,4463	25,6
C4-2	(2)	(5)	-0,11	1648,7	0,8256	47,3
C5-2	(4)	(5)	-0,83	1136,2	0,1792	10,3
C6-2	(1)	(7)	-1,62	460,8	0,6657	38,1
C7-2	(7)	(4)	-1,72	172,1	0,1317	7,5
C8-2	(8)	(5)	-0,91	1421,4	1,0208	58,5
T1-2	(1)	(3)	1,27	1175,0	0	0,0
T2-2	(2)	(4)	0,50	1009,2	1,5708	90,0
T3-2	(2)	(6)	0,46	1118,0	0	0,0
T4-2	(7)	(8)	0,89	1127,4	1,0657	61,1
T5-2	(8)	(9)	0,90	743,0	0	0,0

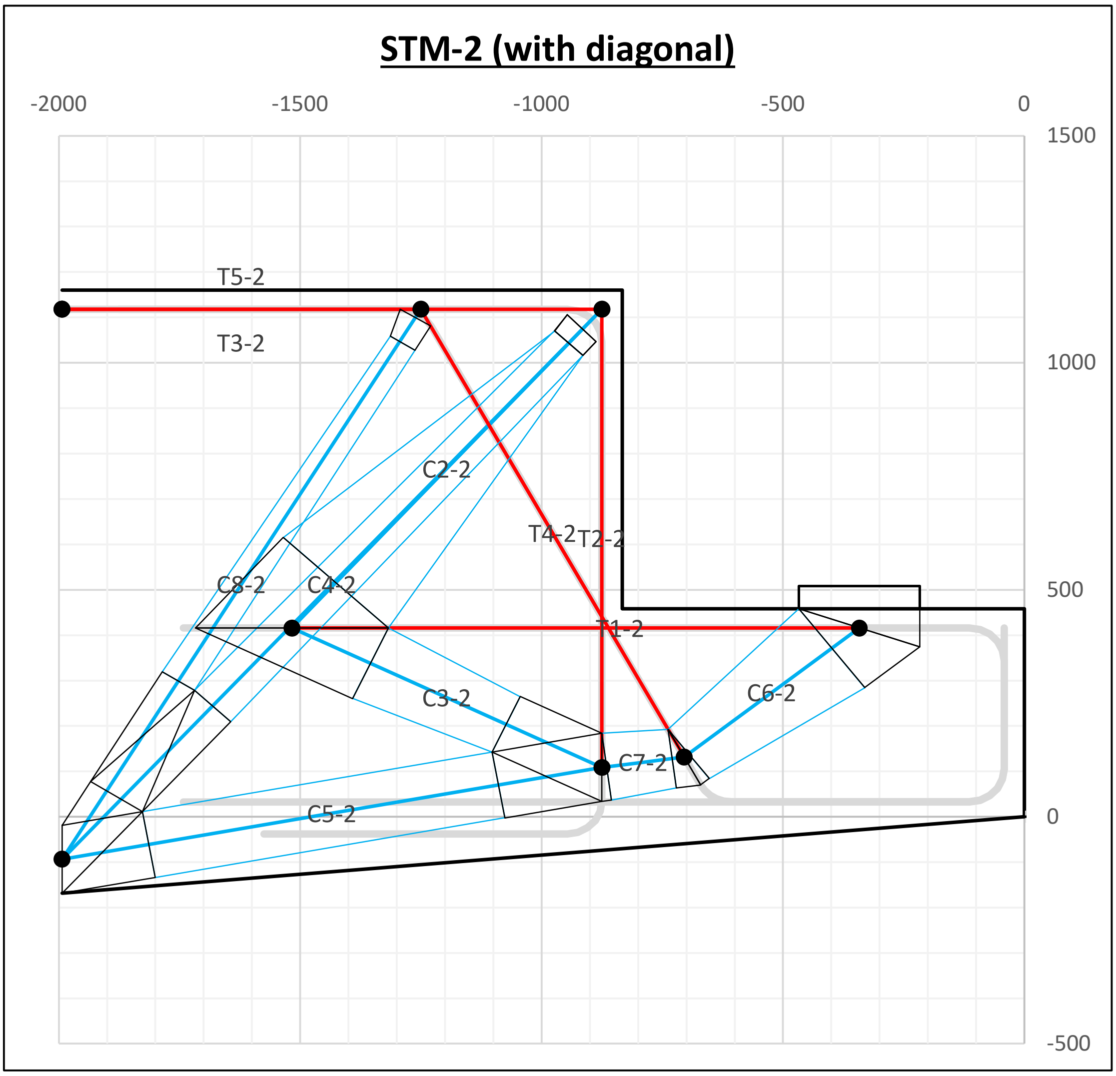

2.4 STM-3 (Combined)

	Node (j)	Node (k)	$F_{unit,STM1}$	$F_{unit,STM2}$	F_{unit}	Length	Angles	
			0,1	0,9	[-]	[mm]	[rad]	[°]
C1	(1)	(4)	-2,00		-0,20	615,2	0,5228	30,0
C2	(2)	(3)	-0,78	-0,57	-0,60	951,3	0,8300	47,6
C3	(3)	(4)	-1,34	-0,98	-1,02	711,7	0,4463	25,6
C4	(2)	(5)	-1,23	-0,11	-0,22	1648,7	0,8256	47,3
C5	(4)	(5)	-0,54	-0,83	-0,80	1136,2	0,1792	10,3
C6	(1)	(7)		-1,62	-1,46	460,8	0,6657	38,1
C7	(7)	(4)		-1,72	-1,55	172,1	0,1317	7,5
C8	(8)	(5)		-0,91	-0,82	1421,4	1,0208	58,5
T1	(1)	(3)	1,74	1,27	1,32	1175,0	0	0
T2	(2)	(4)	1,48	0,50	0,60	1009,2	1,5708	90,0
T3	(2)	(6)	1,36	0,46	0,55	1118,0	0	0
T4	(7)	(8)		0,89	0,80	1127,4	1,0657	61,1
T5	(8)	(6)		0,90	0,81	743,0	0	0

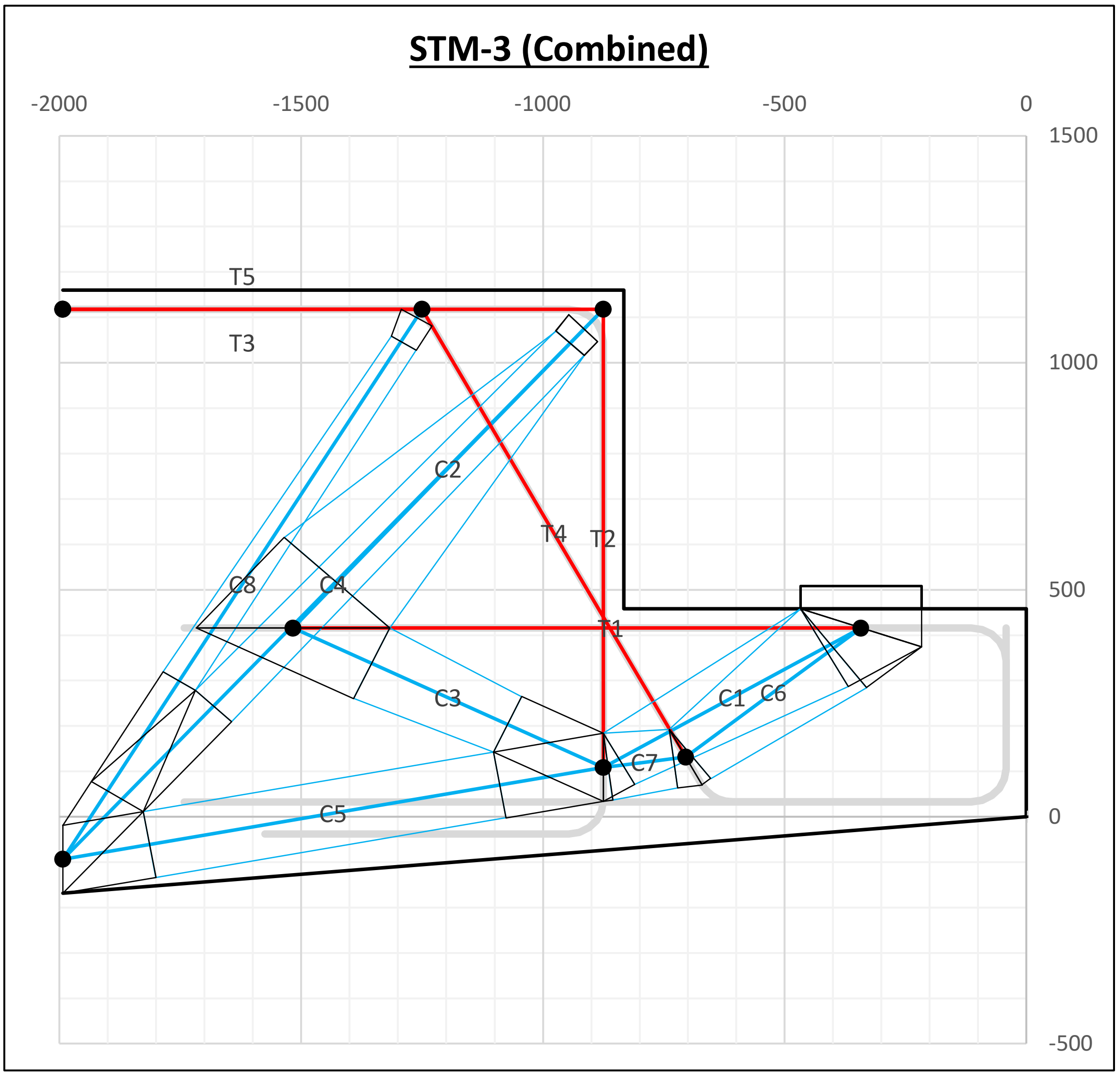

2.5 Node dimensions

Node (1)	T1	F	C1	C6		CCT
$a_{(1)}$	-	263,7	263,7	263,7		[mm]
$w_{(1)}$	-	250,0	197,6	220,5		[mm]
$b_{(1)}$	-	84,0	174,7	144,7		[mm]

Node (2)	T2	T3	C2	C4		CTT
$a_{(2)}$	-	-	84,9	84,9		[mm]
$w_{(2)}$	-	-	79,5	80,0		[mm]
$b_{(2)}$	-	-	-	-		[mm]

Node (3)	T1	C2	C3			CCT
$a_{(3)}$	-	400,0	400,0			[mm]
$w_{(3)}$	-	295,2	172,6			[mm]
$b_{(3)}$	-	269,9	360,8			[mm]

Node (4)	T2	C1	C3	C5	C7	CCT
$a_{(4)}$	-	150,0	231,1	252,1	150,0	[mm]
$w_{(4)}$	-	130,0	135,3	147,6	148,7	[mm]
$b_{(4)}$	-	74,9	187,3	204,3	19,7	[mm]

Node (5)	C4	C5	C8	Internal		CCC
$a_{(5)}$	288,1	245,1	294,8	168,9		[mm]
$w_{(5)}$	101,7	147,6	78,4	125,9		[mm]
$b_{(5)}$	269,6	195,6	284,2	112,5		[mm]

Node (7)	T4	C6	C7			CCT
$a_{(7)}$	-	140,0	140,0			[mm]
$w_{(7)}$	-	138,2	130,4			[mm]
$b_{(7)}$	-	22,4	51,1			[mm]

Node (8)	T4	T5	C8			CTT
$a_{(8)}$	-	-	-			[mm]
$w_{(8)}$	-	-	59,8			[mm]
$b_{(8)}$	-	-	-			[mm]

2,6 Checks

2.6.1 Compressive strength of struts

Strut i	C1	C2	C3	C4	C5	C6	C7	C8	
$F_{unit,i}$	-0,200	-0,595	-1,018	-0,218	-0,800	-1,457	-1,545	-0,818	[-]
Tension	Yes	Yes	Yes	Yes	Yes	Yes	Yes	Yes	
$\sigma_{Rd,max,c}$	10,56	10,56	10,56	10,56	10,56	10,56	10,56	10,56	[N/mm^2]
L_c	615,2	951,3	711,7	1648,7	1136,2	460,8	172,1	1421,4	[mm]
$w_{c,eff}$	130,0	79,5	135,3	80,0	147,6	138,2	130,4	59,8	[mm]
$C_{max,C,i}$	-1372,4	-839,2	-1428,9	-844,9	-1558,6	-1459,4	-1376,5	-632,0	[kN/m]
$F_{max,C,i}$	6852,9	1409,9	1404,1	3873,2	1948,3	1001,4	890,9	773,0	[kN/m]

2.6.2 Compressive strength of nodes

Strut	C1	C2	C3	C4	C5	C6	C7	C8	
Node (j)	(1)	(2)	(3)	(2)	(4)	(1)	(7)	(8)	
Type	CCT	CTT	CCT	CTT	CCT	CCT	CCT	CTT	
k	0,85	0,75	0,85	0,75	0,85	0,85	0,85	0,75	[-]
$\sigma_{Rd,max,(j)}$	14,96	13,20	14,96	13,20	14,96	14,96	14,96	13,20	[N/mm^2]
$w_{i(j)}$	197,6	79,5	172,6	80,0	147,6	220,5	130,4	59,8	[mm]
$C_{max,i(j)}$	-2956,3	-1049,0	-2582,8	-1056,1	-2208,0	-3298,1	-1950,1	-790,0	[kN/m]
$F_{max,i(j)}$	14762,0	1762,4	2538,0	4841,5	2760,1	2263,2	1262,2	966,2	[kN/m]
Node (k)	(4)	(3)	(4)	(5)	(5)	(7)	(4)	(5)	
Type	CCT	CCT	CCT	CCC	CCC	CCT	CCT	CCC	
k	0,85	0,85	0,85	1,00	1,00	0,85	0,85	1,00	[-]
$\sigma_{Rd,max,(k)}$	14,96	14,96	14,96	17,60	17,60	14,96	14,96	17,60	[N/mm^2]
$w_{i(k)}$	130,0	295,2	135,3	101,7	147,6	138,2	148,7	78,4	[mm]
$C_{max,i(k)}$	-1944,2	-4415,8	-2024,2	-1790,2	-2597,7	-2067,5	-2224,6	-1380,0	[kN/m]
$F_{max,i(k)}$	9708,3	7418,8	1989,1	8206,9	3247,2	1418,7	1439,8	1687,7	[kN/m]

2.6.3 Compressive strength of internal nodes

Node (j/k)	(1)	(2)	(4)	(5)	
Strut i_1	C1	C2	C1	C4	
$F_{unit,i,1}$	-0,150	-0,595	-0,174	-0,148	[-]
Strut i_2	C6	C4	C7	C5	
$F_{unit,i,2}$	-1,218	-0,218	-1,532	-0,787	[-]
Strut i_3	-		-	C8	
$F_{unit,i,3}$				-0,427	[-]
F_{unit}	-1,368	-0,813	-1,705	-1,362	[-]
Type	CCT	CTT	CCT	CCC	
k	0,85	0,75	0,85	1,00	[-]
$\sigma_{Rd,max}$	14,96	13,20	14,96	17,60	[N/mm^2]
w	263,7	79,5	150,0	150,0	[mm]
C_{max}	-3945,5	-1049,0	-2244,0	-2640,0	[kN/m]
F_{max}	2883,6	1291,0	1316,0	1937,6	[kN/m]

2.6.4 Yield strength of ties

Ties	T1	T2	T3	T4	T5		
$F_{unit,i}$	1,320	0,600	0,550	0,797	0,813	[-]	
Rebar	1	2	2	3	3	[-]	
Ø	24	24	34	24	34	[mm]	(add top rebar)
Corrosion	0%	0%	0%	0%	-	[-]	(at re-entrant corner)
f_{yd}	330	330	330	330	330	[N/mm^2]	
$T_{max,T,ind,i}$	149,3	149,3	299,6	149,3	299,6	[kN]	
$T_{max,T,i}$	995,3	497,6	998,7	995,3	1997,4	[kN/m]	
$F_{max,T,i}$	754,2	830,0	1817,1	1249,5	2457,2	[kN/m]	

2.6.5 Anchorage length of ties

Lower-bound load 754,2 [kN/m] Failure mechanism: T1

Ties	T1	T2	T3	T4	T5	
F_T	995,3	452,2	414,5	600,7	613,0	[kN/m]
$F_{T,ind}$	149,3	135,7	124,4	90,1	92,0	[kN]
f_{bd}	3,04	3,04	3,04	3,04	3,04	[N/mm^2]
σ_{sd}	330,0	299,9	137,0	199,2	101,3	[N/mm^2]
$l_{b,rqd,max}$	651,0	591,6	382,8	393,0	283,1	[mm]
Node (j)	(1)	(2)	(2)	(7)	(8)	
c_d	75,0	-	-	75,0	-	[mm]
p	3,02	-	-	7,75	-	[N/mm^2]
α_1	0,7	-	-	0,7	-	[-]
α_2	0,9	-	-	0,9	-	[-]
α_3	1,0	-	-	1,0	-	[-]
α_4	1,0	-	-	1,0	-	[-]
α_5	0,88	-	-	0,70	-	[-]
$l_{b,min}$	240,0	-	-	240,0	-	[mm]
l_{bd}	375,7	-	-	240,0	-	[mm]
$l_{b,prov}$	2446,8	-	-	1134,4	-	[mm]
Check	Correct	-	-	Correct	-	
Node (k)	(3)	(4)	(6)	(8)	(6)	
c_d	75,0	150,0	-	-	-	[mm]
p	0,74	8,57	-	-	-	[N/mm^2]
α_1	0,7	0,7	-	-	-	[-]
α_2	0,9	0,7	-	-	-	[-]
α_3	1,0	1,0	-	-	-	[-]
α_4	1,0	1,0	-	-	-	[-]
α_5	0,97	0,70	-	-	-	[-]
$l_{b,min}$	240,0	240,0	-	-	-	[mm]
l_{bd}	414,7	240,0	-	-	-	[mm]
$l_{b,prov}$	425,0	891,1	-	-	-	[mm]
Check	Correct	Correct	-	-	-	

3. Kinematic approach (upper-bound approximation)

x_min	98,5	[mm]
Δx	0	[mm]

θ_{Crack}	30,0	[°]
l_{crack}	1008,0	[mm]

	$A_{s,i}$	A_s	f_{yd}	N_S / N_C	Leverarm	Moment	$N_{y\text{-}dir}$
	[mm^2]	[mm^2]	[N/mm^2]	[kN/m]	[mm]	[kNm/m]	[kN/m]
Rebar 1	452	3016	330	995,3	462,0	459,8	0,0
Rebar 2	452	1508	330	497,6	830,9	413,5	497,6
Rebar 3	452	3016	330	995,3	962,5	957,9	871,0
Concrete	-	-	-	1476,9	60,1	88,7	0,0
Total						1919,9	1368,6

Support		
Leverarm:	1363,9	[mm]
Upper-bound load:	1407,6	[kN/m]

Vertical equilibrium	Correct	
Difference in vertical force	39,0	[kN/m]
Concrete shear resistance	53,4	[kN/m]

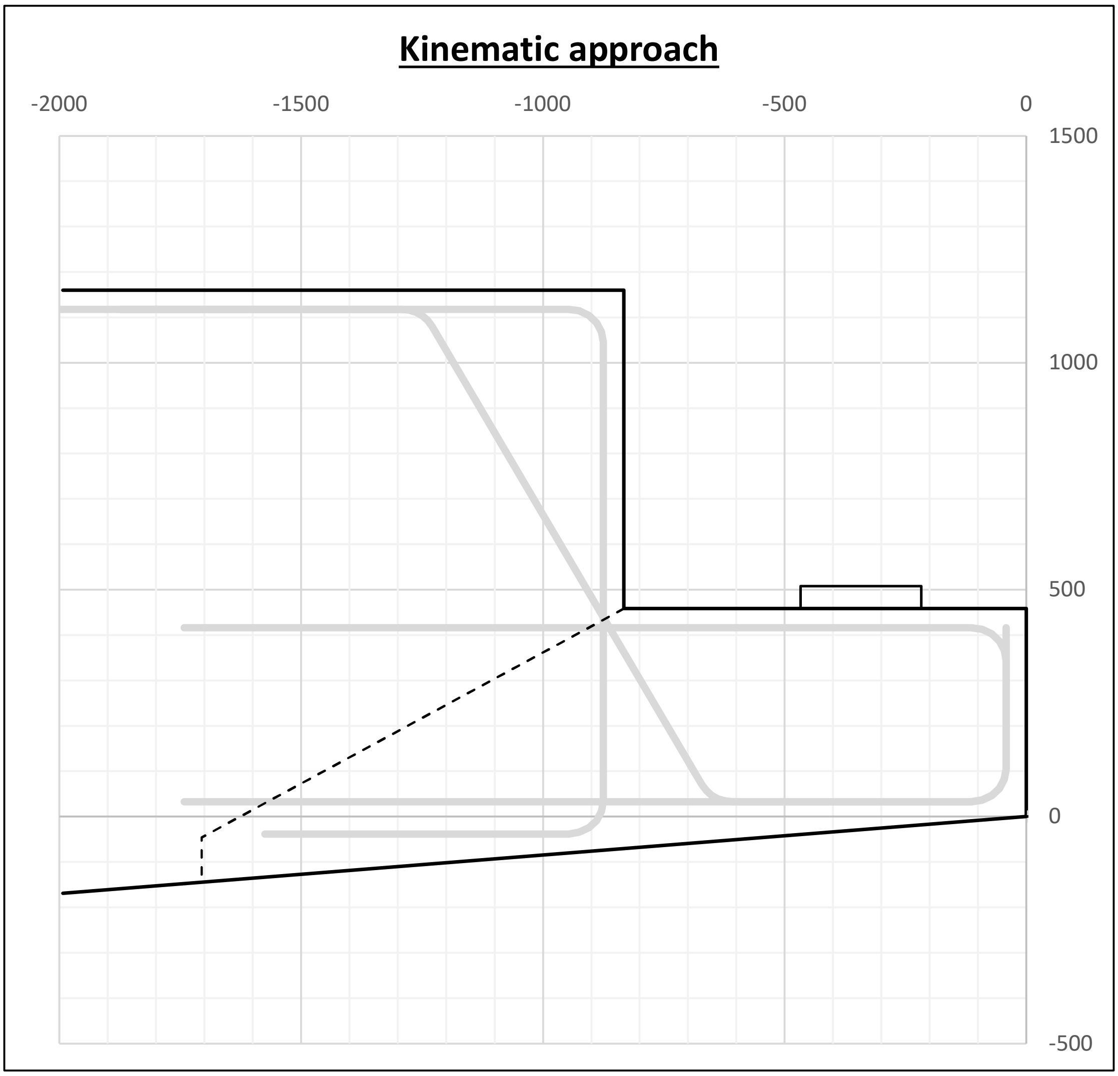

4. Optimisation

4.1 Strut-and-tie approach (Highest lower-bound approximation)

	Stepsize	Max. shift	Steps
Load	0,1	-	10
Node 3	25	300,0	12
Node 4	25	100,0	4
Node 5	25	100,0	4
Node 7	10	100,0	10

min θ 25,0 [°]

Anchorage:	Correct	
Angle (theta):	Correct	
Lower-bound load	754,2	[kN/m]

Limitations on angles				
	Minimum	Maximum	[°]	
θC1	25,0	65,0	30,0	Correct
θC2	25,0	65,0	47,6	Correct
θC3	25,0	65,0	25,6	Correct
θC4	25,0	65,0	47,3	Correct
θC6	25,0	-	38,1	Correct
θC7	-	65,0	7,5	Correct
θC8	25,0	-	58,5	Correct
θC6+θT4	-	155,0	99,2	Correct
θT4-θC7	25,0	-	53,5	Correct
θC8+θT4	25,0	-	119,5	Correct

Governing lower-bound load: 754,2 [kN/m] Failure mechanism: T1

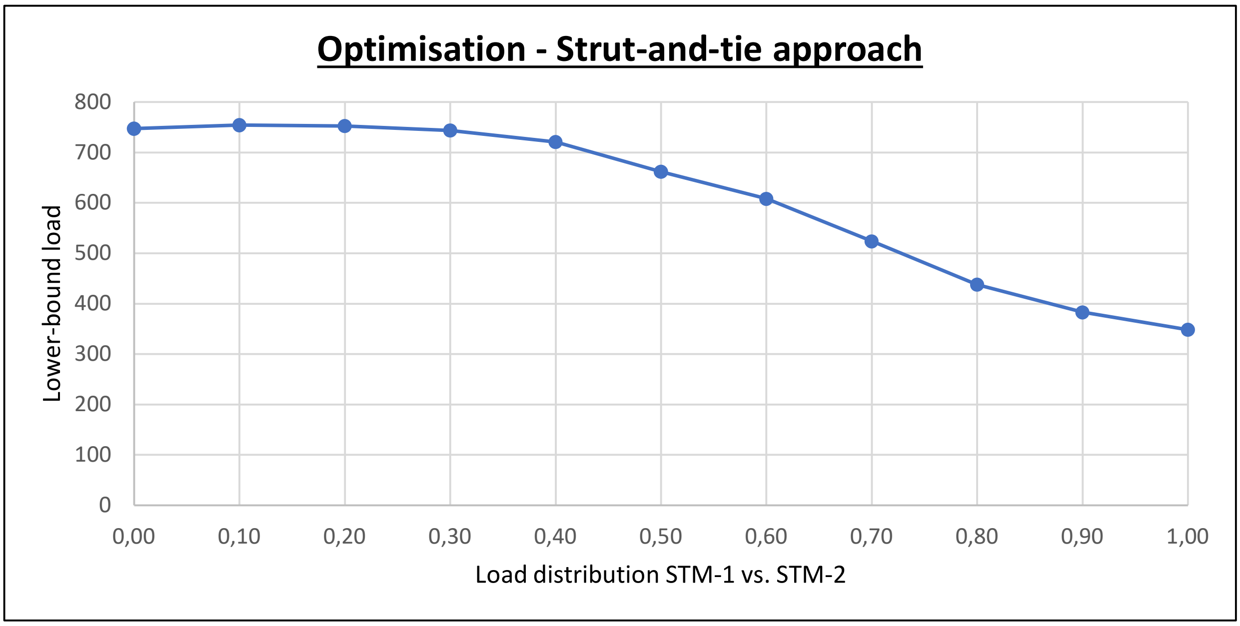

Load distribution		Offset				Load		Limitations	
STM-1	STM-2	Node 3	Node 4	Node 5	Node 7	[kN]	Mechan.	Anchor.	Angle
0,000	1,000	225	75	75	80	747,5	T1	Correct	Correct
0,100	0,900	225	75	75	70	754,2	T1	Correct	Correct
0,200	0,800	225	75	75	60	752,7	T1	Correct	Correct
0,300	0,700	225	75	75	50	743,9	T1	Correct	Correct
0,400	0,600	225	75	50	40	720,6	C7 (strut)	Correct	Correct
0,500	0,500	275	100	50	40	661,7	T1	Correct	Correct
0,600	0,400	275	100	50	30	608,1	T2	Correct	Correct
0,700	0,300	275	100	25	20	523,8	T2	Correct	Correct
0,800	0,200	275	100	25	20	438,1	T2	Correct	Correct
0,900	0,100	175	50	50	10	383,2	T2	Correct	Correct
1,000	0,000	175	50	50	10	348,1	T2	Correct	Correct

4,2 Kinematic approach (Lowest upper-bound approximation)

$\theta_{C,min}$	30,0	[°]
$\theta_{C,max}$	70,0	[°]

θ_{Crack}		30,0	36,7	43,3	50,0	56,7	63,3	70,0	[°]
Rebar 1	Leverarm	462,0	443,3	430,5	421,0	413,4	388,4	366,7	[mm]
	Moment	459,8	441,2	428,4	419,0	411,5	386,5	364,9	[kNm/m]
Rebar 2	Leverarm	830,9	609,8	458,8	346,5	257,5	174,1	106,7	[mm]
	Moment	413,5	303,5	228,3	172,4	128,2	86,7	53,1	[kNm/m]
Rebar 3	Leverarm	962,5	766,7	641,5	555,6	493,7	426,4	374,5	[mm]
	Moment	957,9	763,1	638,5	552,9	491,3	424,4	372,7	[kNm/m]
Concrete	Leverarm	60,1	60,1	60,1	60,1	60,1	77,6	88,3	[mm]
	Moment	88,7	88,7	88,7	88,7	88,7	114,7	130,4	[kNm/m]
ΔX		0,0	0,0	0,0	0,0	0,0	18,0	34,0	[mm]
Total moment		1919,9	1596,4	1383,9	1233,0	1119,7	1012,3	921,2	[kNm/m]
Leverarm support		1363,9	1142,8	991,8	879,5	790,5	707,1	639,7	[mm]
Load support		1407,6	1396,9	1395,4	1402,0	1416,3	1431,5	1440,0	[kN/m]

Governing upper-bound load: 1395,4 [kN/m]

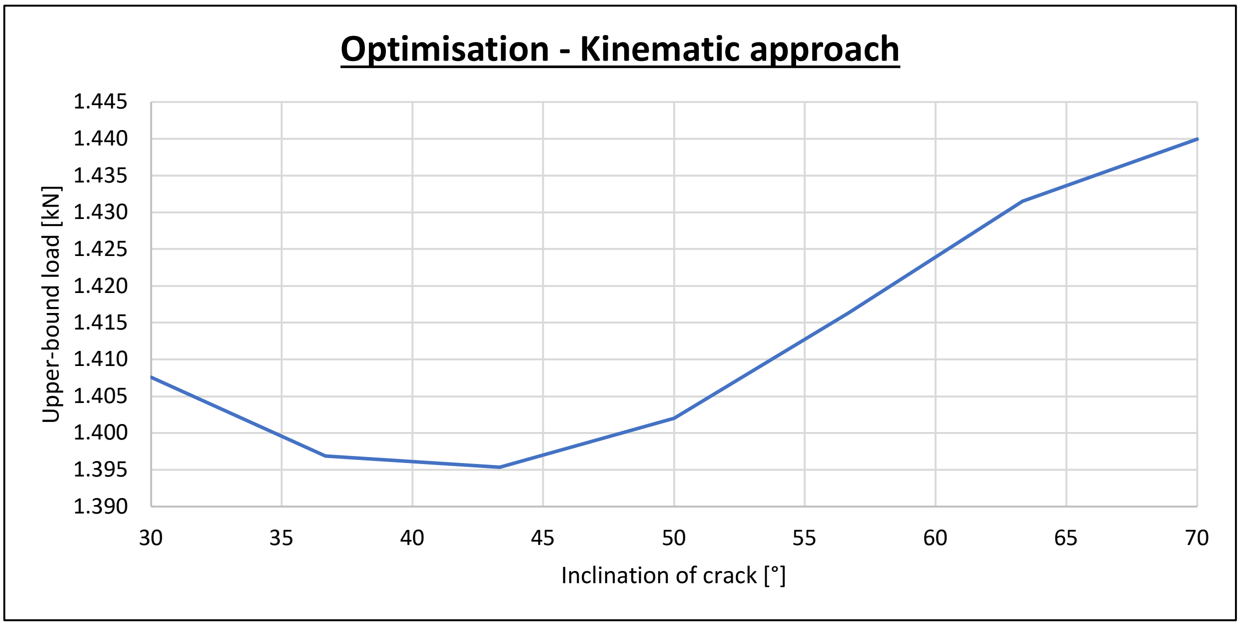

5. Corrosion

	Stepsize	Max
Corrosion	10%	60%

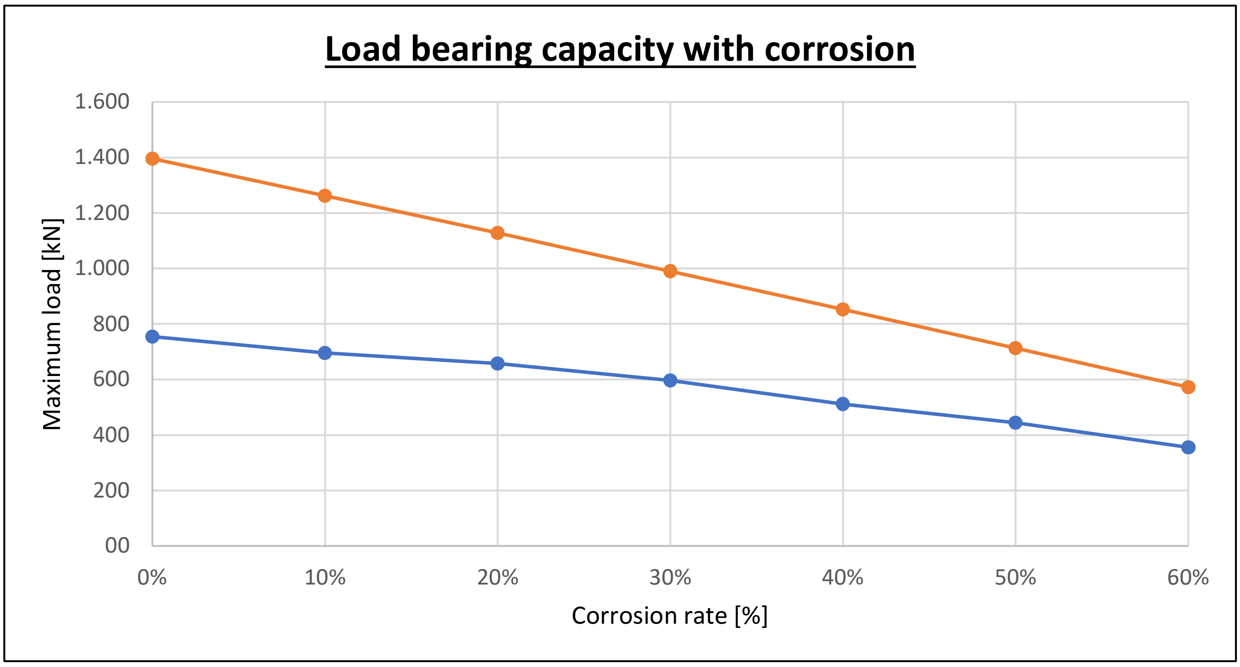

Maximum load	Corrosion							
	0%	10%	20%	30%	40%	50%	60%	
Lower-bound load	754,2	695,7	657,3	596,6	511,4	444,6	355,7	[kN/m]
Failure mechanism	T1	C8 (strut)	T1	T1	T1	T1	T1	
Upper-bound load	1395,4	1262,4	1127,4	990,7	852,7	713,6	572,4	[kN/m]

C.2 Postweg

Analytical parametric tool for load bearing capacity of RC half-joints

Project
Postweg

1. Geometry and material properties

1.1 Concrete

1.1.1 Geometry

a	598	[mm]
b	498	[mm]
c	401	[mm]
d	241	[mm]

Width	1000	[mm]
Cover	35	[mm]
Support	200	[mm]
α	0	[°]

1.1.2 Material

γ_c	1,5	[-]
k_t	1	[-]

α_{cc}	1	[-]
α_{ct}	1	[-]

f_{ck}	35,0	[N/mm^2]
f_{cm}	43,0	[N/mm^2]
f_{cd}	23,3	[N/mm^2]
v'	0,860	[-]

f_{ctm}	3,21	[N/mm^2]
$f_{ctk,0.05}$	2,25	[N/mm^2]
f_{ctd}	1,50	[N/mm^2]
Mean values?		No

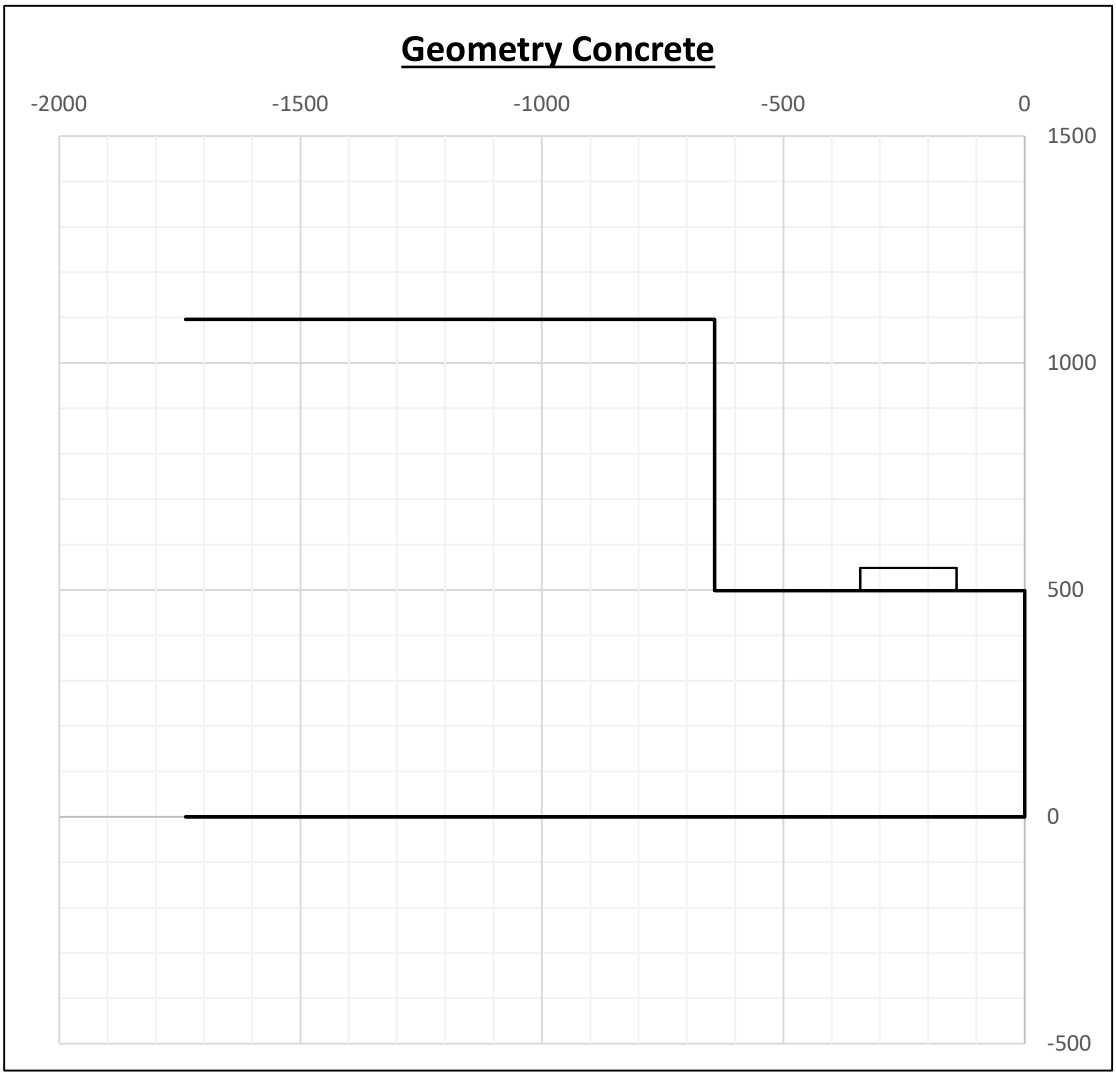

1.2 Reinforcement steel

1.2.1 Geometry

	Rebar 1	Rebar 2	Rebar 3	
Ø	20	25	16	[mm]
$Ø_m$	100	125	80	[mm]
Spacing	100	100	100	[mm]
η_1	1	1	1	[-]
η_2	1	1	1	[-]
η_3	1	1	1	[-]
l_{top}	1142	1000	-	[mm]
l_{bottom}	642	575	-	[mm]
Δ_{top}	5	30	-	[mm]
Δ_{middle}	0	0	-	[mm]
Δ_{bottom}	45	45	-	[mm]
Corrosion	0%	0%	0%	[-]

Include Rebar 3?	Yes

Coordinates Rebar 3		
x	y	
-1650	1018,5	[1]
-1292	1018,5	[2]
-335	90	[3]
-45	90	[4]
		[5]
		[6]

ϕ	2,4	[rad]
	135,9	[°]

1.2.2 Material

$f_{yd,0}$	435	[N/mm^2]
f_{yd}	435	[N/mm^2]

$\alpha_{corr,y}$	0	[-]
	1,23	

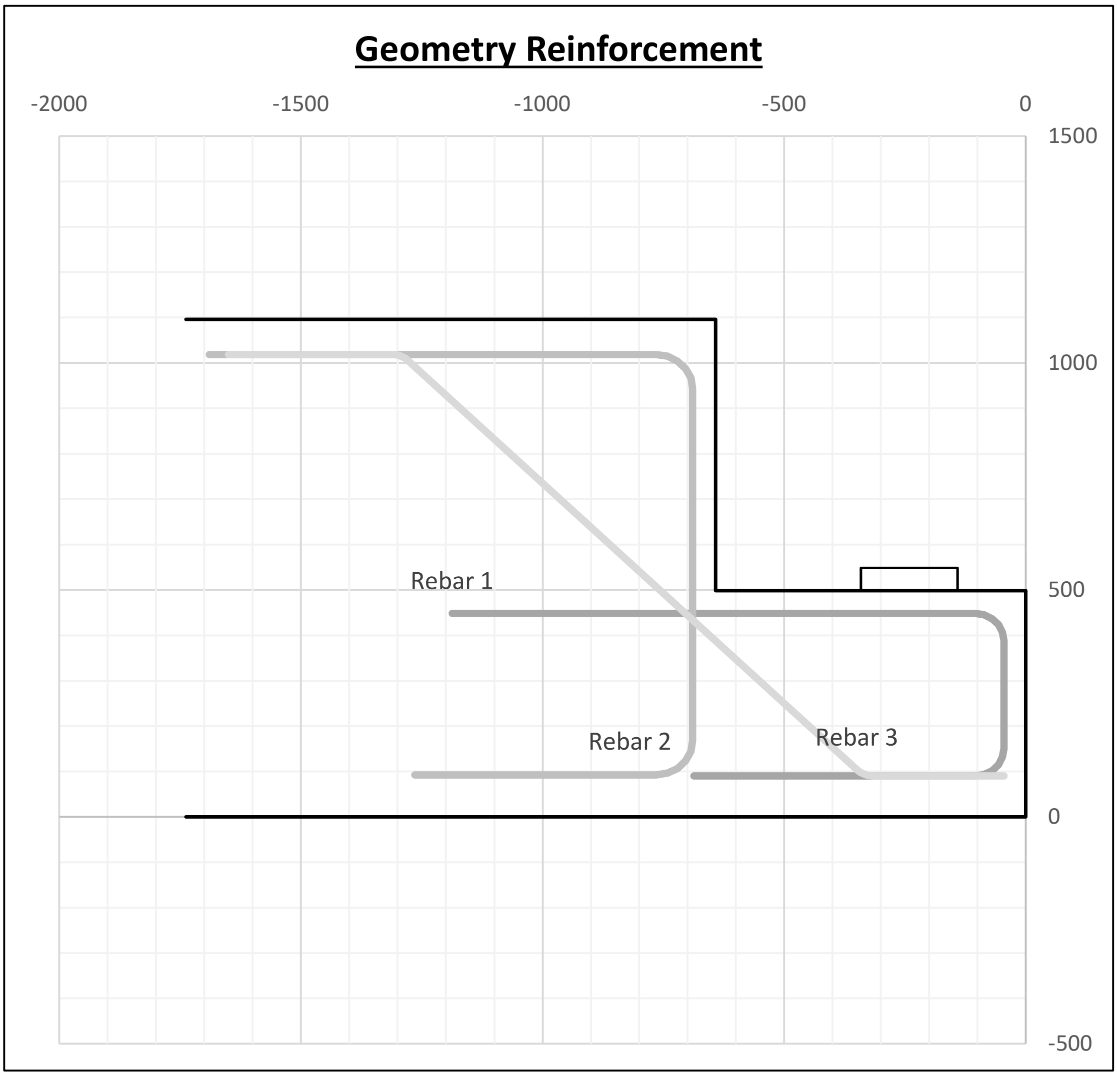

1.3 Pre-stressed steel

1.3.1 Geometry

A_p	1568	[mm^2]
y_p	900	[mm]
Bearing	200	[mm]
Spacing	3372	[mm]

Include prestress?	Yes

1.3.2 Material

σ_{pm}	1208	[N/mm^2]
P_m	1894,6	[kN]

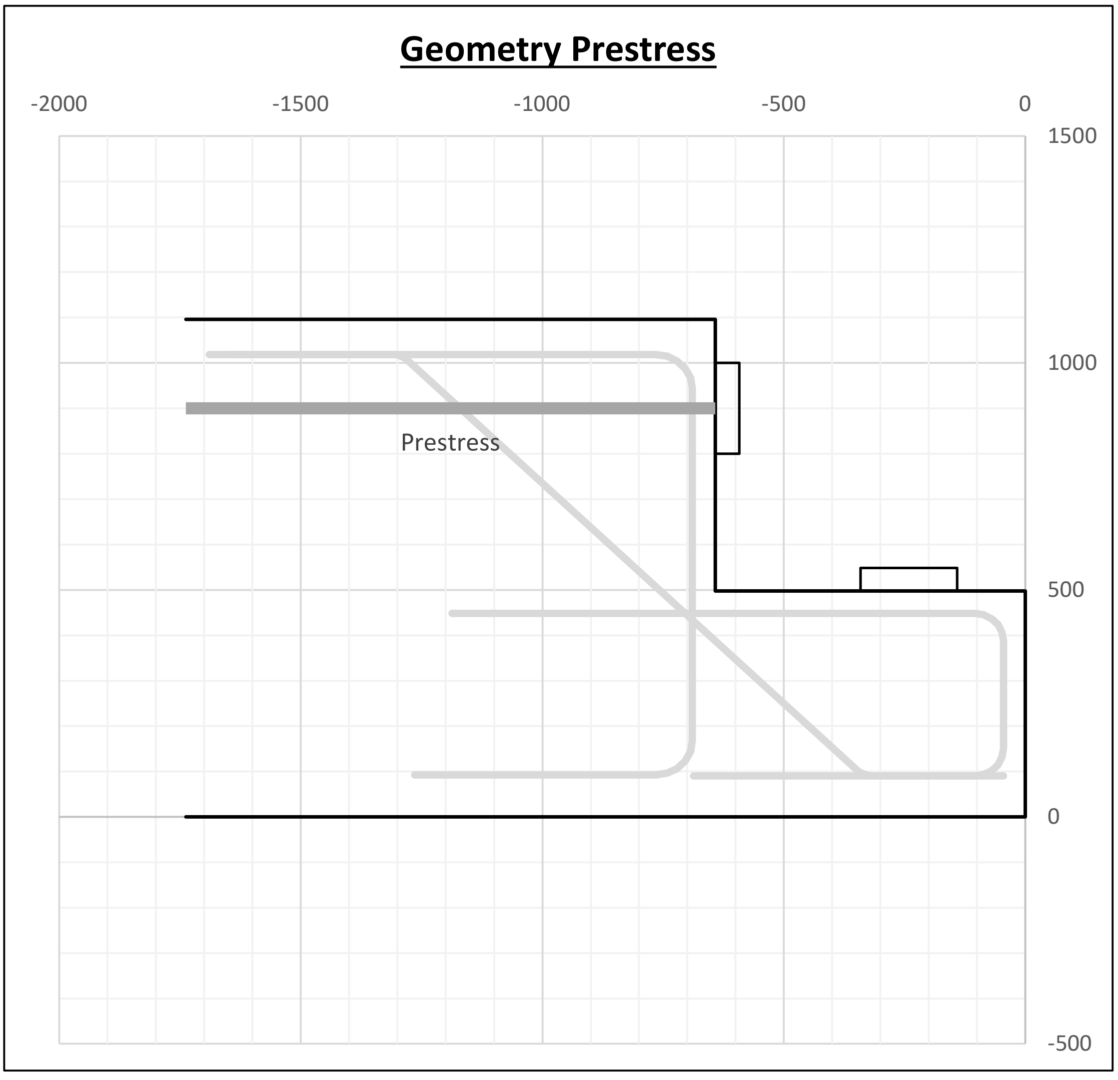

2. Strut-and-tie modelling

2.1 Nodes

	Offset		Coordinates		Type
	x	y	x	y	
(1)	-	-	-241,0	448,0	CCT
(2)	-	0	-689,5	900,0	CTT
(3)	250	-	-937,0	448,0	CCT
(4)	-	60	-689,5	227,5	CCT
(5)	-	40	-1738,0	40,0	CCC
(6)	-		-1738,0	900,0	-
(7)	150		-456,6	208,0	CCT
(8)	-	-	-1292,0	1018,5	CTT
(9)	-	-	-1738,0	1018,5	-

F_{unit}	1,00	[-]

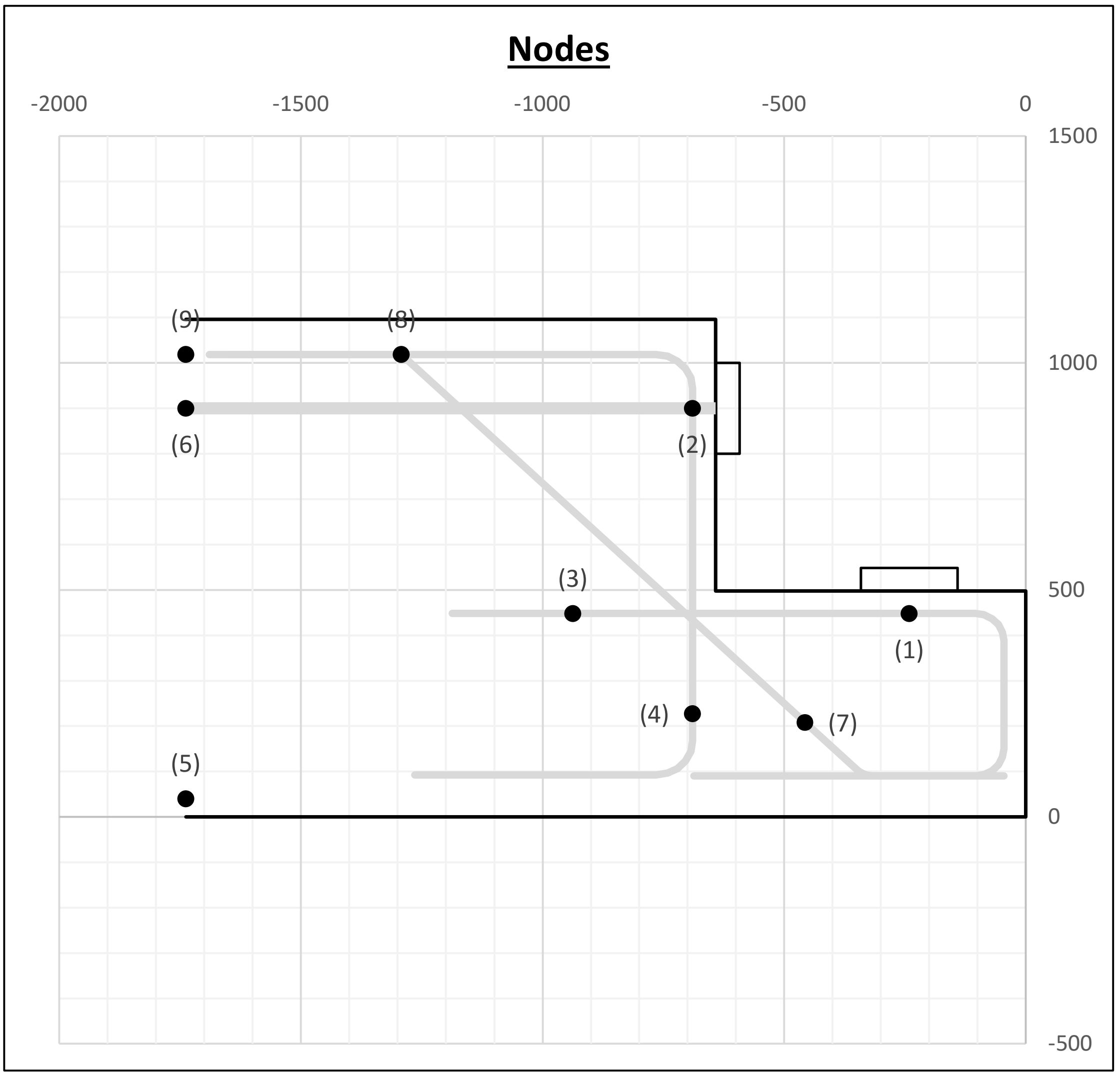

2.2 STM-1 (without diagonal)

	Node (j)	Node (k)	$F_{unit,STM1}$	Length	Angles	
			[-]	[mm]	[rad]	[°]
C1-1	(1)	(4)	-2,27	499,8	0,4569	26,2
C2-1	(2)	(3)	-1,39	515,3	1,0698	61,3
C3-1	(3)	(4)	-1,83	331,5	0,7278	41,7
C4-1	(2)	(5)	-1,39	1356,1	0,6869	39,4
C5-1	(4)	(5)	-0,68	1065,1	0,1770	10,1
T1-1	(1)	(3)	2,03	696,0	0	0,0
T2-1	(2)	(4)	2,10	672,5	1,5708	90,0
P-1	(2)	(6)	1,74	1048,5	0	0,0

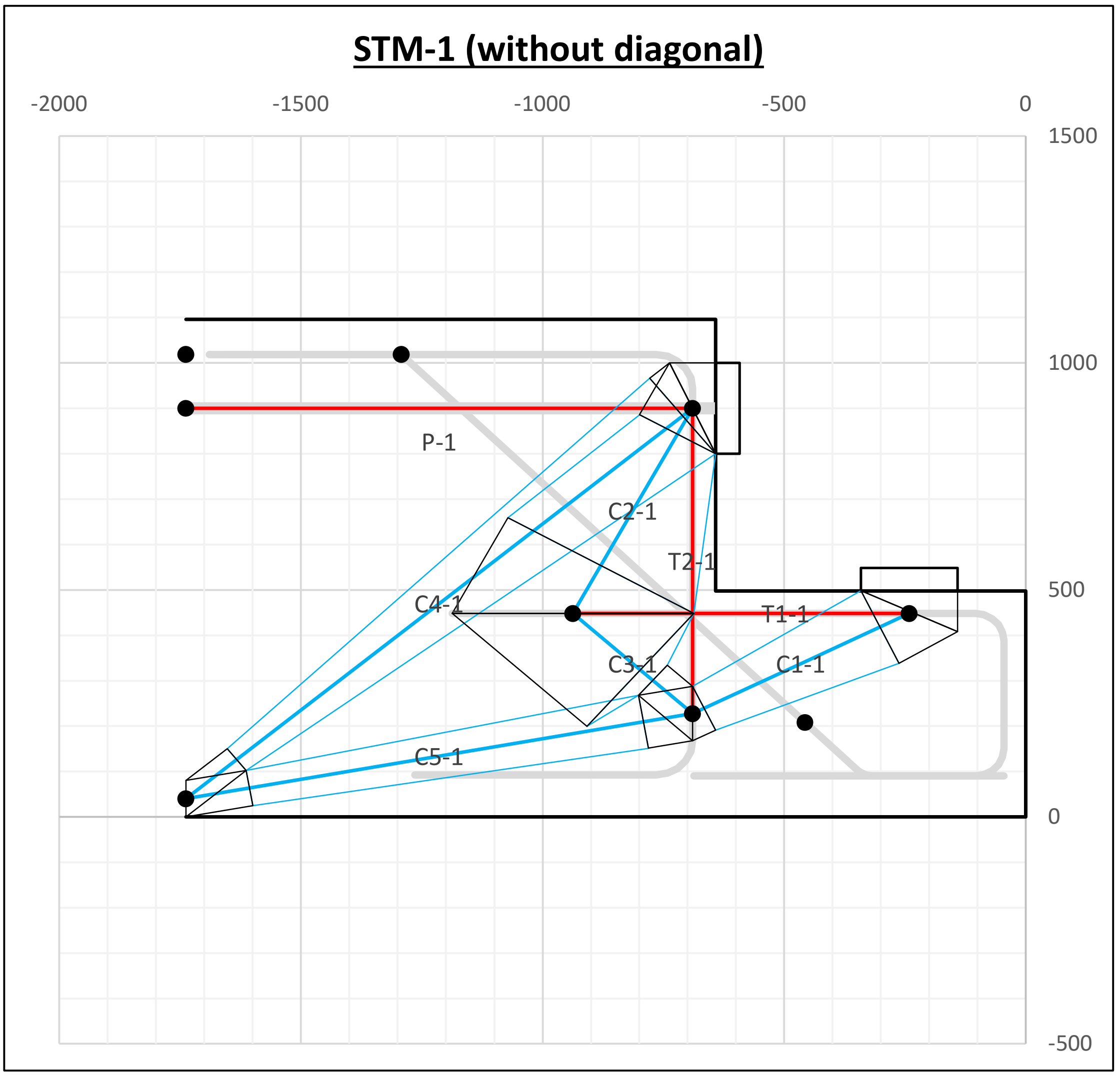

2.3 STM-2 (with diagonal)

	Node (j)	Node (k)	$F_{unit,STM2}$	Length	Angles	
			[-]	[mm]	[rad]	[°]
C2-2	(2)	(3)	-0,61	515,3	1,0698	61,3
C3-2	(3)	(4)	-0,81	331,5	0,7278	41,7
C4-2	(2)	(5)	0,70	1356,1	0,6869	39,4
C5-2	(4)	(5)	-1,53	1065,1	0,1770	10,1
C6-2	(1)	(7)	-1,34	322,6	0,8388	48,1
C7-2	(7)	(4)	-2,12	233,7	-0,0835	-4,8
C8-2	(8)	(5)	-1,29	1075,4	1,1431	65,5
T1-2	(1)	(3)	0,90	696,0	0	0,0
T2-2	(2)	(4)	0,09	672,5	1,5708	90,0
P-2	(2)	(6)	-0,25	1048,5	0	0,0
T4-2	(7)	(8)	1,69	1163,9	0,7703	44,1
T5-2	(8)	(9)	1,75	446,0	0	0,0

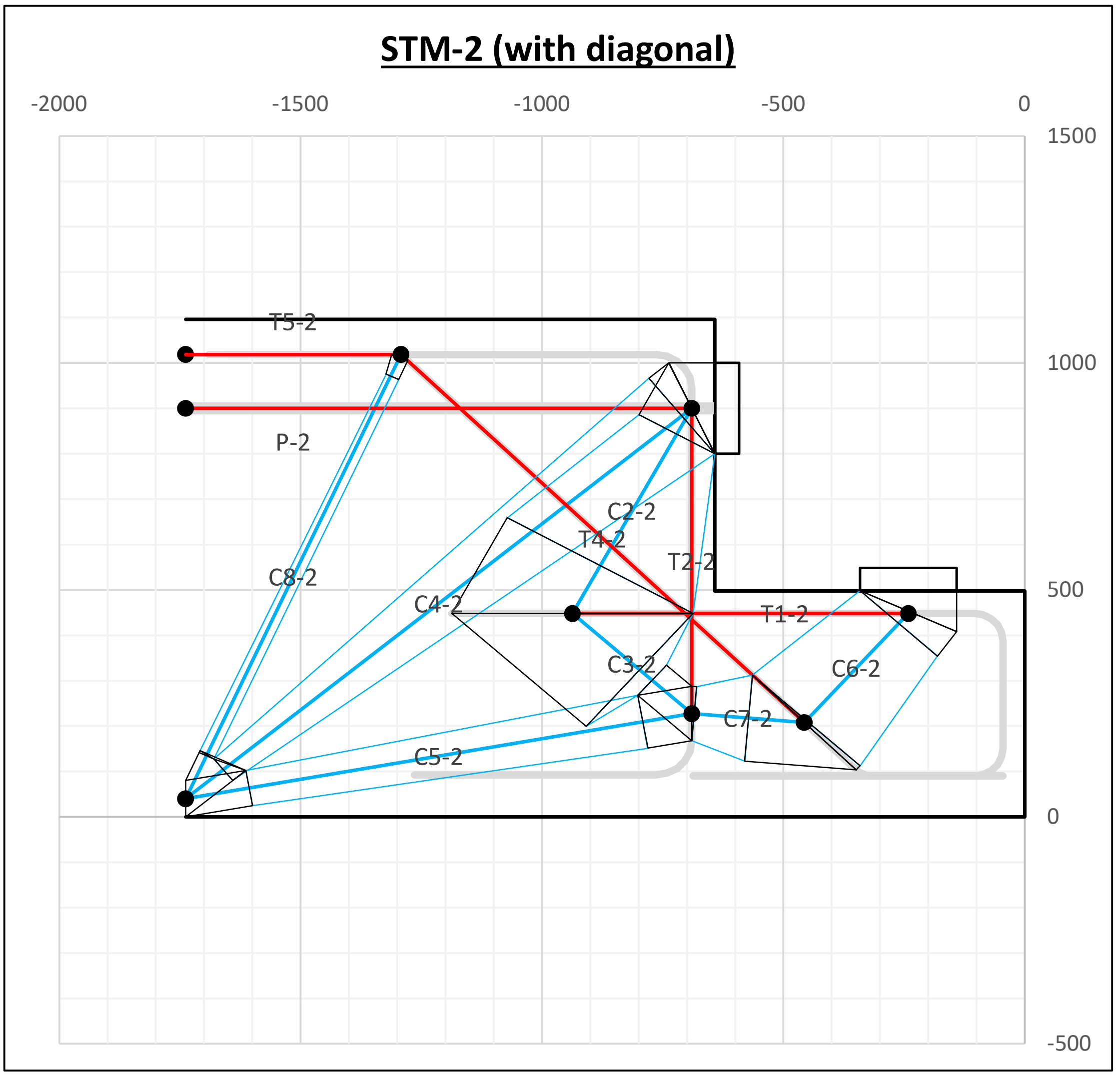

2.4 STM-3 (Combined)

	Node (j)	Node (k)	$F_{unit,STM1}$	$F_{unit,STM2}$	F_{unit}	Length	Angles	
			0,6	0,4	[-]	[mm]	[rad]	[°]
C1	(1)	(4)	-2,27		-1,36	499,8	0,4569	26,2
C2	(2)	(3)	-1,39	-0,61	-1,08	515,3	1,0698	61,3
C3	(3)	(4)	-1,83	-0,81	-1,42	331,5	0,7278	41,7
C4	(2)	(5)	-1,39	0,70	-0,55	1356,1	0,6869	39,4
C5	(4)	(5)	-0,68	-1,53	-1,02	1065,1	0,1770	10,1
C6	(1)	(7)		-1,34	-0,54	322,6	0,8388	48,1
C7	(7)	(4)		-2,12	-0,85	233,7	-0,0835	-4,8
C8	(8)	(5)		-1,29	-0,52	1075,4	1,1431	65,5
T1	(1)	(3)	2,03	0,90	1,58	696,0	0	0
T2	(2)	(4)	2,10	0,09	1,30	672,5	1,5708	90,0
P	(2)	(6)	1,74	-0,25	0,94	1048,5	0	0
T4	(7)	(8)		1,69	0,68	1163,9	0,7703	44,1
T5	(8)	(6)		1,75	0,70	446,0	0	0

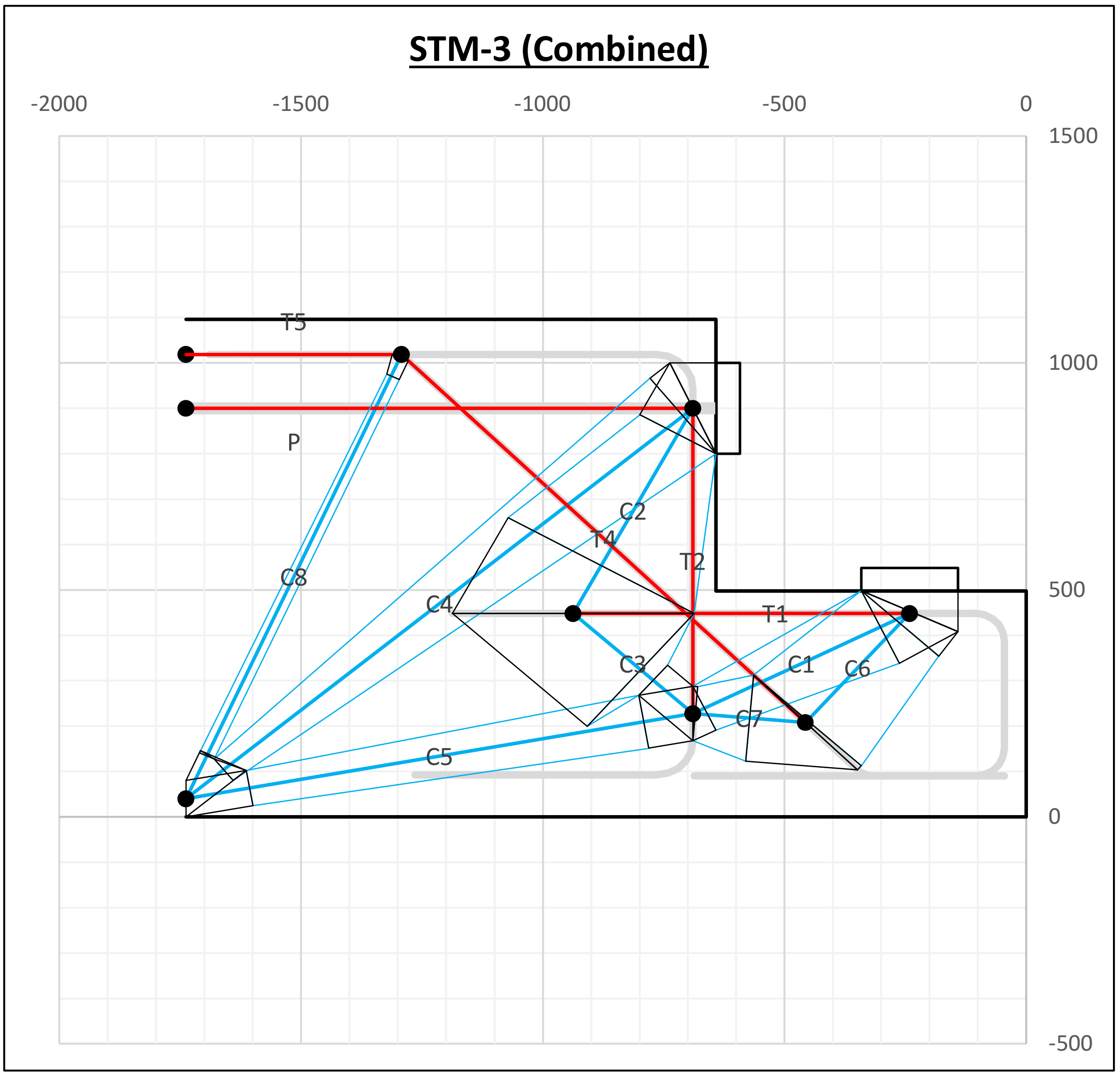

2.5 Node dimensions

Node (1)	T1	F	C1	C6		CCT
$a_{(1)}$	-	223,6	223,6	223,6		[mm]
$w_{(1)}$	-	200,0	178,0	215,6		[mm]
$b_{(1)}$	-	100,0	135,4	59,3		[mm]

Node (2)	T2	P	C2	C4		CTT
$a_{(2)}$	-	221,4	221,4	221,4		[mm]
$w_{(2)}$	-	200,0	179,4	214,9		[mm]
$b_{(2)}$	-	95,0	129,8	53,4		[mm]

Node (3)	T1	C2	C3			CCT
$a_{(3)}$	-	500,0	500,0			[mm]
$w_{(3)}$	-	438,6	332,6			[mm]
$b_{(3)}$	-	240,1	373,3			[mm]

Node (4)	T2	C1	C3	C5	C7	CCT
$a_{(4)}$	-	120,0	114,0	150,2	120,0	[mm]
$w_{(4)}$	-	107,7	89,6	118,1	119,6	[mm]
$b_{(4)}$	-	52,9	70,4	92,8	10,0	[mm]

Node (5)	C4	C5	C8	Internal		CCC
$a_{(5)}$	71,2	161,3	33,5	126,7		[mm]
$w_{(5)}$	61,9	78,8	33,2	104,2		[mm]
$b_{(5)}$	-35,3	140,8	-4,4	72,0		[mm]

Node (7)	T4	C6	C7			CCT
$a_{(7)}$	-	300,0	300,0			[mm]
$w_{(7)}$	-	299,8	190,2			[mm]
$b_{(7)}$	-	11,5	232,0			[mm]

Node (8)	T4	T5	C8			CTT
$a_{(8)}$	-	-	-			[mm]
$w_{(8)}$	-	-	28,8			[mm]
$b_{(8)}$	-	-	-			[mm]

2,6 Checks

2.6.1 *Compressive strength of struts*

Strut i	C1	C2	C3	C4	C5	C6	C7	C8	
$F_{unit,i}$	-1,360	-1,078	-1,422	-0,552	-1,019	-0,538	-0,847	-0,517	[-]
Tension	Yes	Yes	Yes	Yes	Yes	Yes	Yes	Yes	
$\sigma_{Rd,max,c}$	12,04	12,04	12,04	12,04	12,04	12,04	12,04	12,04	[N/mm^2]
L_c	499,8	515,3	331,5	1356,1	1065,1	322,6	233,7	1075,4	[mm]
$w_{c,eff}$	107,7	179,4	89,6	61,9	78,8	215,6	119,6	28,8	[mm]
$C_{max,C,i}$	-1296,6	-2159,8	-1078,8	-744,7	-948,2	-2595,9	-1439,8	-346,5	[kN/m]
$F_{max,C,i}$	953,4	2002,6	758,6	1349,8	930,4	4827,6	1698,9	669,7	[kN/m]

2.6.2 *Compressive strength of nodes*

Strut	C1	C2	C3	C4	C5	C6	C7	C8	
Node (j)	(1)	(2)	(3)	(2)	(4)	(1)	(7)	(8)	
Type	CCT	CTT	CCT	CTT	CCT	CCT	CCT	CTT	
k	0,85	0,75	0,85	0,75	0,85	0,85	0,85	0,75	[-]
$\sigma_{Rd,max,(j)}$	17,06	15,05	17,06	15,05	17,06	17,06	17,06	15,05	[N/mm^2]
$w_{i(j)}$	178,0	179,4	332,6	214,9	118,1	215,6	190,2	28,8	[mm]
$C_{max,i(j)}$	-3035,8	-2699,7	-5673,1	-3234,0	-2014,8	-3677,5	-3244,3	-433,1	[kN/m]
$F_{max,i(j)}$	2232,3	2503,2	3989,3	5861,6	1977,2	6839,1	3828,1	837,2	[kN/m]
Node (k)	(4)	(3)	(4)	(5)	(5)	(7)	(4)	(5)	
Type	CCT	CCT	CCT	CCC	CCC	CCT	CCT	CCC	
k	0,85	0,85	0,85	1,00	1,00	0,85	0,85	1,00	[-]
$\sigma_{Rd,max,(k)}$	17,06	17,06	17,06	20,07	20,07	17,06	17,06	20,07	[N/mm^2]
$w_{i(k)}$	107,7	438,6	89,6	61,9	78,8	299,8	119,6	33,2	[mm]
$C_{max,i(k)}$	-1836,8	-7480,3	-1528,3	-1241,2	-1580,3	-5113,2	-2039,7	-665,8	[kN/m]
$F_{max,i(k)}$	1350,7	6935,9	1074,7	2249,7	1550,7	9509,0	2406,7	1287,1	[kN/m]

2.6.3 *Compressive strength of internal nodes*

Node (j/k)	(1)	(2)	(4)	(5)	
Strut i_1	C1	C2	C1	C4	
$F_{unit,i,1}$	-1,082	-0,874	-1,220	-0,427	[-]
Strut i_2	C6	C4	C7	C5	
$F_{unit,i,2}$	-0,518	-0,535	-0,845	-1,003	[-]
Strut i_3	-		-	C8	
$F_{unit,i,3}$				-0,215	[-]
F_{unit}	-1,601	-1,409	-2,065	-1,644	[-]
Type	CCT	CTT	CCT	CCC	
k	0,85	0,75	0,85	1,00	[-]
$\sigma_{Rd,max}$	17,06	15,05	17,06	20,07	[N/mm^2]
w	223,6	221,4	120,0	80,0	[mm]
C_{max}	-3814,0	-3332,3	-2046,8	-1605,3	[kN/m]
F_{max}	2382,4	2364,7	991,2	976,3	[kN/m]

2.6.4 *Yield strength of ties*

Ties	T1	T2	T3	T4	T5		
$F_{unit,i}$	1,580	1,296	0,945	0,676	0,700	[-]	
Rebar	1	2	P	3	3	[-]	
Ø	20	25	-	16	26	[mm]	(add top rebar)
Corrosion	0%	0%	-	0%	-	[-]	(at re-entrant corner)
f_{yd}	435	435	-	435	435	[N/mm^2]	
$T_{max,T,ind,i}$	136,7	213,5	1894,6	87,5	231,0	[kN]	
$T_{max,T,i}$	1366,6	2135,3	2697,2	874,6	2309,5	[kN/m]	
$F_{max,T,i}$	865,1	1647,8	2855,4	1293,8	3300,7	[kN/m]	

2.6.5 *Anchorage length of ties*

Lower-bound load 669,7 [kN/m] Failure mechanism: C8 (strut)

Ties	T1	T2	T3	T4	T5	
F_T	1058,1	867,9	632,6	452,7	468,6	[kN/m]
$F_{T,ind}$	105,8	86,8	2133,2	45,3	46,9	[kN]
f_{bd}	3,37	3,37	-	3,37	3,37	[N/mm^2]
σ_{sd}	336,8	176,8	-	225,2	88,3	[N/mm^2]
$l_{b,rqd,max}$	499,6	327,9	-	267,2	170,2	[mm]
Node (j)	(1)	(2)	(2)	(7)	(8)	
c_d	50,0	-	-	50,0	-	[mm]
p	3,35	-	-	1,20	-	[N/mm^2]
α_1	1,0	-	-	0,7	-	[-]
α_2	1,0	-	-	0,9	-	[-]
α_3	1,0	-	-	1,0	-	[-]
α_4	1,0	-	-	1,0	-	[-]
α_5	0,87	-	-	0,95	-	[-]
$l_{b,min}$	200,0	-	-	160,0	-	[mm]
l_{bd}	432,7	-	-	167,0	-	[mm]
$l_{b,prov}$	1244,5	-	-	607,5	-	[mm]
Check	Correct	-	-	Correct	-	
Node (k)	(3)	(4)	(6)	(8)	(6)	
c_d	50,0	50,0	-	-	-	[mm]
p	1,27	11,52	-	-	-	[N/mm^2]
α_1	1,0	1,0	-	-	-	[-]
α_2	1,0	1,0	-	-	-	[-]
α_3	1,0	1,0	-	-	-	[-]
α_4	1,0	1,0	-	-	-	[-]
α_5	0,95	0,70	-	-	-	[-]
$l_{b,min}$	200,0	250,0	-	-	-	[mm]
l_{bd}	474,3	250,0	-	-	-	[mm]
$l_{b,prov}$	500,0	737,8	-	-	-	[mm]
Check	Correct	Correct	-	-	-	

3. Kinematic approach (upper-bound approximation)

x_min	114,0	[mm]
Δx	0	[mm]

θ_{Crack}	30,0	[°]
l_{crack}	768,1	[mm]

	$A_{s,i}$	A_s	f_{yd}	N_S / N_C	Leverarm	Moment	$N_{y\text{-}dir}$
	[mm^2]	[mm^2]	[N/mm^2]	[kN/m]	[mm]	[kNm/m]	[kN/m]
Rebar 1	314	3142	435	1366,6	334,0	456,5	0,0
Rebar 2	491	4909	435	2135,3	617,7	1318,9	2135,3
Rebar 3	201	2011	435	874,6	685,9	599,9	609,0
Concrete	-	-	-	1994,3	69,5	138,6	0,0
Total						2514,0	2744,3

Support		
Leverarm:	1066,2	[mm]
Upper-bound load:	2357,9	[kN/m]

Vertical equilibrium	Correct	
Difference in vertical force	-386,4	[kN/m]
Concrete shear resistance	66,7	[kN/m]

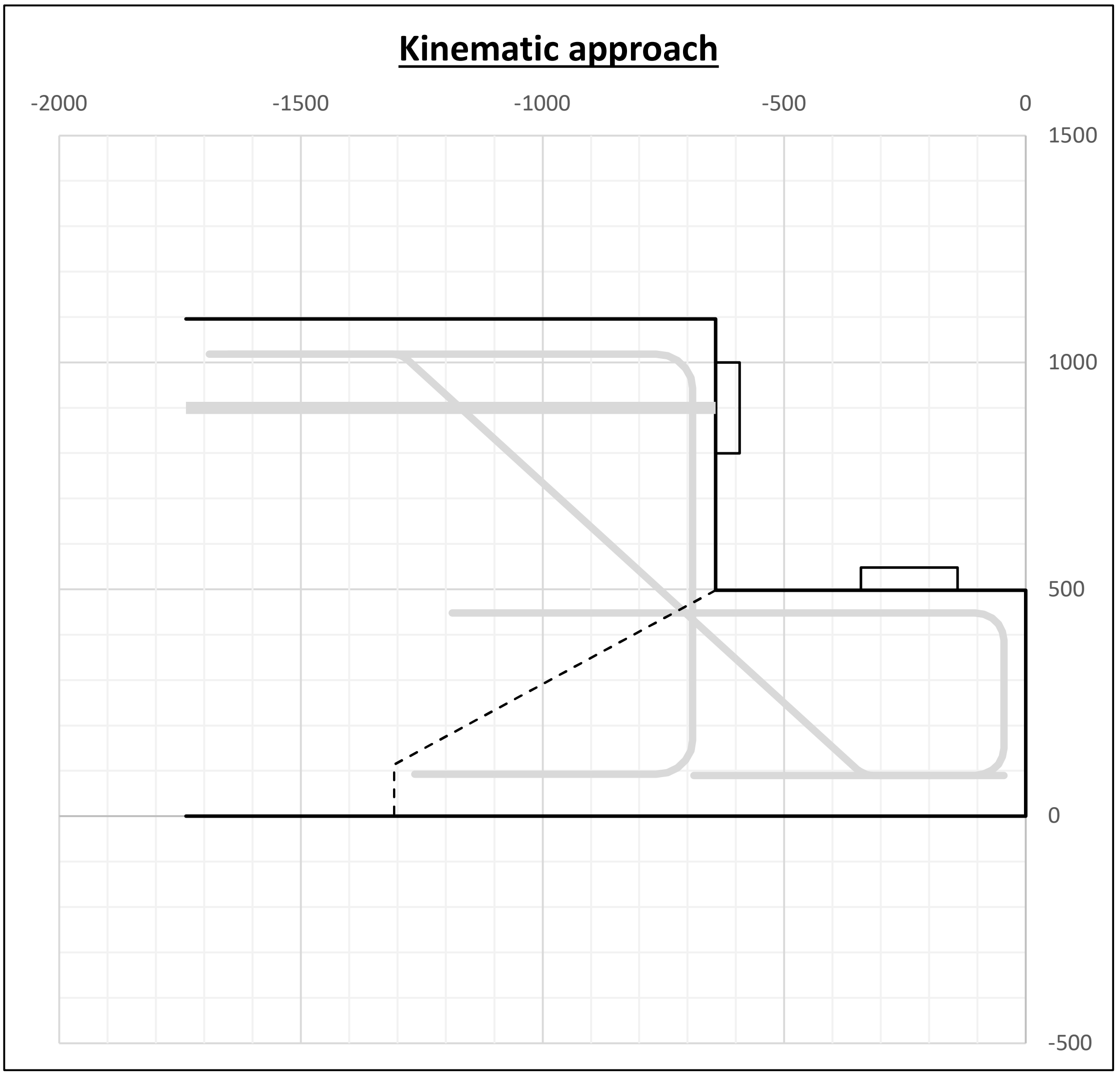

4. Optimisation

4.1 Strut-and-tie approach (Highest lower-bound approximation)

	Stepsize	Max. shift	Steps
Load	0,1	-	10
Node 3	50	300,0	6
Node 4	10	100,0	10
Node 5	10	100,0	10
Node 7	50	250,0	5

min θ 25,0 [°]

Anchorage:	Correct	
Angle (theta):	Correct	
Lower-bound load	669,7	[kN/m]

Limitations on angles				
	Minimum	Maximum	[°]	
θC1	25,0	65,0	26,2	Correct
θC2	25,0	65,0	61,3	Correct
θC3	25,0	65,0	41,7	Correct
θC4	25,0	65,0	39,4	Correct
θC6	25,0	-	48,1	Correct
θC7	-	65,0	-4,8	Correct
θC8	25,0	-	65,5	Correct
θC6+θT4	-	155,0	92,2	Correct
θT4-θC7	25,0	-	48,9	Correct
θC8+θT4	25,0	-	109,6	Correct

Governing lower-bound load: 669,7 [kN/m] Failure mechanism: C8 (strut)

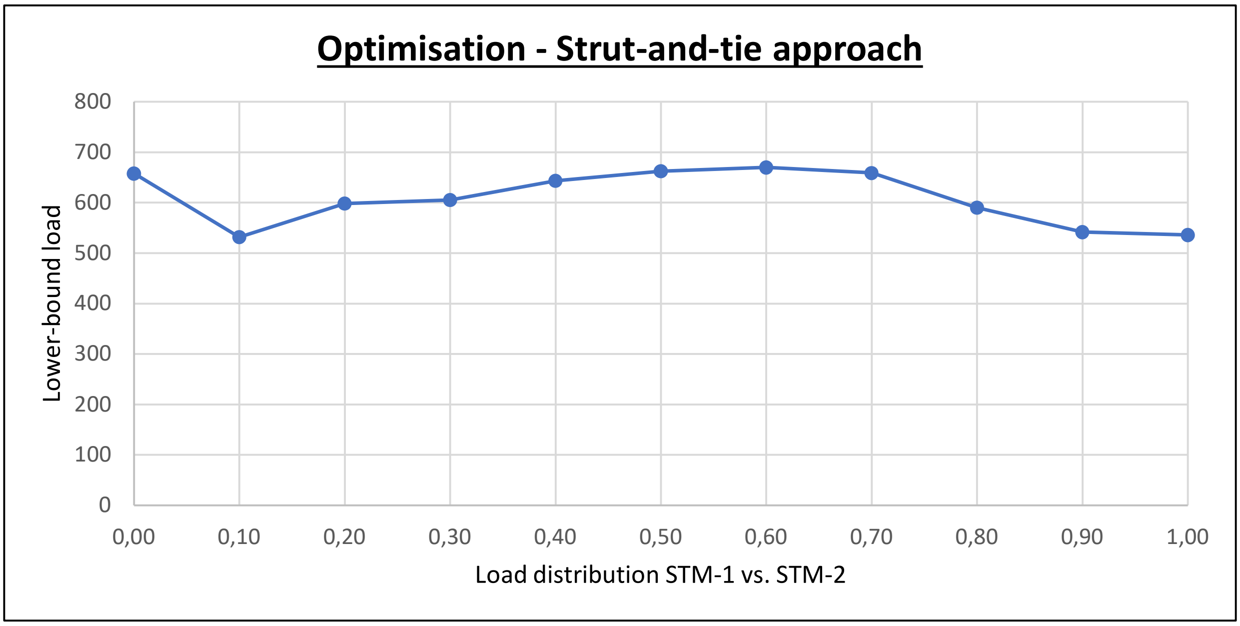

Load distribution		Offset				Load		Limitations	
STM-1	STM-2	Node 3	Node 4	Node 5	Node 7	[kN]	Mechan.	Anchor.	Angle
0,000	1,000	250	70	100	250	657,8	C8 (strut)	Correct	Correct
0,100	0,900	200	40	40	200	531,9	C8 (strut)	Correct	Correct
0,200	0,800	200	40	40	200	598,4	C8 (strut)	Correct	Correct
0,300	0,700	200	50	40	200	605,4	C8 (strut)	Correct	Correct
0,400	0,600	250	50	40	200	643,1	C3 (strut)	Correct	Correct
0,500	0,500	250	70	60	200	662,2	C8 (strut)	Correct	Correct
0,600	0,400	250	60	40	150	669,7	C8 (strut)	Correct	Correct
0,700	0,300	250	70	100	100	658,9	C8 (strut)	Correct	Correct
0,800	0,200	250	50	30	50	590,2	C3 (strut)	Correct	Correct
0,900	0,100	250	50	50	50	541,6	C3 (strut)	Correct	Correct
1,000	0,000	250	60	40	50	536,2	C4 (strut)	Correct	Correct

4,2 Kinematic approach (Lowest upper-bound approximation)

$\theta_{C,min}$	30,0	[°]
$\theta_{C,max}$	70,0	[°]

θ_{Crack}		30,0	36,7	43,3	50,0	56,7	63,3	70,0	[°]
Rebar 1	Leverarm	334,0	334,0	334,0	334,0	334,0	334,0	334,0	[mm]
	Moment	456,5	456,5	456,5	456,5	456,5	456,5	456,5	[kNm/m]
Rebar 2	Leverarm	617,7	468,4	359,6	274,7	205,1	145,4	92,3	[mm]
	Moment	1318,9	1000,1	767,8	586,7	437,9	310,4	197,0	[kNm/m]
Rebar 3	Leverarm	685,9	563,0	480,5	422,1	379,2	346,9	322,1	[mm]
	Moment	599,9	492,4	420,3	369,2	331,6	303,4	281,7	[kNm/m]
Concrete	Leverarm	69,5	69,5	69,5	69,5	69,5	69,5	69,5	[mm]
	Moment	138,6	138,6	138,6	138,6	138,6	138,6	138,6	[kNm/m]
ΔX		0,0	0,0	0,0	0,0	0,0	0,0	0,0	[mm]
Total moment		2514,0	2087,6	1783,1	1551,0	1364,7	1208,9	1073,9	[kNm/m]
Leverarm support		1066,2	916,9	808,1	723,2	653,6	593,9	540,8	[mm]
Load support		2357,9	2277,0	2206,7	2144,4	2088,0	2035,7	1985,8	[kN/m]

Governing upper-bound load: 1985,8 [kN/m]

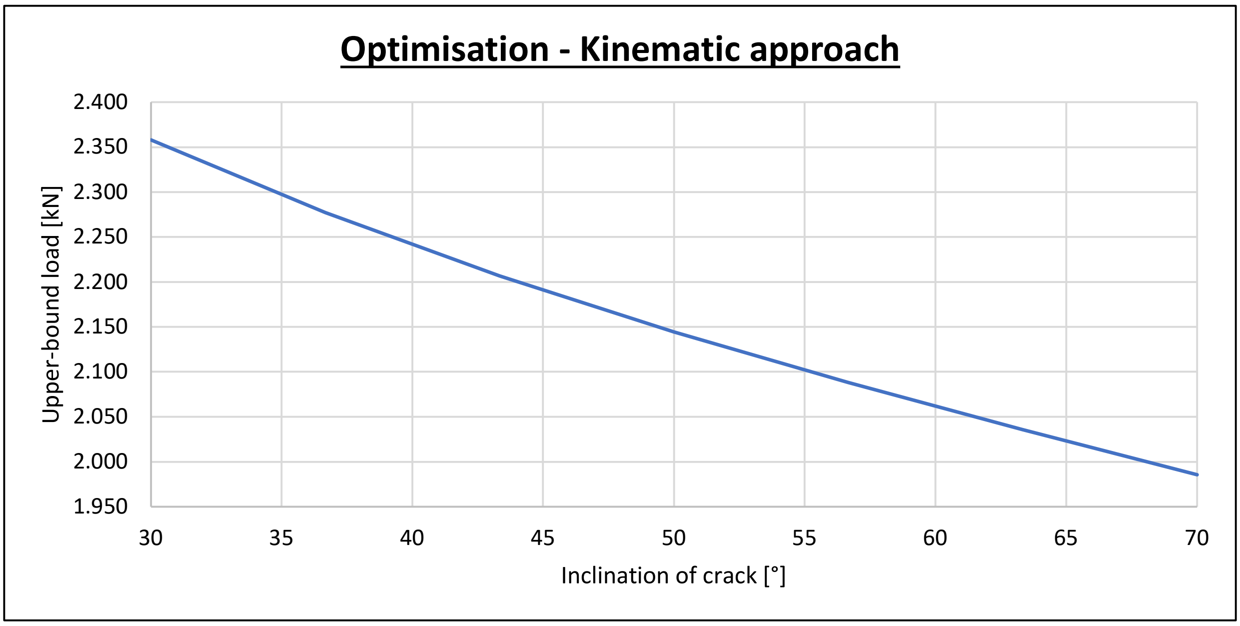

5. Corrosion

	Stepsize	Max
Corrosion	10%	60%

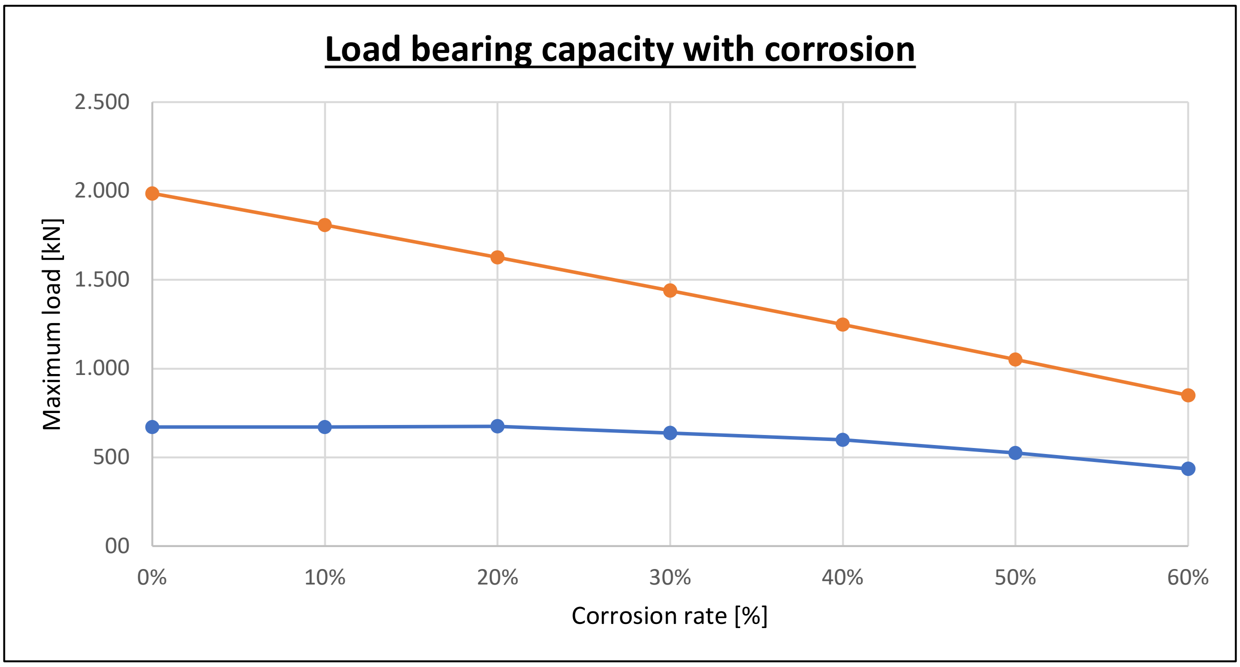

Maximum load	Corrosion							
	0%	10%	20%	30%	40%	50%	60%	
Lower-bound load	669,7	669,7	674,9	637,1	598,4	523,7	435,5	[kN/m]
Failure mechanism	C8 (strut)	C8 (strut)	T1	T1	C8 (strut)	T1	T1	
Upper-bound load	1985,8	1808,6	1626,3	1439,1	1247,2	1050,5	849,2	[kN/m]

C.3 Purmerend

Analytical parametric tool for load bearing capacity of RC half-joints

Project
Purmerend

1. Geometry and material properties

1.1 Concrete

1.1.1 Geometry

a	348	[mm]
b	384	[mm]
c	450	[mm]
d	320	[mm]

Width	1000	[mm]
Cover	30	[mm]
Support	200	[mm]
α	4,68	[°]

1.1.2 Material

γ_c	1,5	[-]
k_t	1	[-]

α_{cc}	1	[-]
α_{ct}	1	[-]

f_{ck}	30,0	[N/mm^2]
f_{cm}	38,0	[N/mm^2]
f_{cd}	20,0	[N/mm^2]
v'	0,880	[-]

f_{ctm}	2,90	[N/mm^2]
$f_{ctk,0.05}$	2,03	[N/mm^2]
f_{ctd}	1,35	[N/mm^2]
Mean values?		No

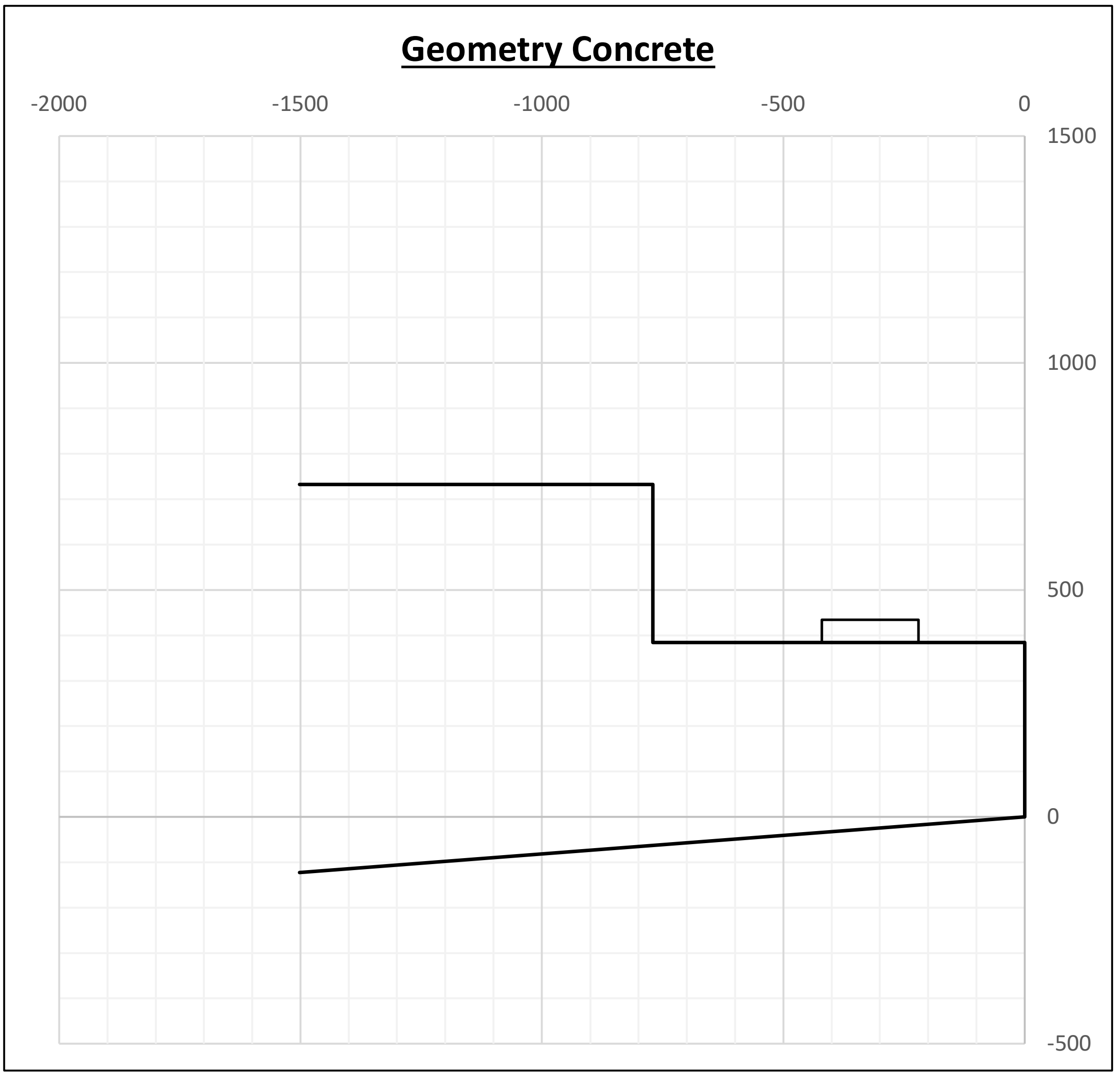

1.2 Reinforcement steel

1.2.1 Geometry

	Rebar 1	Rebar 2	Rebar 3	
Ø	25	25		[mm]
$Ø_m$	125	125		[mm]
Spacing	125	250		[mm]
η_1	1	1		[-]
η_2	1	1		[-]
η_3	1	1		[-]
l_{top}	1400	700	-	[mm]
l_{bottom}	1000	250	-	[mm]
Δ_{top}	0	0	-	[mm]
Δ_{middle}	0	0	-	[mm]
Δ_{bottom}	0	0	-	[mm]
Corrosion	0%	0%	0%	[-]

Include Rebar 3?	No

Coordinates Rebar 3		
x	y	
		[1]
		[2]
		[3]
		[4]
		[5]
		[6]

ϕ		[rad]
		[°]

1.2.2 Material

$f_{yd,0}$	330	[N/mm^2]
f_{yd}	330	[N/mm^2]

$\alpha_{corr,y}$	0	[-]

1,23

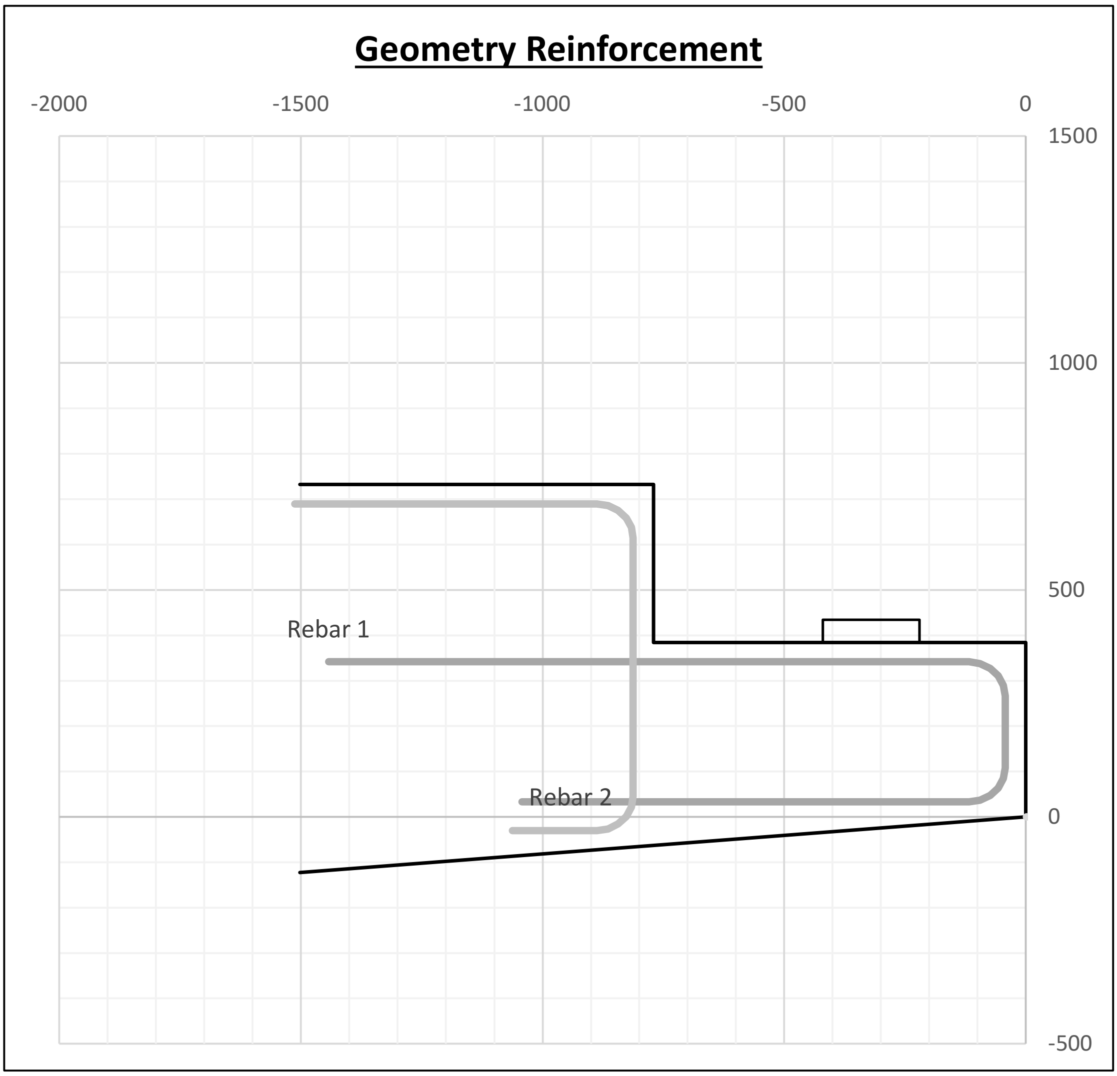

1.3 Pre-stressed steel

1.3.1 Geometry

A_p		[mm^2]
y_p		[mm]
Bearing		[mm]
Spacing		[mm]

Include prestress?	No

1.3.2 Material

σ_{pm}		[N/mm^2]
P_m		[kN]

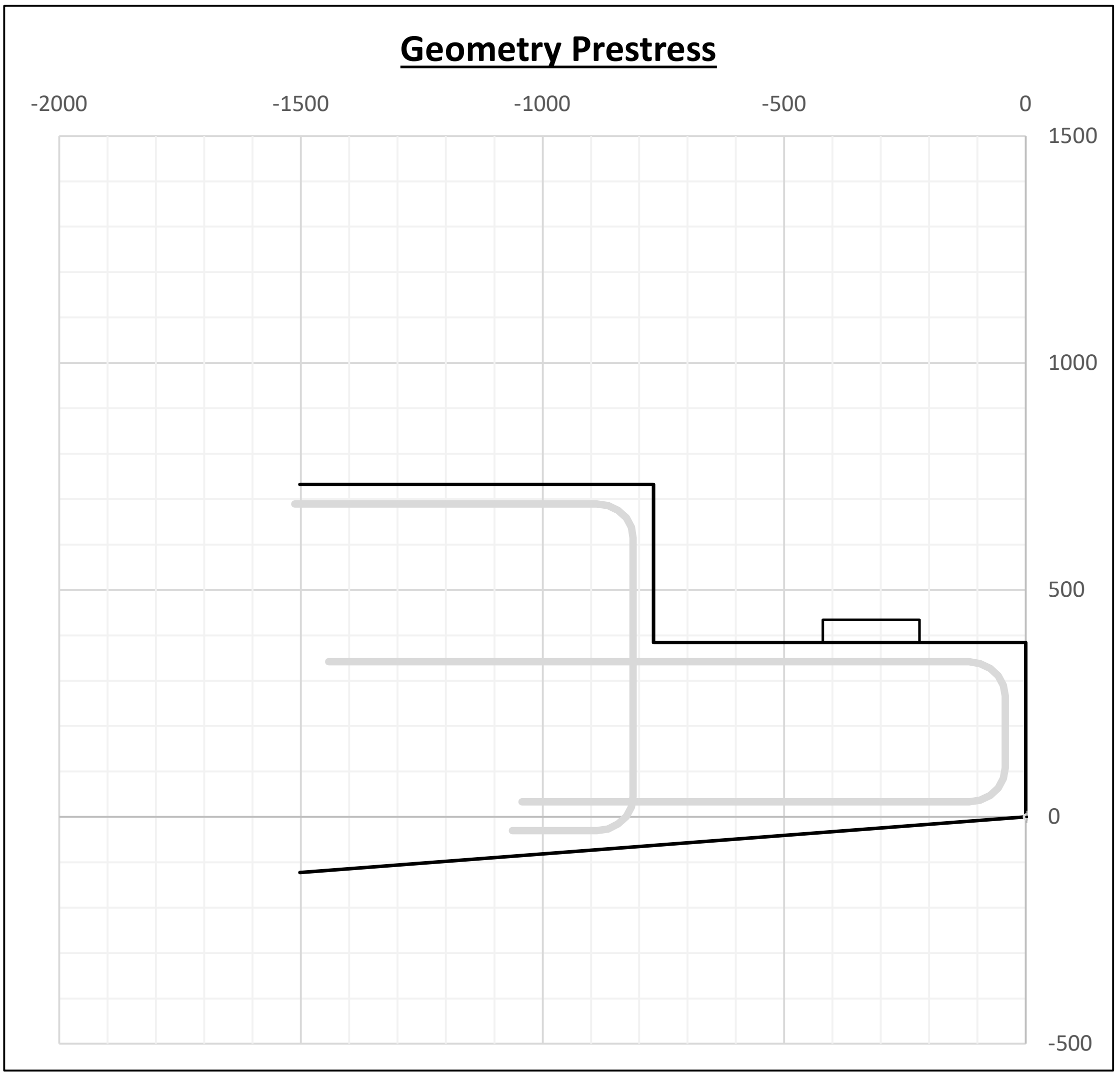

2. Strut-and-tie modelling

2.1 Nodes

	Offset		Coordinates		Type
	x	y	x	y	
(1)	-	-	-320,0	341,5	CCT
(2)	-	0	-812,5	689,5	CTT
(3)	225	-	-1217,5	341,5	CCT
(4)	-	60	-812,5	104,8	CCT
(5)	-	70	-1502,0	-53,0	CCC
(6)	-		-1502,0	689,5	-
(7)	25				CCT
(8)	-	-			CTT
(9)	-	-			-

F_{unit}	1,00	[-]

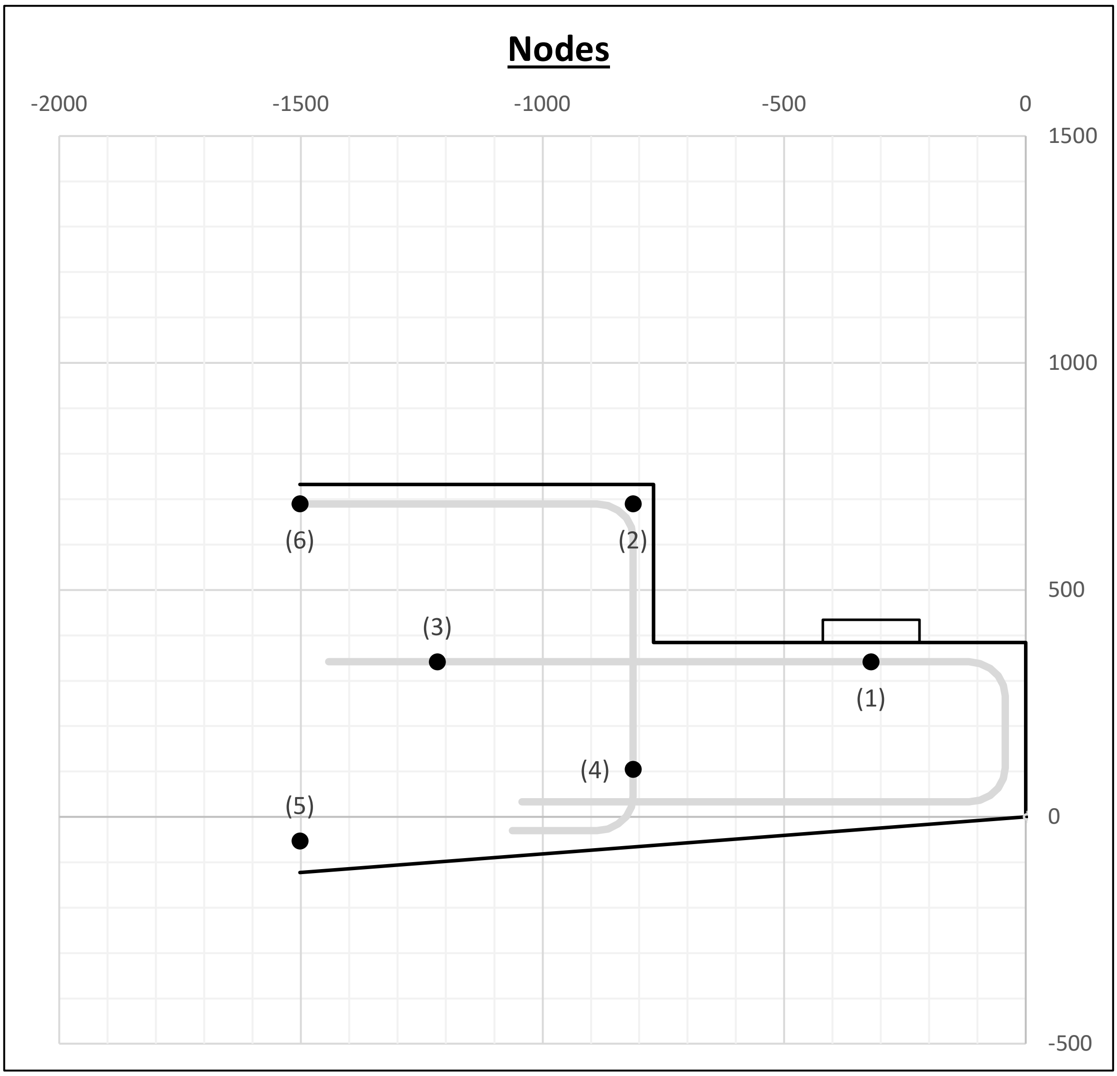

2.2 STM-1 (without diagonal)

	Node (j)	Node (k)	$F_{unit,STM1}$	Length	Angles	
			[-]	[mm]	[rad]	[°]
C1-1	(1)	(4)	-2,31	546,4	0,4479	25,7
C2-1	(2)	(3)	-1,11	534,0	0,7098	40,7
C3-1	(3)	(4)	-1,43	469,1	0,5288	30,3
C4-1	(2)	(5)	-1,10	1013,2	0,8224	47,1
C5-1	(4)	(5)	-0,86	707,3	0,2250	12,9
T1-1	(1)	(3)	2,08	897,5	0	0,0
T2-1	(2)	(4)	1,53	584,7	1,5708	90,0
T3-1	(2)	(6)	1,59	689,5	0	0,0

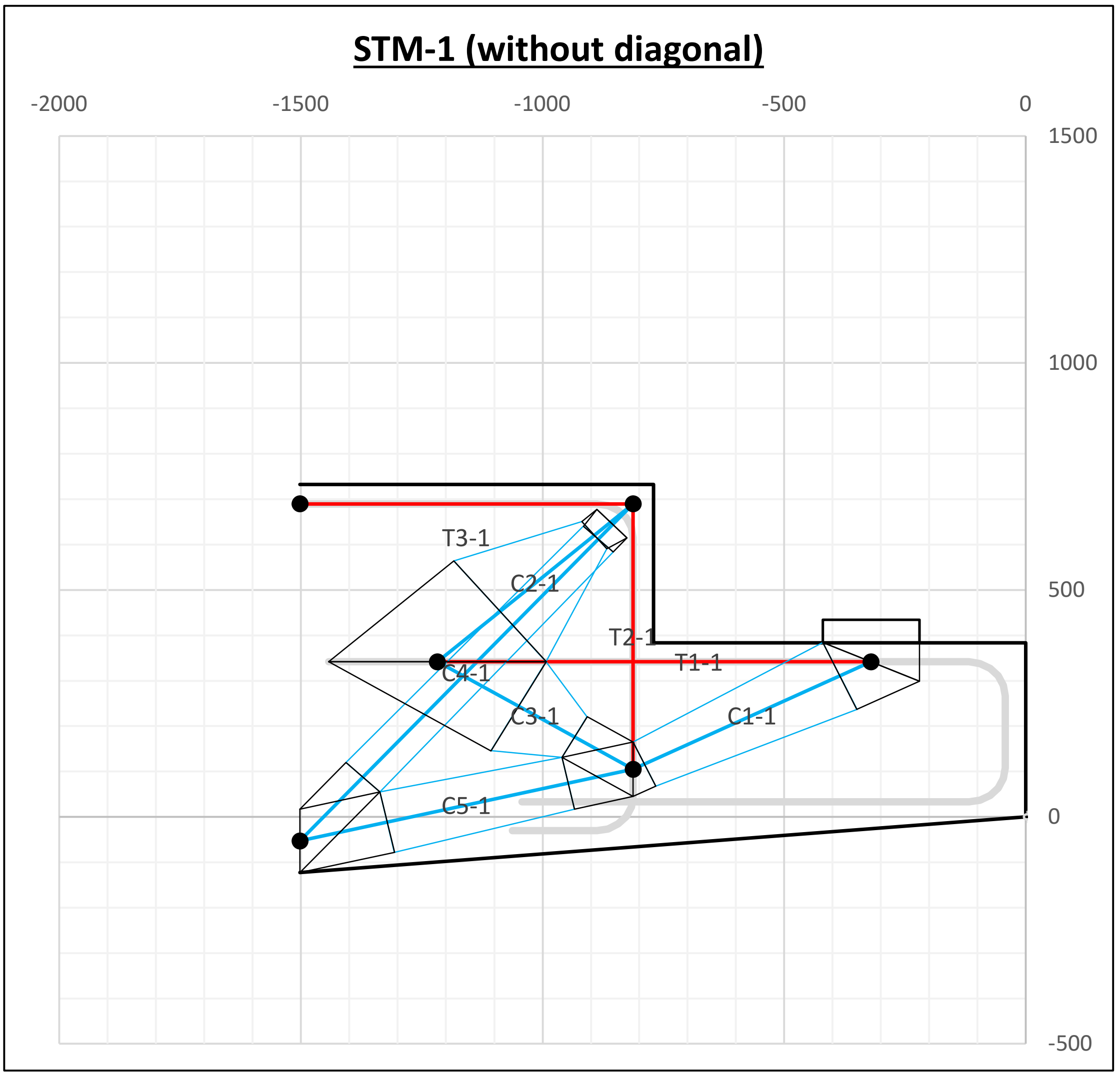

2.5 Node dimensions

Node (1)	T1	F	C1			CCT
$a_{(1)}$	-	217,3	217,3			[mm]
$w_{(1)}$	-	200,0	163,2			[mm]
$b_{(1)}$	-	85,0	143,5			[mm]

Node (2)	T2	T3	C2	C4		CTT
$a_{(2)}$	-	-	88,4	88,4		[mm]
$w_{(2)}$	-	-	78,8	83,8		[mm]
$b_{(2)}$	-	-	-	-		[mm]

Node (3)	T1	C2	C3			CCT
$a_{(3)}$	-	450,0	450,0			[mm]
$w_{(3)}$	-	293,3	227,0			[mm]
$b_{(3)}$	-	341,3	388,5			[mm]

Node (4)	T2	C1	C3	C5		CCT
$a_{(4)}$	-	120,0	151,4	170,9		[mm]
$w_{(4)}$	-	108,2	103,6	117,0		[mm]
$b_{(4)}$	-	52,0	110,4	124,6		[mm]

Node (5)	C4	C5				CCC
$a_{(5)}$	169,4	242,6				[mm]
$w_{(5)}$	95,3	136,5				[mm]
$b_{(5)}$	140,0	200,6				[mm]

Node (7)						
$a_{(7)}$						[mm]
$w_{(7)}$						[mm]
$b_{(7)}$						[mm]

Node (8)						
$a_{(8)}$						[mm]
$w_{(8)}$						[mm]
$b_{(8)}$						[mm]

2,6 Checks

2.6.1 Compressive strength of struts

Strut i	C1	C2	C3	C4	C5				
$F_{unit,i}$	-2,309	-1,111	-1,435	-1,102	-0,864				[-]
Tension	Yes	Yes	Yes	Yes	Yes	Yes	Yes	Yes	
$\sigma_{Rd,max,c}$	10,56	10,56	10,56	10,56	10,56				[N/mm^2]
L_c	546,4	534,0	469,1	1013,2	707,3				[mm]
$w_{c,eff}$	108,2	78,8	103,6	83,8	117,0				[mm]
$C_{max,C,i}$	-1142,2	-832,1	-1094,1	-884,4	-1235,3				[kN/m]
$F_{max,C,i}$	494,7	749,2	762,6	802,9	1429,4				[kN/m]

2.6.2 Compressive strength of nodes

Strut	C1	C2	C3	C4	C5				
Node (j)	(1)	(2)	(3)	(2)	(4)				
Type	CCT	CTT	CCT	CTT	CCT				
k	0,85	0,75	0,85	0,75	0,85				[-]
$\sigma_{Rd,max,(j)}$	14,96	13,20	14,96	13,20	14,96				[N/mm^2]
$w_{i(j)}$	163,2	78,8	227,0	83,8	117,0				[mm]
$C_{max,i(j)}$	-2442,0	-1040,1	-3396,4	-1105,6	-1750,0				[kN/m]
$F_{max,i(j)}$	1057,7	936,5	2367,3	1003,6	2025,0				[kN/m]
Node (k)	(4)	(3)	(4)	(5)	(5)				
Type	CCT	CCT	CCT	CCC	CCC				
k	0,85	0,85	0,85	1,00	1,00				[-]
$\sigma_{Rd,max,(k)}$	14,96	14,96	14,96	17,60	17,60				[N/mm^2]
$w_{i(k)}$	108,2	293,3	103,6	95,3	136,5				[mm]
$C_{max,i(k)}$	-1618,1	-4387,4	-1550,0	-1676,7	-2401,9				[kN/m]
$F_{max,i(k)}$	700,8	3950,3	1080,4	1522,1	2779,5				[kN/m]

2.6.3 Compressive strength of internal nodes

Node (j/k)		(2)		(5)	
Strut i_1		C2		C4	
$F_{unit,i,1}$		-1,107		-0,750	[-]
Strut i_2		C4		C5	
$F_{unit,i,2}$		-1,101		-0,842	[-]
Strut i_3					
$F_{unit,i,3}$					[-]
F_{unit}		-2,208		-1,592	[-]
Type		CTT		CCC	
k		0,75		1,00	[-]
$\sigma_{Rd,max}$		13,20		17,60	[N/mm^2]
w		78,8		140,0	[mm]
C_{max}		-1040,1		-2464,0	[kN/m]
F_{max}		471,0		1547,7	[kN/m]

2.6.4 Yield strength of ties

Ties	T1	T2	T3				
$F_{unit,i}$	2,081	1,531	1,592			[-]	
Rebar	1	2	2			[-]	
Ø	25	25	35			[mm]	(add top rebar)
Corrosion	0%	0%	0%	-	-	[-]	(at re-entrant corner)
f_{yd}	330	330	330			[N/mm^2]	
$T_{max,T,ind,i}$	162,0	162,0	317,5			[kN]	
$T_{max,T,i}$	1295,9	648,0	1270,0			[kN/m]	
$F_{max,T,i}$	622,7	423,2	797,7			[kN/m]	

2.6.5 Anchorage length of ties

Lower-bound load 423,2 [kN/m] Failure mechanism: T2

Ties	T1	T2	T3			
F_T	880,8	648,0	673,8			[kN/m]
$F_{T,ind}$	110,1	162,0	168,4			[kN]
f_{bd}	3,04	3,04	3,04			[N/mm^2]
σ_{sd}	224,3	330,0	175,1			[N/mm^2]
$l_{b,rqd,max}$	460,9	678,2	503,7			[mm]
Node (j)	(1)	(2)	(2)			
c_d	62,5	-	-			[mm]
p	2,12	-	-			[N/mm^2]
α_1	1,0	-	-			[-]
α_2	1,0	-	-			[-]
α_3	1,0	-	-			[-]
α_4	1,0	-	-			[-]
α_5	0,92	-	-			[-]
$l_{b,min}$	250,0	-	-			[mm]
l_{bd}	421,9	-	-			[mm]
$l_{b,prov}$	1621,7	-	-			[mm]
Check	Correct	-	-			
Node (k)	(3)	(4)	(6)			
c_d	62,5	125,0	-			[mm]
p	0,68	7,34	-			[N/mm^2]
α_1	1,0	0,7	-			[-]
α_2	1,0	0,7	-			[-]
α_3	1,0	1,0	-			[-]
α_4	1,0	1,0	-			[-]
α_5	0,97	0,71	-			[-]
$l_{b,min}$	250,0	250,0	-			[mm]
l_{bd}	448,4	250,0	-			[mm]
$l_{b,prov}$	450,0	412,8	-			[mm]
Check	Correct	Correct	-			

3. Kinematic approach (upper-bound approximation)

x_min	86,4	[mm]
Δx	0	[mm]

θ_{Crack}	30,0	[°]
l_{crack}	840,5	[mm]

	$A_{s,i}$	A_s	f_{yd}	N_S / N_C	Leverarm	Moment	$N_{y\text{-}dir}$
	[mm^2]	[mm^2]	[N/mm^2]	[kN/m]	[mm]	[kNm/m]	[kN/m]
Rebar 1	491	3927	330	1295,9	377,7	489,5	0,0
Rebar 2	491	1963	330	648,0	685,4	444,1	648,0
Rebar 3	-	-	-	0,0	0,0	0,0	0,0
Concrete	-	-	-	1295,9	52,7	68,3	0,0
Total						1001,9	648,0

Support		
Leverarm:	1177,9	[mm]
Upper-bound load:	850,6	[kN/m]

Vertical equilibrium	Fail	
Difference in vertical force	202,6	[kN/m]
Concrete shear resistance	46,8	[kN/m]

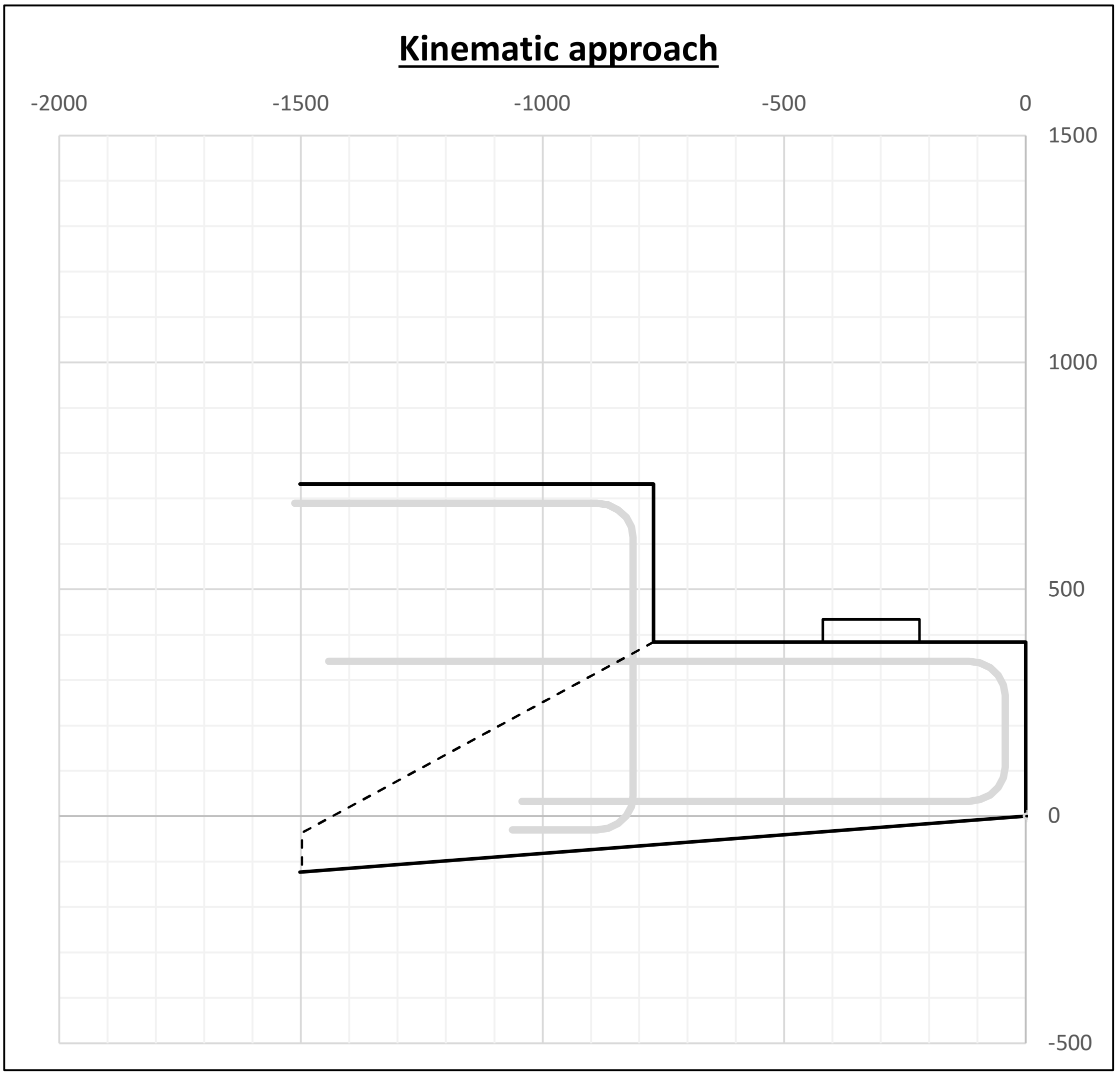

4. Optimisation

4.1 Strut-and-tie approach (Highest lower-bound approximation)

	Stepsize	Max. shift	Steps
Load	0,1	-	10
Node 3	25	400,0	16
Node 4	10	100,0	10
Node 5	10	100,0	10
Node 7	25	100,0	4

min θ 25,0 [°]

Anchorage:	Correct	
Angle (theta):	Correct	
Lower-bound load	423,2	[kN/m]

Limitations on angles				
	Minimum	Maximum	[°]	
θC1	25,0	65,0	25,7	Correct
θC2	25,0	65,0	40,7	Correct
θC3	25,0	65,0	30,3	Correct
θC4	25,0	65,0	47,1	Correct

Governing lower-bound load: 423,2 [kN/m] Failure mechanism: T2

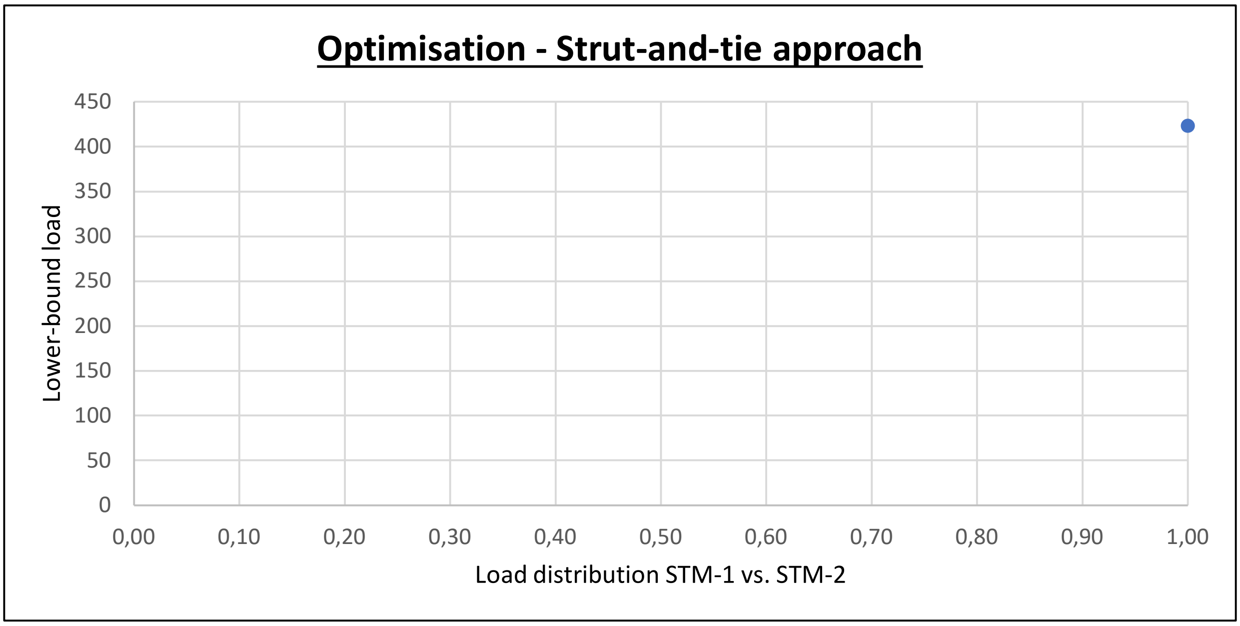

Load distribution		Offset				Load		Limitations	
STM-1	STM-2	Node 3	Node 4	Node 5	Node 7	[kN]	Mechan.	Anchor.	Angle
1,000	0,000	225	60	70	25	423,2	T2	Correct	Correct

4,2 Kinematic approach (Lowest upper-bound approximation)

$\theta_{C,min}$	30,0	[°]
$\theta_{C,max}$	70,0	[°]

θ_{Crack}		30,0	36,7	43,3	50,0	56,7	63,3	70,0	[°]
Rebar 1	Leverarm	124,9	113,3	106,0	101,0	96,6	92,7	90,1	[mm]
	Moment	161,8	146,8	137,4	130,9	125,2	120,1	116,8	[kNm/m]
Rebar 2	Leverarm	247,4	166,7	114,9	77,9	49,0	25,4	5,8	[mm]
	Moment	160,3	108,0	74,5	50,5	31,8	16,5	3,7	[kNm/m]
Rebar 3	Leverarm	0,0	0,0	0,0	0,0	0,0	0,0	0,0	[mm]
	Moment	0,0	0,0	0,0	0,0	0,0	0,0	0,0	[kNm/m]
Concrete	Leverarm	202,3	205,6	207,6	208,9	210,3	211,6	212,3	[mm]
	Moment	262,1	266,4	269,0	270,8	272,5	274,2	275,1	[kNm/m]
ΔX		217,0	222,0	225,0	227,0	229,0	231,0	232,0	[mm]
Total moment		584,2	521,3	480,9	452,1	429,5	410,8	395,6	[kNm/m]
Leverarm support		739,9	659,2	607,4	570,4	541,5	517,9	498,3	[mm]
Load support		789,6	790,7	791,7	792,6	793,1	793,2	793,9	[kN/m]

Governing upper-bound load: 789,6 [kN/m]

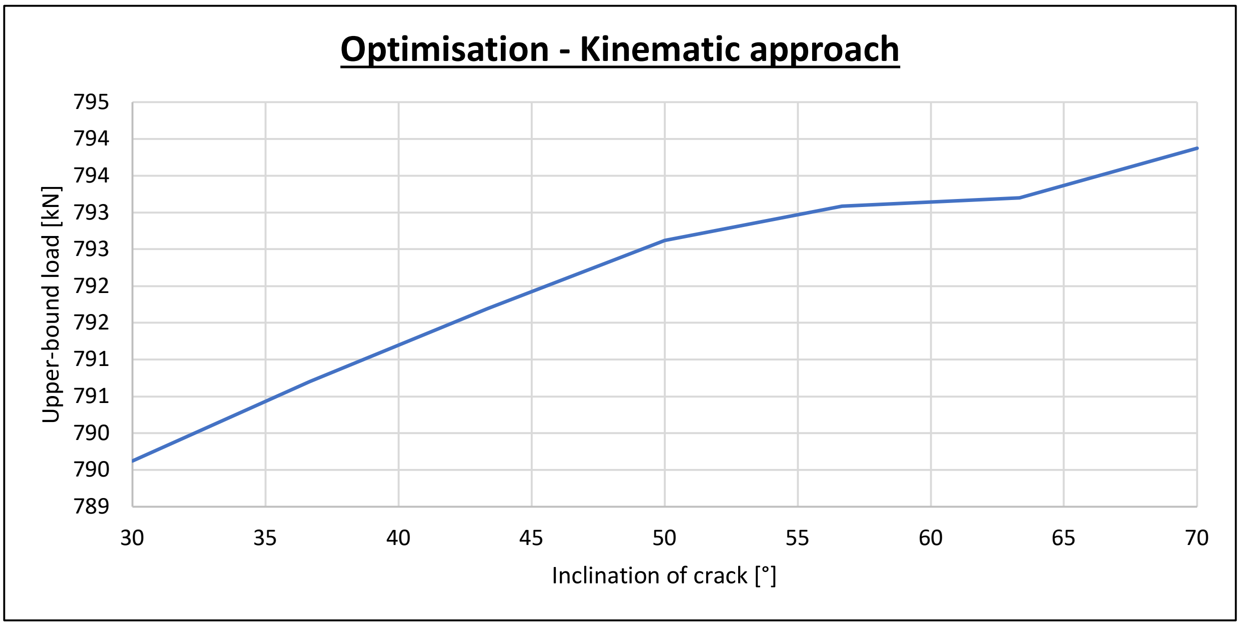

5. Corrosion

	Stepsize	Max
Corrosion	10%	60%

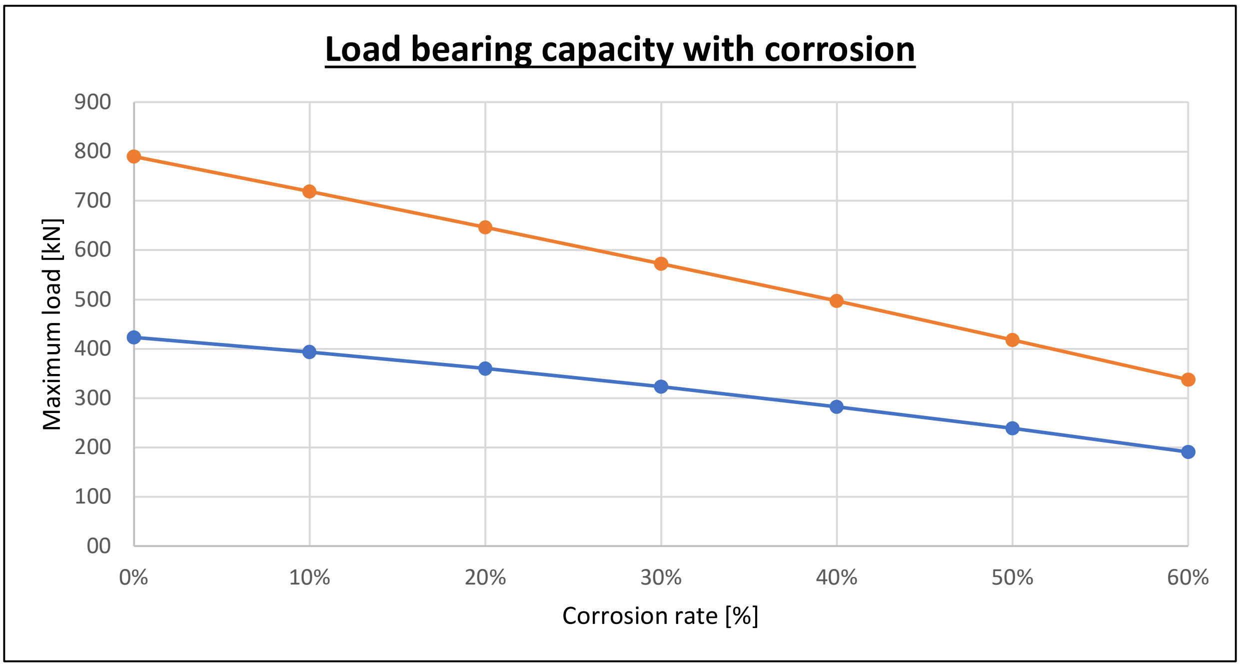

Maximum load	Corrosion							
	0%	10%	20%	30%	40%	50%	60%	
Lower-bound load	423,2	393,5	360,0	323,4	282,8	238,8	191,0	[kN/m]
Failure mechanism	T2	T2	T2	T2	T2	T2	T2	
Upper-bound load	789,6	718,8	646,5	572,7	497,2	418,1	337,4	[kN/m]

C.4 Tegelen

Analytical parametric tool for load bearing capacity of RC half-joints

Project
Tegelen

1. Geometry and material properties

1.1 Concrete

1.1.1 Geometry

a	615	[mm]
b	480	[mm]
c	375	[mm]
d	225	[mm]

Width	1000	[mm]
Cover	30	[mm]
Support	200	[mm]
α	7,33	[°]

1.1.2 Material

γ_c	1,5	[-]
k_t	1	[-]

α_{cc}	1	[-]
α_{ct}	1	[-]

f_{ck}	35,0	[N/mm^2]
f_{cm}	43,0	[N/mm^2]
f_{cd}	23,3	[N/mm^2]
v'	0,860	[-]

f_{ctm}	3,21	[N/mm^2]
$f_{ctk,0.05}$	2,25	[N/mm^2]
f_{ctd}	1,50	[N/mm^2]
Mean values?		No

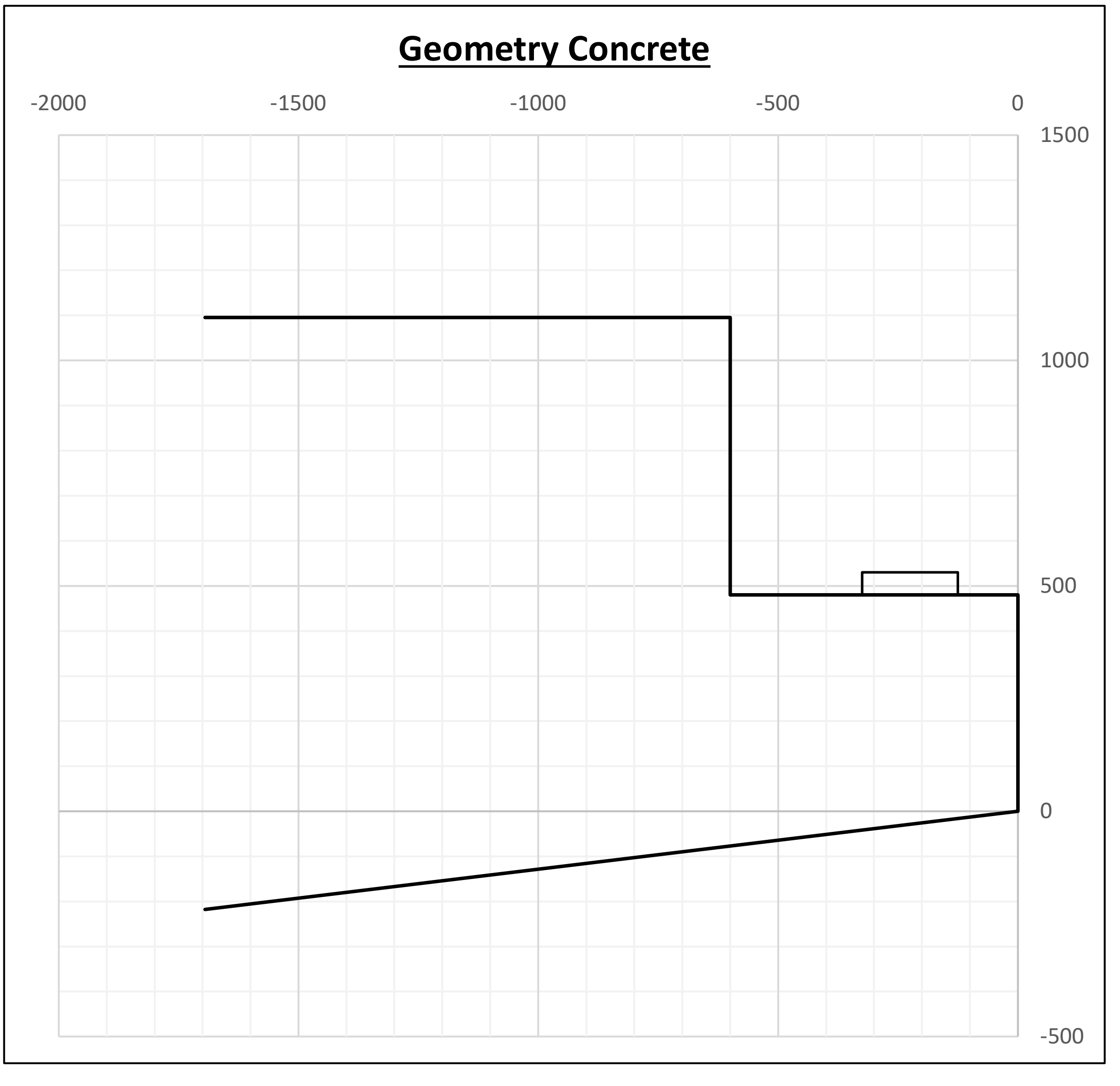

1.2 Reinforcement steel

1.2.1 *Geometry*

	Rebar 1	Rebar 2	Rebar 3	
Ø	32	20	20	[mm]
$Ø_m$	112,5	100	100	[mm]
Spacing	200	100	200	[mm]
η_1	1	1	1	[-]
η_2	1	1	1	[-]
η_3	1	1	1	[-]
l_{top}	970	700	-	[mm]
l_{bottom}	500	200	-	[mm]
Δ_{top}	0	0	-	[mm]
Δ_{middle}	0	0	-	[mm]
Δ_{bottom}	0	0	-	[mm]
Corrosion	0%	0%	0%	[-]

Include Rebar 3?	Yes

Coordinates Rebar 3		
x	y	
-1700	1055	[1]
-1250	1055	[2]
-200	30,8	[3]
-46	30,8	[4]
-46	200	[5]
		[6]

ϕ	2,4	[rad]
	135,7	[°]

1.2.2 *Material*

$f_{yd,0}$	435	[N/mm^2]
f_{yd}	435	[N/mm^2]

$\alpha_{corr,y}$	0	[-]
	1,23	

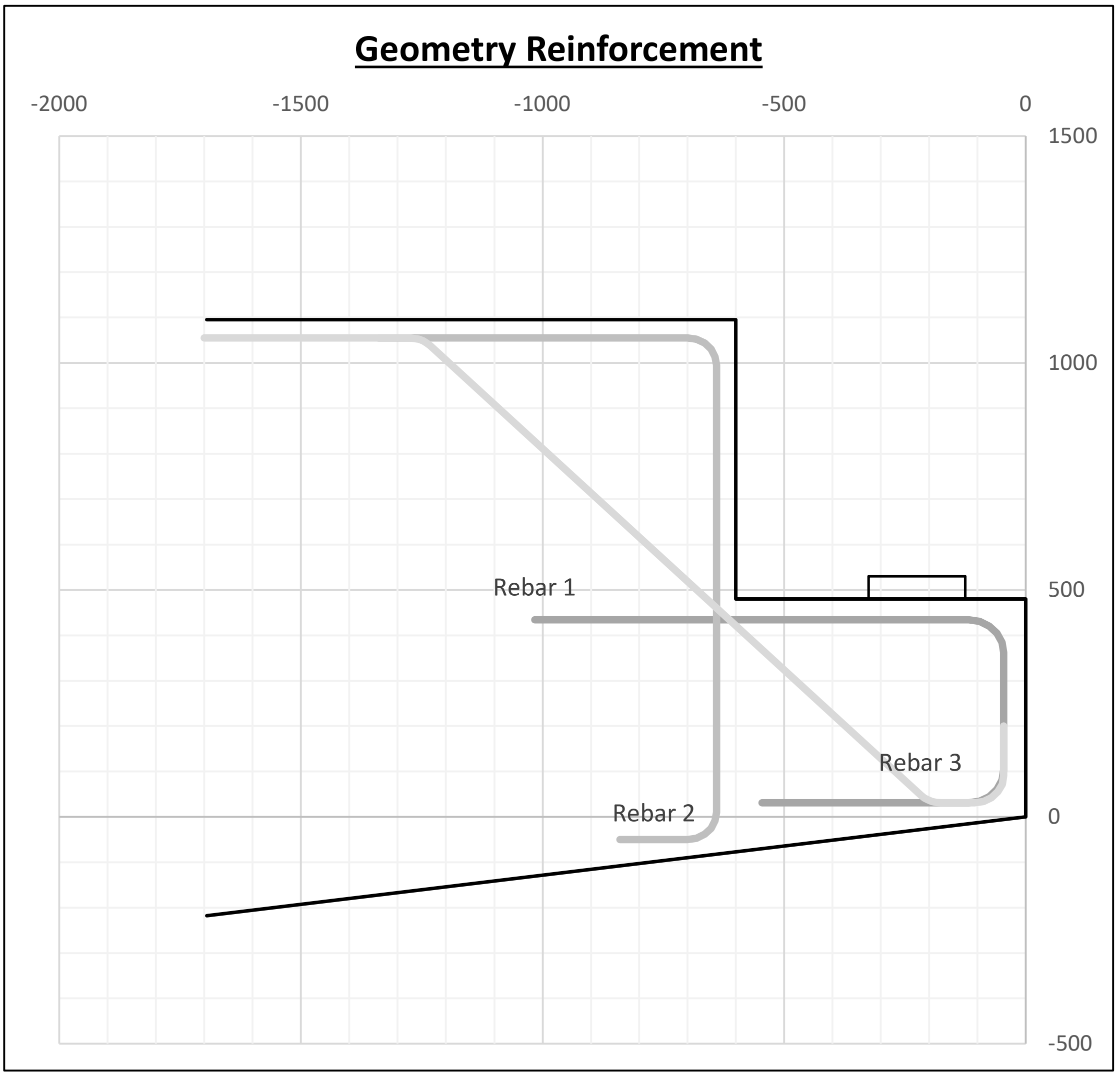

1.3 Pre-stressed steel

1.3.1 Geometry

A_p	1568	[mm^2]
y_p	850	[mm]
Bearing	150	[mm]
Spacing	3000	[mm]

Include prestress?	Yes

1.3.2 Material

σ_{pm}	1208	[N/mm^2]
P_m	1894,6	[kN]

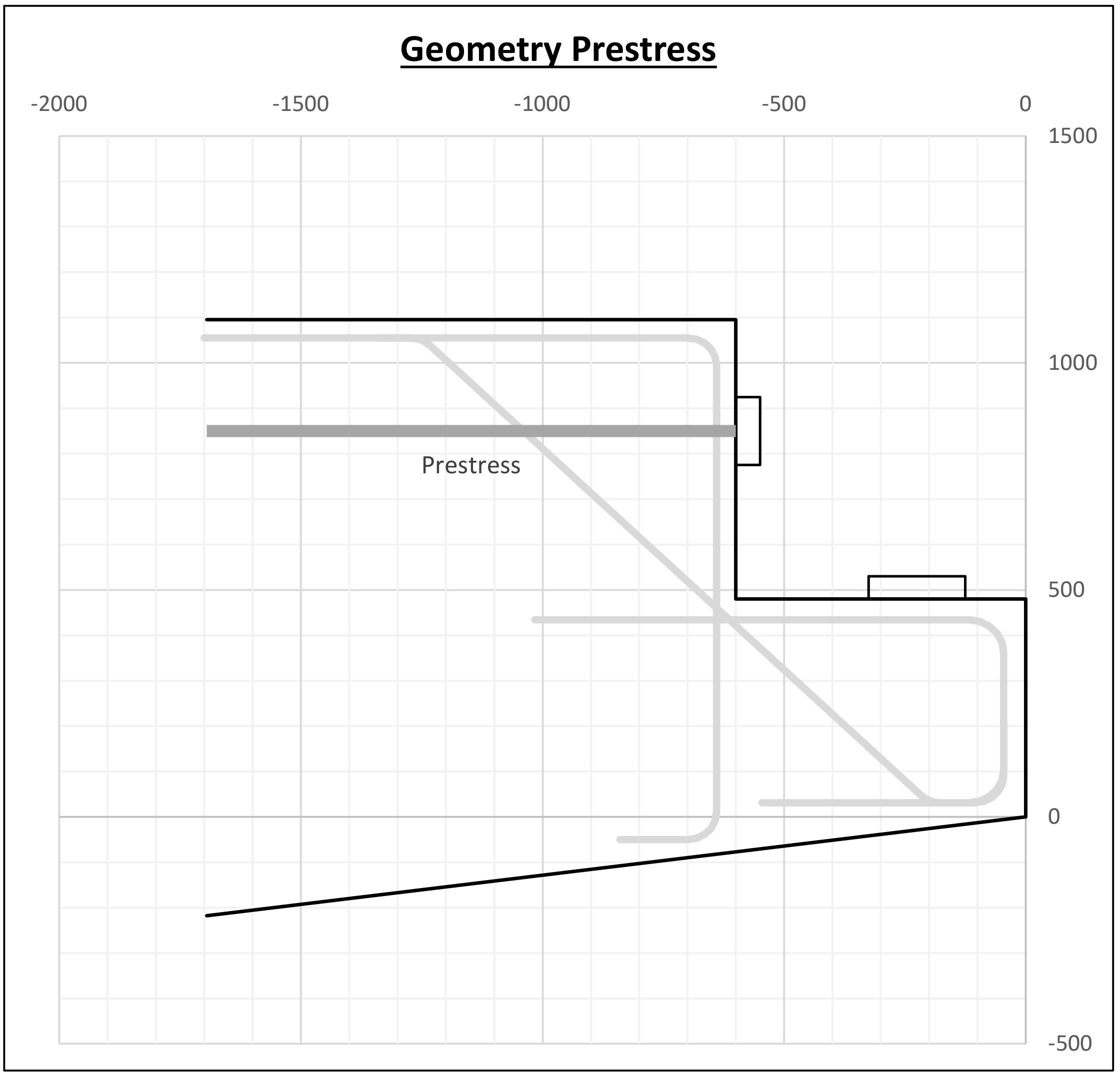

2. Strut-and-tie modelling

2.1 Nodes

	Offset		Coordinates		Type
	x	y	x	y	
(1)	-	-	-225,0	434,0	CCT
(2)	-	0	-640,0	850,0	CTT
(3)	175	-	-841,0	434,0	CCT
(4)	-	100	-640,0	110,0	CCT
(5)	-	75	-1695,0	-143,0	CCC
(6)	-		-1695,0	850,0	-
(7)	200		-360,6	187,5	CCT
(8)	-	-	-1250,0	1055,0	CTT
(9)	-	-	-1695,0	1055,0	-

F_{unit}	1,00	[-]

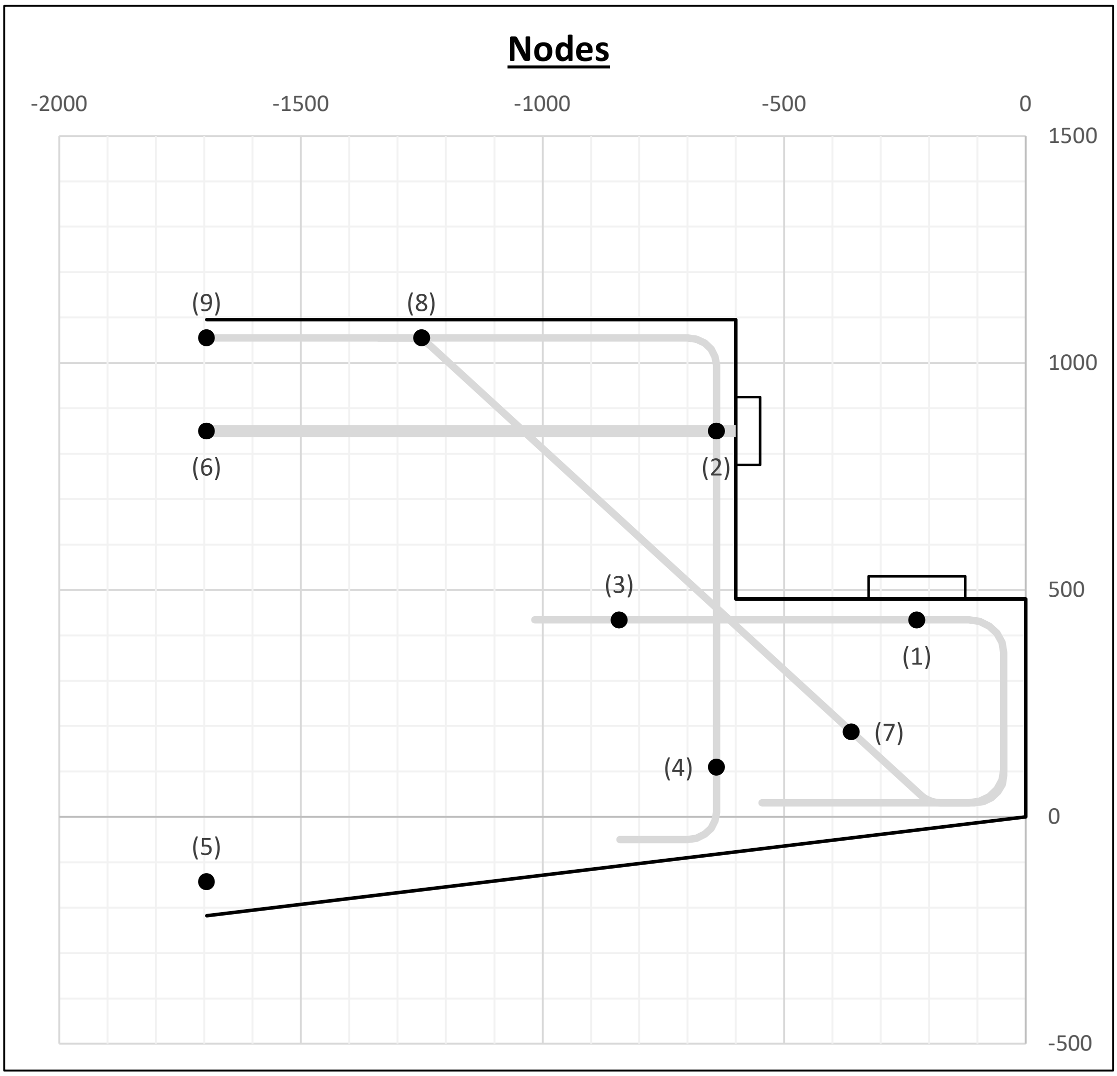

2.2 STM-1 (without diagonal)

	Node (j)	Node (k)	$F_{unit,STM1}$	Length	Angles	
			[-]	[mm]	[rad]	[°]
C1-1	(1)	(4)	-1,62	526,5	0,6629	38,0
C2-1	(2)	(3)	-1,29	462,0	1,1207	64,2
C3-1	(3)	(4)	-1,37	381,3	1,0156	58,2
C4-1	(2)	(5)	-1,26	1448,8	0,7552	43,3
C5-1	(4)	(5)	-0,58	1084,9	0,2354	13,5
T1-1	(1)	(3)	1,28	616,0	0	0,0
T2-1	(2)	(4)	2,03	740,0	1,5708	90,0
P-1	(2)	(6)	1,48	1055,0	0	0,0

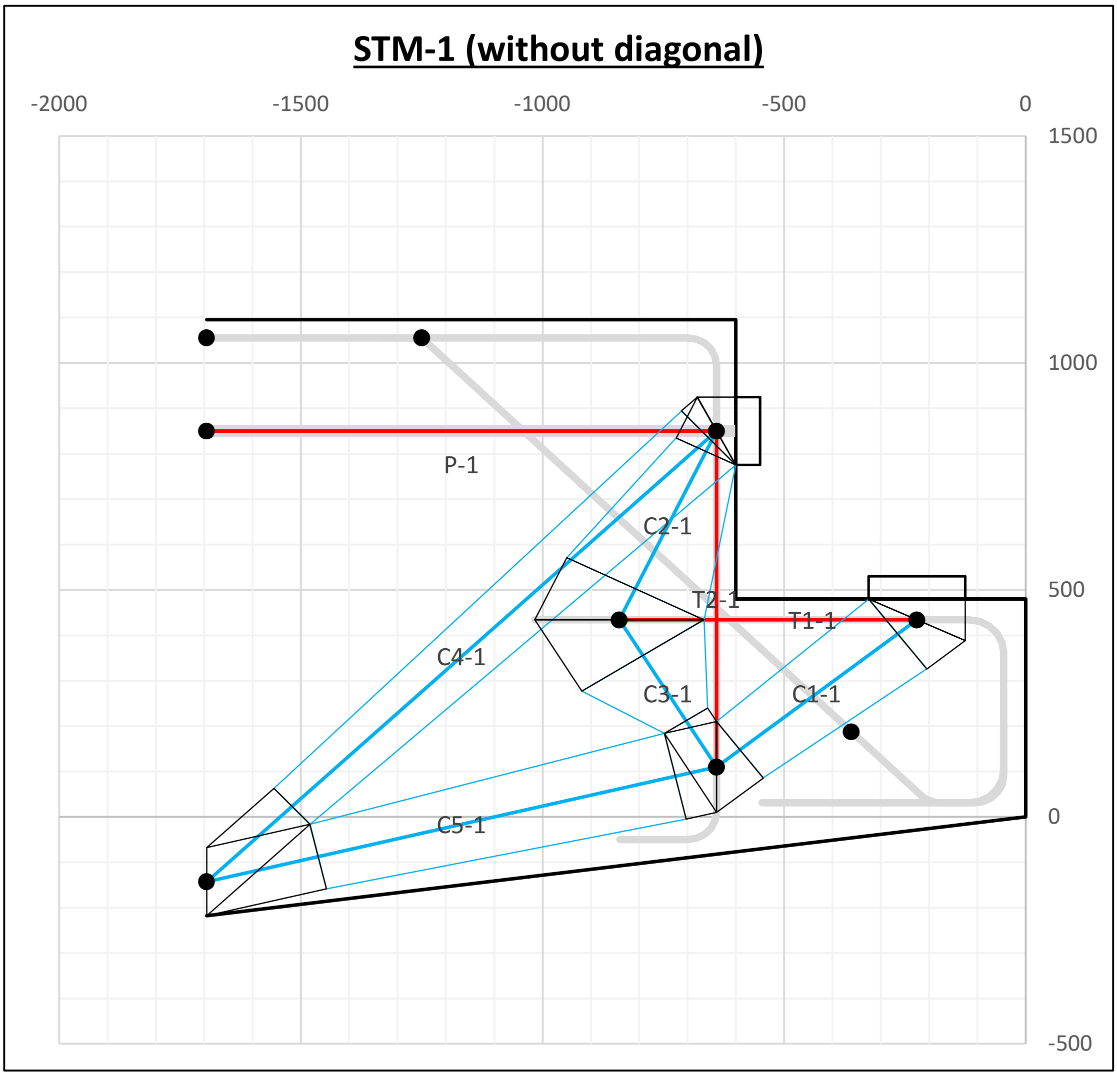

2.3 STM-2 (with diagonal)

	Node (j)	Node (k)	$F_{unit,STM2}$	Length	Angles	
			[-]	[mm]	[rad]	[°]
C2-2	(2)	(3)	-0,55	462,0	1,1207	64,2
C3-2	(3)	(4)	-0,59	381,3	1,0156	58,2
C4-2	(2)	(5)	-0,18	1448,8	0,7552	43,3
C5-2	(4)	(5)	-0,94	1084,9	0,2354	13,5
C6-2	(1)	(7)	-1,14	281,4	1,0677	61,2
C7-2	(7)	(4)	-1,27	289,9	0,2708	15,5
C8-2	(8)	(5)	-0,70	1278,0	1,2151	69,6
T1-2	(1)	(3)	0,55	616,0	0	0,0
T2-2	(2)	(4)	0,62	740,0	1,5708	90,0
P-2	(2)	(6)	0,37	1055,0	0	0,0
T4-2	(7)	(8)	0,94	1242,4	0,7730	44,3
T5-2	(8)	(9)	0,92	445,0	0	0,0

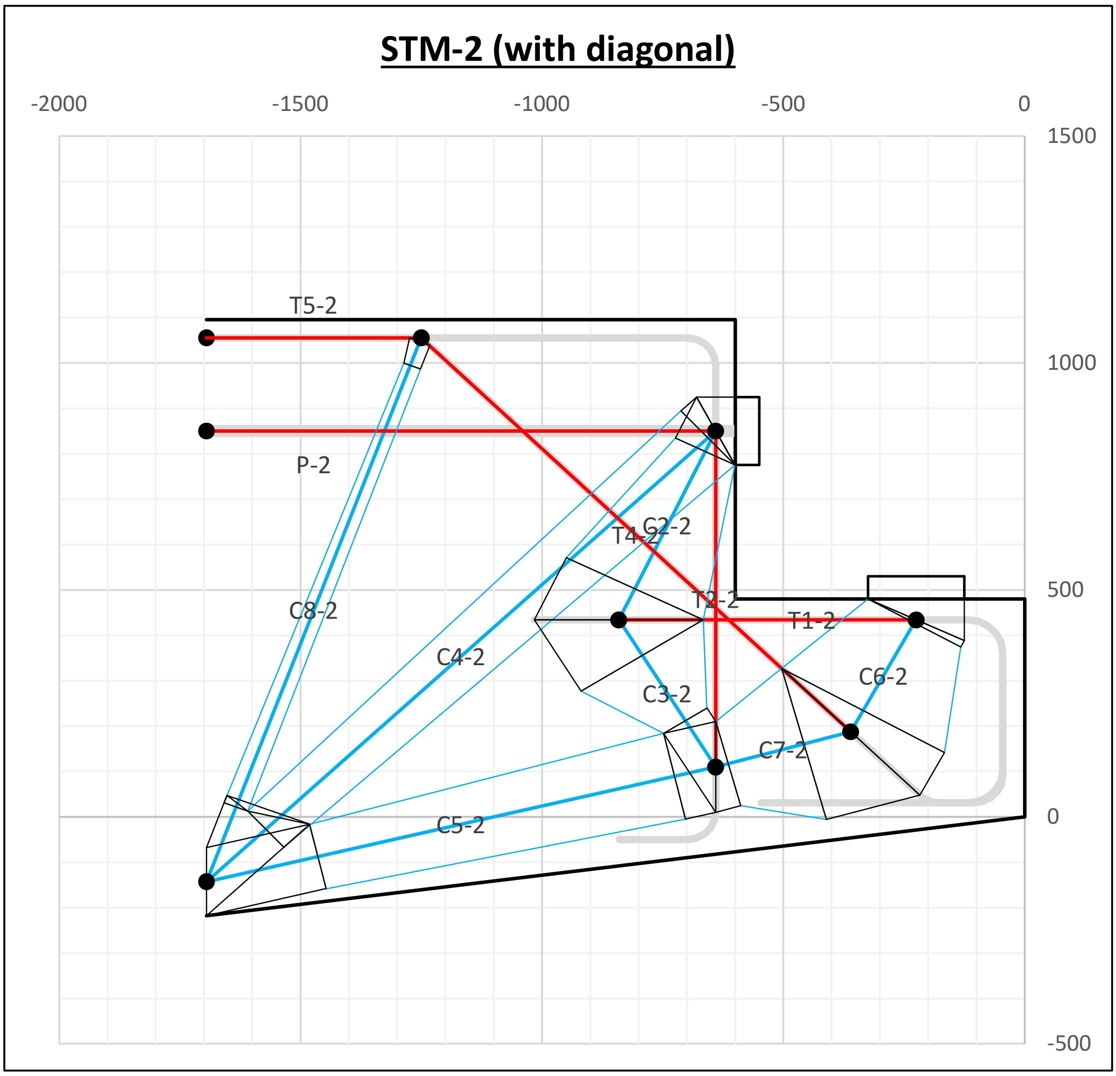

2.4 STM-3 (Combined)

	Node (j)	Node (k)	$F_{unit,STM1}$	$F_{unit,STM2}$	F_{unit}	Length	Angles	
			0,4	0,6	[-]	[mm]	[rad]	[°]
C1	(1)	(4)	-1,62		-0,65	526,5	0,6629	38,0
C2	(2)	(3)	-1,29	-0,55	-0,85	462,0	1,1207	64,2
C3	(3)	(4)	-1,37	-0,59	-0,90	381,3	1,0156	58,2
C4	(2)	(5)	-1,26	-0,18	-0,61	1448,8	0,7552	43,3
C5	(4)	(5)	-0,58	-0,94	-0,80	1084,9	0,2354	13,5
C6	(1)	(7)		-1,14	-0,68	281,4	1,0677	61,2
C7	(7)	(4)		-1,27	-0,76	289,9	0,2708	15,5
C8	(8)	(5)		-0,70	-0,42	1278,0	1,2151	69,6
T1	(1)	(3)	1,28	0,55	0,84	616,0	0	0
T2	(2)	(4)	2,03	0,62	1,18	740,0	1,5708	90,0
P	(2)	(6)	1,48	0,37	0,81	1055,0	0	0
T4	(7)	(8)		0,94	0,57	1242,4	0,7730	44,3
T5	(8)	(6)		0,92	0,55	445,0	0	0

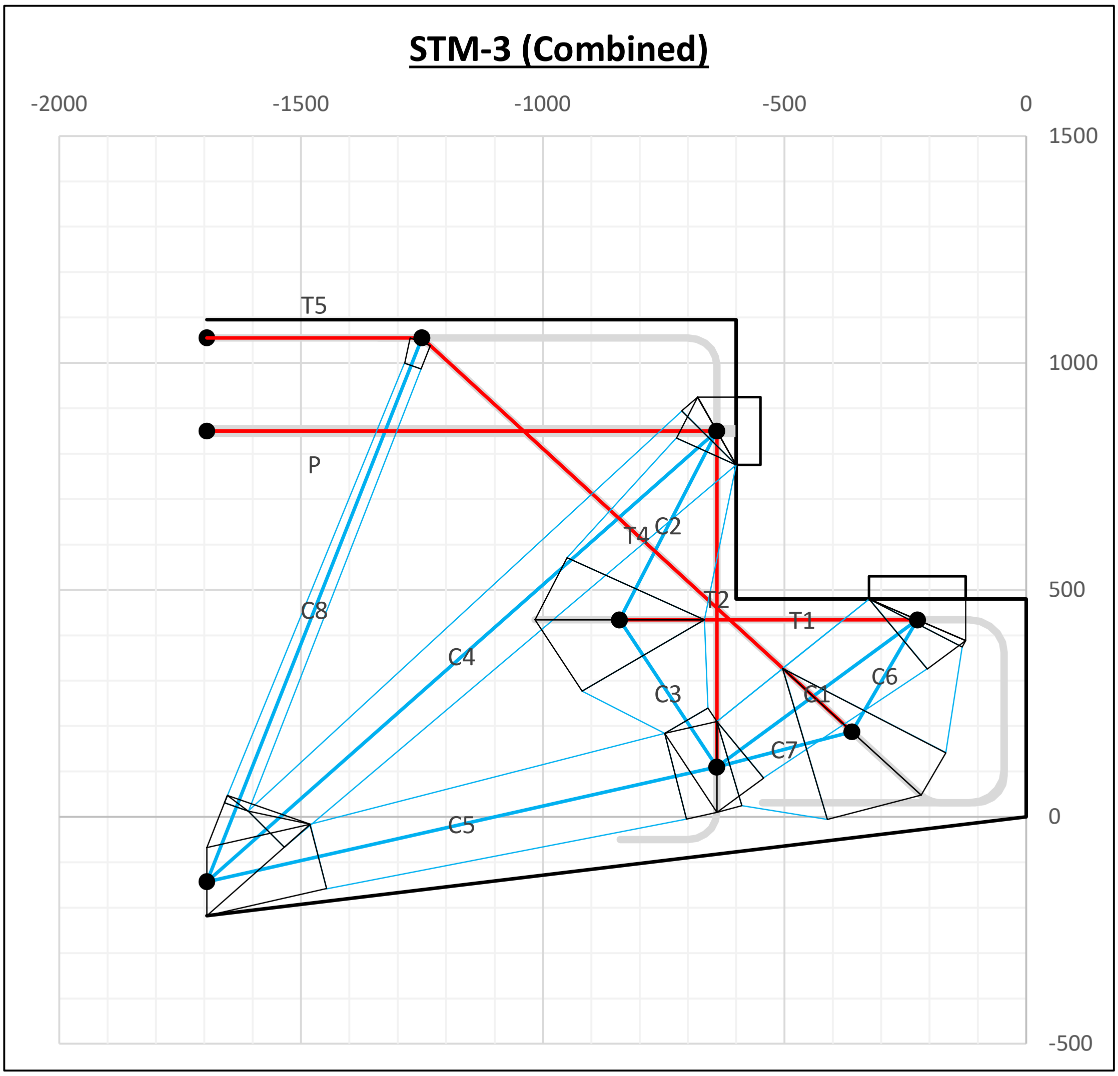

2.5 Node dimensions

Node (1)	T1	F	C1	C6		CCT
$a_{(1)}$	-	220,1	220,1	220,1		[mm]
$w_{(1)}$	-	200,0	195,6	219,6		[mm]
$b_{(1)}$	-	92,0	101,0	15,8		[mm]

Node (2)	T2	P	C2	C4		CTT
$a_{(2)}$	-	170,0	170,0	170,0		[mm]
$w_{(2)}$	-	150,0	137,3	164,1		[mm]
$b_{(2)}$	-	80,0	100,3	44,6		[mm]

Node (3)	T1	C2	C3			CCT
$a_{(3)}$	-	350,0	350,0			[mm]
$w_{(3)}$	-	315,1	297,4			[mm]
$b_{(3)}$	-	152,3	184,5			[mm]

Node (4)	T2	C1	C3	C5	C7	CCT
$a_{(4)}$	-	200,0	111,1	204,9	200,0	[mm]
$w_{(4)}$	-	157,6	105,4	194,5	192,7	[mm]
$b_{(4)}$	-	123,1	34,9	64,4	53,5	[mm]

Node (5)	C4	C5	C8	Internal		CCC
$a_{(5)}$	131,5	293,7	55,0	219,9		[mm]
$w_{(5)}$	109,2	145,9	52,2	182,6		[mm]
$b_{(5)}$	-73,2	254,9	-17,1	122,5		[mm]

Node (7)	T4	C6	C7			CCT
$a_{(7)}$	-	400,0	400,0			[mm]
$w_{(7)}$	-	385,5	345,7			[mm]
$b_{(7)}$	-	106,6	201,2			[mm]

Node (8)	T4	T5	C8			CTT
$a_{(8)}$	-	-	-			[mm]
$w_{(8)}$	-	-	36,5			[mm]
$b_{(8)}$	-	-	-			[mm]

2,6 Checks

2.6.1 Compressive strength of struts

Strut i	C1	C2	C3	C4	C5	C6	C7	C8	
$F_{unit,i}$	-0,650	-0,848	-0,898	-0,611	-0,797	-0,685	-0,764	-0,422	[-]
Tension	Yes	Yes	Yes	Yes	Yes	Yes	Yes	Yes	
$\sigma_{Rd,max,c}$	12,04	12,04	12,04	12,04	12,04	12,04	12,04	12,04	[N/mm^2]
L_c	526,5	462,0	381,3	1448,8	1084,9	281,4	289,9	1278,0	[mm]
$w_{c,eff}$	157,6	137,3	105,4	109,2	145,9	219,6	192,7	36,5	[mm]
$C_{max,C,i}$	-1897,9	-1653,0	-1269,3	-1315,1	-1756,2	-2643,7	-2320,3	-439,9	[kN/m]
$F_{max,C,i}$	2920,2	1949,5	1412,8	2153,6	2204,8	3860,3	3038,2	1042,1	[kN/m]

2.6.2 Compressive strength of nodes

Strut	C1	C2	C3	C4	C5	C6	C7	C8	
Node (j)	(1)	(2)	(3)	(2)	(4)	(1)	(7)	(8)	
Type	CCT	CTT	CCT	CTT	CCT	CCT	CCT	CTT	
k	0,85	0,75	0,85	0,75	0,85	0,85	0,85	0,75	[-]
$\sigma_{Rd,max,(j)}$	17,06	15,05	17,06	15,05	17,06	17,06	17,06	15,05	[N/mm^2]
$w_{i(j)}$	195,6	137,3	297,4	164,1	194,5	219,6	345,7	36,5	[mm]
$C_{max,i(j)}$	-3336,3	-2066,2	-5073,1	-2469,1	-3317,3	-3745,2	-5896,7	-549,9	[kN/m]
$F_{max,i(j)}$	5133,2	2436,8	5646,8	4043,5	4164,6	5468,7	7721,3	1302,6	[kN/m]
Node (k)	(4)	(3)	(4)	(5)	(5)	(7)	(4)	(5)	
Type	CCT	CCT	CCT	CCC	CCC	CCT	CCT	CCC	
k	0,85	0,85	0,85	1,00	1,00	0,85	0,85	1,00	[-]
$\sigma_{Rd,max,(k)}$	17,06	17,06	17,06	20,07	20,07	17,06	17,06	20,07	[N/mm^2]
$w_{i(k)}$	157,6	315,1	105,4	109,2	145,9	385,5	192,7	52,2	[mm]
$C_{max,i(k)}$	-2688,8	-5375,3	-1798,2	-2191,8	-2927,0	-6575,7	-3287,0	-1048,1	[kN/m]
$F_{max,i(k)}$	4136,9	6339,4	2001,5	3589,4	3674,6	9601,7	4304,1	2482,7	[kN/m]

2.6.3 Compressive strength of internal nodes

Node (j/k)	(1)	(2)	(4)	(5)	
Strut i_1	C1	C2	C1	C4	
$F_{unit,i,1}$	-0,577	-0,685	-0,512	-0,445	[-]
Strut i_2	C6	C4	C7	C5	
$F_{unit,i,2}$	-0,683	-0,589	-0,736	-0,775	[-]
Strut i_3	-		-	C8	
$F_{unit,i,3}$				-0,147	[-]
F_{unit}	-1,261	-1,274	-1,248	-1,366	[-]
Type	CCT	CTT	CCT	CCC	
k	0,85	0,75	0,85	1,00	[-]
$\sigma_{Rd,max}$	17,06	15,05	17,06	20,07	[N/mm^2]
w	220,1	170,0	200,0	150,0	[mm]
C_{max}	-3754,9	-2558,5	-3411,3	-3010,0	[kN/m]
F_{max}	2978,8	2008,2	2733,1	2203,2	[kN/m]

2.6.4 *Yield strength of ties*

Ties	T1	T2	T3	T4	T5		
$F_{unit,i}$	0,842	1,182	0,814	0,567	0,553	[-]	
Rebar	1	2	P	3	3	[-]	
Ø	32	20	-	20	30	[mm]	(add top rebar)
Corrosion	0%	0%	-	0%	-	[-]	(at re-entrant corner)
f_{yd}	435	435	-	435	435	[N/mm^2]	
$T_{max,T,ind,i}$	349,8	136,7	1894,6	136,7	307,5	[kN]	
$T_{max,T,i}$	1749,2	1366,6	1998,1	683,3	1537,4	[kN/m]	
$F_{max,T,i}$	2076,4	1156,2	2456,1	1205,7	2781,7	[kN/m]	

2.6.5 *Anchorage length of ties*

Lower-bound load 1042,1 [kN/m] Failure mechanism: C8 (strut)

Ties	T1	T2	T3	T4	T5	
F_T	877,9	1231,7	847,7	590,6	575,9	[kN/m]
$F_{T,ind}$	175,6	123,2	2543,2	118,1	115,2	[kN]
f_{bd}	3,37	3,37	-	3,37	3,37	[N/mm^2]
σ_{sd}	218,3	392,1	-	376,0	163,0	[N/mm^2]
$l_{b,rqd,max}$	518,2	581,6	-	557,7	362,6	[mm]
Node (j)	(1)	(2)	(2)	(7)	(8)	
c_d	100,0	-	-	100,0	-	[mm]
p	5,21	-	-	1,72	-	[N/mm^2]
α_1	0,7	-	-	0,7	-	[-]
α_2	0,9	-	-	0,7	-	[-]
α_3	1,0	-	-	1,0	-	[-]
α_4	1,0	-	-	1,0	-	[-]
α_5	0,79	-	-	0,93	-	[-]
$l_{b,min}$	320,0	-	-	200,0	-	[mm]
l_{bd}	320,0	-	-	254,5	-	[mm]
$l_{b,prov}$	1120,2	-	-	719,4	-	[mm]
Check	Correct	-	-	Correct	-	
Node (k)	(3)	(4)	(6)	(8)	(6)	
c_d	100,0	50,0	-	-	-	[mm]
p	2,27	6,50	-	-	-	[N/mm^2]
α_1	0,7	1,0	-	-	-	[-]
α_2	0,9	1,0	-	-	-	[-]
α_3	1,0	1,0	-	-	-	[-]
α_4	1,0	1,0	-	-	-	[-]
α_5	0,91	0,74	-	-	-	[-]
$l_{b,min}$	320,0	200,0	-	-	-	[mm]
l_{bd}	320,0	430,3	-	-	-	[mm]
$l_{b,prov}$	350,0	434,2	-	-	-	[mm]
Check	Correct	Correct	-	-	-	

3. Kinematic approach (upper-bound approximation)

x_min	127,9	[mm]
Δx	0	[mm]

θ_{Crack}	30,0	[°]
l_{crack}	1104,7	[mm]

	$A_{s,i}$	A_s	f_{yd}	N_S / N_C	Leverarm	Moment	$N_{y\text{-}dir}$
	[mm^2]	[mm^2]	[N/mm^2]	[kN/m]	[mm]	[kNm/m]	[kN/m]
Rebar 1	804	4021	435	1749,2	506,3	885,7	0,0
Rebar 2	314	3142	435	1366,6	916,7	1252,7	1366,6
Rebar 3	314	1571	435	683,3	1060,8	724,8	477,1
Concrete	-	-	-	2238,4	78,0	174,6	0,0
Total						3037,9	1843,7

Support		
Leverarm:	1331,7	[mm]
Upper-bound load:	2281,3	[kN/m]

Vertical equilibrium	Fail	
Difference in vertical force	437,5	[kN/m]
Concrete shear resistance	74,9	[kN/m]

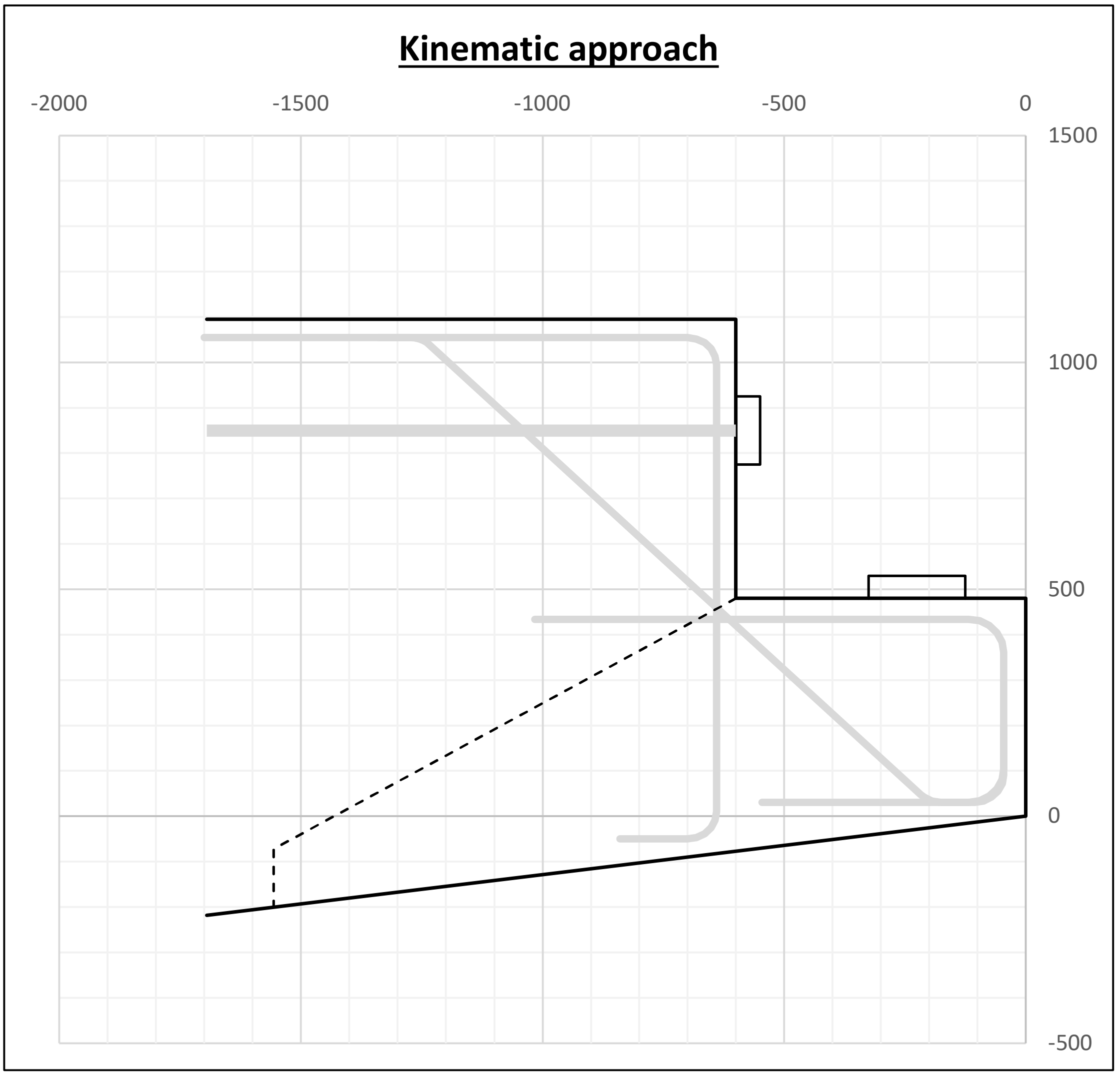

4. Optimisation

4.1 Strut-and-tie approach (Highest lower-bound approximation)

	Stepsize	Max. shift	Steps
Load	0,1	-	10
Node 3	25	200,0	8
Node 4	25	200,0	8
Node 5	25	200,0	8
Node 7	50	200,0	4

min θ 25,0 [°]

Anchorage:	Correct	
Angle (theta):	Correct	
Lower-bound load	1042,1	[kN/m]

Limitations on angles				
	Minimum	Maximum	[°]	
θC1	25,0	65,0	38,0	Correct
θC2	25,0	65,0	64,2	Correct
θC3	25,0	65,0	58,2	Correct
θC4	25,0	65,0	43,3	Correct
θC6	25,0	-	61,2	Correct
θC7	-	65,0	15,5	Correct
θC8	25,0	-	69,6	Correct
θC6+θT4	-	155,0	105,5	Correct
θT4-θC7	25,0	-	28,8	Correct
θC8+θT4	25,0	-	113,9	Correct

Governing lower-bound load: 1042,1 [kN/m] Failure mechanism: C8 (strut)

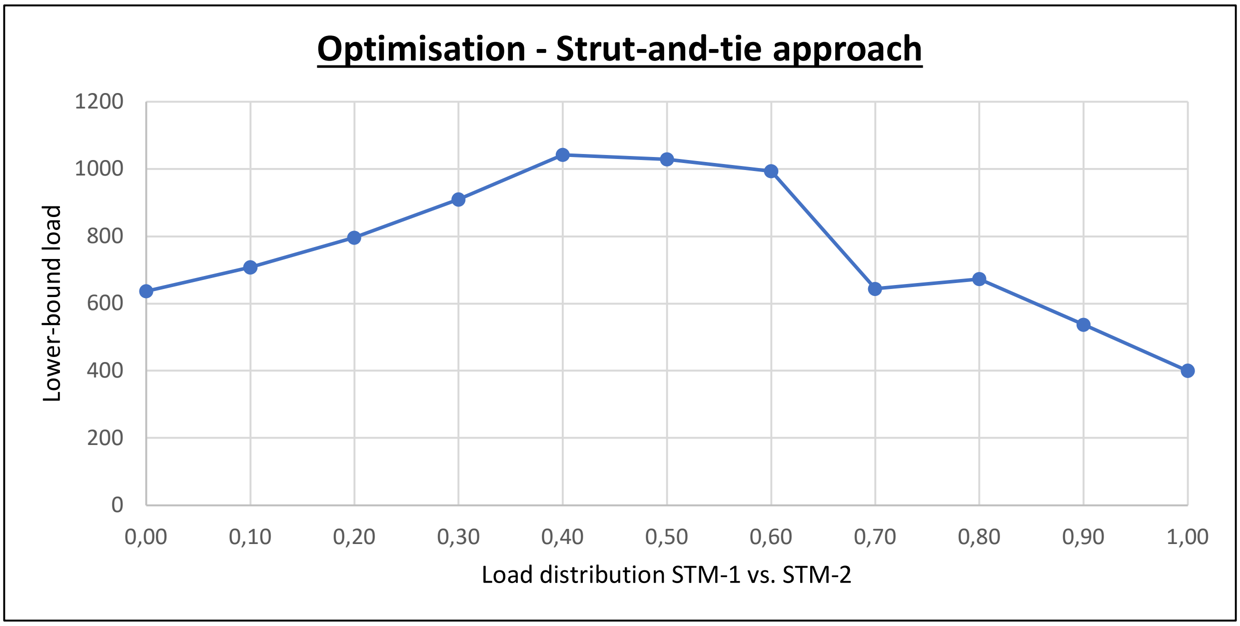

Load distribution		Offset				Load		Limitations	
STM-1	STM-2	Node 3	Node 4	Node 5	Node 7	[kN]	Mechan.	Anchor.	Angle
0,000	1,000	175	100	175	200	636,8	C8 (strut)	Correct	Correct
0,100	0,900	175	100	175	200	707,6	C8 (strut)	Correct	Correct
0,200	0,800	175	100	175	200	796,0	C8 (strut)	Correct	Correct
0,300	0,700	175	100	175	200	909,7	C8 (strut)	Correct	Correct
0,400	0,600	175	100	75	200	1042,1	C8 (strut)	Correct	Correct
0,500	0,500	175	125	50	200	1029,5	C8 (strut)	Correct	Correct
0,600	0,400	175	100	50	100	993,4	C8 (strut)	Correct	Correct
0,700	0,300	175	175	25	200	644,0	C8 (strut)	Correct	Correct
0,800	0,200	175	175	25	50	673,2	C5 (strut)	Correct	Correct
0,900	0,100	175	200	25	50	537,0	C4 (strut)	Correct	Correct
1,000	0,000	175	200	25	50	400,1	C4 (strut)	Correct	Correct

4,2 Kinematic approach (Lowest upper-bound approximation)

$\theta_{C,min}$	30,0	[°]
$\theta_{C,max}$	70,0	[°]

θ_{Crack}		30,0	36,7	43,3	50,0	56,7	63,3	70,0	[°]
Rebar 1	Leverarm	83,0	86,1	86,3	85,5	83,2	80,4	78,1	[mm]
	Moment	145,2	150,6	151,0	149,5	145,5	140,7	136,6	[kNm/m]
Rebar 2	Leverarm	183,5	137,4	100,2	70,3	45,0	23,5	5,2	[mm]
	Moment	250,7	187,8	137,0	96,1	61,5	32,1	7,1	[kNm/m]
Rebar 3	Leverarm	214,1	178,4	150,5	129,2	111,6	97,2	85,7	[mm]
	Moment	146,3	121,9	102,8	88,3	76,3	66,4	58,6	[kNm/m]
Concrete	Leverarm	304,6	298,6	295,3	293,3	292,6	292,6	292,6	[mm]
	Moment	681,8	668,4	660,9	656,5	655,0	655,0	655,0	[kNm/m]
ΔX		329,0	320,0	315,0	312,0	311,0	311,0	311,0	[mm]
Total moment		1224,1	1128,7	1051,8	990,3	938,2	894,2	857,2	[kNm/m]
Leverarm support		598,5	552,4	515,2	485,3	460,0	438,5	420,2	[mm]
Load support		2045,4	2043,2	2041,3	2040,6	2039,7	2039,2	2040,0	[kN/m]

Governing upper-bound load: 2039,2 [kN/m]

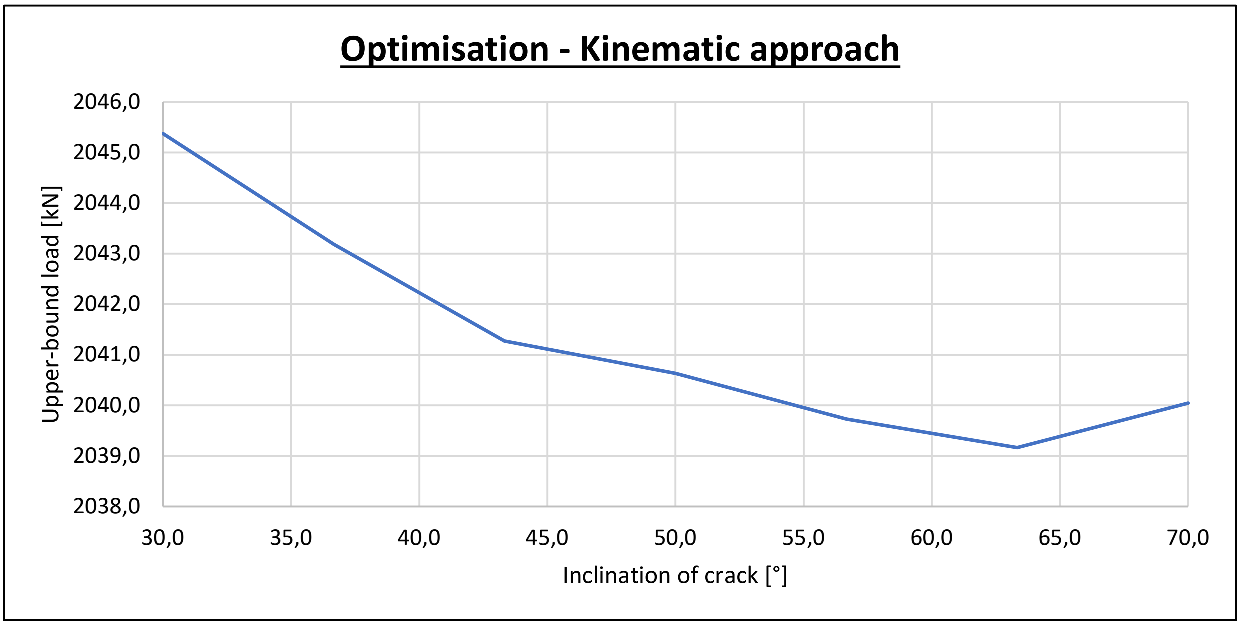

5. Corrosion

	Stepsize	Max
Corrosion	10%	60%

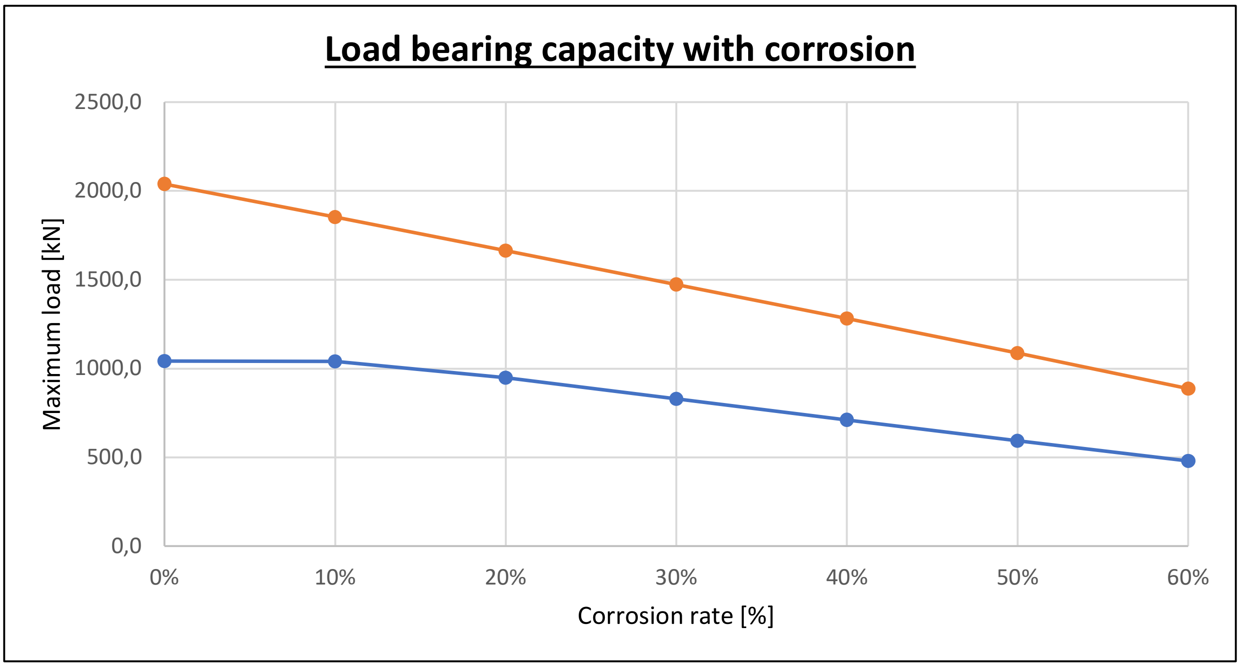

Maximum load	Corrosion							
	0%	10%	20%	30%	40%	50%	60%	
Lower-bound load	1042,1	1040,6	948,3	829,7	711,2	592,7	480,8	[kN/m]
Failure mechanism	C8 (strut)	T2	T4	T4	T4	T4	T2	
Upper-bound load	2039,2	1851,8	1663,5	1474,5	1282,4	1087,4	886,7	[kN/m]

C.5 Deventer-Bathmen

Analytical parametric tool for load bearing capacity of RC half-joints

Project
Deventer

1. Geometry and material properties

1.1 Concrete

1.1.1 *Geometry*

a	620	[mm]
b	400	[mm]
c	225	[mm]
d	225	[mm]

Width	1000	[mm]
Cover	30	[mm]
Support	200	[mm]
α	0	[°]

1.1.2 *Material*

γ_c	1,5	[-]
k_t	1	[-]

α_{cc}	1	[-]
α_{ct}	1	[-]

f_{ck}	35,0	[N/mm^2]
f_{cm}	43,0	[N/mm^2]
f_{cd}	23,3	[N/mm^2]
v'	0,860	[-]

f_{ctm}	3,21	[N/mm^2]
$f_{ctk,0.05}$	2,25	[N/mm^2]
f_{ctd}	1,50	[N/mm^2]
Mean values?		No

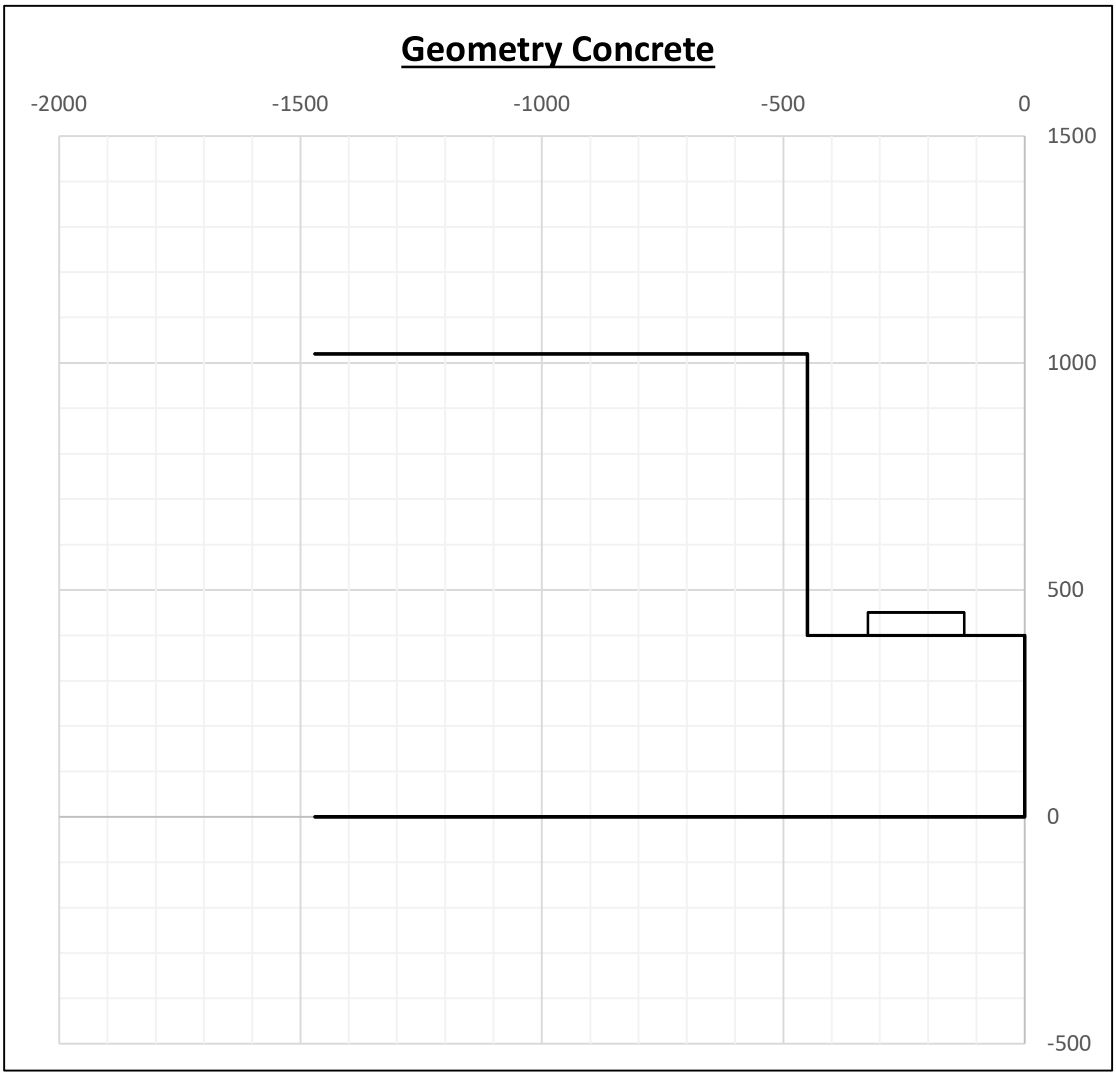

1.2 Reinforcement steel

1.2.1 Geometry

	Rebar 1	Rebar 2	Rebar 3	
Ø	25	25	25	[mm]
$Ø_m$	125	125	125	[mm]
Spacing	150	150	150	[mm]
η_1	1	1	1	[-]
η_2	1	1	1	[-]
η_3	1	1	1	[-]
l_{top}	1400	1000	-	[mm]
l_{bottom}	1000	300	-	[mm]
Δ_{top}	0	0	-	[mm]
Δ_{middle}	0	0	-	[mm]
Δ_{bottom}	0	0	-	[mm]
Corrosion	0%	0%	0%	[-]

Include Rebar 3?	Yes

Coordinates Rebar 3		
x	y	
-1500	977,5	[1]
-1000	997,5	[2]
-250	42,5	[3]
-42,5	42,5	[4]
-42,5	340	[5]
		[6]

ϕ	2,2	[rad]
	128,1	[°]

1.2.2 Material

$f_{yd,0}$	330	[N/mm^2]
f_{yd}	330	[N/mm^2]

$\alpha_{corr,y}$	0	[-]
	1,23	

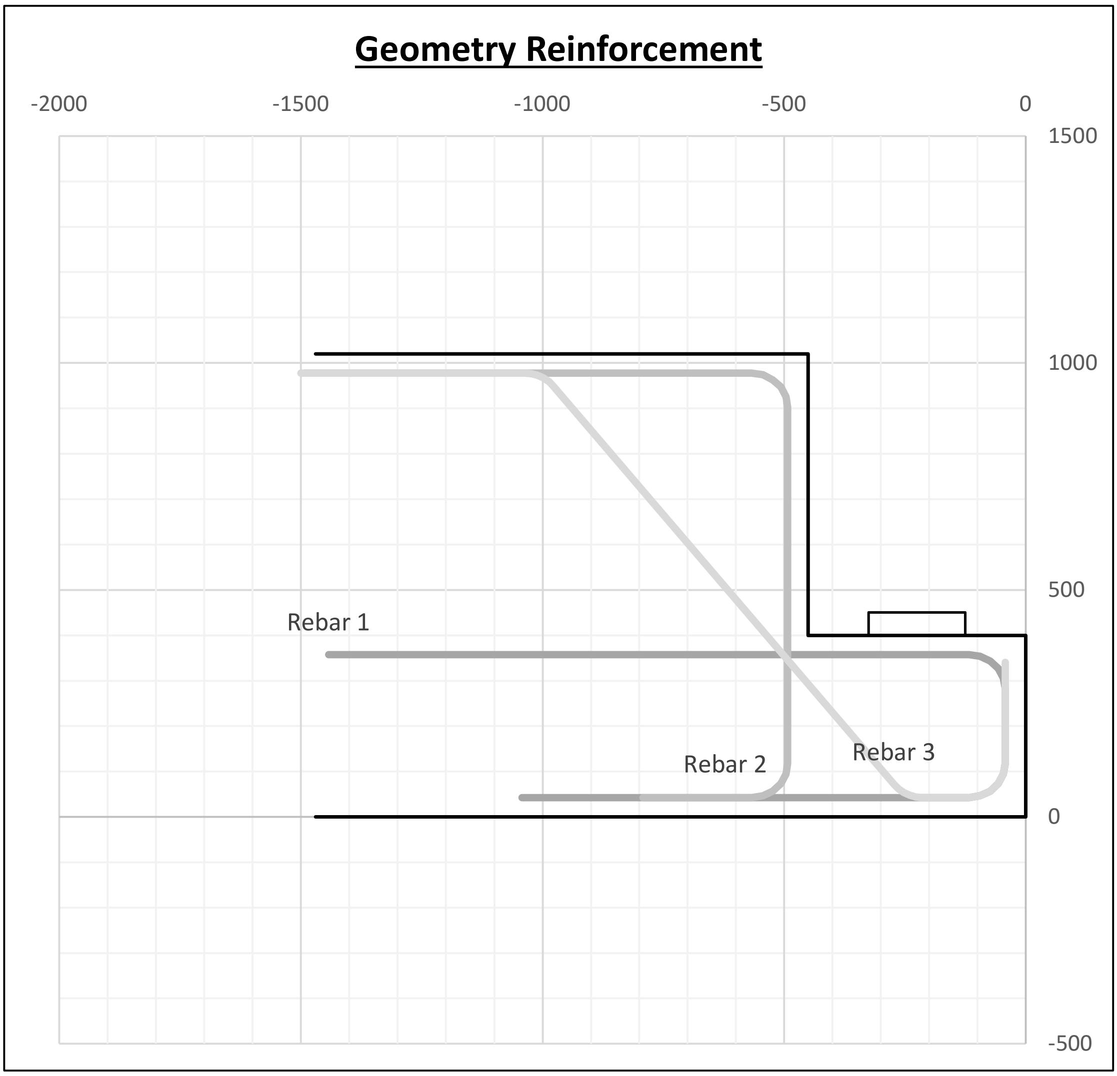

1.3 Pre-stressed steel

1.3.1 Geometry

A_p		[mm^2]
y_p		[mm]
Bearing		[mm]
Spacing		[mm]

Include prestress?	No

1.3.2 Material

σ_{pm}		[N/mm^2]
P_m		[kN]

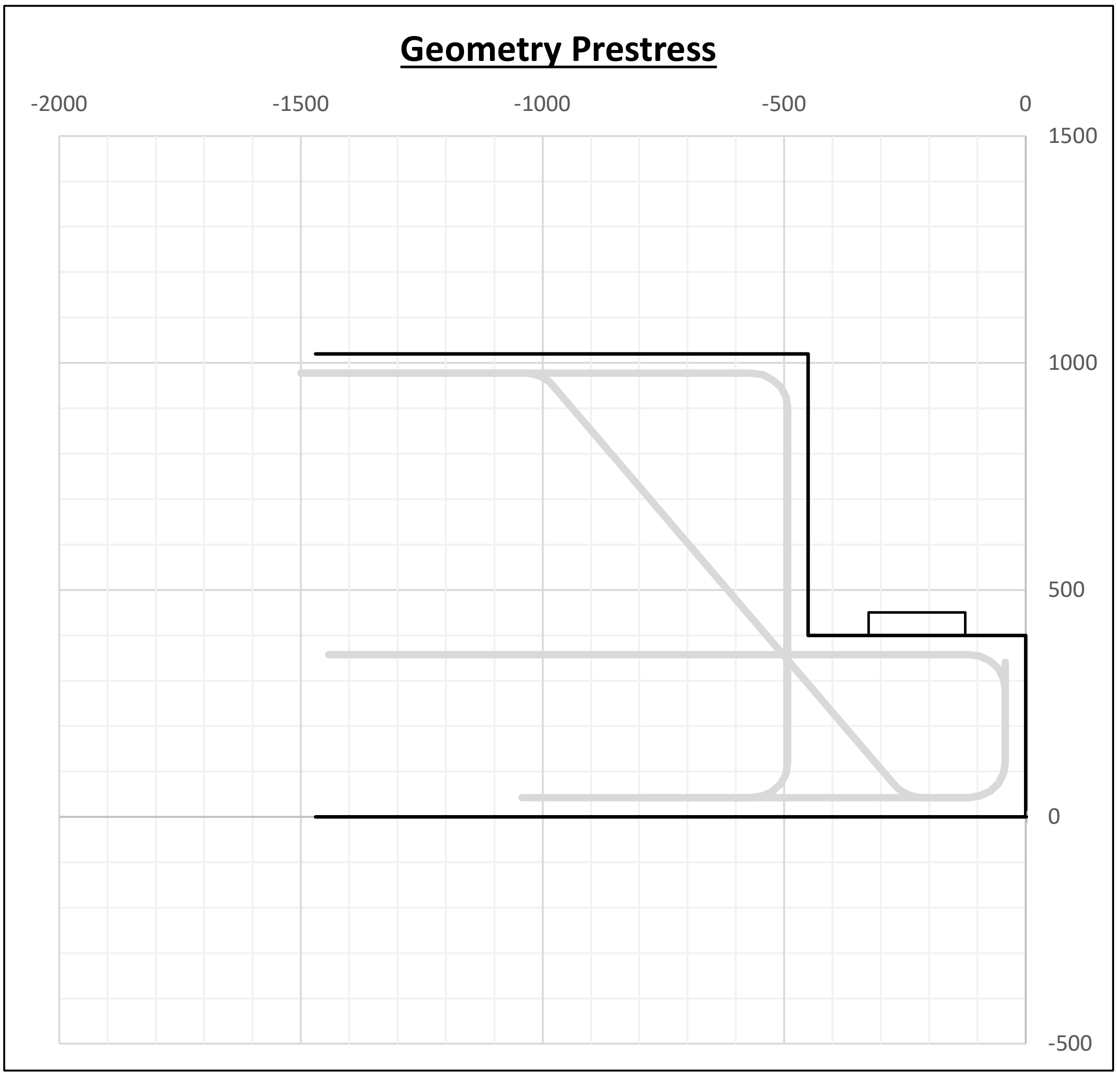

2. Strut-and-tie modelling

2.1 Nodes

	Offset		Coordinates		Type
	x	y	x	y	
(1)	-	-	-225,0	357,5	CCT
(2)	-	0	-492,5	977,5	CTT
(3)	550	-	-892,5	357,5	CCT
(4)	-	50	-492,5	167,5	CCT
(5)	-	75	-1470,0	75,0	CCC
(6)	-		-1470,0	977,5	-
(7)	125		-349,7	169,5	CCT
(8)	-	-	-1000,0	997,5	CTT
(9)	-	-	-1470,0	977,5	-

F_{unit}	1,00	[-]

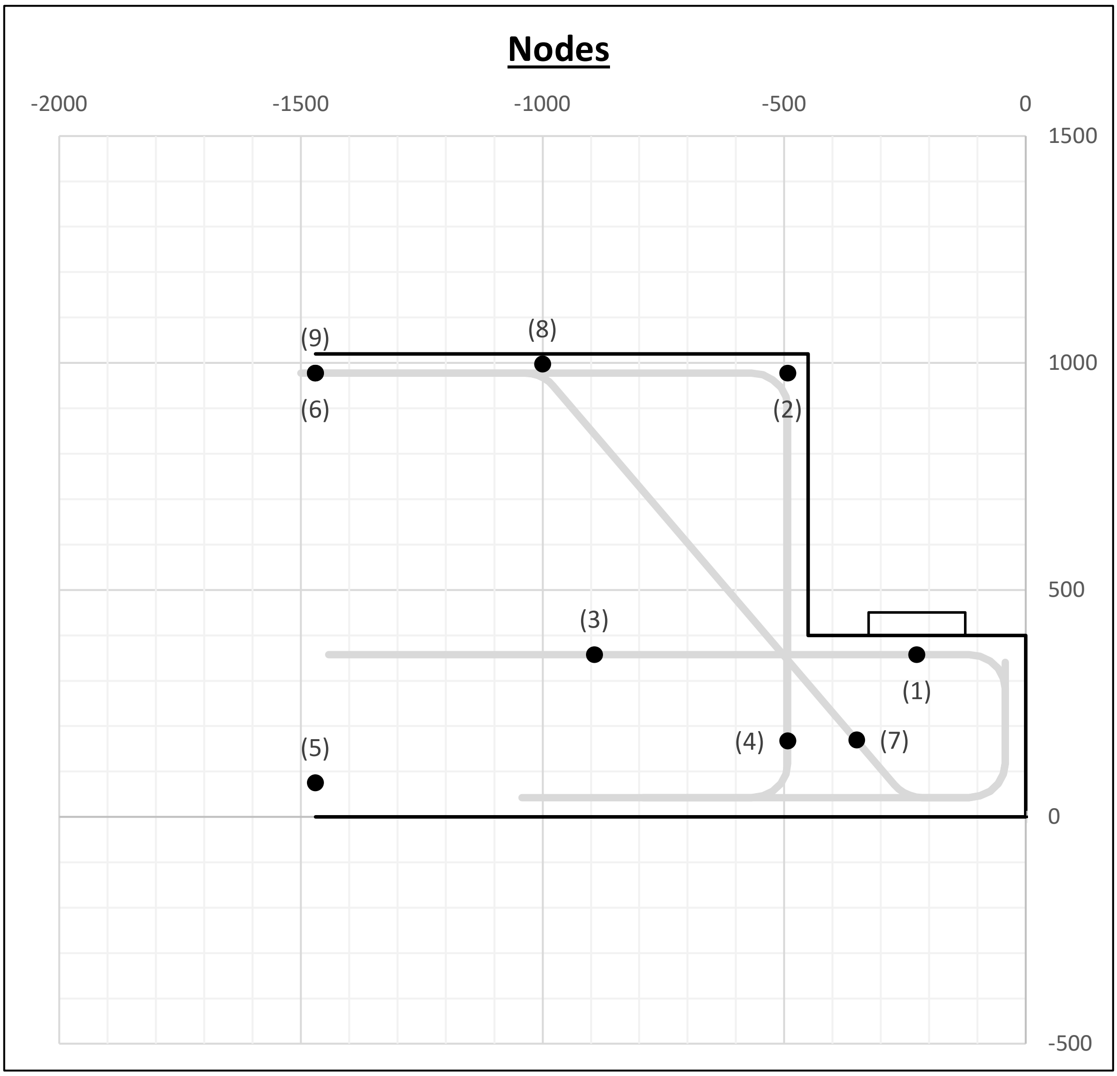

2.2 STM-1 (without diagonal)

	Node (j)	Node (k)	$F_{unit,STM1}$	Length	Angles	
			[-]	[mm]	[rad]	[°]
C1-1	(1)	(4)	-1,73	328,1	0,6176	35,4
C2-1	(2)	(3)	-0,61	737,8	0,9978	57,2
C3-1	(3)	(4)	-1,19	442,8	0,4434	25,4
C4-1	(2)	(5)	-1,43	1330,4	0,7455	42,7
C5-1	(4)	(5)	-0,33	981,9	0,0943	5,4
T1-1	(1)	(3)	1,41	667,5	0	0,0
T2-1	(2)	(4)	1,48	810,0	1,5708	90,0
T3-1	(2)	(6)	1,38	977,5	0	0,0

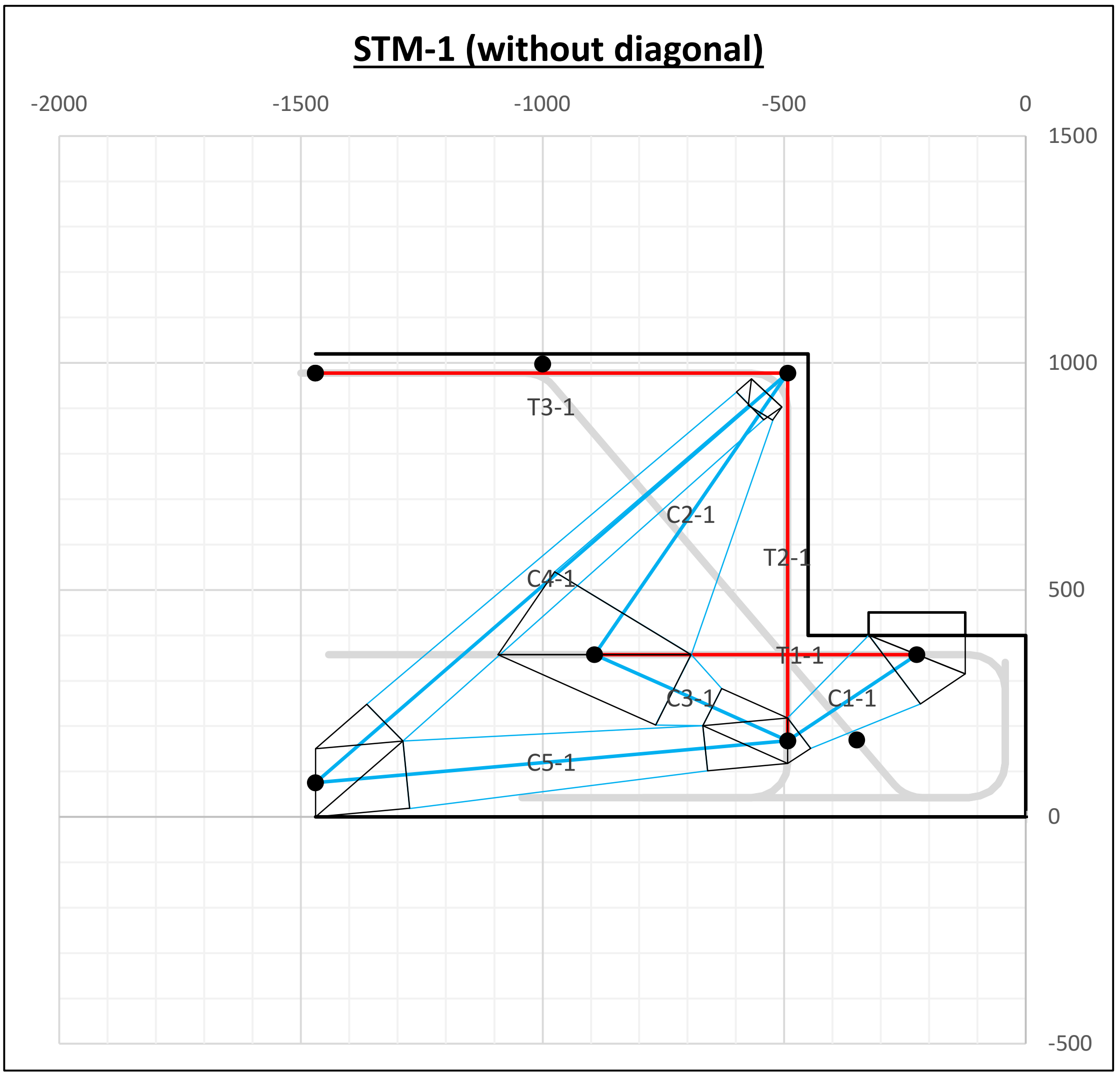

2.3 STM-2 (with diagonal)

	Node (j)	Node (k)	$F_{unit,STM2}$	Length	Angles	
			[-]	[mm]	[rad]	[°]
C2-2	(2)	(3)	-0,29	737,8	0,9978	57,2
C3-2	(3)	(4)	-0,56	442,8	0,4434	25,4
C4-2	(2)	(5)	0,10	1330,4	0,7455	42,7
C5-2	(4)	(5)	-0,93	981,9	0,0943	5,4
C6-2	(1)	(7)	-1,20	225,6	0,9851	56,4
C7-2	(7)	(4)	-1,43	142,8	0,0139	0,8
C8-2	(8)	(5)	-1,10	1035,3	1,0996	63,0
T1-2	(1)	(3)	0,66	667,5	0	0,0
T2-2	(2)	(4)	0,17	810,0	1,5708	90,0
T3-2	(2)	(6)	0,08	977,5	0	0,0
T4-2	(7)	(8)	1,25	1052,8	0,9051	51,9
T5-2	(8)	(9)	1,27	470,4	0	0,0

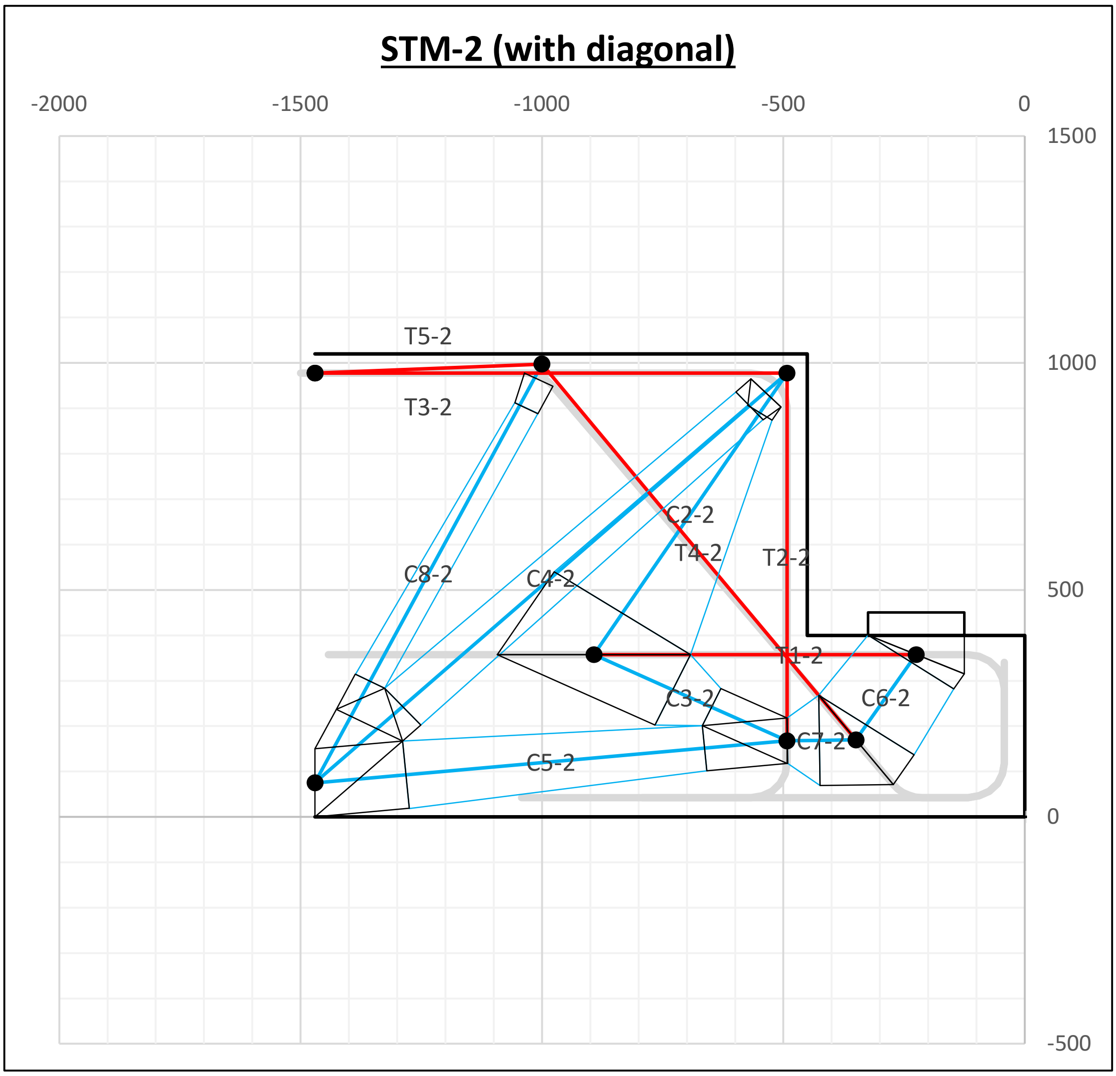

2.4 STM-3 (Combined)

	Node (j)	Node (k)	$F_{unit,STM1}$	$F_{unit,STM2}$	F_{unit}	Length	Angles	
			0,4	0,6	[-]	[mm]	[rad]	[°]
C1	(1)	(4)	-1,73		-0,69	328,1	0,6176	35,4
C2	(2)	(3)	-0,61	-0,29	-0,42	737,8	0,9978	57,2
C3	(3)	(4)	-1,19	-0,56	-0,81	442,8	0,4434	25,4
C4	(2)	(5)	-1,43	0,10	-0,51	1330,4	0,7455	42,7
C5	(4)	(5)	-0,33	-0,93	-0,69	981,9	0,0943	5,4
C6	(1)	(7)		-1,20	-0,72	225,6	0,9851	56,4
C7	(7)	(4)		-1,43	-0,86	142,8	0,0139	0,8
C8	(8)	(5)		-1,10	-0,66	1035,3	1,0996	63,0
T1	(1)	(3)	1,41	0,66	0,96	667,5	0	0
T2	(2)	(4)	1,48	0,17	0,70	810,0	1,5708	90,0
T3	(2)	(6)	1,38	0,08	0,60	977,5	0	0
T4	(7)	(8)		1,25	0,75	1052,8	0,9051	51,9
T5	(8)	(6)		1,27	0,76	470,4	0	0

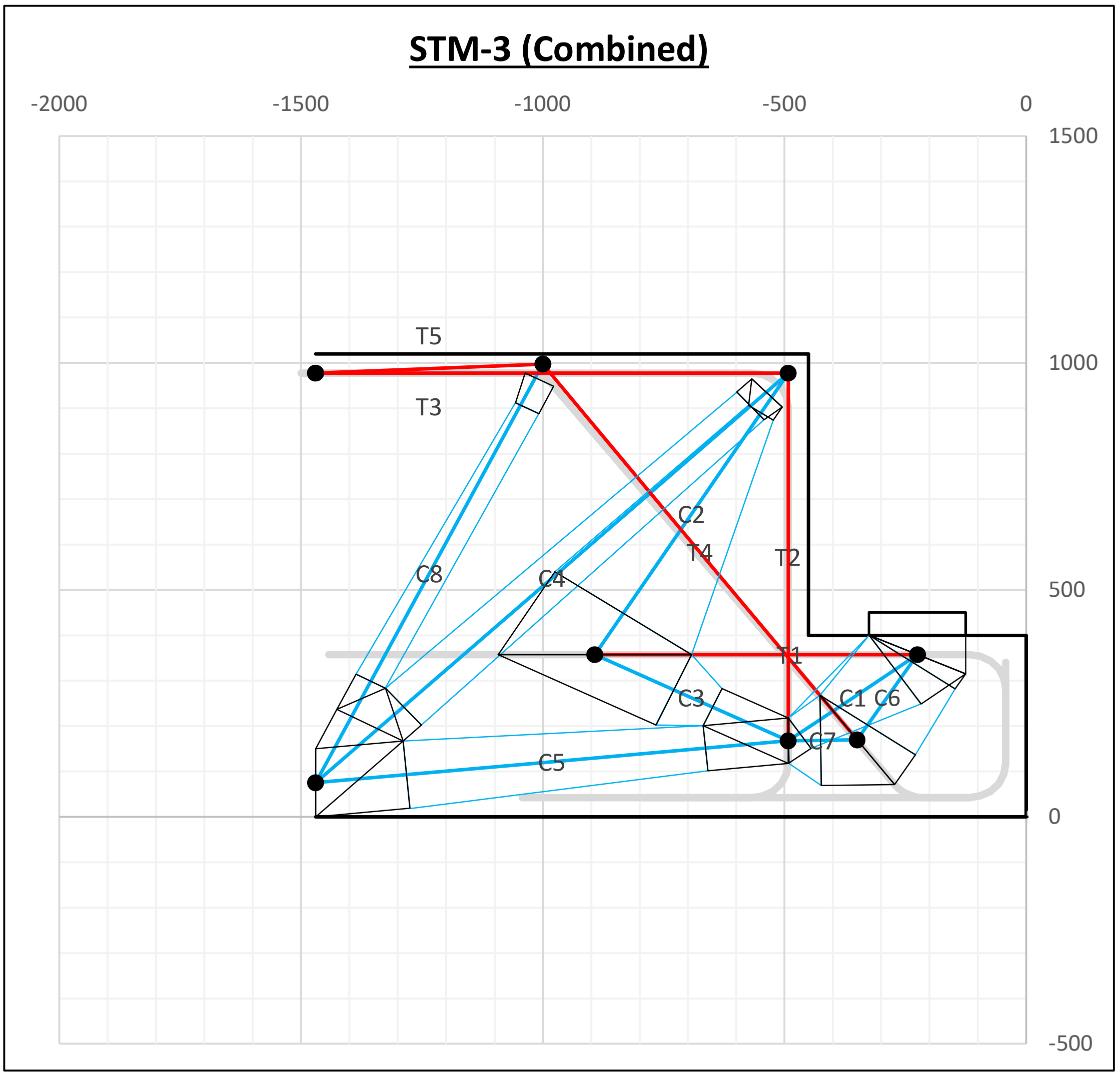

2.5 Node dimensions

Node (1)	T1	F	C1	C6		CCT
$a_{(1)}$	-	217,3	217,3	217,3		[mm]
$w_{(1)}$	-	200,0	185,1	213,7		[mm]
$b_{(1)}$	-	85,0	113,8	39,7		[mm]

Node (2)	T2	T3	C2	C4		CTT
$a_{(2)}$	-	-	88,4	88,4		[mm]
$w_{(2)}$	-	-	60,3	83,4		[mm]
$b_{(2)}$	-	-	-	-		[mm]

Node (3)	T1	C2	C3			CCT
$a_{(3)}$	-	400,0	400,0			[mm]
$w_{(3)}$	-	336,1	171,6			[mm]
$b_{(3)}$	-	216,9	361,3			[mm]

Node (4)	T2	C1	C3	C5	C7	CCT
$a_{(4)}$	-	100,0	176,3	194,4	100,0	[mm]
$w_{(4)}$	-	81,5	90,3	99,6	100,0	[mm]
$b_{(4)}$	-	57,9	151,4	166,9	1,4	[mm]

Node (5)	C4	C5	C8	Internal		CCC
$a_{(5)}$	121,8	246,4	110,3	181,8		[mm]
$w_{(5)}$	110,2	149,3	68,1	153,5		[mm]
$b_{(5)}$	51,8	196,0	86,8	97,4		[mm]

Node (7)	T4	C6	C7			CCT
$a_{(7)}$	-	250,0	250,0			[mm]
$w_{(7)}$	-	237,4	198,7			[mm]
$b_{(7)}$	-	78,5	151,7			[mm]

Node (8)	T4	T5	C8			CTT
$a_{(8)}$	-	-	-			[mm]
$w_{(8)}$	-	-	53,6			[mm]
$b_{(8)}$	-	-	-			[mm]

2,6 Checks

2.6.1 Compressive strength of struts

Strut i	C1	C2	C3	C4	C5	C6	C7	C8	
$F_{unit,i}$	-0,691	-0,416	-0,815	-0,511	-0,690	-0,720	-0,860	-0,660	[-]
Tension	Yes	Yes	Yes	Yes	Yes	Yes	Yes	Yes	
$\sigma_{Rd,max,c}$	12,04	12,04	12,04	12,04	12,04	12,04	12,04	12,04	[N/mm^2]
L_c	328,1	737,8	442,8	1330,4	981,9	225,6	142,8	1035,3	[mm]
$w_{c,eff}$	81,5	60,3	90,3	83,4	99,6	213,7	100,0	53,6	[mm]
$C_{max,C,i}$	-981,6	-726,2	-1087,5	-1004,0	-1198,6	-2572,4	-1203,9	-645,7	[kN/m]
$F_{max,C,i}$	1421,0	1746,0	1335,2	1963,1	1736,3	3572,6	1400,0	978,4	[kN/m]

2.6.2 Compressive strength of nodes

Strut	C1	C2	C3	C4	C5	C6	C7	C8	
Node (j)	(1)	(2)	(3)	(2)	(4)	(1)	(7)	(8)	
Type	CCT	CTT	CCT	CTT	CCT	CCT	CCT	CTT	
k	0,85	0,75	0,85	0,75	0,85	0,85	0,85	0,75	[-]
$\sigma_{Rd,max,(j)}$	17,06	15,05	17,06	15,05	17,06	17,06	17,06	15,05	[N/mm^2]
$w_{i(j)}$	185,1	60,3	171,6	83,4	99,6	213,7	198,7	53,6	[mm]
$C_{max,i(j)}$	-3157,4	-907,7	-2927,3	-1255,0	-1698,1	-3644,2	-3389,9	-807,1	[kN/m]
$F_{max,i(j)}$	4570,9	2182,5	3594,0	2453,9	2459,7	5061,2	3942,0	1223,0	[kN/m]
Node (k)	(4)	(3)	(4)	(5)	(5)	(7)	(4)	(5)	
Type	CCT	CCT	CCT	CCC	CCC	CCT	CCT	CCC	
k	0,85	0,85	0,85	1,00	1,00	0,85	0,85	1,00	[-]
$\sigma_{Rd,max,(k)}$	17,06	17,06	17,06	20,07	20,07	17,06	17,06	20,07	[N/mm^2]
$w_{i(k)}$	81,5	336,1	90,3	110,2	149,3	237,4	100,0	68,1	[mm]
$C_{max,i(k)}$	-1390,6	-5733,1	-1540,7	-2211,5	-2996,6	-4048,6	-1705,5	-1366,4	[kN/m]
$F_{max,i(k)}$	2013,1	13785,1	1891,6	4324,4	4340,7	5622,9	1983,3	2070,4	[kN/m]

2.6.3 Compressive strength of internal nodes

Node (j/k)	(1)	(2)	(4)	(5)	
Strut i_1	C1	C2	C1	C4	
$F_{unit,i,1}$	-0,588	-0,407	-0,563	-0,376	[-]
Strut i_2	C6	C4	C7	C5	
$F_{unit,i,2}$	-0,708	-0,511	-0,860	-0,687	[-]
Strut i_3	-		-	C8	
$F_{unit,i,3}$				-0,300	[-]
F_{unit}	-1,296	-0,918	-1,423	-1,363	[-]
Type	CCT	CTT	CCT	CCC	
k	0,85	0,75	0,85	1,00	[-]
$\sigma_{Rd,max}$	17,06	15,05	17,06	20,07	[N/mm^2]
w	217,3	60,3	100,0	150,0	[mm]
C_{max}	-3706,6	-907,7	-1705,7	-3010,0	[kN/m]
F_{max}	2859,4	989,3	1198,6	2209,0	[kN/m]

2.6.4 *Yield strength of ties*

Ties	T1	T2	T3	T4	T5		
$F_{unit,i}$	0,961	0,696	0,601	0,748	0,761	[-]	
Rebar	1	2	2	3	3	[-]	
Ø	25	25	35	25	35	[mm]	(add top rebar)
Corrosion	0%	0%	0%	0%	-	[-]	(at re-entrant corner)
f_{yd}	330	330	330	330	330	[N/mm^2]	
$T_{max,T,ind,i}$	162,0	162,0	317,5	162,0	317,5	[kN]	
$T_{max,T,i}$	1079,9	1079,9	2116,6	1079,9	2116,6	[kN/m]	
$F_{max,T,i}$	1123,5	1550,8	3520,7	1444,3	2779,9	[kN/m]	

2.6.5 *Anchorage length of ties*

Lower-bound load 978,4 [kN/m] Failure mechanism: C8 (strut)

Ties	T1	T2	T3	T4	T5	
F_T	940,4	681,3	588,2	731,6	745,0	[kN/m]
$F_{T,ind}$	141,1	102,2	88,2	109,7	111,7	[kN]
f_{bd}	3,37	3,37	3,37	3,37	3,37	[N/mm^2]
σ_{sd}	287,4	208,2	91,7	223,5	116,1	[N/mm^2]
$l_{b,rqd,max}$	532,9	386,1	238,1	414,5	301,5	[mm]
Node (j)	(1)	(2)	(2)	(7)	(8)	
c_d	75,0	-	-	75,0	-	[mm]
p	4,89	-	-	2,68	-	[N/mm^2]
α_1	1,0	-	-	1,0	-	[-]
α_2	1,0	-	-	1,0	-	[-]
α_3	1,0	-	-	1,0	-	[-]
α_4	1,0	-	-	1,0	-	[-]
α_5	0,80	-	-	0,89	-	[-]
$l_{b,min}$	250,0	-	-	250,0	-	[mm]
l_{bd}	428,6	-	-	370,2	-	[mm]
$l_{b,prov}$	1533,1	-	-	754,2	-	[mm]
Check	Correct	-	-	Correct	-	
Node (k)	(3)	(4)	(6)	(8)	(6)	
c_d	75,0	75,0	-	-	-	[mm]
p	0,31	13,92	-	-	-	[N/mm^2]
α_1	1,0	1,0	-	-	-	[-]
α_2	1,0	1,0	-	-	-	[-]
α_3	1,0	1,0	-	-	-	[-]
α_4	1,0	1,0	-	-	-	[-]
α_5	0,99	0,70	-	-	-	[-]
$l_{b,min}$	250,0	250,0	-	-	-	[mm]
l_{bd}	526,3	270,3	-	-	-	[mm]
$l_{b,prov}$	750,0	442,8	-	-	-	[mm]
Check	Correct	Correct	-	-	-	

3. Kinematic approach (upper-bound approximation)

x_min	99,8	[mm]
Δx	0	[mm]

θ_{Crack}	30,0	[°]
l_{crack}	600,4	[mm]

	$A_{s,i}$	A_s	f_{yd}	N_S / N_C	Leverarm	Moment	$N_{y\text{-}dir}$
	[mm^2]	[mm^2]	[N/mm^2]	[kN/m]	[mm]	[kNm/m]	[kN/m]
Rebar 1	491	3272	330	1079,9	257,7	278,3	0,0
Rebar 2	491	3272	330	1079,9	477,4	515,6	1079,9
Rebar 3	491	3272	330	1079,9	536,2	579,0	849,3
Concrete	-	-	-	1746,9	60,9	106,4	0,0
Total						1479,3	1929,2

Support		
Leverarm:	744,9	[mm]
Upper-bound load:	1985,8	[kN/m]

Vertical equilibrium	Correct	
Difference in vertical force	56,6	[kN/m]
Concrete shear resistance	58,5	[kN/m]

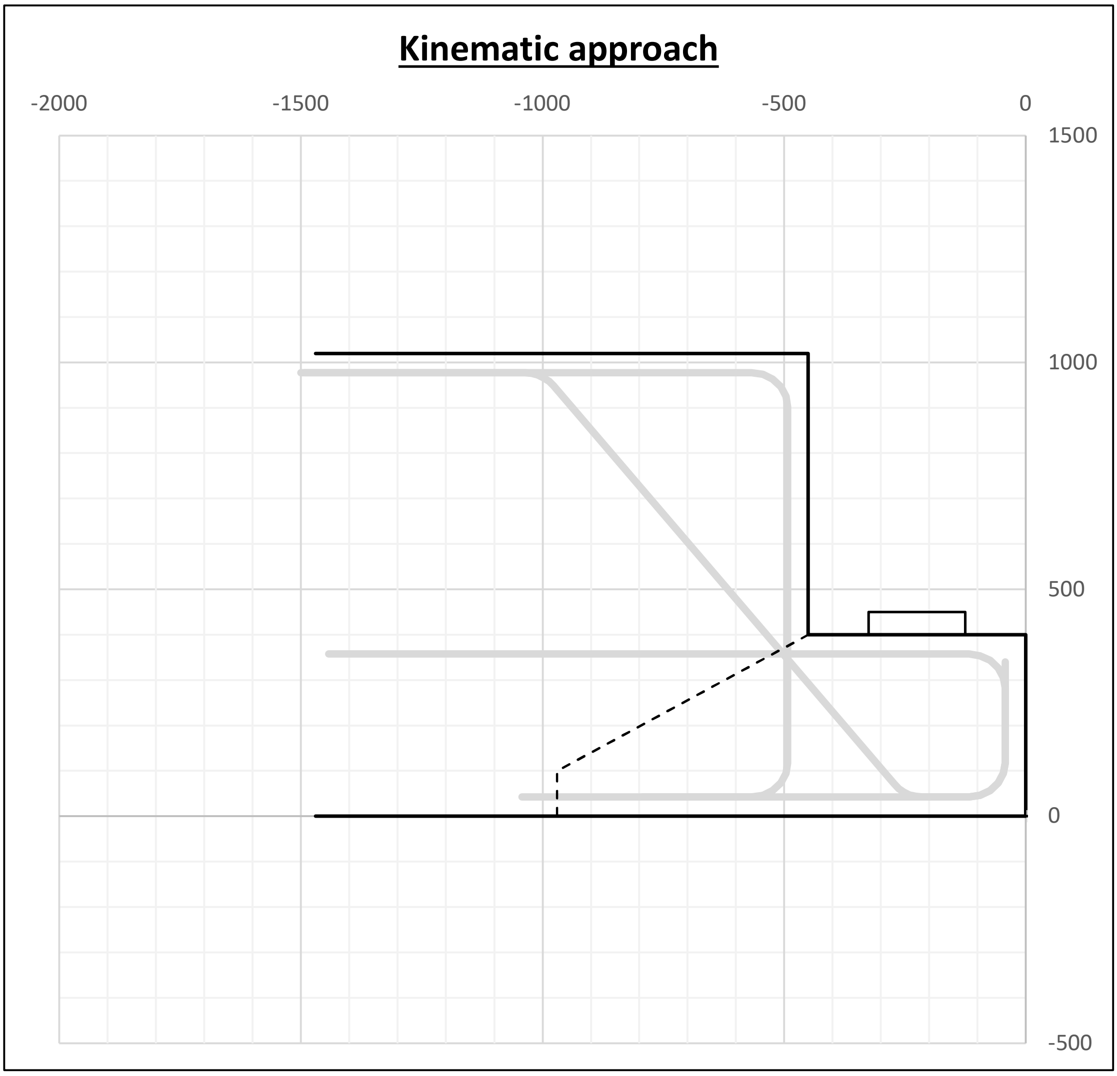

4. Optimisation

4.1 Strut-and-tie approach (Highest lower-bound approximation)

	Stepsize	Max. shift	Steps
Load	0,1	-	10
Node 3	50	600,0	12
Node 4	25	100,0	4
Node 5	25	100,0	4
Node 7	25	150,0	6

min θ 25,0 [°]

Anchorage:	Correct	
Angle (theta):	Correct	
Lower-bound load	978,4	[kN/m]

Limitations on angles				
	Minimum	Maximum	[°]	
θC1	25,0	65,0	35,4	Correct
θC2	25,0	65,0	57,2	Correct
θC3	25,0	65,0	25,4	Correct
θC4	25,0	65,0	42,7	Correct
θC6	25,0	-	56,4	Correct
θC7	-	65,0	0,8	Correct
θC8	25,0	-	63,0	Correct
θC6+θT4	-	155,0	108,3	Correct
θT4-θC7	25,0	-	51,1	Correct
θC8+θT4	25,0	-	114,9	Correct

Governing lower-bound load: 978,4 [kN/m] Failure mechanism: C8 (strut)

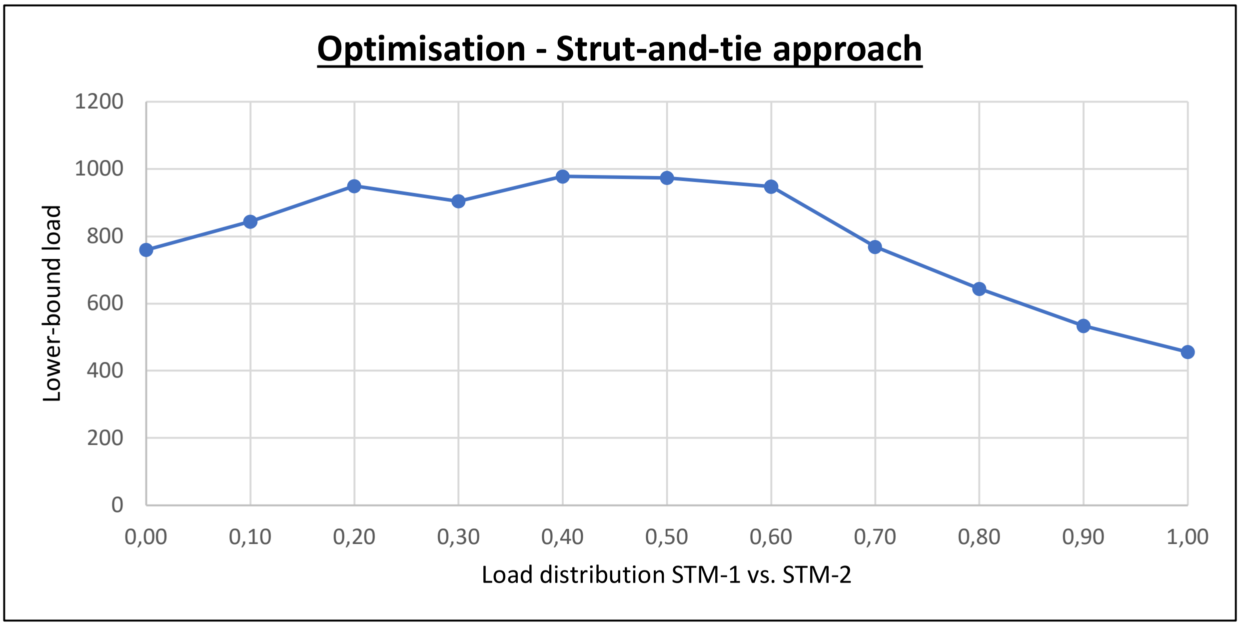

Load distribution		Offset				Load		Limitations	
STM-1	STM-2	Node 3	Node 4	Node 5	Node 7	[kN]	Mechan.	Anchor.	Angle
0,000	1,000	550	50	75	150	759,7	C8 (strut)	Correct	Correct
0,100	0,900	550	50	75	150	844,1	C8 (strut)	Correct	Correct
0,200	0,800	550	50	75	150	949,6	C8 (strut)	Correct	Correct
0,300	0,700	550	50	50	150	904,1	C8 (strut)	Correct	Correct
0,400	0,600	550	50	75	125	978,4	C8 (strut)	Correct	Correct
0,500	0,500	550	50	75	100	973,8	(2) Inner	Correct	Correct
0,600	0,400	550	50	75	50	947,4	C1 (strut)	Correct	Correct
0,700	0,300	550	50	50	50	768,8	(2) Inner	Correct	Correct
0,800	0,200	550	50	50	25	643,6	(2) Inner	Correct	Correct
0,900	0,100	550	50	50	25	533,9	(2) Inner	Correct	Correct
1,000	0,000	550	50	50	25	456,1	(2) Inner	Correct	Correct

4,2 Kinematic approach (Lowest upper-bound approximation)

$\theta_{C,min}$	30,0	[°]
$\theta_{C,max}$	70,0	[°]

θ_{Crack}		30,0	36,7	43,3	50,0	56,7	63,3	70,0	[°]
Rebar 1	Leverarm	257,7	257,7	237,7	225,7	212,7	197,7	184,7	[mm]
	Moment	278,3	278,3	256,7	243,7	229,7	213,5	199,4	[kNm/m]
Rebar 2	Leverarm	477,4	360,7	254,5	182,5	125,3	78,1	40,2	[mm]
	Moment	515,6	389,5	274,8	197,1	135,3	84,4	43,4	[kNm/m]
Rebar 3	Leverarm	536,2	439,1	344,5	285,2	238,4	198,6	167,0	[mm]
	Moment	579,0	474,2	372,0	308,0	257,5	214,4	180,3	[kNm/m]
Concrete	Leverarm	60,9	60,9	79,9	87,9	96,5	106,5	115,2	[mm]
	Moment	106,4	106,4	139,5	153,5	168,7	186,1	201,3	[kNm/m]
ΔX		0,0	0,0	20,0	32,0	45,0	60,0	73,0	[mm]
Total moment		1479,3	1248,4	1043,1	902,3	791,2	698,4	624,4	[kNm/m]
Leverarm support		744,9	628,2	522,0	450,0	392,8	345,6	307,7	[mm]
Load support		1985,8	1987,3	1998,3	2005,0	2014,0	2020,8	2029,4	[kN/m]

Governing upper-bound load: 1985,8 [kN/m]

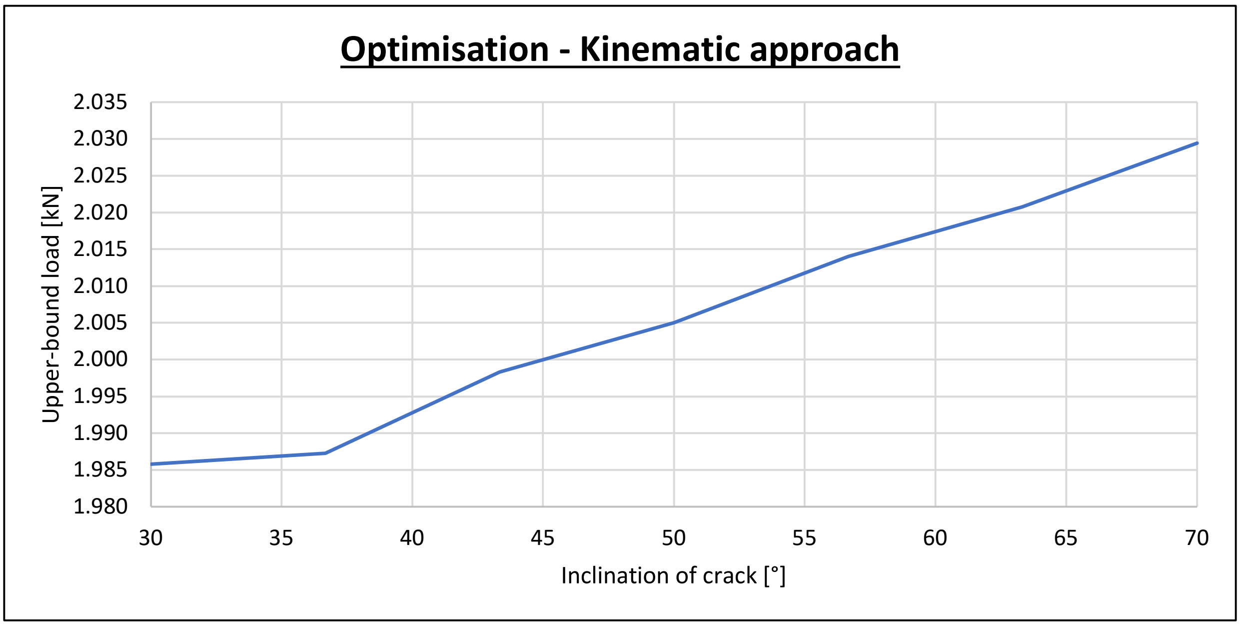

5. Corrosion

	Stepsize	Max
Corrosion	10%	60%

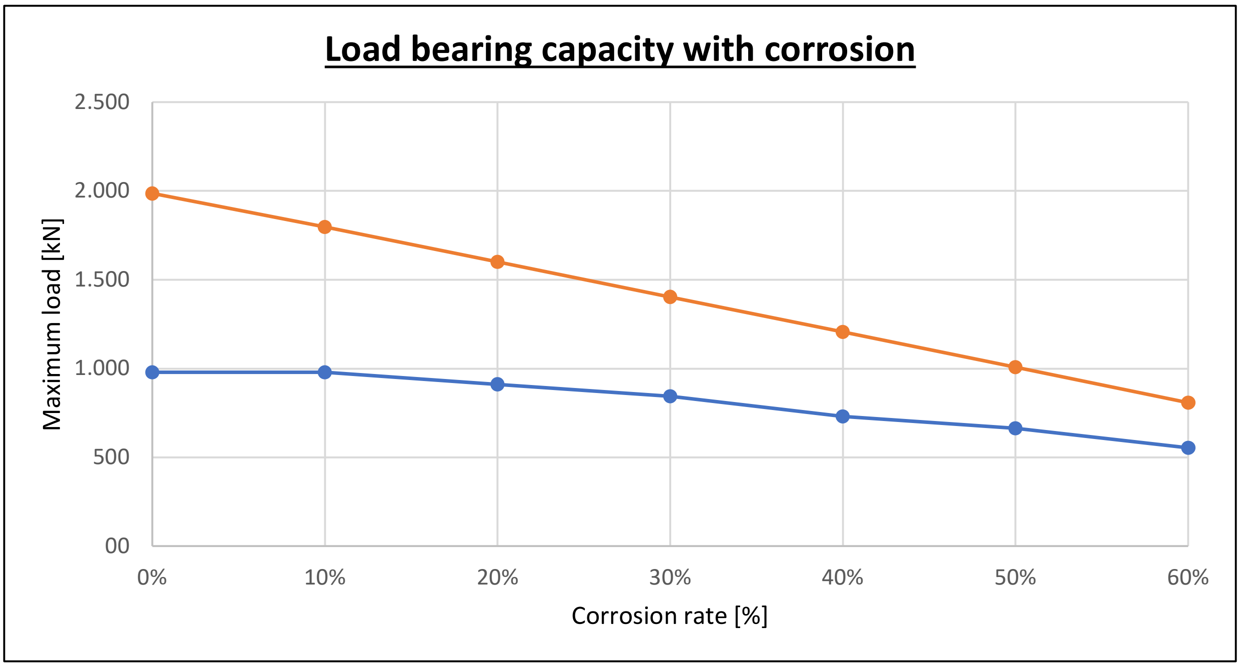

Maximum load	Corrosion							
	0%	10%	20%	30%	40%	50%	60%	
Lower-bound load	978,4	978,4	911,7	844,1	731,8	663,8	554,1	[kN/m]
Failure mechanism	C8 (strut)	C8 (strut)	T1	C8 (strut)	T4	T1	T1	
Upper-bound load	1985,8	1796,8	1600,3	1403,3	1205,8	1007,5	808,4	[kN/m]

C.6 Category A1 for numerical analysis

Analytical parametric tool for load bearing capacity of RC half-joints

Project
Numerical

1. Geometry and material properties

1.1 Concrete

1.1.1 *Geometry*

a	375	[mm]
b	325	[mm]
c	130	[mm]
d	130	[mm]

Width	1000	[mm]
Cover	30	[mm]
Support	150	[mm]
α	0	[°]

1.1.2 *Material*

γ_c	1,5	[-]
k_t	1	[-]

α_{cc}	1	[-]
α_{ct}	1	[-]

f_{ck}	53,0	[N/mm^2]
f_{cm}	53,0	[N/mm^2]
f_{cd}	53,0	[N/mm^2]
v'	0,788	[-]

f_{ctm}	3,90	[N/mm^2]
$f_{ctk,0.05}$	3,90	[N/mm^2]
f_{ctd}	3,90	[N/mm^2]
Mean values?		Yes

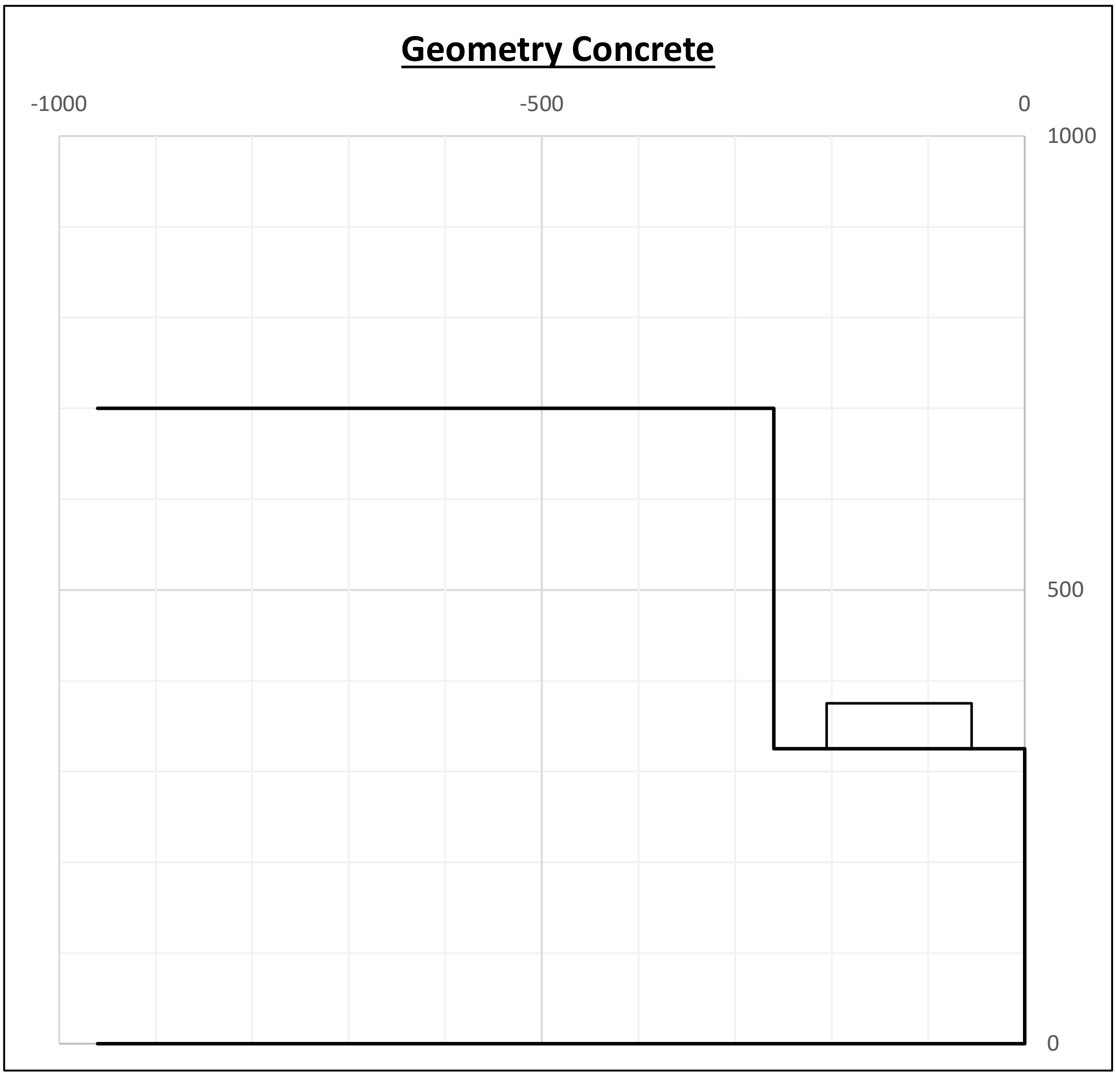

1.2 Reinforcement steel

1.2.1 Geometry

	Rebar 1	Rebar 2	Rebar 3	
Ø	12	12	8	[mm]
$Ø_m$	60	60	60	[mm]
Spacing	120	120	120	[mm]
η_1	1	1	1	[-]
η_2	1	1	1	[-]
η_3	1	1	1	[-]
l_{top}	800	600	-	[mm]
l_{bottom}	800	500	-	[mm]
Δ_{top}	0	0	-	[mm]
Δ_{middle}	0	0	-	[mm]
Δ_{bottom}	0	0	-	[mm]
Corrosion	0%	0%	0%	[-]

Include Rebar 3?	No

Coordinates Rebar 3		
x	y	
-896	664	[1]
-527	664	[2]
-165	36	[3]
-36	36	[4]
-36	289	[5]
		[6]

ϕ		[rad]
		[°]

1.2.2 Material

$f_{yd,0}$	400	[N/mm^2]
f_{yd}	400	[N/mm^2]

$\alpha_{corr,y}$	0	[-]

1,23

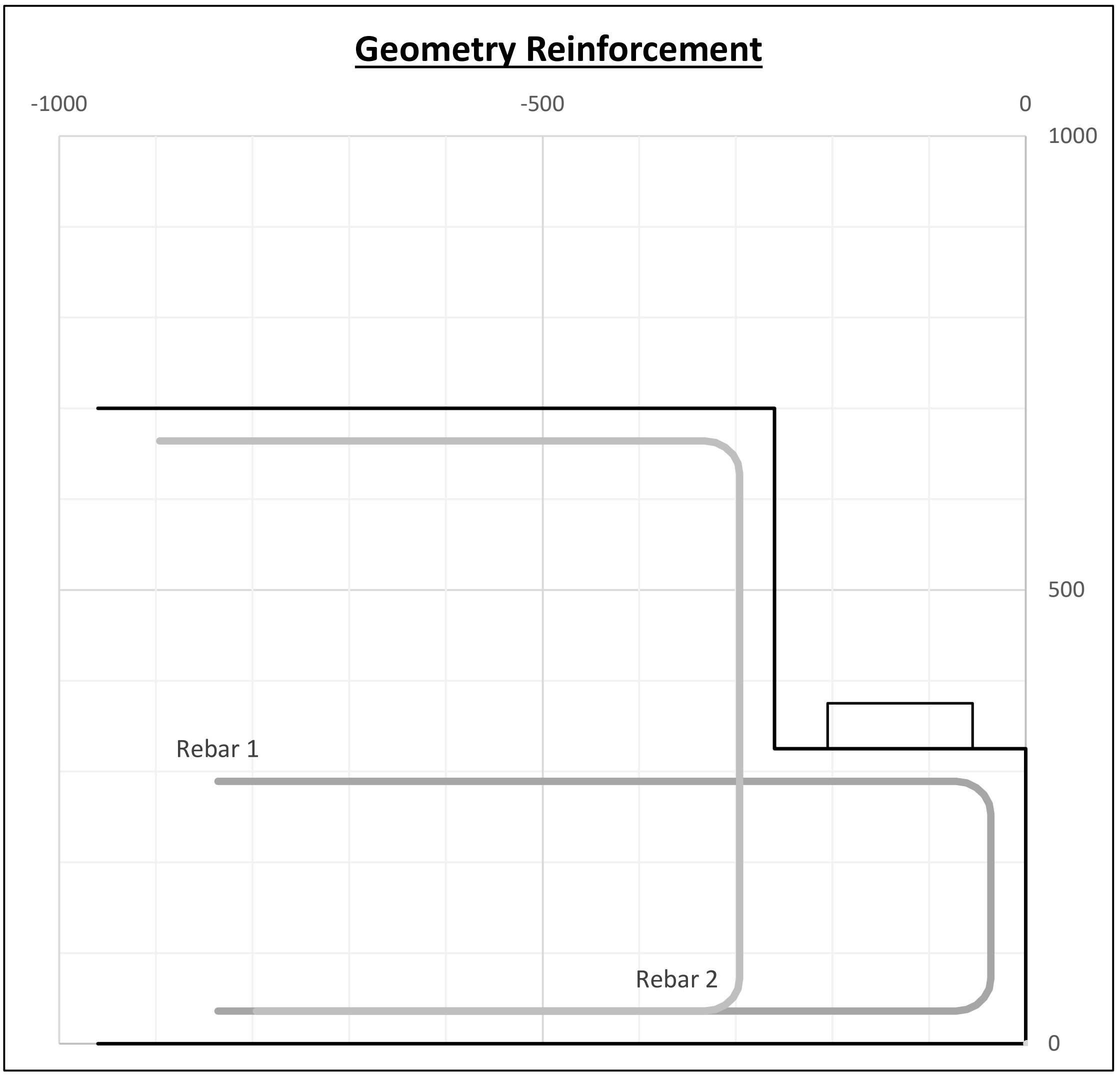

1.3 Pre-stressed steel

1.3.1 Geometry

A_p		[mm^2]
y_p		[mm]
Bearing		[mm]
Spacing		[mm]

Include prestress?	No

1.3.2 Material

σ_{pm}		[N/mm^2]
P_m		[kN]

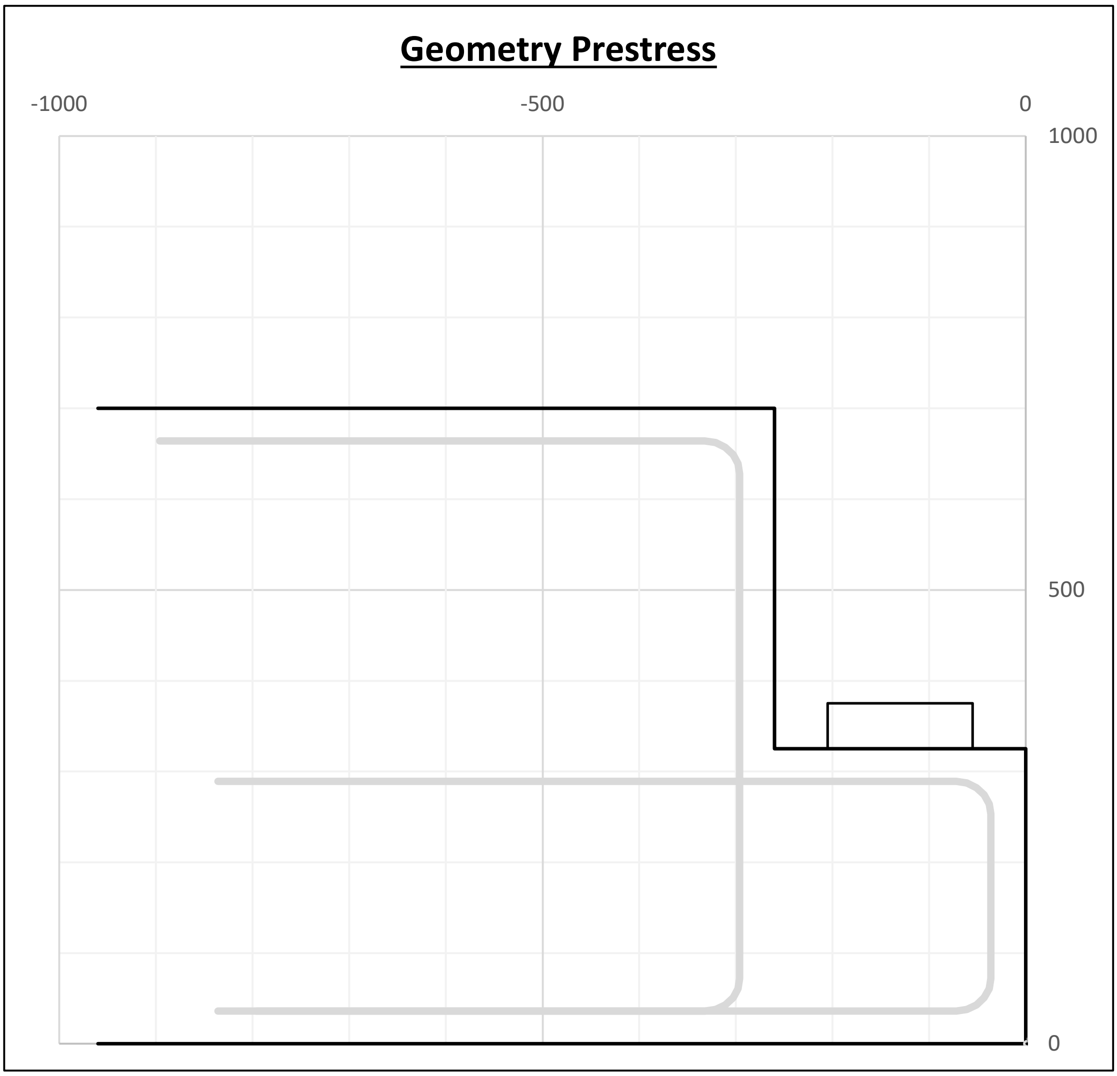

2. Strut-and-tie modelling

2.1 Nodes

	Offset		Coordinates		Type
	x	y	x	y	
(1)	-	-	-130,0	289,0	CCT
(2)	-	0	-296,0	664,0	CTT
(3)	110	-	-726,0	289,0	CCT
(4)	-	15	-296,0	87,0	CCT
(5)	-	15	-960,0	15,0	CCC
(6)	-		-960,0	664,0	-
(7)	5				CCT
(8)	-	-			CTT
(9)	-	-			-

F_{unit}	1,00	[-]

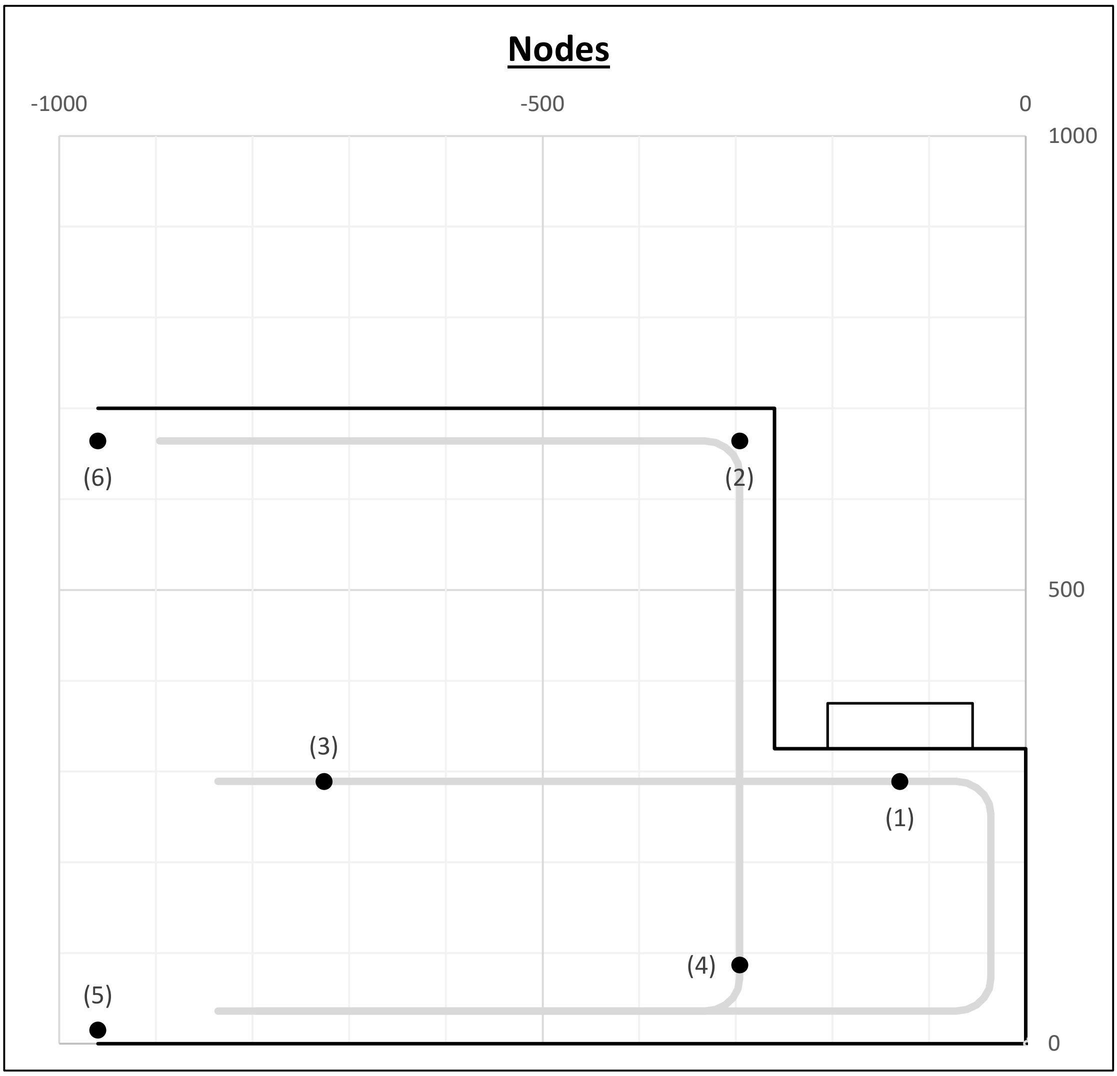

2.2 STM-1 (without diagonal)

	Node (j)	Node (k)	$F_{unit,STM1}$	Length	Angles	
			[-]	[mm]	[rad]	[°]
C1-1	(1)	(4)	-1,29	261,5	0,8829	50,6
C2-1	(2)	(3)	-0,38	570,5	0,7172	41,1
C3-1	(3)	(4)	-0,59	475,1	0,4392	25,2
C4-1	(2)	(5)	-1,39	928,5	0,7740	44,3
C5-1	(4)	(5)	-0,29	667,9	0,1080	6,2
T1-1	(1)	(3)	0,82	596,0	0	0,0
T2-1	(2)	(4)	1,22	577,0	1,5708	90,0
T3-1	(2)	(6)	1,28	664,0	0	0,0

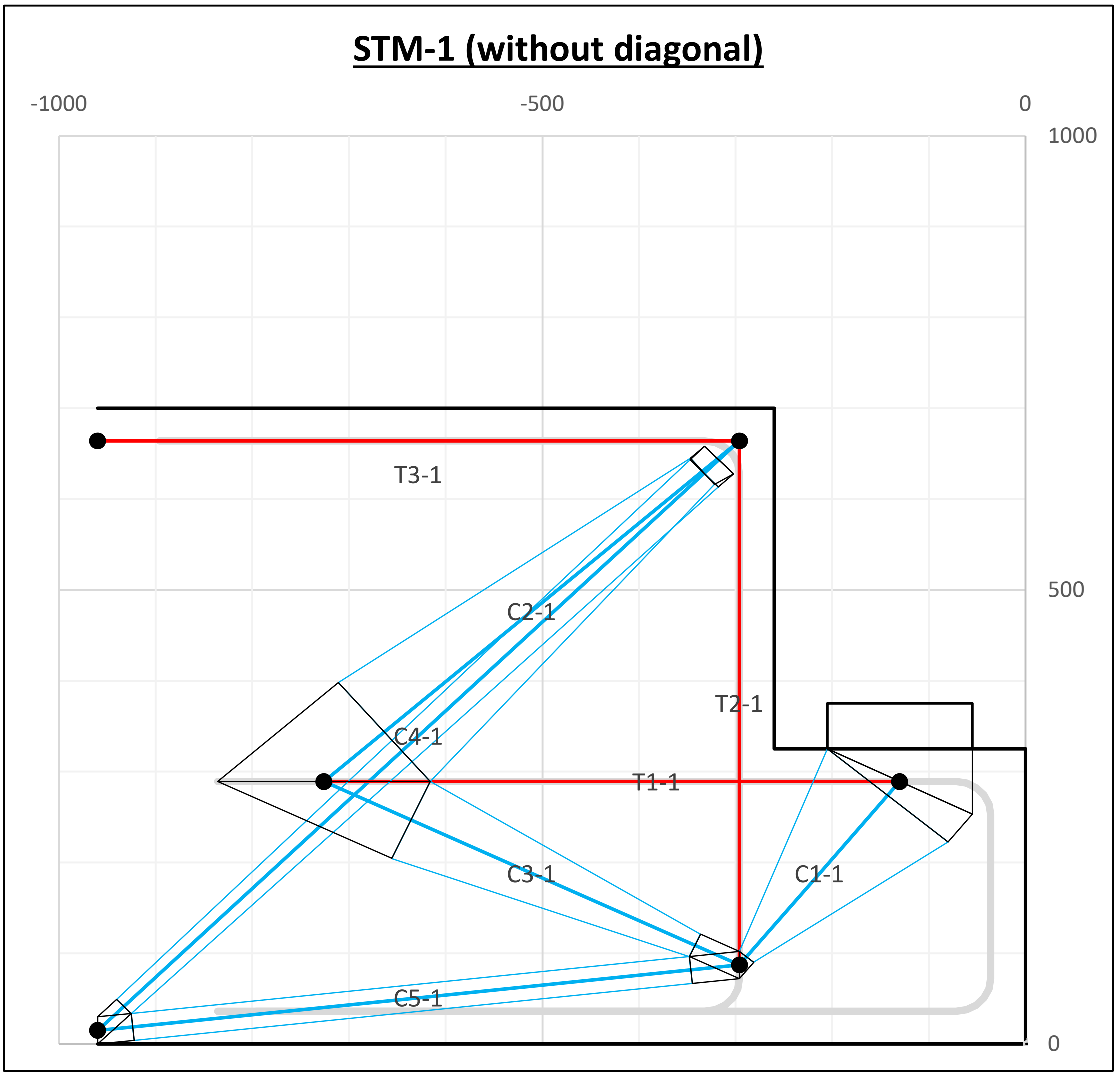

2.5 Node dimensions

Node (1)	T1	F	C1			CCT
$a_{(1)}$	-	166,4	166,4			[mm]
$w_{(1)}$	-	150,0	161,6			[mm]
$b_{(1)}$	-	72,0	39,6			[mm]

Node (2)	T2	T3	C2	C4		CTT
$a_{(2)}$	-	-	42,4	42,4		[mm]
$w_{(2)}$	-	-	38,3	41,7		[mm]
$b_{(2)}$	-	-	-	-		[mm]

Node (3)	T1	C2	C3			CCT
$a_{(3)}$	-	220,0	220,0			[mm]
$w_{(3)}$	-	144,6	93,5			[mm]
$b_{(3)}$	-	165,8	199,1			[mm]

Node (4)	T2	C1	C3	C5		CCT
$a_{(4)}$	-	30,0	52,2	57,3		[mm]
$w_{(4)}$	-	19,0	27,2	29,8		[mm]
$b_{(4)}$	-	23,2	44,6	49,0		[mm]

Node (5)	C4	C5				CCC
$a_{(5)}$	34,7	48,3				[mm]
$w_{(5)}$	21,5	29,8				[mm]
$b_{(5)}$	27,3	38,0				[mm]

Node (7)						
$a_{(7)}$						[mm]
$w_{(7)}$						[mm]
$b_{(7)}$						[mm]

Node (8)						
$a_{(8)}$						[mm]
$w_{(8)}$						[mm]
$b_{(8)}$						[mm]

2,6 Checks

2.6.1 Compressive strength of struts

Strut i	C1	C2	C3	C4	C5				
$F_{unit,i}$	-1,294	-0,382	-0,590	-1,386	-0,289				[-]
Tension	Yes	Yes	Yes	Yes	Yes	Yes	Yes	Yes	
$\sigma_{Rd,max,c}$	25,06	25,06	25,06	25,06	25,06				[N/mm^2]
L_c	261,5	570,5	475,1	928,5	667,9				[mm]
$w_{c,eff}$	19,0	38,3	27,2	21,5	29,8				[mm]
$C_{max,C,i}$	-477,3	-959,2	-680,4	-537,6	-747,4				[kN/m]
$F_{max,C,i}$	368,7	2512,8	1153,1	387,9	2582,7				[kN/m]

2.6.2 Compressive strength of nodes

Strut	C1	C2	C3	C4	C5				
Node (j)	(1)	(2)	(3)	(2)	(4)				
Type	CCT	CTT	CCT	CTT	CCT				
k	0,85	0,75	0,85	0,75	0,85				[-]
$\sigma_{Rd,max,(j)}$	35,50	31,32	35,50	31,32	35,50				[N/mm^2]
$w_{i(j)}$	161,6	38,3	93,5	41,7	29,8				[mm]
$C_{max,i(j)}$	-5736,8	-1199,0	-3320,7	-1307,6	-1058,8				[kN/m]
$F_{max,i(j)}$	4432,2	3141,0	5627,5	943,4	3658,8				[kN/m]
Node (k)	(4)	(3)	(4)	(5)	(5)				
Type	CCT	CCT	CCT	CCC	CCC				
k	0,85	0,85	0,85	1,00	1,00				[-]
$\sigma_{Rd,max,(k)}$	35,50	35,50	35,50	41,76	41,76				[N/mm^2]
$w_{i(k)}$	19,0	144,6	27,2	21,5	29,8				[mm]
$C_{max,i(k)}$	-676,2	-5133,1	-963,9	-896,0	-1245,6				[kN/m]
$F_{max,i(k)}$	522,4	13447,0	1633,5	646,5	4304,4				[kN/m]

2.6.3 Compressive strength of internal nodes

Node (j/k)		(2)		(5)	
Strut i_1		C2		C4	
$F_{unit,i,1}$		-0,381		-0,991	[-]
Strut i_2		C4		C5	
$F_{unit,i,2}$		-1,386		-0,288	[-]
Strut i_3					
$F_{unit,i,3}$					[-]
F_{unit}		-1,767		-1,279	[-]
Type		CTT		CCC	
k		0,75		1,00	[-]
$\sigma_{Rd,max}$		31,32		41,76	[N/mm^2]
w		38,3		30,0	[mm]
C_{max}		-1199,0		-1252,9	[kN/m]
F_{max}		678,6		979,7	[kN/m]

2.6.4 Yield strength of ties

Ties	T1	T2	T3				
$F_{unit,i}$	0,822	1,220	1,279			[-]	
Rebar	1	2	2			[-]	
Ø	12	12	22			[mm]	(add top rebar)
Corrosion	0%	0%	0%	-	-	[-]	(at re-entrant corner)
f_{yd}	400	400	400			[N/mm^2]	
$T_{max,T,ind,i}$	45,2	45,2	152,1			[kN]	
$T_{max,T,i}$	377,0	377,0	1267,1			[kN/m]	
$F_{max,T,i}$	458,7	309,1	990,8			[kN/m]	

2.6.5 Anchorage length of ties

Lower-bound load 309,1 [kN/m] Failure mechanism: T2

Ties	T1	T2	T3			
F_T	254,0	377,0	395,3			[kN/m]
$F_{T,ind}$	30,5	45,2	47,4			[kN]
f_{bd}	8,78	8,78	8,78			[N/mm^2]
σ_{sd}	269,5	400,0	124,8			[N/mm^2]
$l_{b,rqd,max}$	92,1	136,7	78,2			[mm]
Node (j)	(1)	(2)	(2)			
c_d	60,0	-	-			[mm]
p	2,06	-	-			[N/mm^2]
α_1	0,7	-	-			[-]
α_2	0,7	-	-			[-]
α_3	1,0	-	-			[-]
α_4	1,0	-	-			[-]
α_5	0,92	-	-			[-]
$l_{b,min}$	120,0	-	-			[mm]
l_{bd}	120,0	-	-			[mm]
$l_{b,prov}$	1191,1	-	-			[mm]
Check	Correct	-	-			
Node (k)	(3)	(4)	(6)			
c_d	60,0	60,0	-			[mm]
p	0,35	8,47	-			[N/mm^2]
α_1	0,7	0,7	-			[-]
α_2	0,7	0,7	-			[-]
α_3	1,0	1,0	-			[-]
α_4	1,0	1,0	-			[-]
α_5	0,99	0,70	-			[-]
$l_{b,min}$	120,0	120,0	-			[mm]
l_{bd}	120,0	120,0	-			[mm]
$l_{b,prov}$	220,0	550,5	-			[mm]
Check	Correct	Correct	-			

3. Kinematic approach (upper-bound approximation)

x_min	9,5	[mm]
Δx	0	[mm]

θ_{Crack}	45,0	[°]
l_{crack}	446,2	[mm]

	$A_{s,i}$	A_s	f_{yd}	N_S / N_C	Leverarm	Moment	$N_{y\text{-}dir}$
	[mm^2]	[mm^2]	[N/mm^2]	[kN/m]	[mm]	[kNm/m]	[kN/m]
Rebar 1	113	942	400	377,0	279,5	105,4	0,0
Rebar 2	113	942	400	377,0	279,5	105,4	377,0
Rebar 3	-	-	-	0,0	0,0	0,0	0,0
Concrete	-	-	-	377,0	5,8	2,2	0,0
Total						212,9	377,0

Support		
Leverarm:	445,5	[mm]
Upper-bound load:	477,9	[kN/m]

Vertical equilibrium	Fail	
Difference in vertical force	101,0	[kN/m]
Concrete shear resistance	6,8	[kN/m]

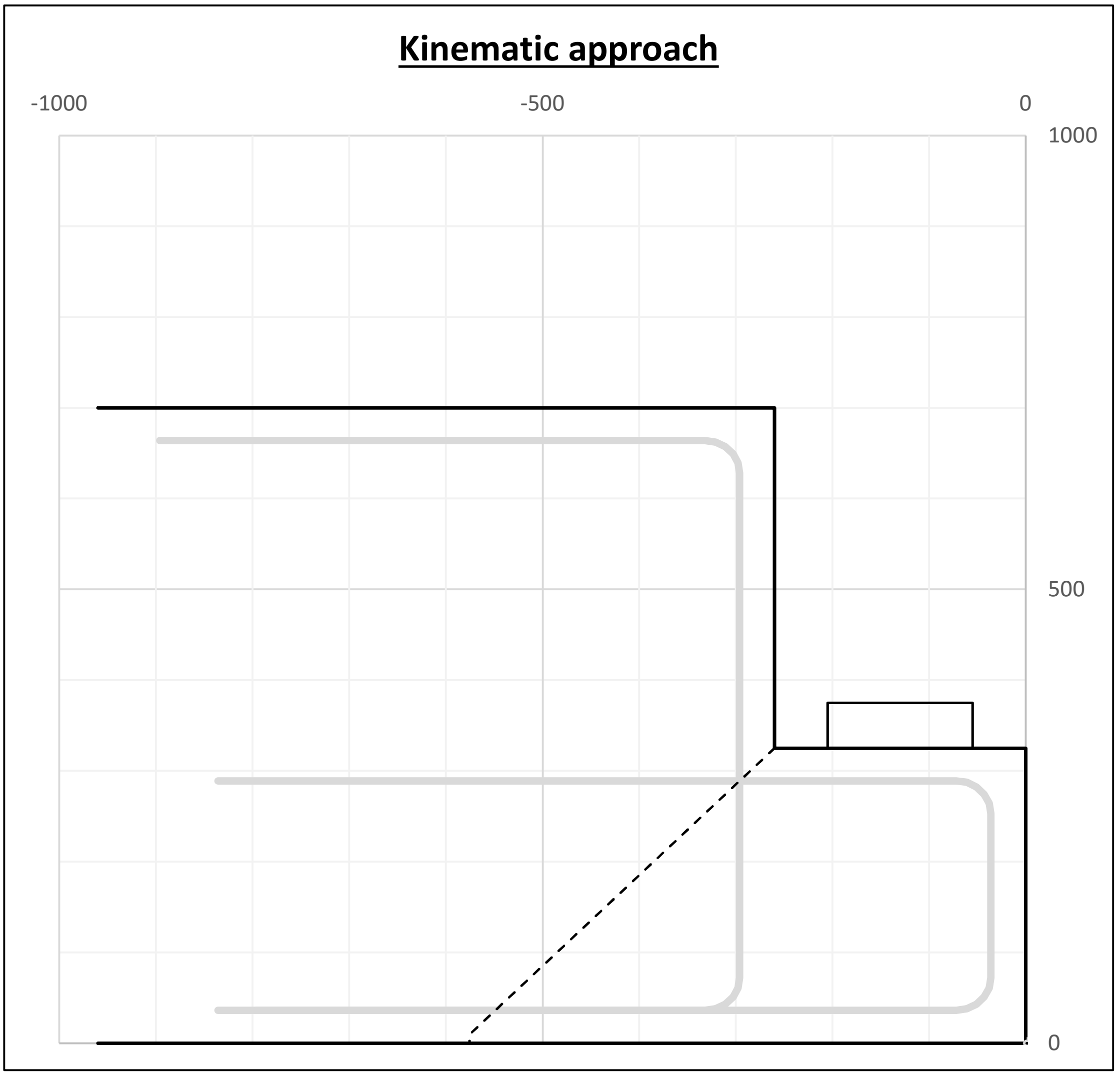

4. Optimisation

4.1 Strut-and-tie approach (Highest lower-bound approximation)

	Stepsize	Max. shift	Steps
Load	0,1	-	10
Node 3	10	150,0	15
Node 4	5	50,0	10
Node 5	5	50,0	10
Node 7	5	50,0	10

Limitations on angles				
	Minimum	Maximum	[°]	
θC1	25,0	65,0	50,6	Correct
θC2	25,0	65,0	41,1	Correct
θC3	25,0	65,0	25,2	Correct
θC4	25,0	65,0	44,3	Correct

min θ 25,0 [°]

Anchorage:	Correct	
Angle (theta):	Correct	
Lower-bound load	309,1	[kN/m]

Governing lower-bound load: 309,1 [kN/m] Failure mechanism: T2

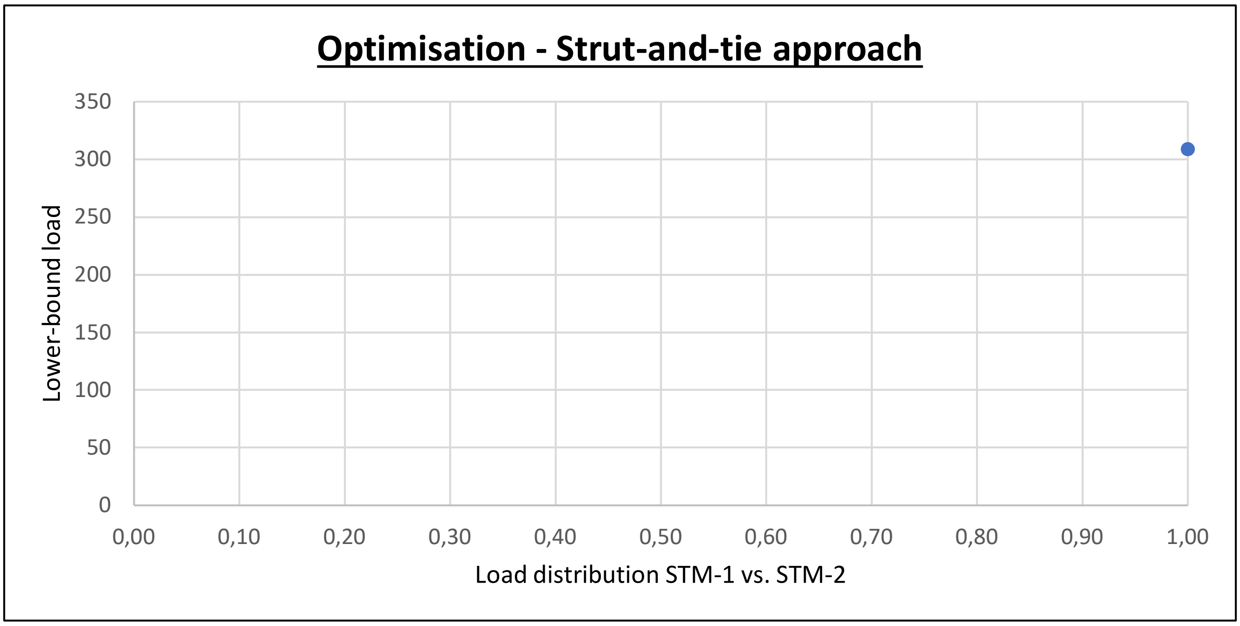

Load distribution		Offset				Load		Limitations	
STM-1	STM-2	Node 3	Node 4	Node 5	Node 7	[kN]	Mechan.	Anchor.	Angle
1,000	0,000	110	15	15	5	309,1	T2	Correct	Correct

4,2 Kinematic approach (Lowest upper-bound approximation)

$\theta_{C,min}$	30,0	[°]
$\theta_{C,max}$	70,0	[°]

θ_{Crack}		30,0	36,7	43,3	50,0	56,7	63,3	70,0	[°]
Rebar 1	Leverarm	197,5	180,5	164,5	148,5	134,5	120,5	108,5	[mm]
	Moment	74,5	68,1	62,0	56,0	50,7	45,4	40,9	[kNm/m]
Rebar 2	Leverarm	368,5	254,8	176,5	118,8	76,2	42,6	16,6	[mm]
	Moment	138,9	96,1	66,6	44,8	28,7	16,1	6,3	[kNm/m]
Rebar 3	Leverarm	0,0	0,0	0,0	0,0	0,0	0,0	0,0	[mm]
	Moment	0,0	0,0	0,0	0,0	0,0	0,0	0,0	[kNm/m]
Concrete	Leverarm	61,0	72,3	83,0	93,7	103,0	112,3	120,3	[mm]
	Moment	23,0	27,3	31,3	35,3	38,8	42,3	45,4	[kNm/m]
ΔX		82,0	99,0	115,0	131,0	145,0	159,0	171,0	[mm]
Total moment		236,4	191,4	159,9	136,1	118,2	103,8	92,5	[kNm/m]
Leverarm support		534,5	420,8	342,5	284,8	242,2	208,6	182,6	[mm]
Load support		442,2	454,8	466,7	477,8	488,3	497,8	506,7	[kN/m]

Governing upper-bound load: 442,2 [kN/m]

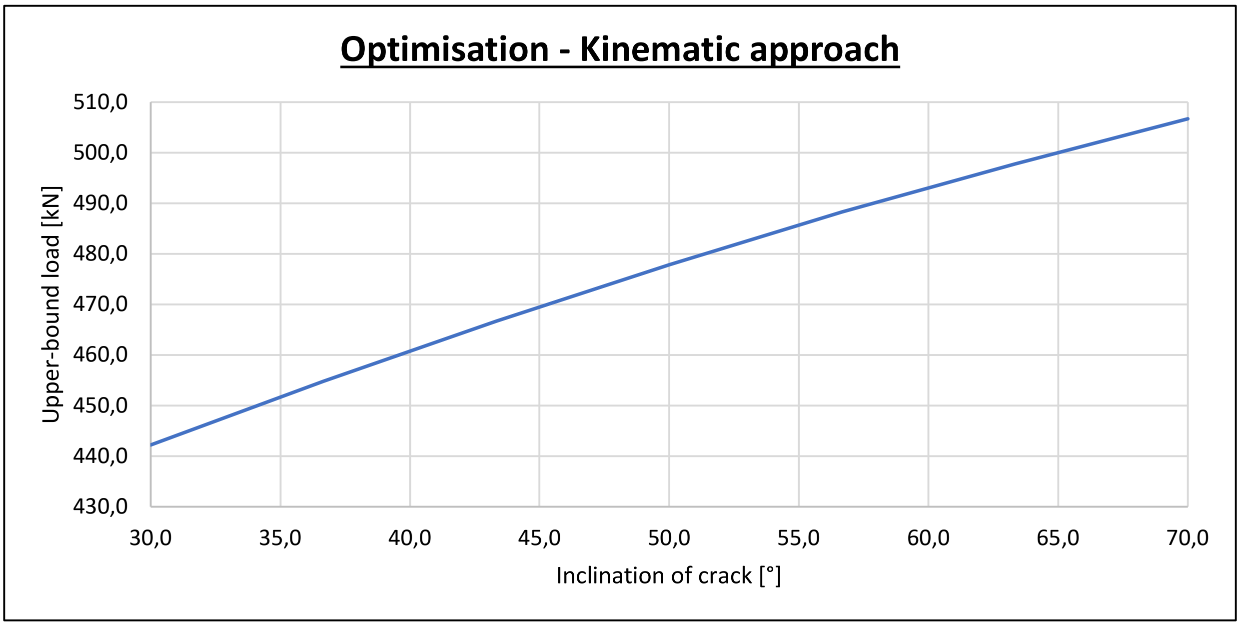

5. Corrosion

	Stepsize	Max
Corrosion	10%	60%

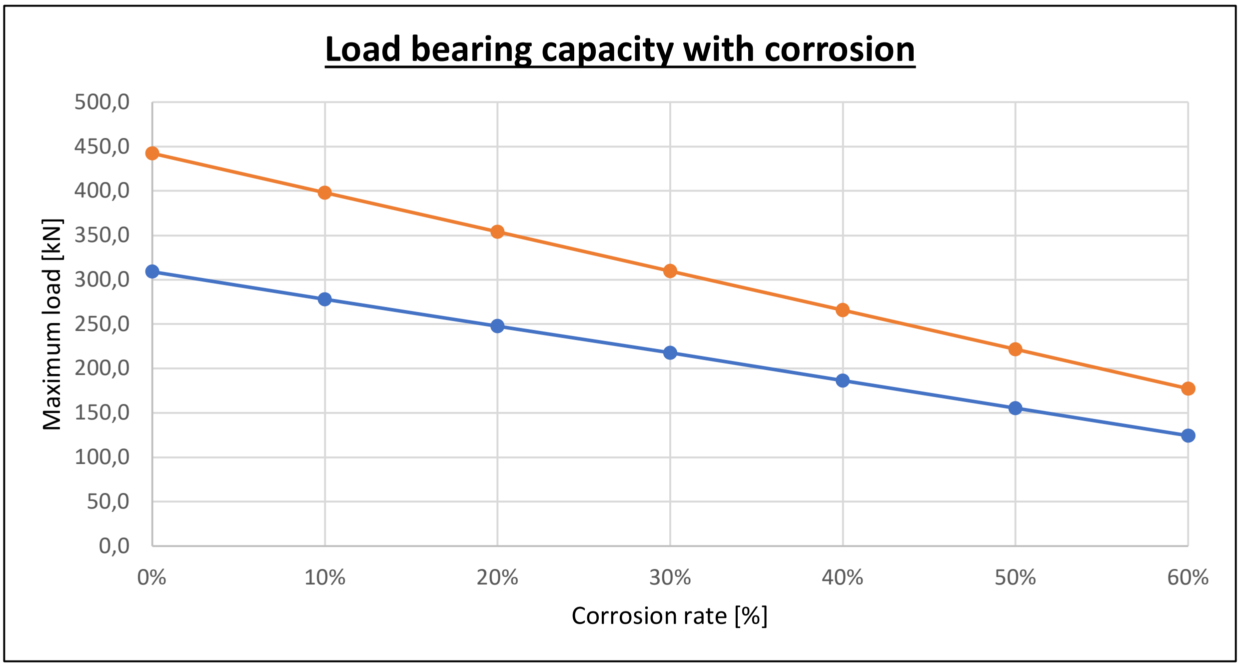

Maximum load	Corrosion							
	0%	10%	20%	30%	40%	50%	60%	
Lower-bound load	309,1	278,2	247,7	217,7	186,6	155,5	124,6	[kN/m]
Failure mechanism	T2	T2	T2	T2	T2	T2	T2	
Upper-bound load	442,2	398,2	354,1	310,0	265,8	221,6	177,3	[kN/m]

C.7 Category A2 for numerical analysis

Analytical parametric tool for load bearing capacity of RC half-joints

Project
Numerical

1. Geometry and material properties

1.1 Concrete

1.1.1 Geometry

a	375	[mm]
b	325	[mm]
c	130	[mm]
d	130	[mm]

Width	1000	[mm]
Cover	30	[mm]
Support	150	[mm]
α	0	[°]

1.1.2 Material

γ_c	1,5	[-]
k_t	1	[-]

α_{cc}	1	[-]
α_{ct}	1	[-]

f_{ck}	53,0	[N/mm^2]
f_{cm}	53,0	[N/mm^2]
f_{cd}	53,0	[N/mm^2]
v'	0,788	[-]

f_{ctm}	3,90	[N/mm^2]
$f_{ctk,0.05}$	3,90	[N/mm^2]
f_{ctd}	3,90	[N/mm^2]
Mean values?		Yes

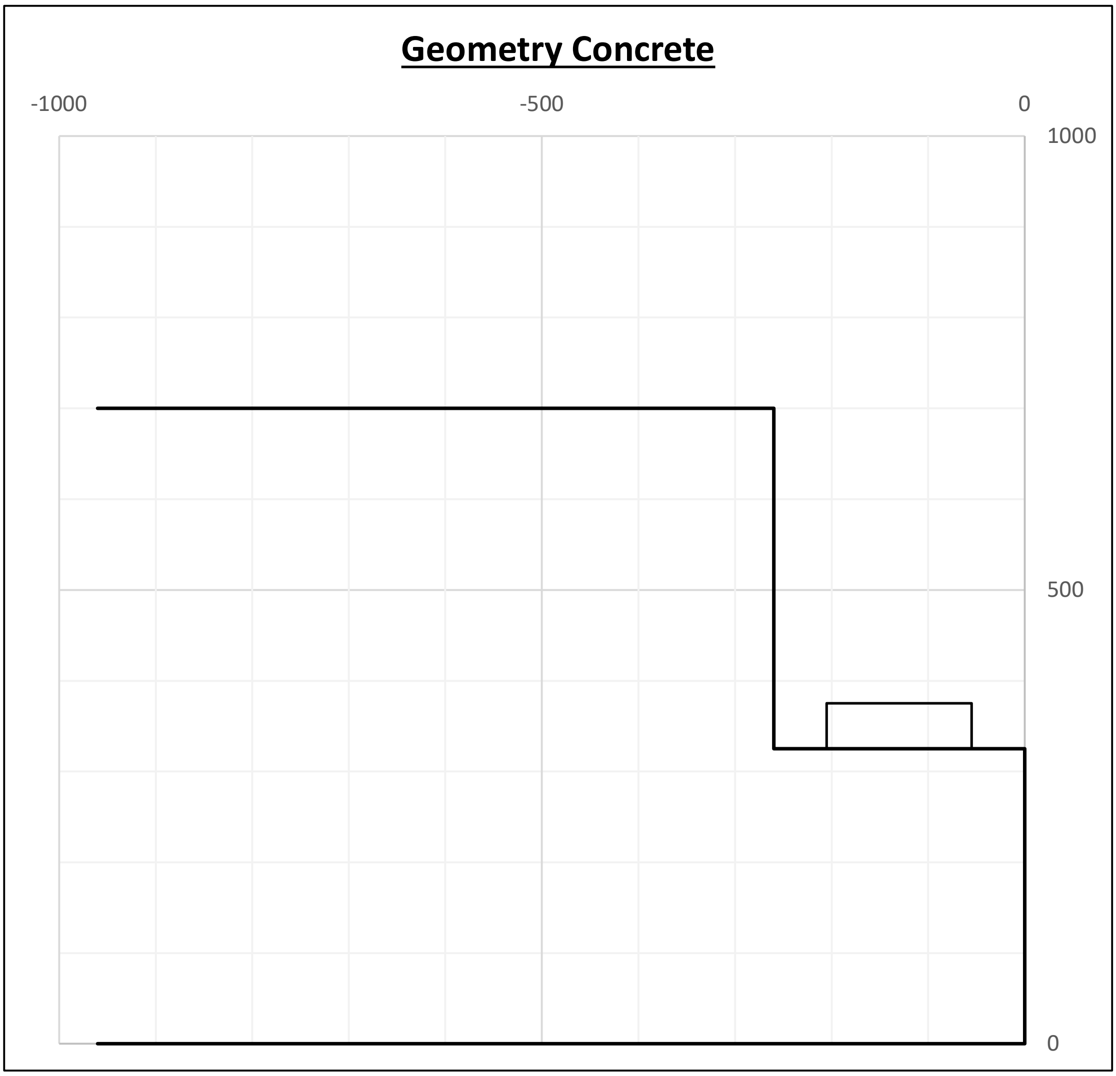

1.2 Reinforcement steel

1.2.1 Geometry

	Rebar 1	Rebar 2	Rebar 3	
Ø	12	12	8	[mm]
$Ø_m$	60	60	60	[mm]
Spacing	120	120	120	[mm]
η_1	1	1	1	[-]
η_2	1	1	1	[-]
η_3	1	1	1	[-]
l_{top}	800	600	-	[mm]
l_{bottom}	800	500	-	[mm]
Δ_{top}	0	0	-	[mm]
Δ_{middle}	0	0	-	[mm]
Δ_{bottom}	0	0	-	[mm]
Corrosion	0%	0%	0%	[-]

Include Rebar 3?	Yes

Coordinates Rebar 3		
x	y	
-896	664	[1]
-527	664	[2]
-165	36	[3]
-36	36	[4]
-36	289	[5]
		[6]

ϕ	2,1	[rad]
	120,0	[°]

1.2.2 Material

$f_{yd,0}$	400	[N/mm^2]
f_{yd}	400	[N/mm^2]

$\alpha_{corr,y}$	0	[-]

1,23

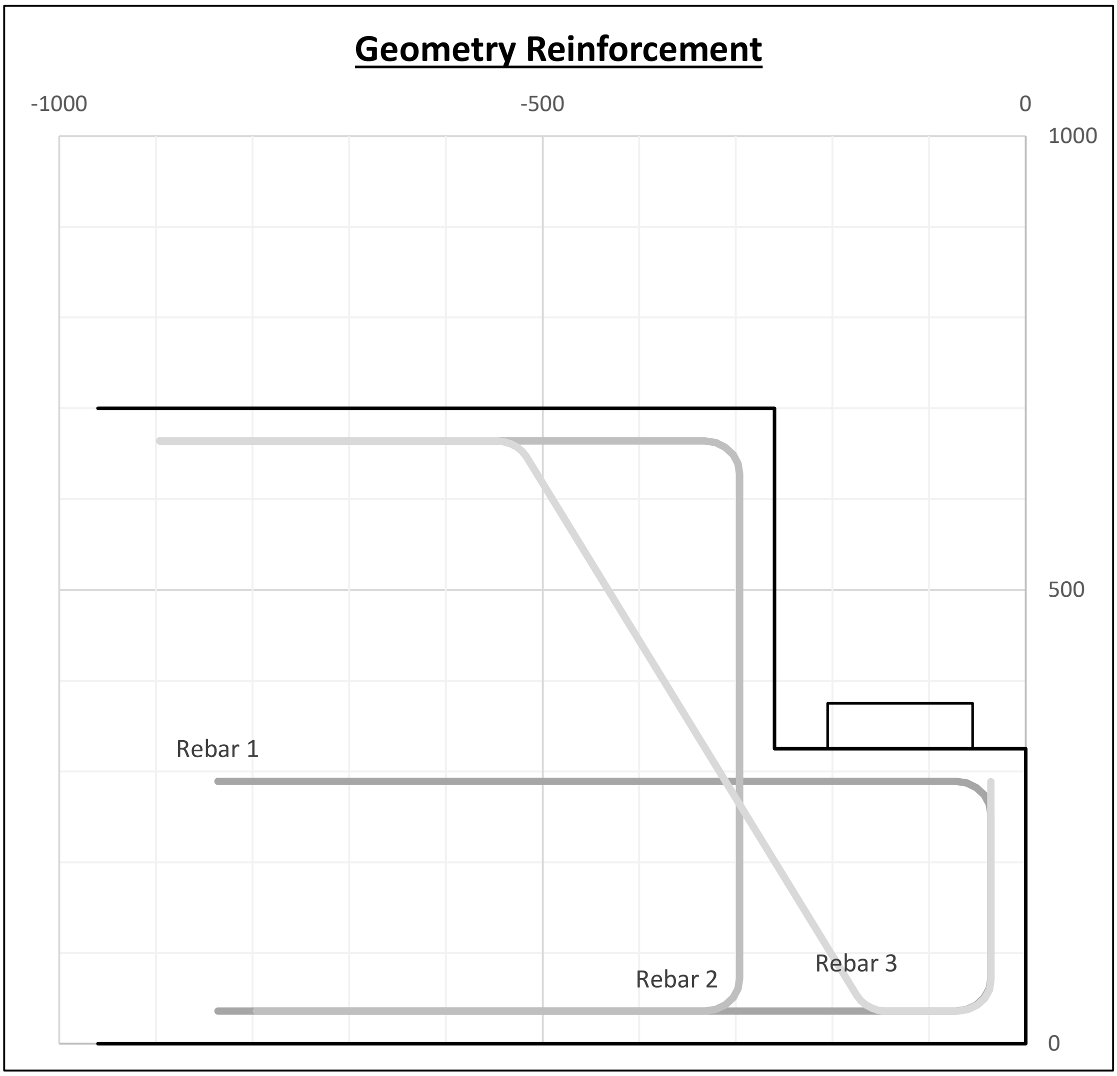

1.3 Pre-stressed steel

1.3.1 Geometry

A_p		[mm^2]
y_p		[mm]
Bearing		[mm]
Spacing		[mm]

Include prestress?	No

1.3.2 Material

σ_{pm}		[N/mm^2]
P_m		[kN]

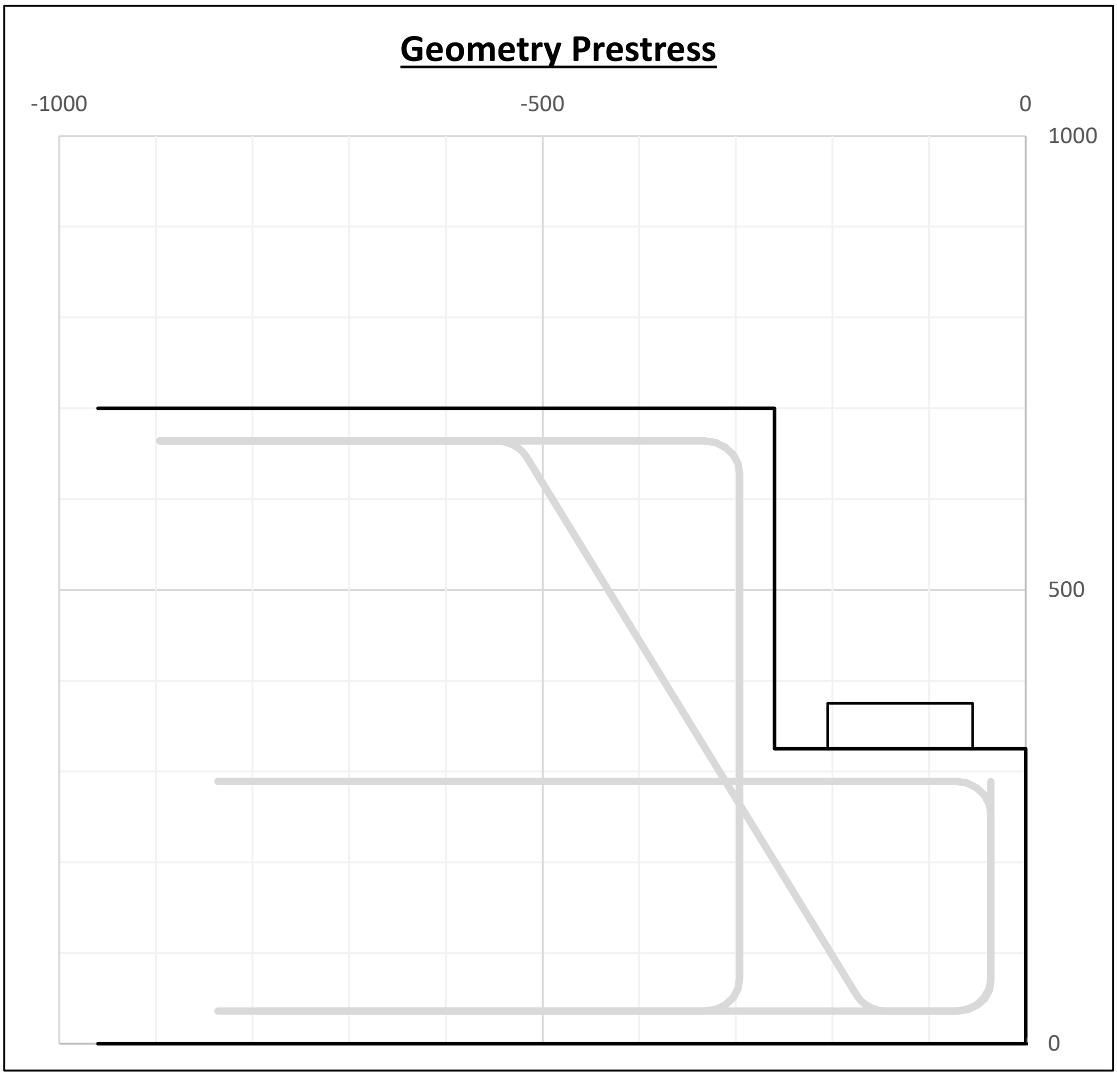

2. Strut-and-tie modelling

2.1 Nodes

	Offset		Coordinates		Type
	x	y	x	y	
(1)	-	-	-130,0	289,0	CCT
(2)	-	0	-296,0	664,0	CTT
(3)	120	-	-716,0	289,0	CCT
(4)	-	20	-296,0	92,0	CCT
(5)	-	15	-960,0	15,0	CCC
(6)	-		-960,0	664,0	-
(7)	35		-192,3	83,3	CCT
(8)	-	-	-527,0	664,0	CTT
(9)	-	-	-960,0	664,0	-

F_{unit}	1,00	[-]

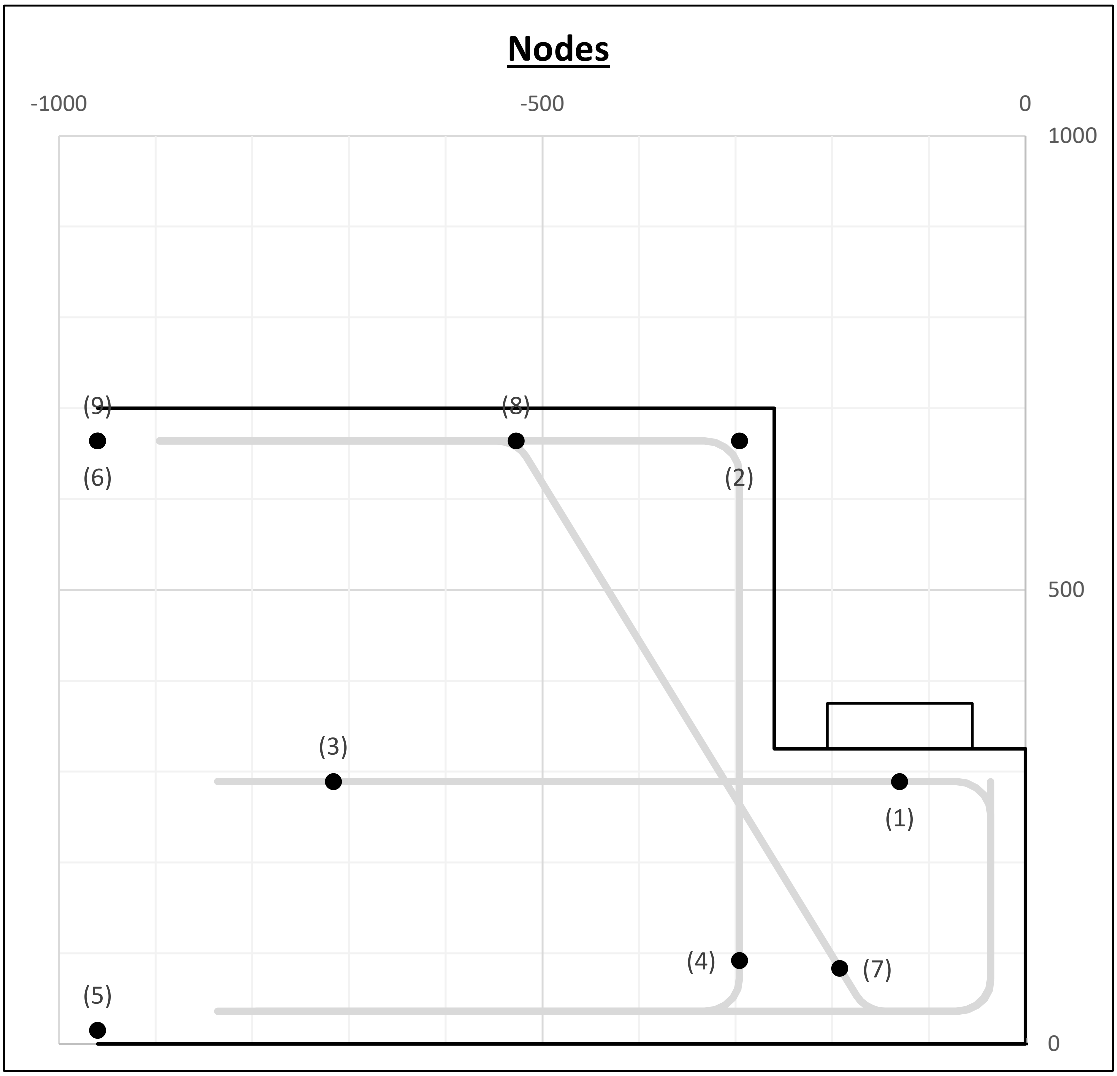

2.2 STM-1 (without diagonal)

	Node (j)	Node (k)	$F_{unit,STM1}$	Length	Angles	
			[-]	[mm]	[rad]	[°]
C1-1	(1)	(4)	-1,31	257,6	0,8706	49,9
C2-1	(2)	(3)	-0,39	563,0	0,7289	41,8
C3-1	(3)	(4)	-0,61	463,9	0,4386	25,1
C4-1	(2)	(5)	-1,38	928,5	0,7740	44,3
C5-1	(4)	(5)	-0,29	668,4	0,1154	6,6
T1-1	(1)	(3)	0,84	586,0	0	0,0
T2-1	(2)	(4)	1,23	572,0	1,5708	90,0
T3-1	(2)	(6)	1,28	664,0	0	0,0

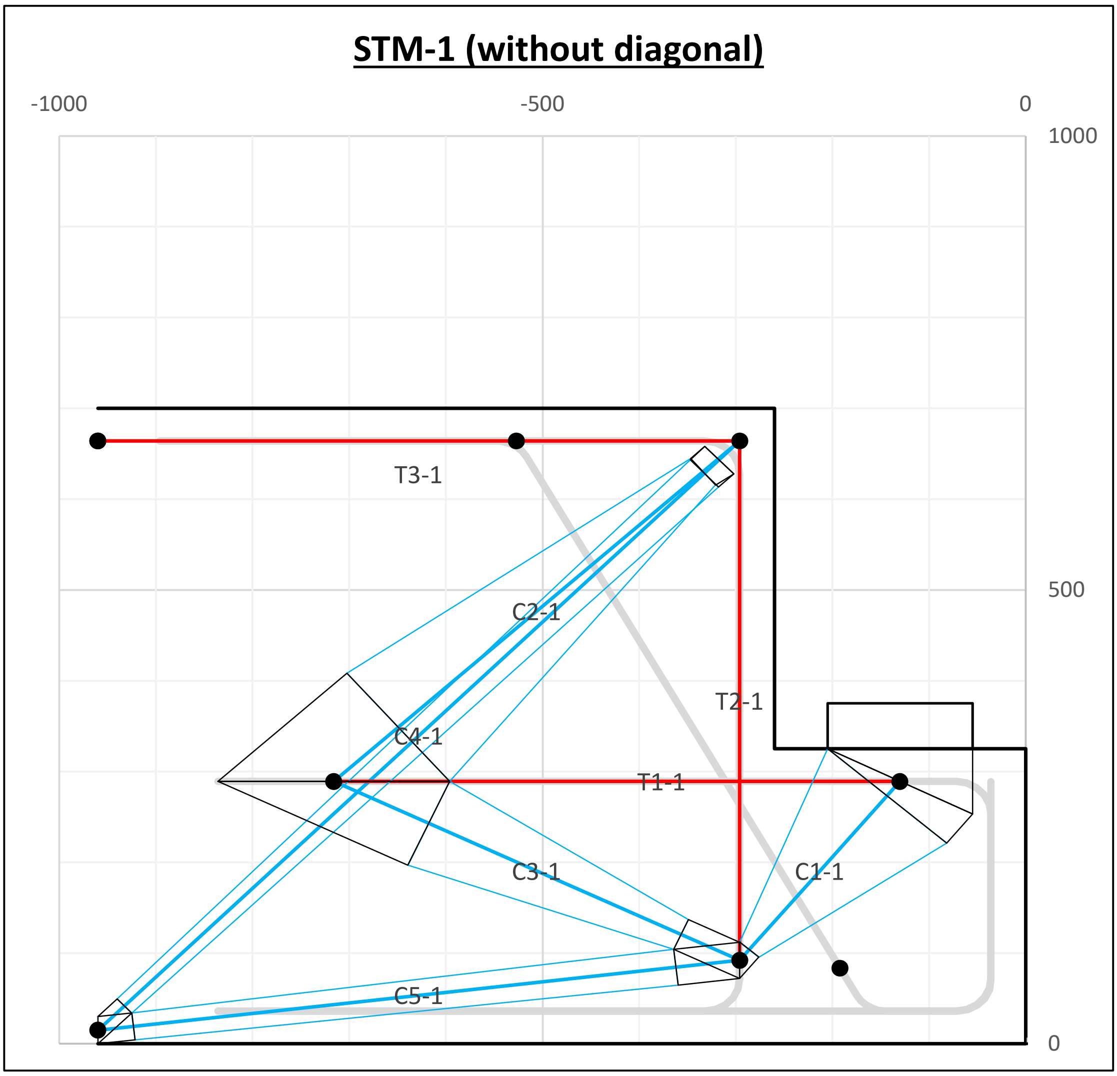

2.3 STM-2 (with diagonal)

	Node (j)	Node (k)	$F_{unit,STM2}$ [-]	Length [mm]	Angles [rad]	Angles [°]
C2-2	(2)	(3)	-0,14	563,0	0,7289	41,8
C3-2	(3)	(4)	-0,22	463,9	0,4386	25,1
C4-2	(2)	(5)	0,23	928,5	0,7740	44,3
C5-2	(4)	(5)	-0,73	668,4	0,1154	6,6
C6-2	(1)	(7)	-1,04	214,9	1,2767	73,1
C7-2	(7)	(4)	-0,93	104,1	-0,0833	-4,8
C8-2	(8)	(5)	-1,29	780,2	0,9824	56,3
T1-2	(1)	(3)	0,30	586,0	0	0,0
T2-2	(2)	(4)	-0,07	572,0	1,5708	90,0
T3-2	(2)	(6)	-0,06	664,0	0	0,0
T4-2	(7)	(8)	1,24	670,2	1,0479	60,0
T5-2	(8)	(9)	1,34	433,0	0	0,0

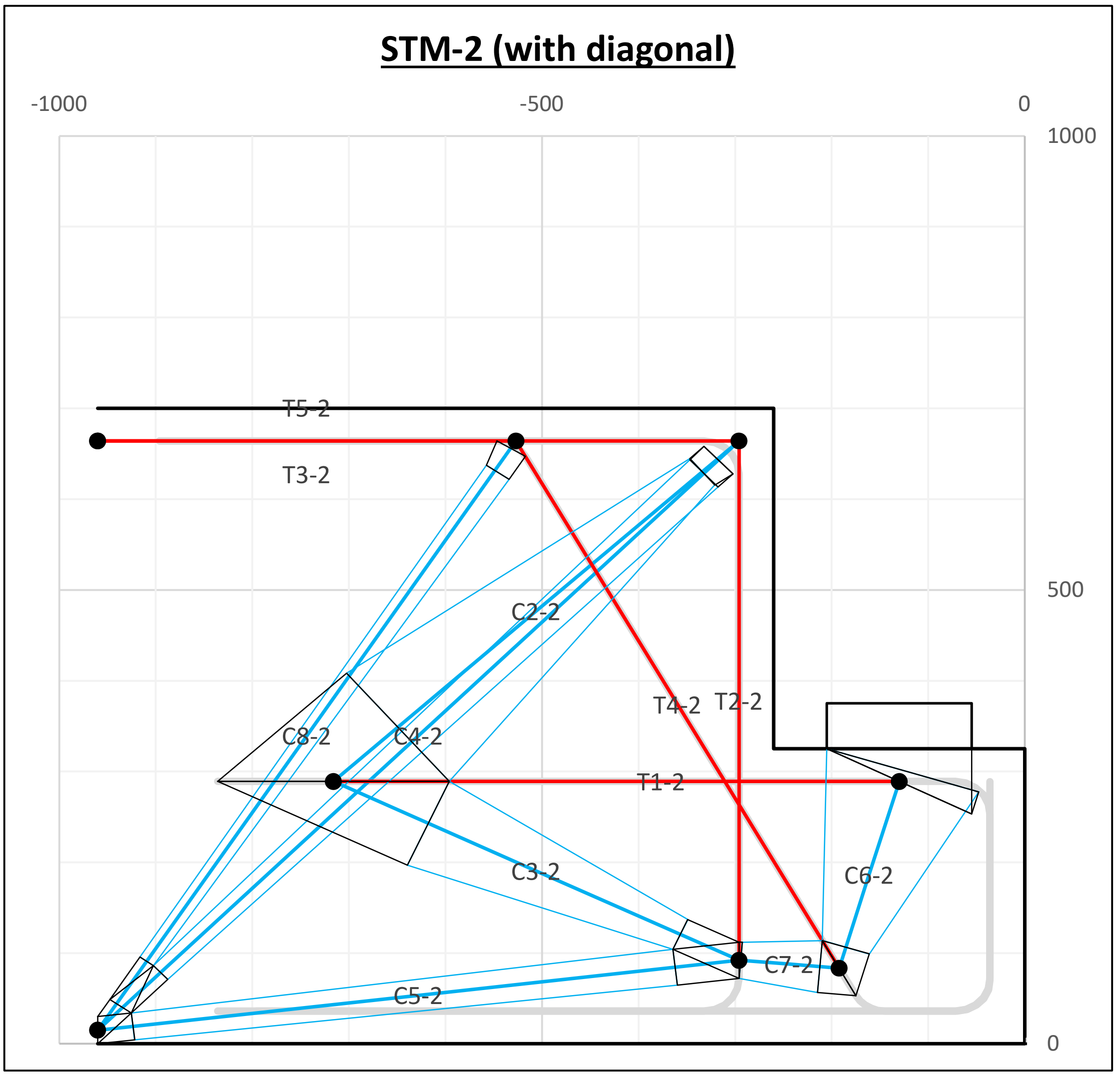

2.4 STM-3 (Combined)

	Node (j)	Node (k)	$F_{unit,STM1}$	$F_{unit,STM2}$	F_{unit}	Length	Angles	
			0,7	0,3	[-]	[mm]	[rad]	[°]
C1	(1)	(4)	-1,31		-0,92	257,6	0,8706	49,9
C2	(2)	(3)	-0,39	-0,14	-0,31	563,0	0,7289	41,8
C3	(3)	(4)	-0,61	-0,22	-0,49	463,9	0,4386	25,1
C4	(2)	(5)	-1,38	0,23	-0,90	928,5	0,7740	44,3
C5	(4)	(5)	-0,29	-0,73	-0,42	668,4	0,1154	6,6
C6	(1)	(7)		-1,04	-0,31	214,9	1,2767	73,1
C7	(7)	(4)		-0,93	-0,28	104,1	-0,0833	-4,8
C8	(8)	(5)		-1,29	-0,39	780,2	0,9824	56,3
T1	(1)	(3)	0,84	0,30	0,68	586,0	0	0
T2	(2)	(4)	1,23	-0,07	0,84	572,0	1,5708	90,0
T3	(2)	(6)	1,28	-0,06	0,88	664,0	0	0
T4	(7)	(8)		1,24	0,37	670,2	1,0479	60,0
T5	(8)	(6)		1,34	0,40	433,0	0	0

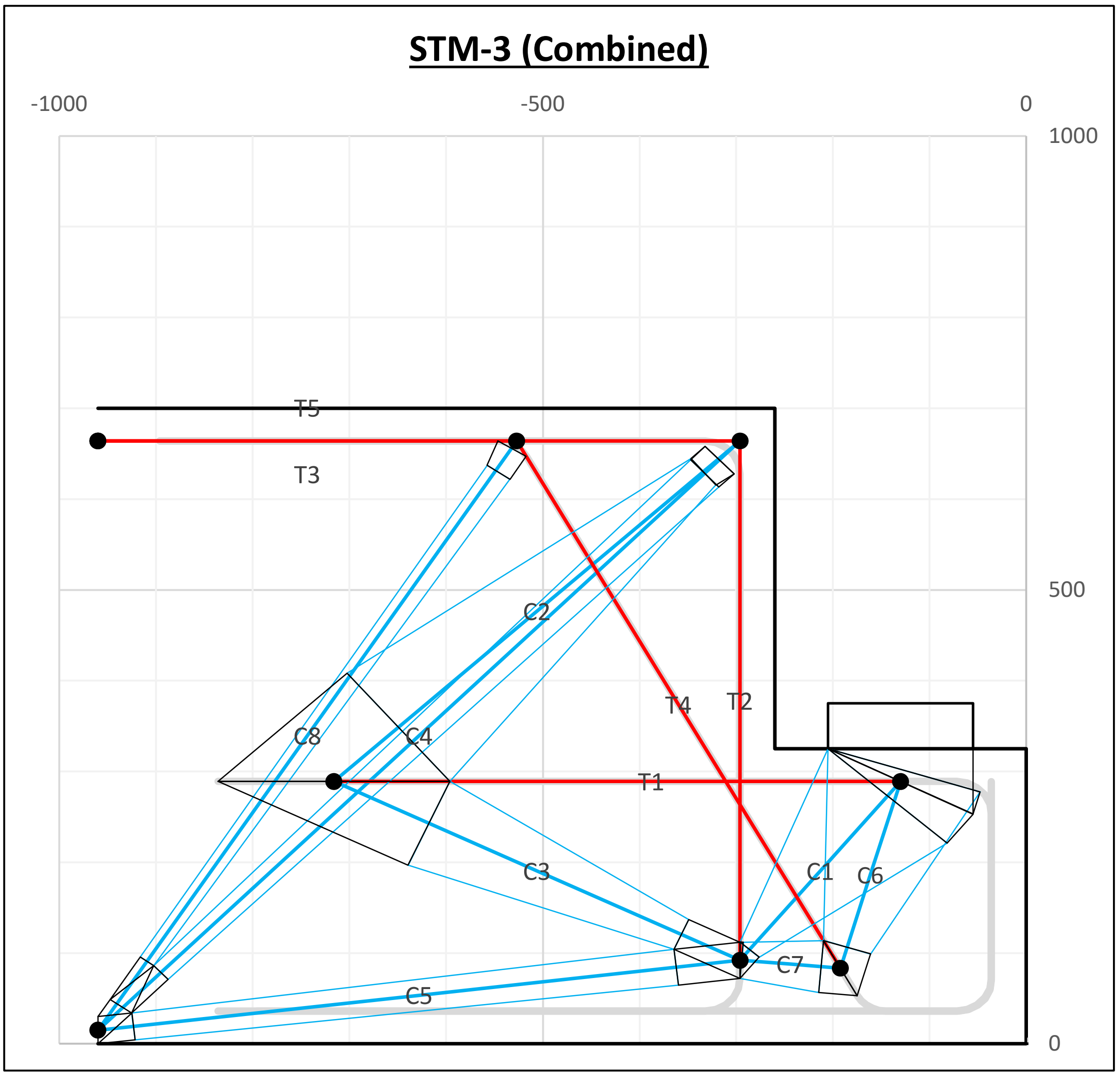

2.5 Node dimensions

Node (1)	T1	F	C1	C6		CCT
$a_{(1)}$	-	166,4	166,4	166,4		[mm]
$w_{(1)}$	-	150,0	161,1	164,4		[mm]
$b_{(1)}$	-	72,0	41,6	25,4		[mm]

Node (2)	T2	T3	C2	C4		CTT
$a_{(2)}$	-	-	42,4	42,4		[mm]
$w_{(2)}$	-	-	39,0	41,7		[mm]
$b_{(2)}$	-	-	-	-		[mm]

Node (3)	T1	C2	C3			CCT
$a_{(3)}$	-	240,0	240,0			[mm]
$w_{(3)}$	-	159,8	101,9			[mm]
$b_{(3)}$	-	179,0	217,3			[mm]

Node (4)	T2	C1	C3	C5	C7	CCT
$a_{(4)}$	-	40,0	68,8	75,5	40,0	[mm]
$w_{(4)}$	-	25,8	36,2	39,7	39,9	[mm]
$b_{(4)}$	-	30,6	58,5	64,2	3,3	[mm]

Node (5)	C4	C5	C8	Internal		CCC
$a_{(5)}$	56,9	48,7	58,4	35,1		[mm]
$w_{(5)}$	21,5	29,8	16,6	26,7		[mm]
$b_{(5)}$	52,7	38,5	56,0	22,7		[mm]

Node (7)	T4	C6	C7			CCT
$a_{(7)}$	-	70,0	70,0			[mm]
$w_{(7)}$	-	51,0	57,5			[mm]
$b_{(7)}$	-	47,9	39,9			[mm]

Node (8)	T4	T5	C8			CTT
$a_{(8)}$	-	-	-			[mm]
$w_{(8)}$	-	-	28,2			[mm]
$b_{(8)}$	-	-	-			[mm]

2,6 Checks

2.6.1 Compressive strength of struts

Strut i	C1	C2	C3	C4	C5	C6	C7	C8	
$F_{unit,i}$	-0,915	-0,314	-0,493	-0,899	-0,424	-0,313	-0,278	-0,388	[-]
Tension	Yes	Yes	Yes	Yes	Yes	Yes	Yes	Yes	
$\sigma_{Rd,max,c}$	25,06	25,06	25,06	25,06	25,06	25,06	25,06	25,06	[N/mm^2]
L_c	257,6	563,0	463,9	928,5	668,4	214,9	104,1	780,2	[mm]
$w_{c,eff}$	25,8	39,0	36,2	21,5	29,8	51,0	39,9	16,6	[mm]
$C_{max,C,i}$	-645,9	-977,3	-907,5	-537,6	-746,7	-1278,9	-998,9	-417,2	[kN/m]
$F_{max,C,i}$	705,6	3109,6	1841,0	598,3	1763,2	4080,0	3591,8	1074,1	[kN/m]

2.6.2 Compressive strength of nodes

Strut	C1	C2	C3	C4	C5	C6	C7	C8	
Node (j)	(1)	(2)	(3)	(2)	(4)	(1)	(7)	(8)	
Type	CCT	CTT	CCT	CTT	CCT	CCT	CCT	CTT	
k	0,85	0,75	0,85	0,75	0,85	0,85	0,85	0,75	[-]
$\sigma_{Rd,max,(j)}$	35,50	31,32	35,50	31,32	35,50	35,50	35,50	31,32	[N/mm^2]
$w_{i(j)}$	161,1	39,0	101,9	41,7	39,7	164,4	57,5	28,2	[mm]
$C_{max,i(j)}$	-5719,0	-1221,7	-3618,0	-1307,6	-1410,5	-5837,2	-2042,2	-884,7	[kN/m]
$F_{max,i(j)}$	6247,7	3887,0	7339,9	1455,2	3330,4	18621,9	7343,6	2277,5	[kN/m]
Node (k)	(4)	(3)	(4)	(5)	(5)	(7)	(4)	(5)	
Type	CCT	CCT	CCT	CCC	CCC	CCT	CCT	CCC	
k	0,85	0,85	0,85	1,00	1,00	0,85	0,85	1,00	[-]
$\sigma_{Rd,max,(k)}$	35,50	35,50	35,50	41,76	41,76	35,50	35,50	41,76	[N/mm^2]
$w_{i(k)}$	25,8	159,8	36,2	21,5	29,8	51,0	39,9	16,6	[mm]
$C_{max,i(k)}$	-915,0	-5674,4	-1285,6	-896,0	-1244,6	-1811,8	-1415,1	-695,4	[kN/m]
$F_{max,i(k)}$	999,6	18054,5	2608,1	997,2	2938,6	5780,0	5088,4	1790,1	[kN/m]

2.6.3 Compressive strength of internal nodes

Node (j/k)	(1)	(2)	(4)	(5)	
Strut i_1	C1	C2	C1	C4	
$F_{unit,i,1}$	-0,886	-0,314	-0,590	-0,643	[-]
Strut i_2	C6	C4	C7	C5	
$F_{unit,i,2}$	-0,310	-0,899	-0,277	-0,421	[-]
Strut i_3	-		-	C8	
$F_{unit,i,3}$				-0,216	[-]
F_{unit}	-1,196	-1,212	-0,867	-1,279	[-]
Type	CCT	CTT	CCT	CCC	
k	0,85	0,75	0,85	1,00	[-]
$\sigma_{Rd,max}$	35,50	31,32	35,50	41,76	[N/mm^2]
w	166,4	39,0	40,0	30,0	[mm]
C_{max}	-5906,6	-1221,7	-1420,0	-1252,9	[kN/m]
F_{max}	4938,2	1007,7	1637,8	979,7	[kN/m]

2.6.4 Yield strength of ties

Ties	T1	T2	T3	T4	T5		
$F_{unit,i}$	0,681	0,837	0,877	0,373	0,402	[-]	
Rebar	1	2	2	3	3	[-]	
Ø	12	12	22	8	18	[mm]	(add top rebar)
Corrosion	0%	0%	0%	0%	-	[-]	(at re-entrant corner)
f_{yd}	400	400	400	400	400	[N/mm^2]	
$T_{max,T,ind,i}$	45,2	45,2	152,1	20,1	101,8	[kN]	
$T_{max,T,i}$	377,0	377,0	1267,1	167,6	848,2	[kN/m]	
$F_{max,T,i}$	553,8	450,2	1444,8	449,2	2110,8	[kN/m]	

2.6.5 Anchorage length of ties

Lower-bound load 449,2 [kN/m] Failure mechanism: T4

Ties	T1	T2	T3	T4	T5	
F_T	305,8	376,2	394,0	167,6	180,5	[kN/m]
$F_{T,ind}$	36,7	45,1	47,3	20,1	21,7	[kN]
f_{bd}	8,78	8,78	8,78	8,78	8,78	[N/mm^2]
σ_{sd}	324,5	399,1	124,4	400,0	85,1	[N/mm^2]
$l_{b,rqd,max}$	110,9	136,4	77,9	91,1	43,6	[mm]
Node (j)	(1)	(2)	(2)	(7)	(8)	
c_d	60,0	-	-	60,0	-	[mm]
p	2,99	-	-	1,47	-	[N/mm^2]
α_1	0,7	-	-	0,7	-	[-]
α_2	0,7	-	-	0,7	-	[-]
α_3	1,0	-	-	1,0	-	[-]
α_4	1,0	-	-	1,0	-	[-]
α_5	0,88	-	-	0,94	-	[-]
$l_{b,min}$	120,0	-	-	100,0	-	[mm]
l_{bd}	120,0	-	-	100,0	-	[mm]
$l_{b,prov}$	1191,1	-	-	453,4	-	[mm]
Check	Correct	-	-	Correct	-	
Node (k)	(3)	(4)	(6)	(8)	(6)	
c_d	60,0	60,0	-	-	-	[mm]
p	0,39	9,74	-	-	-	[N/mm^2]
α_1	0,7	0,7	-	-	-	[-]
α_2	0,7	0,7	-	-	-	[-]
α_3	1,0	1,0	-	-	-	[-]
α_4	1,0	1,0	-	-	-	[-]
α_5	0,98	0,70	-	-	-	[-]
$l_{b,min}$	120,0	120,0	-	-	-	[mm]
l_{bd}	120,0	120,0	-	-	-	[mm]
$l_{b,prov}$	240,0	560,5	-	-	-	[mm]
Check	Correct	Correct	-	-	-	

3. Kinematic approach (upper-bound approximation)

x_min	11,6	[mm]
Δx	0	[mm]

θ_{Crack}	45,0	[°]
l_{crack}	443,2	[mm]

	$A_{s,i}$	A_s	f_{yd}	N_S / N_C	Leverarm	Moment	$N_{y\text{-}dir}$
	[mm^2]	[mm^2]	[N/mm^2]	[kN/m]	[mm]	[kNm/m]	[kN/m]
Rebar 1	113	942	400	377,0	277,4	104,6	0,0
Rebar 2	113	942	400	377,0	277,4	104,6	377,0
Rebar 3	50	419	400	167,6	379,0	63,5	145,2
Concrete	-	-	-	460,7	7,1	3,3	0,0
Total						275,9	522,2

Support		
Leverarm:	443,4	[mm]
Upper-bound load:	622,3	[kN/m]

Vertical equilibrium	Fail	
Difference in vertical force	100,1	[kN/m]
Concrete shear resistance	8,4	[kN/m]

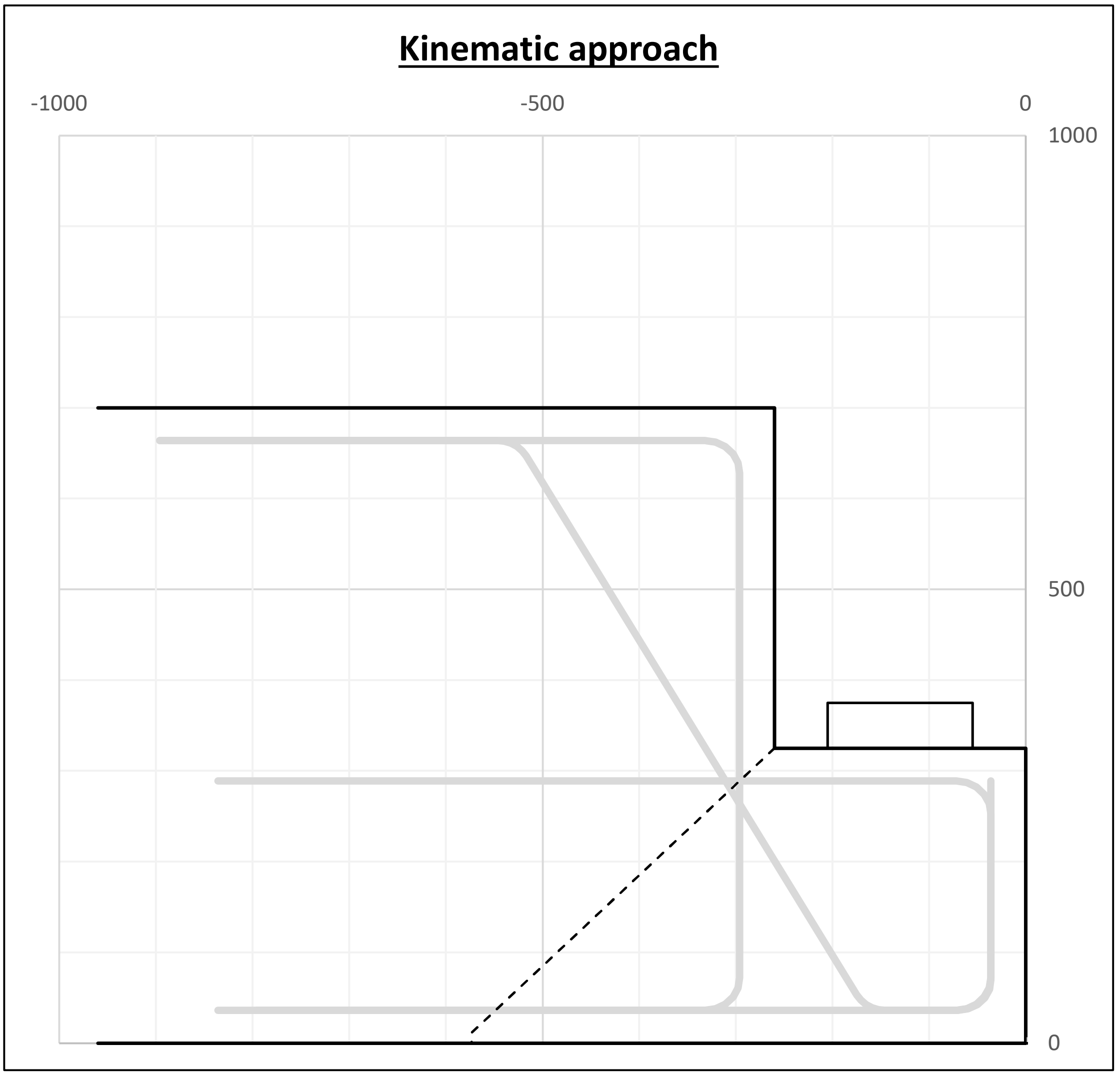

4. Optimisation

4.1 Strut-and-tie approach (Highest lower-bound approximation)

	Stepsize	Max. shift	Steps
Load	0,1	-	10
Node 3	20	150,0	7
Node 4	5	30,0	6
Node 5	5	30,0	6
Node 7	5	50,0	10

min θ 25,0 [°]

Anchorage:	Correct	
Angle (theta):	Correct	
Lower-bound load	449,2	[kN/m]

Limitations on angles				
	Minimum	Maximum	[°]	
θC1	25,0	65,0	49,9	Correct
θC2	25,0	65,0	41,8	Correct
θC3	25,0	65,0	25,1	Correct
θC4	25,0	65,0	44,3	Correct
θC6	25,0	-	73,1	Correct
θC7	-	65,0	-4,8	Correct
θC8	25,0	-	56,3	Correct
θC6+θT4	-	155,0	133,2	Correct
θT4-θC7	25,0	-	64,8	Correct
θC8+θT4	25,0	-	116,3	Correct

Governing lower-bound load: 449,2 [kN/m] Failure mechanism: T4

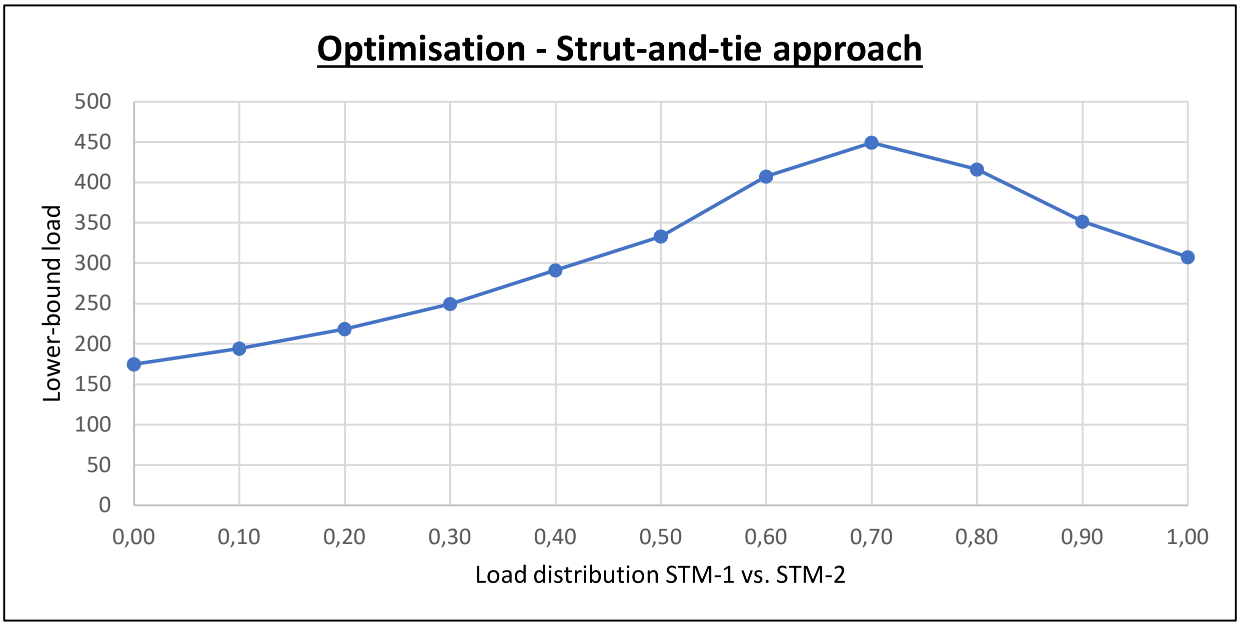

Load distribution		Offset				Load		Limitations	
STM-1	STM-2	Node 3	Node 4	Node 5	Node 7	[kN]	Mechan.	Anchor.	Angle
0,000	1,000	100	5	10	50	174,7	T4	Correct	Correct
0,100	0,900	100	5	10	50	194,1	T4	Correct	Correct
0,200	0,800	100	5	10	50	218,4	T4	Correct	Correct
0,300	0,700	100	5	10	50	249,6	T4	Correct	Correct
0,400	0,600	100	5	10	50	291,2	T4	Correct	Correct
0,500	0,500	100	10	10	50	333,2	T4	Correct	Correct
0,600	0,400	100	10	10	50	407,7	C1 (strut)	Correct	Correct
0,700	0,300	120	20	15	35	449,2	T4	Correct	Correct
0,800	0,200	140	30	15	5	416,2	T2	Correct	Correct
0,900	0,100	140	30	15	5	351,7	T2	Correct	Correct
1,000	0,000	120	20	15	5	307,6	T2	Correct	Correct

4,2 Kinematic approach (Lowest upper-bound approximation)

$\theta_{C,min}$	30,0	[°]
$\theta_{C,max}$	70,0	[°]

θ_{Crack}		30,0	36,7	43,3	50,0	56,7	63,3	70,0	[°]
Rebar 1	Leverarm	208,4	193,4	178,4	162,4	148,4	134,4	123,4	[mm]
	Moment	78,6	72,9	67,3	61,2	55,9	50,7	46,5	[kNm/m]
Rebar 2	Leverarm	387,3	272,2	191,3	130,5	85,3	49,6	22,0	[mm]
	Moment	146,0	102,6	72,1	49,2	32,2	18,7	8,3	[kNm/m]
Rebar 3	Leverarm	426,8	321,7	248,7	193,0	151,3	116,4	88,6	[mm]
	Moment	71,5	53,9	41,7	32,3	25,3	19,5	14,9	[kNm/m]
Concrete	Leverarm	53,7	63,7	73,7	84,4	93,7	103,1	110,4	[mm]
	Moment	24,7	29,4	34,0	38,9	43,2	47,5	50,9	[kNm/m]
ΔX		69,0	84,0	99,0	115,0	129,0	143,0	154,0	[mm]
Total moment		320,9	258,8	215,0	181,6	156,6	136,3	120,5	[kNm/m]
Leverarm support		553,3	438,2	357,3	296,5	251,3	215,6	188,0	[mm]
Load support		579,9	590,6	601,8	612,6	623,3	632,5	641,1	[kN/m]

Governing upper-bound load: 579,9 [kN/m]

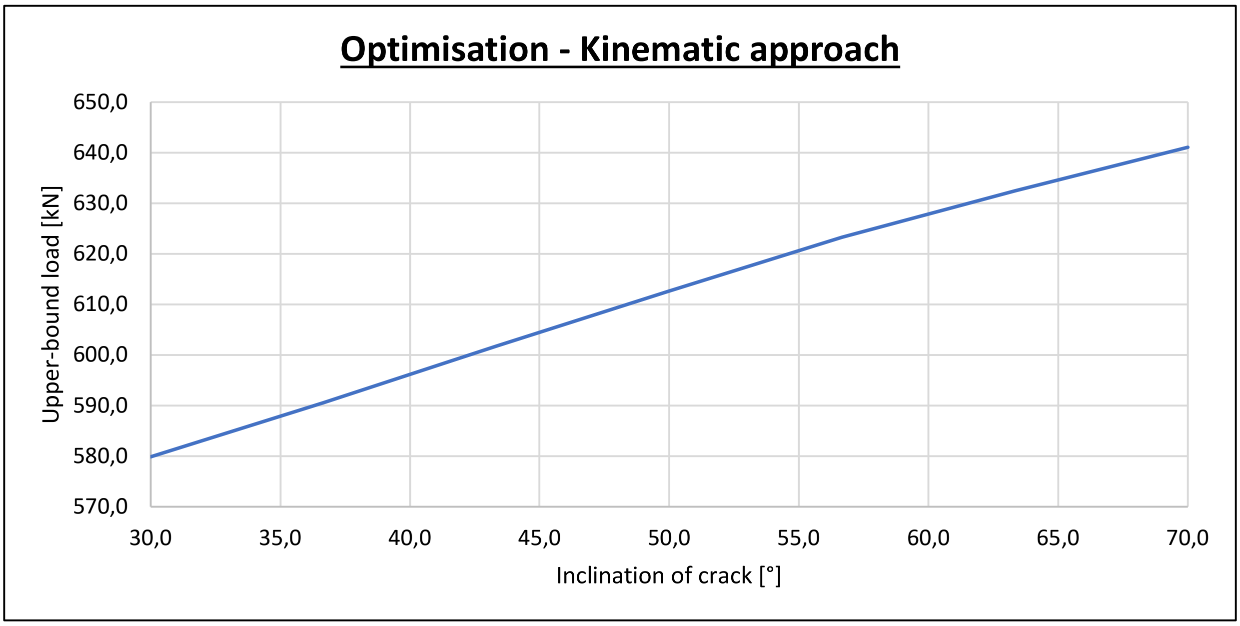

5. Corrosion

	Stepsize	Max
Corrosion	10%	60%

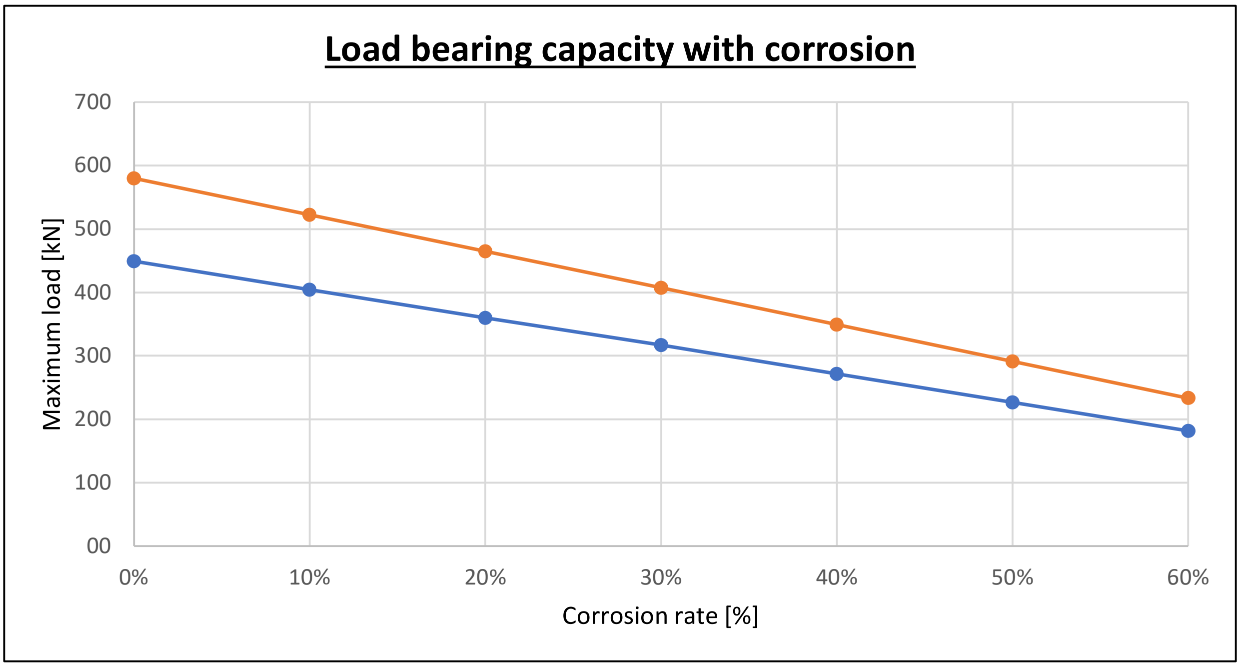

Maximum load	Corrosion							
	0%	10%	20%	30%	40%	50%	60%	
Lower-bound load	449,2	404,3	359,9	317,1	271,8	226,5	181,9	[kN/m]
Failure mechanism	T4	T4	T2	T2	T2	T2	T2	
Upper-bound load	579,9	522,5	464,9	407,3	349,5	291,6	233,5	[kN/m]

Appendix D

Results of Category A1 half-joint

D.1 Category A1 - 10% Corrosion

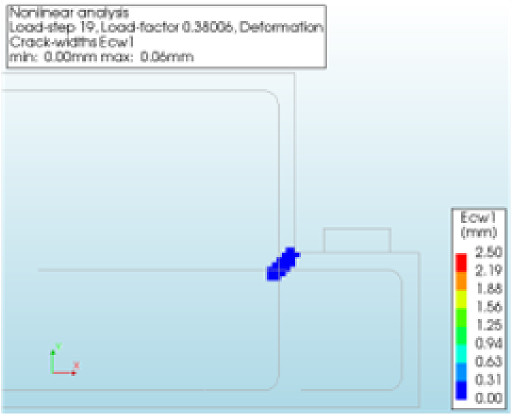

(a) Crackwidth

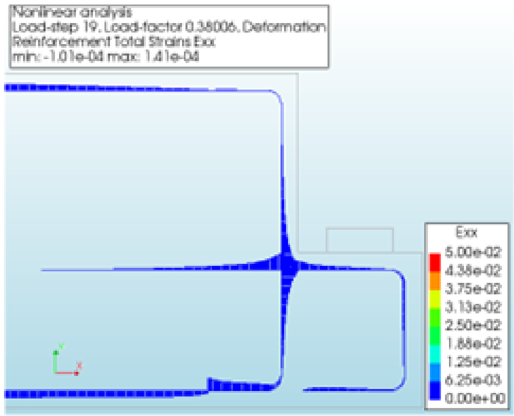

(b) Strain reinforcement

Figure D.1: Crack initiation of concrete

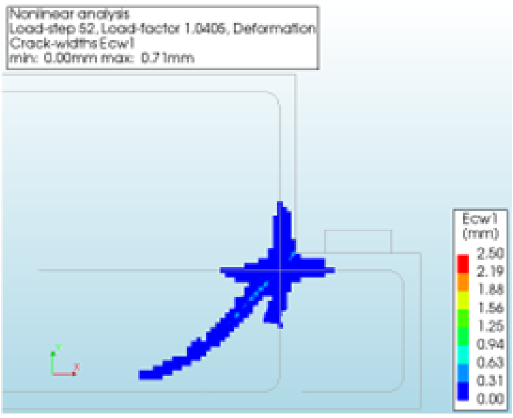

(a) Crackwidth

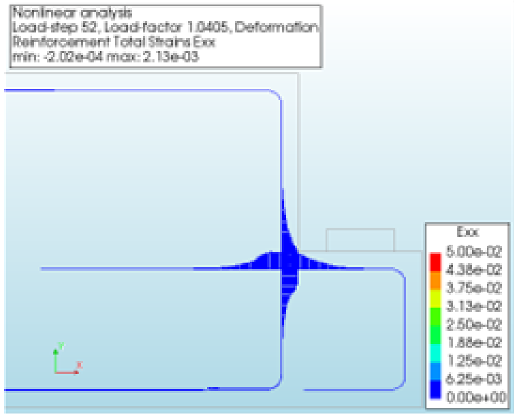

(b) Strain reinforcement

Figure D.2: Start yielding of reinforcement

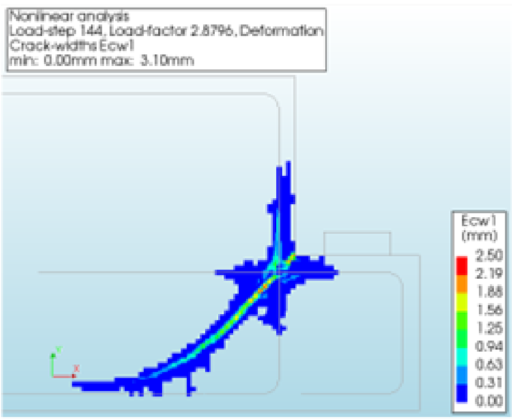

(a) Crackwidth

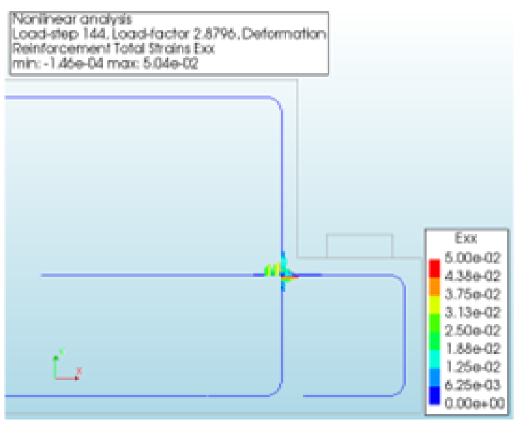

(b) Strain reinforcement

Figure D.3: Ultimate strain of reinforcement reached

D.2 Category A1 - 20% Corrosion

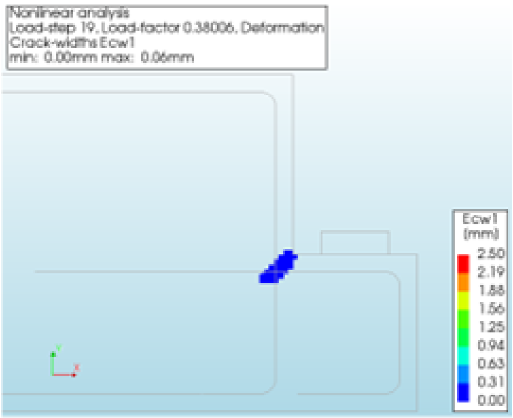

(a) Crackwidth

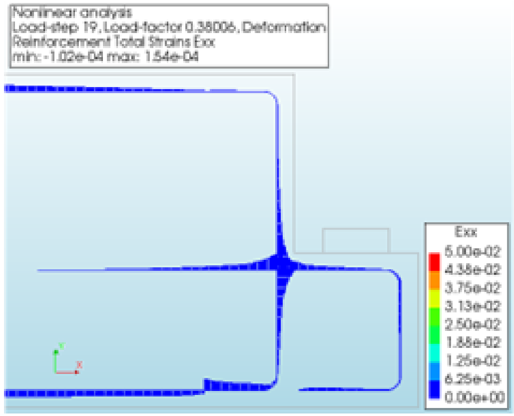

(b) Strain reinforcement

Figure D.4: Crack initiation of concrete

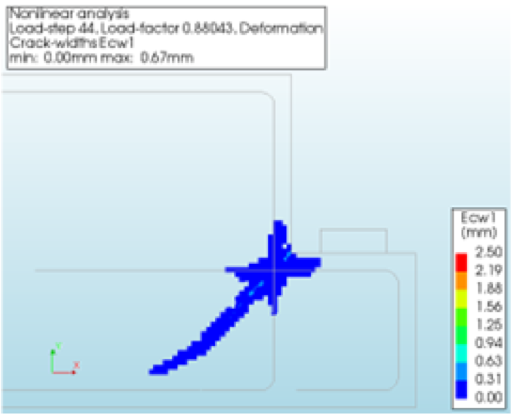

(a) Crackwidth

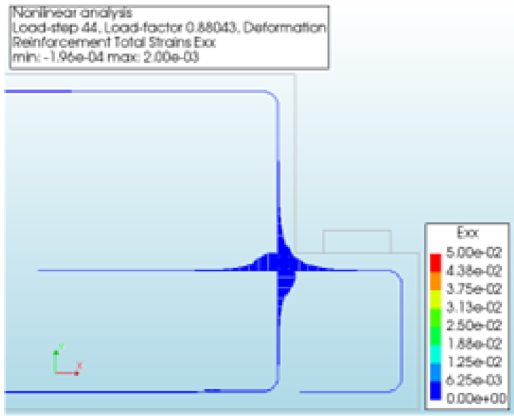

(b) Strain reinforcement

Figure D.5: Start yielding of reinforcement

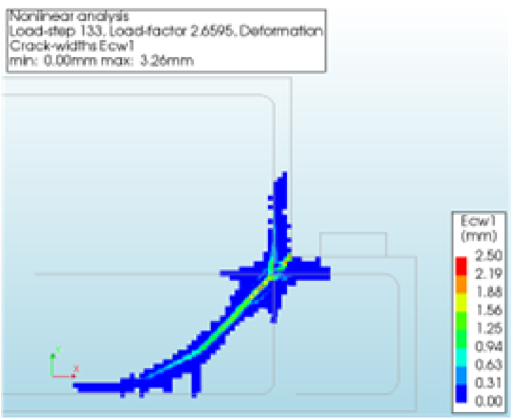

(a) Crackwidth

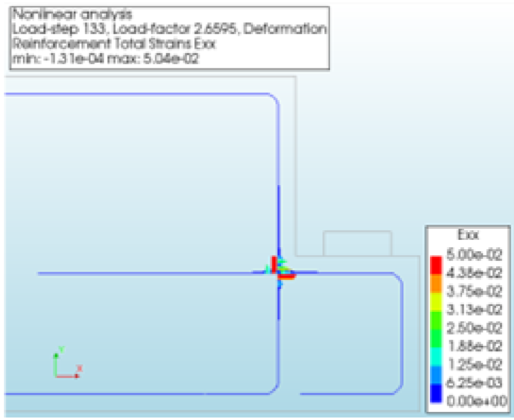

(b) Strain reinforcement

Figure D.6: Ultimate strain of reinforcement reached

D.3 Category A1 - 30% Corrosion

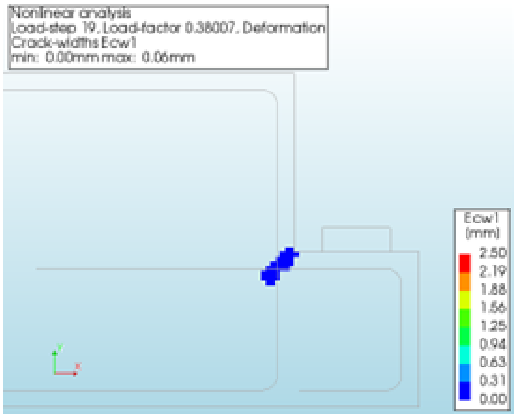

(a) Crackwidth

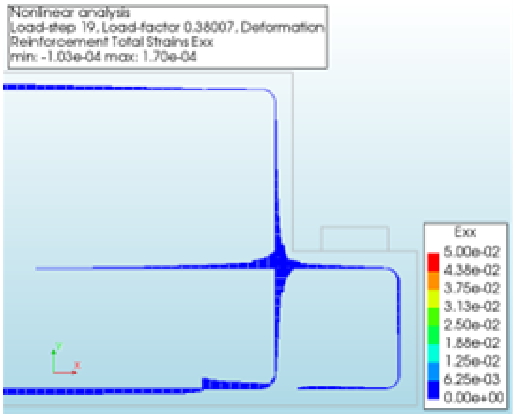

(b) Strain reinforcement

Figure D.7: Crack initiation of concrete

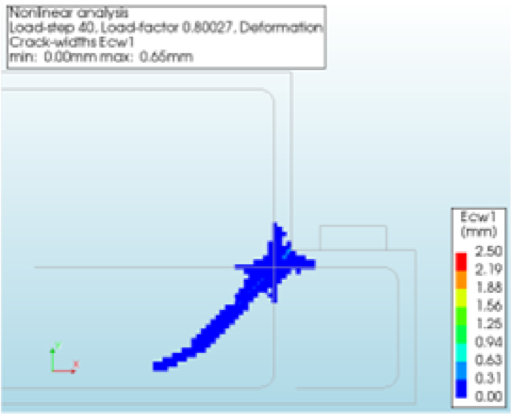

(a) Crackwidth

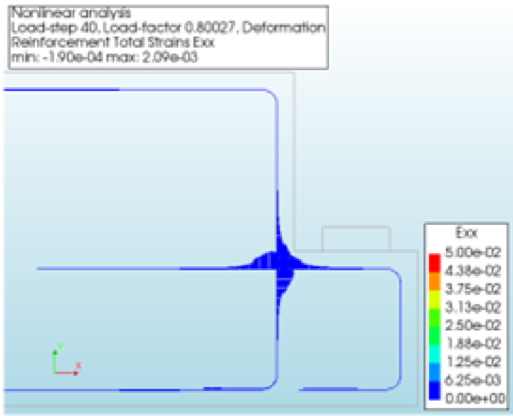

(b) Strain reinforcement

Figure D.8: Start yielding of reinforcement

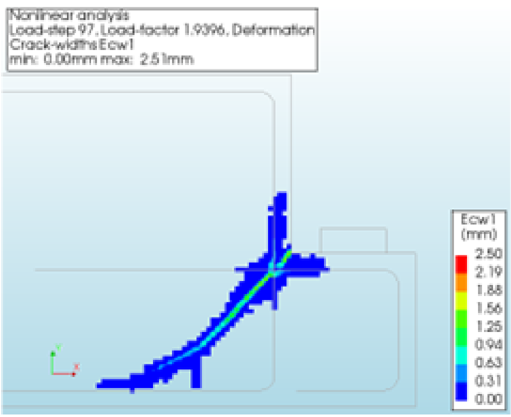

(a) Crackwidth

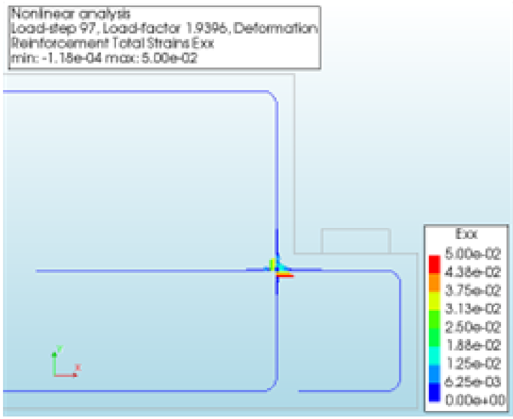

(b) Strain reinforcement

Figure D.9: Ultimate strain of reinforcement reached

D.4 Category A1 - 40% Corrosion

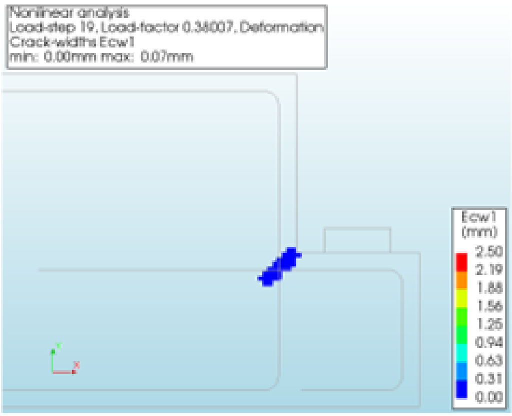

(a) Crackwidth

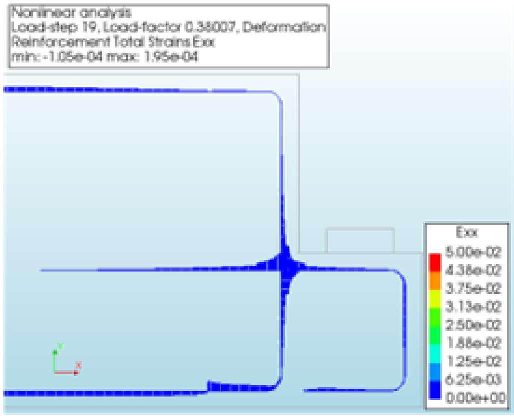

(b) Strain reinforcement

Figure D.10: Crack initiation of concrete

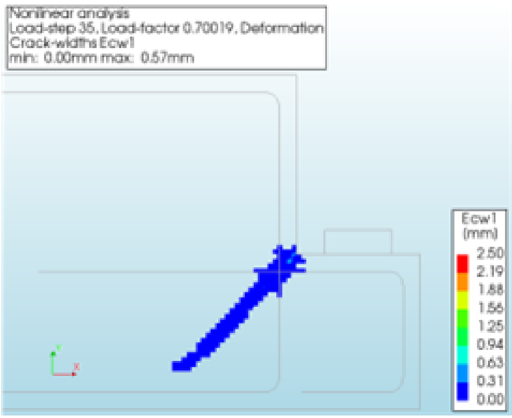

(a) Crackwidth

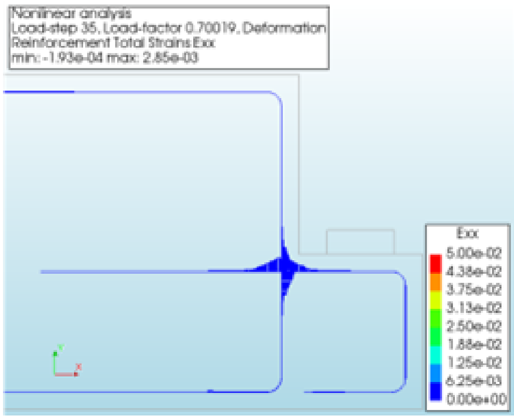

(b) Strain reinforcement

Figure D.11: Start yielding of reinforcement

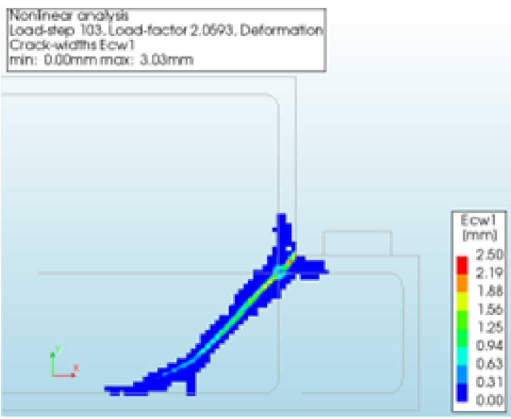

(a) Crackwidth

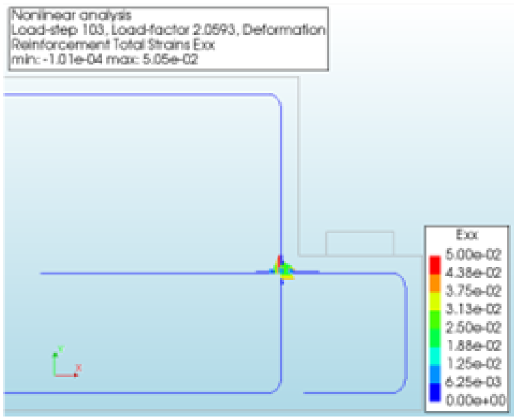

(b) Strain reinforcement

Figure D.12: Ultimate strain of reinforcement reached

D.5 Category A1 - 50% Corrosion

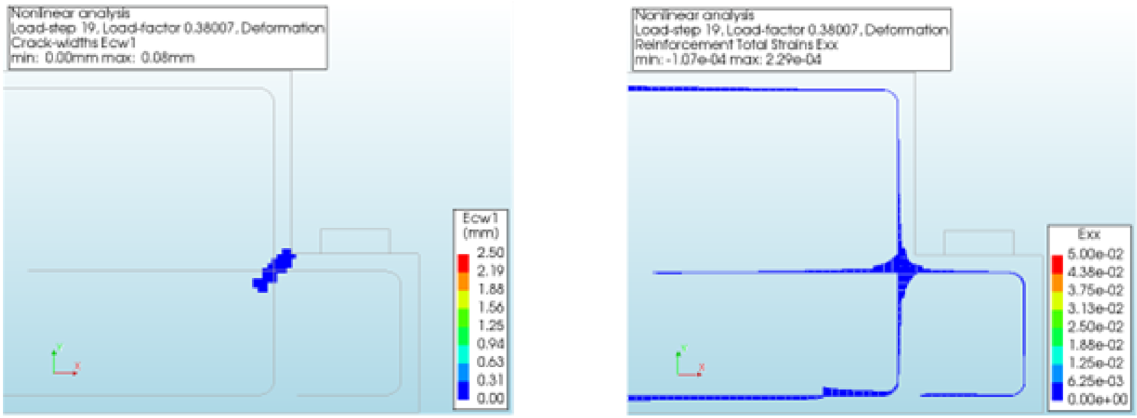

(a) Crackwidth (b) Strain reinforcement

Figure D.13: Crack initiation of concrete

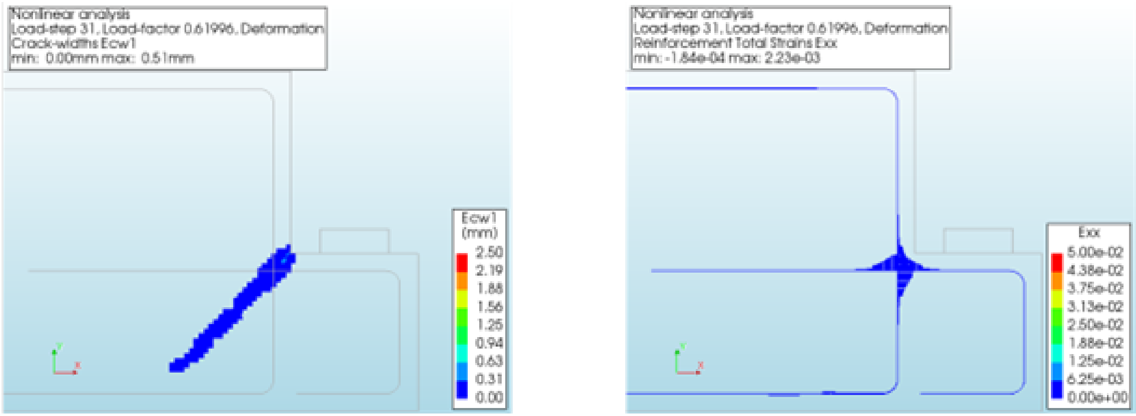

(a) Crackwidth (b) Strain reinforcement

Figure D.14: Start yielding of reinforcement

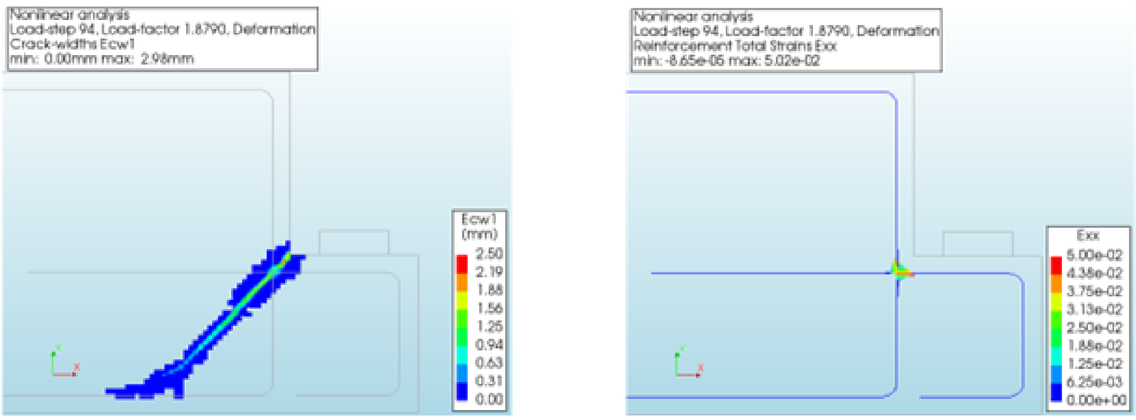

(a) Crackwidth (b) Strain reinforcement

Figure D.15: Ultimate strain of reinforcement reached